12-2011

Controlling Biofouling by Surface Engineering and Molecular Inhibition

Debjyoti Bandyopadhyay
Syracuse University

ABSTRACT

The common theme that binds together all the chapters in this dissertation is *anti-biofouling chemistry*. By utilizing tools of surface engineering and molecular inhibition, a hypothesis driven, systematic approach of controlling the different forms of biofoulings such as protein adsorption, mammalian cell adhesion and biofilm formation is presented. Chapter 1 provides a brief introduction about topics relevant for understanding the studies presented in subsequent chapters. Chapter 2 reports the synthesis of enantiomerically pure alkanethiols that terminate with different stereoisomer's of sugar alcohols, and the effect of chirality of these polyol-terminated self-assembled monolayers (SAMs) on resisting protein adsorption.

Chapter 3 and 4 presents the results on confining adhered mammalian cell (Swiss 3T3 albino fibroblasts) and bacterial (*Escherichia coli*) biofilm respectively, within micrometer sized cell adhesive patterns of methyl-terminated SAMs, surrounded by bioinert chiral polyol-terminated SAMs. Interestingly, SAMs presenting racemic mixture of enantiomeric alkanethiols were found to confine the adhered mammalian cells or biofilm within the micrometer-sized patterns longer than the SAMs presenting either enantiomer.

Chapter 5 presents the synthesis of chiral polyol-terminated alkanephosphonic acids to form SAMs on surface of native metal oxides, particularly TiO_2 and Fe_3O_4, for evaluating the ability of these alkanephosphonate SAMs on TiO_2 to resist the adhesion of mammalian cells (Swiss 3T3 albino fibroblasts) and on Fe_3O_4 to solubilize Fe_3O_4 (magnetite) nanoparticles in aqueous media.

Another approach of controlling biofouling due to biofilm formation is to develop inhibitors for a class of organic molecules called autoinducers secreted by bacteria, which are responsible for regulating bacterial group behavior such as biofilm formation. Chapter 6 reports the synthesis of derivatives of a class of molecules called brominated furanones, which are known to inhibit biofilm formation in *E. coli.* Chapter 7 reports the synthesis of novel squarate based molecules named squarylated homoserine lactones (SHLs), which are structural mimics of the bacterial autoinducer molecules called acylated homoserine lactones (AHLs). The synthesized brominated furanone derivatives and SHLs were found to be non-toxic to *E. coli* and were able to inhibit the biofilm formation by the bacterium.

Controlling Biofouling by Surface Engineering and Molecular Inhibition

by

Debjyoti Bandyopadhyay

M. Phil. (Chemistry), Syracuse University, 2008
M.Sc. (Chemistry), University of Delhi, New Delhi, India, 2005
B.Sc. (Chemistry), University of Delhi, New Delhi, India 2003

Dissertation
Submitted in partial fulfillment of the requirements for the degree of
Doctor of Philosophy in *Chemistry*.

Syracuse University
December 2011

ACKNOWLEDGEMENTS

I would like to thank Professor Yan-Yeung Luk for his continued support and valuable guidance during the course of my graduate studies in Syracuse. Professor Luk's passion for science and his drive for developing new ideas are truly inspiring for any budding scientist. I thank him for believing in me and giving me the opportunity to work in areas of science that were completely new to me. Professor Luk is a truly wonderful person to work with and I have never felt the slightest of hesitation to approach him to discuss matters both professional and personal.

Sincere thanks to Professors Raina, Luk, Dabrowiak, Borer, Kallmerten and Hougland for being on my Ph.D. defense committee. A special thanks to Professor Baldwin for his valuable suggestions and comments on my annual research reports.

I would like to thank my parents, my father Late Krishna Kumar Bandyopadhyay and my mother Mrs Debapriya Bandyopadhyay for their endless love and encouragement during both good and bad times. I specially thank my mother for her efforts and support in every possible way during my application and travel to the United States for my graduate studies. Without my mother, my existence or my Ph.D. would not have been possible. I would like to thank my grandparents Late Sanatan Roy and Gayatri Roy, both of them have been an inspiration for me.

I would like to thank my sister Dr Panchali Bandyopadhyay for her endless love and good wishes and for being the best tutor, I ever had or will have. I would like to thank my brother Debdutta Bandyopadhyay for his love and unspoken support during both good and bad times.

In 2009, I got married to Deepali Prashar, whom I have known for 6 years now. Deepali's selfless love and support has been the source of motivation and happiness during our 6 years of togetherness and my graduate studies. I have truly enjoyed discussing Chemistry with Deepali, be it at work or at home and the experience has always been enriching. I also wish to thank Deepali for conducting the surface plasmon resonance (SPR) and mammalian cell experiments with me. I wish to thank my in laws, Mr. Raj Kumar Prashar and Mrs. Rita Prashar, my brother in laws Anshul Prashar and Mansij Lal and my sister in laws Neelmani Prashar and Rajashree Bandyopadhyay for their prayers and good wishes. I truly love and adore my nephews Ojaswi, Promit and my niece Neelanshi, their very thought has always brought a smile to my face.

I would also like to thank my colleagues and friends from Luk laboratory Dr Preeti Sejwal, Dr Karen Simon, Dr Erik Burton, Dr Sri Kamesh Narasimhan, Dr Ricky Lei Wu, Dr Dawei Cui, Sijie Yang, Deepali Prashar, Nischal Singh, Gauri Shetye and Nisha Varghese for being great friends and colleagues during my stay in Luk laboratory. I would also like to thank all my friends in Syracuse, especially Abhishek Anan for making my stay in Syracuse a truly wonderful and joyous experience and Nikhilesh Dhar for helping me learn bacterial culture. I would also like to thank the wonderful office staff at the Department of Chemistry for all their help during my 5 years of stay at Syracuse University. A special thanks to Dr Deborah Kerwood for helping me with analysis of spectral data.

Last but not the least; I would like to thank God, the invisible life giving driving force that has always been there for me and guided me through all the good and bad times.

Debjyoti Bandyopadhyay

TABLE OF CONTENTS

Chapter 5

Chapter 6

LIST OF FIGURES

LIST OF SCHEMES

Chapter 7

LIST OF TABLE

Chapter 1

Chemistry and Surface Engineering using Self-Assembled Monolayers for Contolling Biofouling – *Integration of different knowledge for an interdisciplinary problem*

1.1 Overview

Biofouling due to protein adsorption,[1-2] mammalian cell adhesion[3-4] and biofilm formation,[5-6] poses a daunting problem for both industry and biomedical research. Biocompatibility is one of the most desirable characteristic of biomaterials. Often the performance of a biomaterial, prosthesis, or medical device is compromised due to biofoulings such as protein adsorption, mammalian cell adhesion and biofilm formation. One approach for controlling biofouling is to engineer surfaces that can resist the various biofouling processes.[1] The other approach is to develop structural mimics for a class of organic molecules called autoinducers secreted by bacteria, which regulate the population (quorum) sensing of bacteria.[7] These mimics can inhibit certain bacterial group behavior such as biofilm formation.[8]

Protein Adsorption and Mammalian Cell Adhesion

The surfaces of metals or metal oxides spontaneously adsorb adventitious material because the adsorbed materials decrease the free energy of the interface between the surface and the surrounding environment.[9] Hence, proteins also have a tendency to adsorb onto essentially any natural or non-natural surface. Biologically active proteins remain folded in their native conformations with their hydrophobic residues buried inside

and hydrophilic residues exposed.[10-11] Solvation is essential for maintaining the native conformation of the protein. When protein is exposed to a hydrophobic surface, it gets desolvated and denatures to facilitate hydrophobic interaction with the surface. Protein adsorption on a surface is a complicated multistep process. It involves among other processes a) reversible adsorption of the native protein, b) partial denaturation or orientation change, c) desorption of the partially denatured protein from the surface or d) complete denaturation and immobilization on the surface.[12] The process of protein adsorption on a surface is a function of solution conditions such as pH, ionic strength, co-solute concentration, temperature and the surface charge density of the protein or the surface can also vary with pH or ionic strength. It is believed that proteins have the highest tendency to adsorb onto surfaces at their isoelectric point[13] and that this tendency decreases with increasing ionic strength of the solution. Furthermore, electrostatics alone cannot speculate if a positively charged protein (protein below its isoelectric point) can adsorb onto a negatively charged surface or cannot adsorb onto a positively charged surface, since pH or ionic strength can alter the surface charge density and screen the surface charges on both the protein and the surface.

The native structure of a protein is partially lost when it adsorbs on to almost any surface. Apart from implantable prosthesis or medical devices, non-specific protein adsorption is a major challenge for developing multi-array protein assays requiring proper orientation and non-denatured protein structure in a small area.[14-15] Such arrays allow parallel read-out of information concerning protein function. Similar arrays are also being developed for peptides,[16] cells and tissues.[17]

Non-specific adsorption of serum proteins is one of the first events for the identification of an implanted biomaterial by the immune cells.[4] It is imperative to present such chemistry on the surface of a biomaterial that can minimize the level of protein adsorption and prevent adhesion of immune cells on the implant, which causes implant rejection or life threatening infections.

Biofilm formation

Biofilms are surface attached multicellular communities of bacteria and other microorganisms, found encased in a sticky polysaccharide matrix called extracellular polymeric substance (EPS).[5] The EPS is comprised of nucleic acids, proteins and polysaccharides. The EPS allows the initial attachment of the bacteria to different surfaces and protects the bacteria from environmental stress and dehydration. The composition and quantity of EPS varies depending upon the type of microorganism, age of the biofilm and the environmental conditions under which the biofilm exists, such as varying amounts of nutrients, humidity, temperature and pH.[18] The fact that biofilms can exists under a variety of environmental conditions, suggests that microorganisms are capable of responding to changes in their environment and control the composition of the EPS and adhesive abilities depending on the surface on which they attach. The attached bacterial cells in a biofilm express genes in a pattern, which is very different from their planktonic counterparts.[19] For example, biofilm bacteria unlike planktonic bacteria lack flagella or pilli needed for motility.[20] Biofilms are highly differentiated structure and have open water channels to allow exchange of nutrients.[21-22] Biofilms can form on both living and non-living surfaces and occur most commonly in natural, industrial and hospital settings.[23] Biofilms cause serious problems for public health[6, 24] and various

industries.[25] In an industrial setting, biofilms cause corrosion, product contamination, blockage in water pipelines or mechanical blockage of machine parts.[25] Biofilm formation is a complex process and is associated with five stages, which begins with attachment of the planktonic bacterial cells on the surface, microcolony formation, secretion of polysaccharides, maturation of the biofilm and eventual dispersal of the bacterial cells from the biofilm (Figure 1.1).[18] In a clinical setting, biofilms are a leading cause of infections associated with medical devices and implants, sutures and exit sites.[23, 26] For example, *P. aeruginosa* and Gram-positive cocci is associated with infected contact lenses; *E. coli* and other Gram-negative rods are associated with urinary catheter cystitis and *S. aureus* and *S. epidermis* are associated with infected mechanical heart valves.[6]

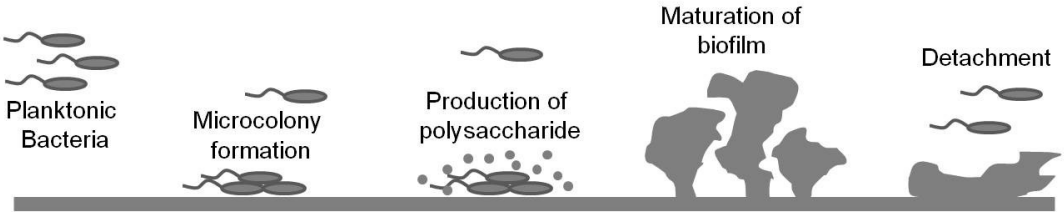

Figure 1.1 The five stages of biofilm formation on surfaces

Self-Assembled Monolayers (SAMs) as Model Substrates for Studying Biofouling

Self-assembled monolayers (SAMs) on gold films,[1, 27-29] that have well-defined and ordered structures at both molecular and topographical-level,[30-31] have provided a platform to deconvolute such a complex problem of biofouling. The present chapter primarily focuses on self-assembled monolayers (SAMs) of alkanethiols on gold (Au) and provides an introduction on SAMs as an interface for studying various chemical and biological processes. This chapter will discuss topics relevant for the reader, to

understand the studies presented in the forthcoming chapters, including methods for preparing substrates for SAMs, nature of the gold (Au)-alkanethiolate bond and structure of alkanethiolate SAMs on gold (Au). We will discuss oblique angle deposition as a means of introducing structural anisotropy in gold films,[32-33] since obliquely deposited gold films will be used as substrates for forming alkanethiolate SAMs for the studies presented in the forthcoming chapters. We will discuss surface plasmon resonance (SPR) as a method to study adsorption of proteins on the surface of gold. We will also introduce microcontact printing as a means for forming patterned SAMs of *n*-alkanethiol (pentadecanethiol) on the surface of gold. Such patterned substrates will be used to study how cell-resistant bioinert SAMs can confine adhered mammalian cells and bacterial biofilm within cell-adhesive micrometer sized patterns formed by the pentadecanethiol SAMs. Eventually, we will shift focus away from surface engineering and explore the use of designed organic molecules to control biofouling via molecular inhibition. The common theme that binds together all the chapters in this thesis is *anti-biofouling chemistry*. We utilize tools of surface engineering and molecular inhibition and describe a hypothesis driven, systematic approach for controlling the different forms of biofouling. Hence, a brief introduction about topics relevant for understanding the studies presented in subsequent chapters is desirable.

1.2 Self-Assembled Monolayers (SAMs)

Metal or metal oxide thin films and nanoparticles have wide applications in materials science and biomedical engineering. The surfaces coated with adventitious materials lack defined structure, reproducible properties or functions and hence do not have any practical applications in the field of material science and nanotechnology. Adsorption of

adventitious materials alters the interfacial properties of the surfaces of metal or metal oxide thin films and nanoparticles, without any definite control over their function. Self-assembled monolayers (SAMs) are a convenient system for tailoring the properties of surfaces of metals and metal oxides. SAMs are crystalline or semi-crystalline assemblies formed by spontaneous adsorption of molecular components from solution or gas phase onto surfaces of solids and liquids. The molecules, which form SAMs, have a "headgroup" which have specific affinity for the underlying substrate. For example, thiols, can be bound to the surfaces of copper,[34] silver,[34-35] gold,[36-39] mercury,[40] platinum[41] and palladium[42-43] and phosphonic acid can be bound to native oxide surfaces of metals or alloys such as iron,[44] steel,[45] aluminum,[45-46] copper,[45] zirconium,[46] titanium[46-47] and even mica.[48]

1.3 Substrates for Supporting Self-Assembled Monolayers (SAMs)

"Substrate" is the surface on which SAMs form. SAMs can either form on metal or metal oxide thin films supported on glass or silicon slabs or on surface of nanoparticles, nanocolloids and nanocrystals. The type of substrate used for forming SAMs depends firstly on the "headgroup" of the SAM and secondly on the intended application of the SAM. In case of biological assays involving mammalian or bacterial cells, it is preferable to use metals or metal oxides, which are nontoxic to the cells. Glass slides supporting semitransparent polycrystalline gold films are commonly used as model substrates for studying tissue-biomaterial interactions.[49] A thin film of primer or adhesive layer of titanium or chromium (1-5 nm) is deposited first on the glass slides, to improve the adhesion of metals such as gold that do not bind strongly to the surface of native oxides such as silicon dioxide or glass.[39]

The substrates for forming SAMs are prepared by physical vapor deposition (PVD) methods such as thermal or electron beam (e-beam) evaporation, electrodeposition and electroless deposition. Metal thin films deposited on glass or silicon are composed of contiguous islands or grains of metal of varying sizes (~10 to 1000 nm) and tend to have a dominant (111) texture.[34, 43, 50] The films are polycrystalline and the morphology of the grains is determined by the method of deposition.[51-52] Since small grain size minimizes the roughness in the edges of the grains, metal thins films with small grain sizes are desirable for a number of applications such as microcontact printing and etching.[39] The composition of the thin films determines the morphology of the grains. Metals with higher melting point such as palladium (1552 °C) and platinum (1772 °C) tend to have small grain sizes (~15-30 nm) but metals with lower melting point such as gold (1064 °C) tend to have larger grain sizes (~45-60 nm).[43]

1.4 Nature of the Gold (Au)-Alkanethiolate Bond

Although SAMs of alkanethiols on gold have been studied extensively, the nature of the metal-thiol bond and the arrangement of the sulfur groups on the underlying gold substrate are not well understood. Studies conducted by Dubois et al. in ultra high vacuum (UHV) suggests that there is significant degree of charge transfer to sulfur in thiolates during SAM formation.[53-54] The adsorption of dimethyl disulfide on Au (111) was found to occur dessociatively and the desorption of the disulfide was found to be an activated process, with an energy barrier close to 30 kcal/mol.[53] Studies conducted in solution phase have yielded values of activation energy which are lower (~20-25 kcal/mol),[55-56] and sometimes significantly lower (~15 kcal/mol) than values of activation energy obtained from studies in UHV.[57] Since UHV measurements do not have

interference from factors such as heats of solution of the adsorbates and heats of immersion of substrates (common in solution phase studies), homolytic Au-S bond strength is believed to be of the order of ca.-50 kcal/mol.[39] Formation of alkanethiolate likely proceeds by oxidative addition of an alkanethiol on gold, but what happens to the hydrogen of the thiol, is still intriguing.[58-60] While in vacuum, hydrogen may be lost as dihydrogen (H_2) from a thiol by reductive elimination; in solution, the liberated H_2 may oxidize to form water by dissolved molecular oxygen.[39] The formation of alkanethiolates on gold (Au) by dialkyl disulfides (equation 1) or alkanethiols (equation 2) can be described using the equations in Scheme 1.1.

Scheme 1.1

$$RS\text{-}SR + 2\,Au^{\circ} \longrightarrow 2\,(Au\,(I)^{-}SR) \qquad \text{Equation 1}$$

$$R\text{-}SH + Au^{\circ} \longrightarrow Au\,(I)^{-}SR + 1/2\,H_2 \qquad \text{Equation 2}$$

1.5 Structure of Self-Assembled Monolayers of Alkanethiolates on Gold (Au)

The SAMs of alkanethiolates on gold are pseudo crystalline assemblies, with the alkane chains having an extended all-trans conformation. An additional parameter, which is the tilt angle (α), describes the orientation of the alkane chains with respect to the surface normal. The tilt angle (α) is the angle, which the long axis of the fully extended, all-trans alkane chain makes with the surface normal (Figure 1.2A). The tilt angle (α) can be either negative (-α) or positive (+α) with respect to the surface normal. In case of alkanethiolates, α is positive and close to 30° (Figure 1.2B).[39] The formation of alkanethiolate SAMs on gold is a stepwise process, which begins with the initial

physisorption of the alkanethiols on gold followed by chemisorption or the gold-alkanethiol bond formation and finally the secondary reorganization giving an ordered SAM structure.

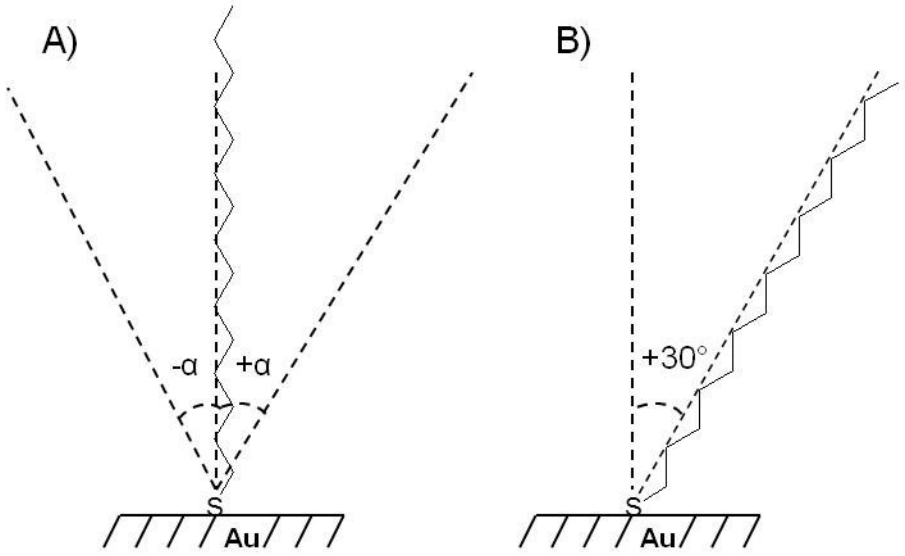

Figure 1.2 Schematic representation of (A) all-trans conformation of long chain alkanethiolates on the surface of gold, with tilt angle (α). (B) Tilt angle α ~30° in case of alkanethiolates on gold.

1.6 Introducing Structural Anisotropy in Gold (Au) Films

Gold films deposited without any preferred direction, lack structural anisotropy and are referred to as uniformly deposited films.[61-62] Uniformly deposited gold films are prepared by depositing the gold on substrates which are mounted on a planetary which makes the substrates rotate in an epicyclical motion about the vertical axis of the evaporator. The epicyclical motion is associated with a constantly varying polar angle (θ) and azimuthal angle (φ) (Figure 1.3 A). Due to the epicyclical motion of the substrates, deposition occurs without any preferred direction (Figure 1.3 B). Oblique angle deposition can

introduce structural anisotropy in gold films.[32-33] During oblique angle deposition the substrates are held stationary during the deposition and the metal vapors deposit at a measured and fixed angle (40°-60°) from the surface normal of the substrates (Figure 1.3 C).

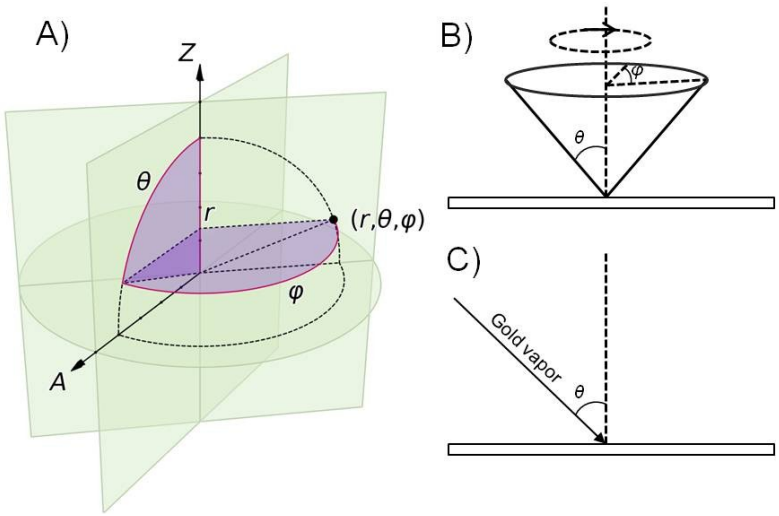

Figure 1.3 (A) A spherical coordinate system depicting the distance from the origin (r), polar angle (θ) and azimuthal angle (φ), for a point in space with the coordinates (r, θ, φ). (B) Schematic representation showing the variation of the polar angle (θ) and azimuthal angle (φ) during uniform deposition. The cone in the figure constitutes the set of all vectors representing the direction of incidence of the gold atoms. (C) Schematic representation showing the variation of the polar angle (θ), with fixed azimuthal angle (φ), during oblique deposition.

1.7 Uniform Alignment of Liquid Crystals on Anisotropic Gold (Au) Films

Abbott and co-workers showed that such obliquely deposited gold films are anisotropic and have a corrugated tin roof-like structure (Figure 1.4A). The corrugations have amplitude of 1-2 nm and wavelength ranging from 5-50 nm.[32-33] Abbott and co-workers discovered that the obliquely deposited anisotropic gold films could uniformly align liquid crystals, while preferred orientation of liquid crystals was not observed on uniformly deposited gold films.[33] The nematic liquid crystal formed by 4,4'-pentyl-cyanobiphenyl (5CB) (Figure 1.4) can have two preferred orientation on anisotropic gold films, one is azimuthal orientation, where the liquid crystal aligns parallel to the plane of the substrate and other is polar orientation, where the liquid crystal aligns perpendicular to the plane of the gold film. Abbott and co-workers discovered that liquid crystal formed 5CB has a preferred orientation on anisotropic gold films, where the azimuthal orientation of liquid crystal is perpendicular to corrugations on the surface of anisotropic gold films (Figure 1.4B).[61, 63] When the anisotropic gold films support SAMs of alkanethiols, the azimuthal orientations of the liquid crystal formed by 5CB was found to depend on the number of carbon atoms in the alkanethiols. While alkanethiols with odd number of carbons oriented the liquid crystal perpendicular to the corrugations, alkanethiols with even number of carbons oriented the liquid crystal parallel to the corrugations.[32, 61, 64-66]

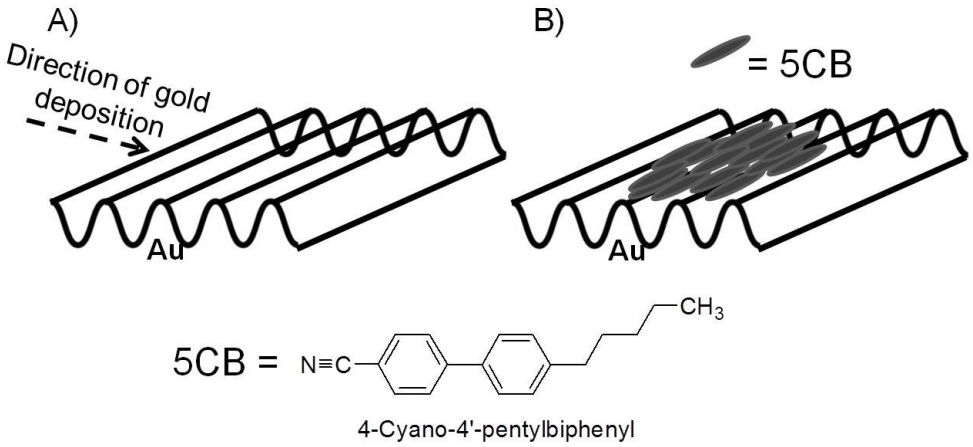

Figure 1.4 Schematic illustrations of the structure of anisotropic gold films deposited by oblique angle deposition with a corrugated tin roof-like structure (A), uniform alignment of 5CB on anisotropic gold film, where the azimuthal orientation of the liquid crystal is perpendicular to the corrugations on the surface of the gold film.

1.8 Measuring Protein Adsorption on Surface of Gold (Au) Using Surface Plasmon Resonance (SPR)

Surface plasmon resonance (SPR) is a widely used technique, to quantify the amount of protein adsorbed on the surface of gold films.[27, 67-69] SPR allows *in situ* measurement of protein adsorption in real-time and is more useful than *ex situ* techniques such as ellipsometry,[70] which require rinsing and drying of the substrates that might cause desorption of weakly adsorbed proteins. The gold films can support SAMs of alkanethiols and hence SPR is compatible with studying non-specific and specific adsorption of proteins on SAMs. Surface plasmons are surface electromagnetic waves, which propagate in a direction parallel to the metal-dielectric interface. Since the surface plasmon waves are at the interface between the metal and the external medium, these

waves are very sensitive to processes occurring at such an interface such as adsorption of molecules or biomolecules on the metal surface. In order to excite the surface plasmons one can use a light beam (visible or infrared). The incident light should be plane polarized where the electric field vector of the incident light oscillates in a plane parallel to the plane of incidence of the light. Resonance occurs when at a given wavelength (λ) and angle of incidence (θ) of the incident light, a decrease in the intensity of the reflected light is observed. The angle of minimum reflectivity (θ_m) is the angle at which the reflected light has the minimum intensity (Figure 1.5A). The angle of minimum reflectivity (θ_m) is sensitive to the refractive index of the gold-solution interface. Protein adsorption at the gold-solution interface changes the refractive index of the interface, causing a change in the angle of minimum reflectivity (θ_m). While some SPR instruments measure the change in the angle of minimum reflectivity ($\Delta\theta_m$)[67] (Figure 1.5B), others measure the change in reflectivity (ΔR), to estimate amount of adsorbed biomolecules (proteins).[68-69]

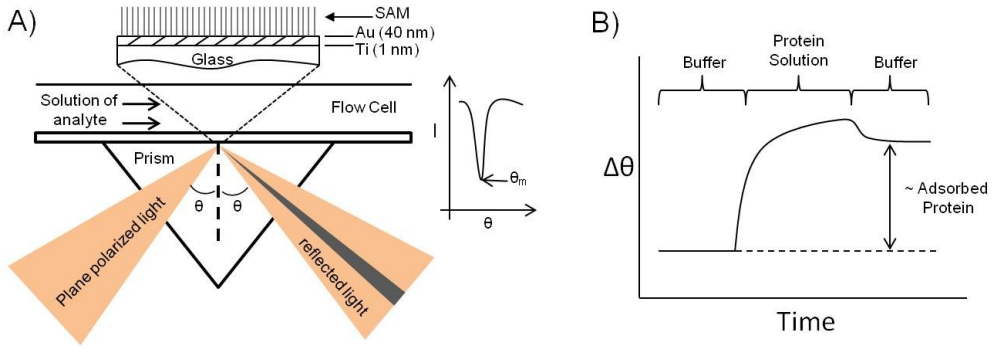

Figure 1.5 (A) Schematic diagram showing the setup of the SPR experiment, for measuring adsorption of proteins on self-assembled monolayers (SAMs) of alkanethiolate on gold. Plane polarized light is incident on the sample at an angle of incidence (θ_m), which is associated with a decrease in the intensity of the reflected light. The angle of incidence θ_m is referred to as the angle of minimum reflectivity and is a function of the refractive index of the gold-solution interface. The adsorption of proteins at the interface will cause a change in the refractive index of the interface and hence a change in the angle of minimum reflectivity. Adsorption of proteins causes a change in the angle of minimum reflectivity ($\Delta\theta = \theta_m - \theta_m°$), which is measured by the SPR instrument. (B) A typical sample trace from an SPR experiment which plots the change in the angle of minimum reflectivity ($\Delta\theta = \theta_m - \theta_m°$) versus time. Buffer is flowed in first followed by the protein solution, which is then replaced by the buffer again. The amount of protein adsorption is estimated from the difference in the $\Delta\theta$ values after and before exposing the SAMs to the protein solution. Figure adapted and modified from the work by Mrksich and co-workers.[67]

1.9 Confining Adhered Mammalian Cell and Biofilm on Patterned Self-Assembled Monolayers on Gold (Au)

Microcontact printing is a soft-lithographic technique for printing micrometer sized patterns of alkanethiols on gold.[71] The process of microcontact printing is very similar to the process of stamping ink patterns on piece of paper, the difference being that the "ink" in case of microcontact printing, is able to chemically bond with the underlying substrate and form SAMs. If needed, the patterned substrate can then be soaked in a solution of a second alkanethiol, to form a different SAM on the bare regions of the gold. The stamp used for microcontact printing is made of polydimethylsiloxane (PDMS). PDMS is the choice material for stamps used in microcontact printing because PDMS is an elastomeric material with low surface energy and hence can transfer patterns with efficiency and high fidelity.[72-73] The elastomeric nature of the PDMS stamp allows conformal contact between the stamp and the underlying substrate and is useful for molecular scale printing of SAMs. For microconatct printing, the PDMS stamp is wetted with a solution of n-alkanethiol (2 mM) in ethanol and dried under a stream of nitrogen gas, placed on the substrate to allow conformal contact for about 20 seconds and then removed carefully. The substrate is then rinsed profusely with ethanol, dried under a stream of nitrogen gas and then if needed, soaked in a solution of a second alkanethiol (Figure 1.6).[71] These substrates can allow the patterning of mammalian cell adhesion or biofilm formation when the SAMs formed by the second alkanethiol for example oligo(ethylene glycol)-terminated alkanethiol, are resistant to either mammalian cell adhesion[29, 31, 74] or bacterial biofilm formation.[75-76]

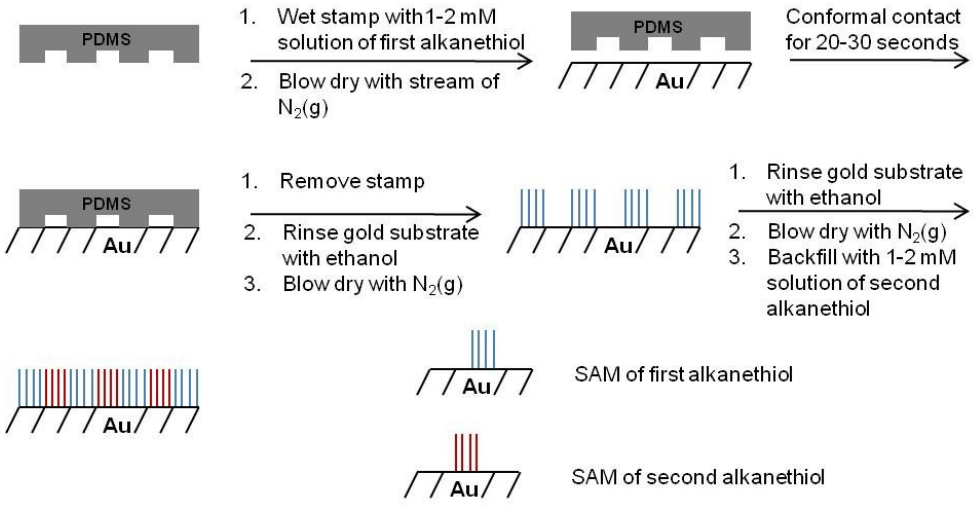

Figure 1.6 Schematic diagram showing the various steps involved in microcontact printing self-assembled monolayers (SAMs) of *n*-alkanethiols on gold.

1.10 Enhancing the Bioinertness of Bioinert Self-Assembled Monolayers on Anisotropic Gold (Au) Films

Mammalian cell adhesion on a surface is initiated by selective binding of the cell surface receptor integrin and the tripeptide Arg-Gly-Asp (RGD) presented by extra cellular matrix (ECM) proteins fibronectin and vitronectin,[77] which is the key event for initiating vital cell activities.[78] Since protein adsorption is a prerequisite for mammalian cell adhesion, a surface that can resist the adsorption of proteins, can in principle resist the adhesion of mammalian cells. Self-assembled monolayers (SAMs) presenting tri(ethylene glycol) (EG_3OH) or hexa(ethylene glycol) (EG_6OH) on gold are known to resist the adsorption of proteins, adhesion of mammalian cells, biofilm formation and are termed bioinert SAMs.[27-29, 75-76, 79] The topography of the gold films is also reported to influence the bioinert properties of EG_3OH SAMs. Luk and co-workers recently showed that EG_3OH SAMs on gold films deposited at a higher oblique angle (θ_L), are more

resistant to mammalian cell adhesion than EG_3OH SAMs on gold films deposited at a smaller oblique angle (θ_S) (Figure 1.7 B).[31] In this work, a gradient nanotopography was prepared by depositing gold on glass substrates at a fixed azimuthal direction but constantly varying polar angle (gradient gold). The regions of the gold slides deposited at a higher polar angle were associated with higher topography than the regions of the gold slide deposited at lower polar angles. Cell-adhesive patterned SAMs of 1-pentadecanethiol ($HS(CH_2)_{14}CH_3$), surrounded by cell-resistant SAMs of $HS(CH_2)_{12}(OCH_2CH_2)_3OH$ (Figure 1.7 A and B) were formed on the deposited gold film and the adhesion of Swiss 3T3 albino fibroblast was studied along the topographic gradient. Once the cells proliferated within the cell-adhesive patterns and became confluent, the higher topography regions confined the adhered mammalian cells within the cell adhesive micropatterns for 25 days, which was 4 times longer than observed on planar gold films.

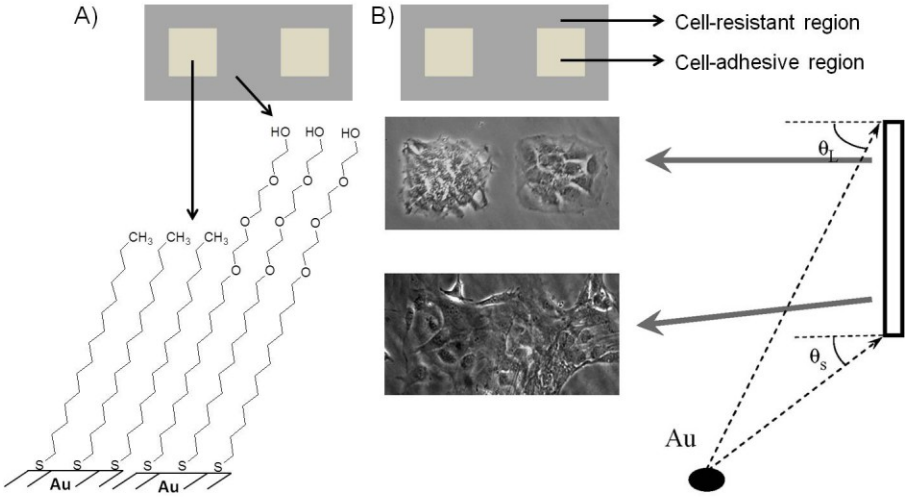

Figure 1.7 (A) Patterned SAMs of pentadecanethiol surrounded tri(ethylene glycol)-terminated alkanethiol SAMs on gold. (B) Optical micrographs showing that the mammalian cells (Swiss 3T3 albino fibroblast) are confined within the cell-adhesive microcontact printed patterns of pentadecanethiol SAMs, surrounded by cell-resistant tri(ethylene glycol)-terminated SAMs on gradient gold films. Adhered mammalian cells remained confined within the cell-adhesive micropatterns for a longer time in regions of the gold substrate deposited at large oblique angles (θ_L) than at small oblique angles (θ_S). Figure adapted and modified from the work by Luk and co-workers.[31]

Mrksich and co-workers have demonstrated that a polyol-terminated monolayer, in which the polyol has a stereochemistry of D-mannitol is comparable to tri(ethylene glycol)-terminated monolayer in its ability to resist protein adsorption. Interestingly, D-mannitol-terminated monolayers could confine mammalian cell adhesion significantly longer than tri(ethylene glycol)-terminated monolayers.[74] The D-mannitol-terminated monolayers have also been demonstrated to resist formation of bacterial biofilms

significantly longer than tri(ethylene glycol)-terminated monolayers.[76] Although protein adsorption does not strictly correlate with both mammalian cell adhesion or biofilm formation,[80-83] a surface demonstrating long term resistance to both mammalian cell adhesion and biofilm formation is on a gross scale resistant to protein adsorption.[68] Enantiomeric surfaces have been demonstrated to show different level of mammalian cell adhesion.[84-85] The polyol-terminated monolayers can be used to tailor surfaces with rich stereochemistry but there is no study to correlate the stereochemistry of the surface with the effectiveness of resisting different forms of biofouling such as protein adsorption,[2, 79] mammalian cell adhesion[4, 86] and biofilm formation.[6]

In the next three chapters, we provide a detailed study of how the stereochemistry of the surface influences the bioinertness of the surface to prevent protein adsorption (Chapter 2), mammalian cell adhesion (Chapter 3) and biofilm formation (Chapter 4). Chapter 2 reports the synthesis of enantiomerically pure alkanethiols that terminate in different stereoisomers of sugar alcohols, and the effect of chirality of these polyol-terminated self-assembled monolayers (SAMs) on resisting the adsorption of proteins such as bovine serum albumin (BSA), lysozyme and fibrinogen which is one of the stickiest proteins known. Self-assembled monolayers (SAMs) presenting a “racemic” mixture of the chiral polyol-terminated alkanethiols were found to be more resistant to protein adsorption than SAMs formed by the enantiomers alone. Note that the mixtures called "racemic" in this dissertation mean "nearly equimolar scalemic mixtures," as they are prepared by mixing the two pure enantiomers. A truly racemic mixture, as from a synthesis that produces both enantiomers, would have almost exactly equimolar amounts

of each enantiomer. Physical mixing can typically produce a mixture that is equimolar within 1-2%.

Chapter 3 and 4 presents the results on confining adhered mammalian cell (Swiss 3T3 albino fibroblasts) and bacterial (*Escherichia coli*) biofilm, respectively, within micrometer sized cell adhesive patterns of methyl-terminated SAMs, surrounded by bioinert chiral polyol-terminated SAMs. Interestingly, SAMs presenting a racemic mixture of enantiomeric alkanethiols were found to confine adhered mammalian cells or biofilm within the micrometer sized patterns longer than the SAMs presenting either enantiomer. Hence, a racemic enhancement in the bioinertness of these polyol SAMs was observed towards resisting protein adsorption, mammalian cell adhesion and biofilm formation. In addition to the racemic enhancement in bioinertness of these chiral polyol SAMs, enantiomeric and diasteriomeric polyol SAMs exhibited different ability to resist the adhesion of mammalian cells.

Chapter 5 presents the synthesis of chiral polyol-terminated alkanephosphonic acids to form SAMs on surface of native metal oxides, particularly TiO_2 and Fe_3O_4, for evaluating the ability of these alkanephosphonate SAMs on TiO_2 to resist the adhesion of mammalian cells (Swiss 3T3 albino fibroblasts) and on Fe_3O_4 to solubilize Fe_3O_4 (magnetite) nanoparticles in aqueous media.

Another approach of controlling biofouling due to biofilm formation is to develop inhibitors for a class of organic molecules called autoinducers secreted by bacteria, which are responsible for regulating bacterial group behavior such as biofilm formation. Chapter 6 reports the synthesis of derivatives of a class of molecules called brominated furanones, which are known to inhibit biofilm formation in *E. coli.* These brominated furanone

compounds are considered structural mimics of two classes of signaling molecules which are associated with quorum sensing in gram-negative bacteria such as *E. coli*. Among the two kinds of signaling molecules, one class of signaling molecules are referred to as autoinducer-1 (AI-1) or acylated homoserine lactones (AHLs) and the other class of signaling molecules are referred to as autoinducer-2 (AI-2) or borate complexes or derivatives of 4,5-dihydroxy-2,3-pentanedione.[8, 87] Chapter 7 reports the synthesis of a new library of novel squarate based molecules named squarylated homoserine lactones (SHLs),[88] which are structural mimics of the bacterial autoinducer molecules called AHLs. The synthesized brominated furanones and SHLs were found to be non-toxic to *E. coli* and were able to inhibit the biofilm formation by the bacterium.

The last chapter (Chapter 8) provides a brief literature survey and summarizes the results presented in this dissertation together with future work.

Chapter 2

Stereochemical effects and Enhancement of Resisting Biofouling Due to Protein Adsorption on Chiral Monolayers[*]

Summary

Self-assembled monolayers (SAMs) of alkanethiols on gold, presenting the sugar alcohol D-mannitol, have been reported to be more resistant to the different biofouling processes such as mammalian cell adhesion and biofilm formation, than SAMs presenting tri(ethylene glycol) (EG_3OH). While such sugar alcohols possess a rich stereochemistry, there is no study on the correlation between the chirality of the surface chemistry and the effectiveness of resisting biofouling. Here, the synthesis of enantiomerically pure alkanethiols that terminate with different stereoisomer's of sugar alcohols, and the effect of chirality of these polyol-terminated SAMs on resisting protein adsorption is reported. Interestingly, while both enantiomers of gulitol- and mannonamide-terminated monolayer resisted adsorption of proteins (bovine serum albumin, lysozyme and fibrinogen), the monolayers formed by the racemic mixture of either pair of enantiomers exhibited stronger antifouling chemistry against protein adsorption than monolayers formed by one enantiomer alone. These results are consistent with a kosmotrope theory, which suggests

[*] Reproduced in part with permission from *Anti-Fouling Chemistry of Chiral Monolayers: Enhancing Biofilm Resistance on Racemic Surface* Debjyoti Bandyopadhyay, Deepali Prashar and Yan-Yeung Luk***** *Langmuir*, **2011**, 27 (10), 6124–6131. Copyright 2011 American Chemical Society. Verbatim text in Arial font size 10 and identical figures are indicated in the legend.

that molecules that can stabilize native protein folding can also resist protein adsorption and other biofoulings.

2.1 Background and Significance

2.1.1 Strategies and theories for controlling biofouling

Adhesive interactions between a surface and biological entities, including proteins, mammalian cells and bacteria govern the fundamental science of biofouling. It is intriguing that all these processes including protein adsorption, mammalian cell adhesion (under conditions that permit proliferation), bacteria attachment and biofilm formation occur ubiquitously on many surfaces. To understand and control these biofoulings, self-assembled monolayers (SAMs) on gold films[1, 27-29] that have well-defined and ordered structures at both molecular and topographical-level[30-31] have provided a platform to deconvolute such a complex problem. While protein adsorption seems to be the most basic element of biofouling, the surface chemistry of resisting protein adsorption does not strictly correlate with the effectiveness to resist bacteria attachment and mammalian cell adhesion.[80-83] Nevertheless, the starting point for developing an anti-fouling chemistry often begins with a protein-resistant surface.

During the 90's, Whitesides and co-workers at Harvard discovered that self-assembled monolayers (SAMs) presenting oligo(ethylene glycol) (OEG) on gold, are resistant to protein adsorption.[28, 70] A number of theories have been put forth to explain the resistance of bioinert SAMs towards protein adsorption.[74, 89-97] While these surface chemistries exhibit different degree of bio-inertness, there is no single chemistry that broadly resists all biofouling processes.[80, 83] Among these knowledge and surface chemistries, a recurring class of functional groups that are resistant to protein adsorption and cell adhesion are sugars and sugar derivatives.[95,74,76] One claim that bioinert SAMs should only possess hydrogen bond acceptors and not donors[94] (example: OEG) was refuted when Mrksich and co-

workers showed that SAMs presenting D-mannitol (a sugar alcohol possessing multiple hydroxyl groups), was more resistant to mammalian cell adhesion than SAMs presenting tri(ethylene glycol) (EG_3OH).[74] It was recently shown by Ren and co-workers that SAMs presenting D-mannitol were more resistant to biofilm formation than SAMs presenting EG_3OH.[76]

2.1.2 The "kosmotrope theory"- a new basis for bioinert surfaces

Surveying among many hypothesis for bio-inert chemistries,[74, 89-97] the notion that organic molecules that can stabilize protein structure can also prevent biofouling when immobilized on surface is particularly appealing.[74, 92, 96] However, the mechanism for how certain additives stabilize protein folding whereas others destabilize folding is a still difficult subject of intense studies.[98] For example, the Hofmeister series[99] (Figure 2.1) provides two empirical collections of ions that either stabilize or destabilize protein folding, termed kosmotropes and chaotropes, respectively.

$$SO_4^{2-} > F^- > Cl^- > NO_3^- > Br^- > I^- > ClO_4^- > SCN^-$$

Figure 2.1 The ions at the right end of the series are called chaotropes and act to salt proteins into solution, while the ions on the left are called kosmotropes and act to salt proteins out of solution.

While the old studies suggested that the effect of kosmotropic ions on protein stability is due to long-range effects mediated by water solvation, recent studies show that such effects were more likely to involve direct interactions of the ions with the proteins.[100-103] However, kosmotropic organic osmolytes are believed to stabilize protein structure by exerting a long range effect on solvent water.[98] Two well-known phenomena further support this phenomenon of long-range

solvation by water. First, it is a known fact that polyols such as glycerol and sucrose stabilize protein structure.[104-106] Second, sucrose can easily form aqueous-based density gradients which do not "dissolve" into a homogenous solution, suggesting that the water molecules between the sucrose molecules have different dynamics along the density gradient.[107] For these reasons, it is believed that the multiple hydroxyl groups on the polyol SAMs such as SAMs presenting D-mannitol, can be solvated with multiple water molecules, which creates an interface that prevents protein or biological entities such as mammalian cells or bacteria from approaching or attaching to the surface. Luk et al. have very aptly represented how the polyol SAMs are able to template water structure. The multiple hydroxyl groups of the polyol moiety of these SAMs can template an interfacial water structure that can make the surface invisible to biological entities.[74, 92] In case of biofilm formation such biological entities might include the bacterial cells, secreted extracellular polymeric substance (EPS), proteins, nucleic acids and the subsequently formed biofilm. In case of mammalian cell adhesion, the biological entities might include the mammalian cells together with intracellular or extracellular proteins (Figure 2.2).

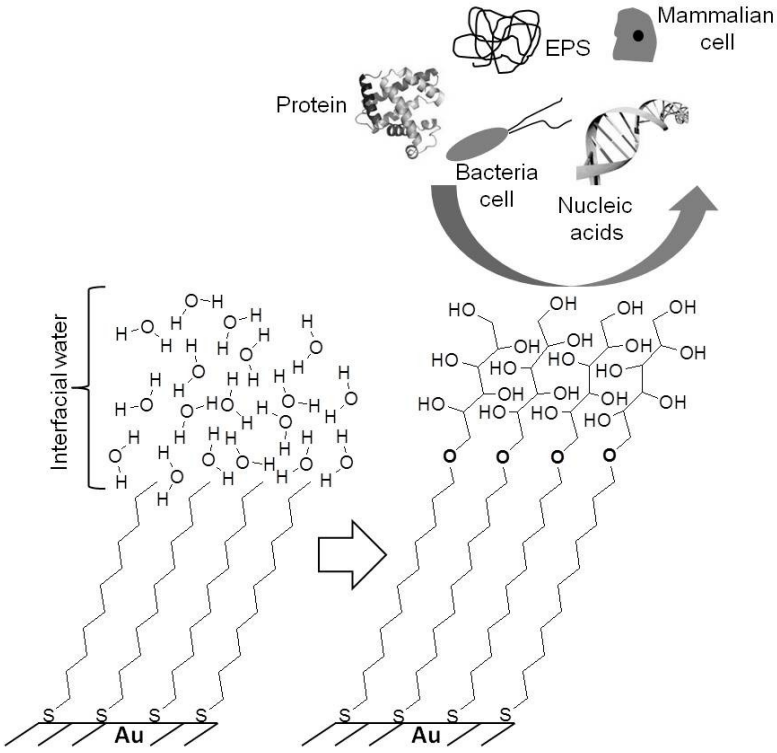

Figure 2.2 Interfacial water structure templated by polyol-terminated self-assembled monolayer (SAM) on gold. The interfacial water structure makes the surface invisible to biological entities such as bacterial and mammalian cells, extracellular polymeric substances (EPS) during biofilm formation, proteins and nucleic acids.

While these sugar alcohols possess a rich stereochemistry, there is no study on the correlation between the chirality of the surface chemistry and the effectiveness of the surface in resisting biofouling. Furthermore, biofilm formation and mammalian cell adhesion involve multiple steps and it is not clear how certain surfaces are able to resist these biofouling processes. Here, the synthesis of enantiomerically pure alkanethiols that terminate with different stereoisomer's of sugar alcohols, and the effect of chirality of these polyol-terminated SAMs on resisting protein adsorption is reported. The enhancement of anti-fouling

chemistry of these polyol-terminated SAMs, by using monolayers that consists of a racemic mixture of alkanethiols is also reported.

2.2 Results and Discussion

To examine the resistance of monolayers of chiral polyols towards protein adsorption, alditol-terminated alkanethiols (D-gulitol, **1** and L-gulitol, **1′**) and aldonamide-terminated alkanethiols (D-mannonamide, **2** and L-mannonamide, **2′**) (Scheme 2.1) were synthesized. Resistance of protein adsorption does not strictly correlate with resistance of bacterial attachment and mammalian cell adhesion.[80-83] In the extreme cases, hydrophobic surfaces may exhibit short-term resistance to mammalian cell adhesion (see Chapter 3) and bacterial cell attachment (see Chapter 4). However, protein adsorption on the hydrophobic surface can temporarily render the surface hydrated and bio-inert. Protein adsorption is intimately accompanied with, and sometimes a prerequisite for,[27, 78] cell adhesion. Hence, surface plasmon resonance (SPR)[27] was utilized to examine protein adsorption and resistance towards protein adsorption of SAMs presenting D-gulitol (**1**), L-gulitol (**1′**), D-mannonamide (**2**), L-mannonamide (**2′**), racemic mixture of the enantiomers and were compared to SAMs presenting methyl groups.

Scheme 2.1

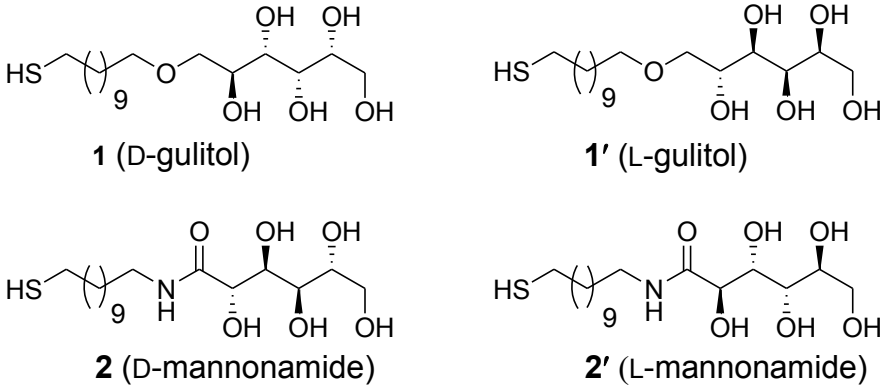

Surface plasmon resonance (SPR)[27, 74] was used to measure the adsorption of protein (bovine serum albumin, fibrinogen and lysozyme) on SAMs formed by $CH_3(CH_2)_{14}SH$, D-gulitol-terminated alkanethiol (**1**), L-gulitol-terminated alkanethiol (**1′**), or the racemic mixture of the two enantiomers (**1** and **1′**). Figure 2.3 shows the data for the adsorption of bovine serum albumin (BSA) on the four SAMs formed on a SPR array chip. Phosphate buffered saline (1× PBS, pH 7.42) was first introduced to the SAMs for 7 min, and then followed by the PBS containing BSA (0.5 mg/mL) for 8 min. Pure PBS was introduced again to observe the amount of adsorbed protein. The amount of protein, which adsorbed irreversibly on the SAMs was calculated from the difference in the SPR intensity measured from the difference of pixel intensity units (ΔPIU) before and after the SAMs were exposed to the protein solution. The percentage of the monolayer covered by the adsorbed proteins (%ML) was compared to the amount of protein adsorbed on methyl-terminated SAMs, and was estimated by the equation %ML = $(\Delta PIU_{gulitol}/\Delta PIU_{methyl})\times 100$.[91, 95] Self-assembled monolayers (SAMs) presenting D-gulitol and L-gulitol were found to be bioinert, supporting about 4.26 ± 0.74% and 9.57 ± 2.53% monolayer (%ML) respectively of the protein adsorbed on methyl-terminated SAMs. Interestingly, SAMs presenting the racemic mixture of the two enantiomers exhibited little protein adsorption (maximum %ML ≤ 0.66), that was within the noise of the SPR signals.

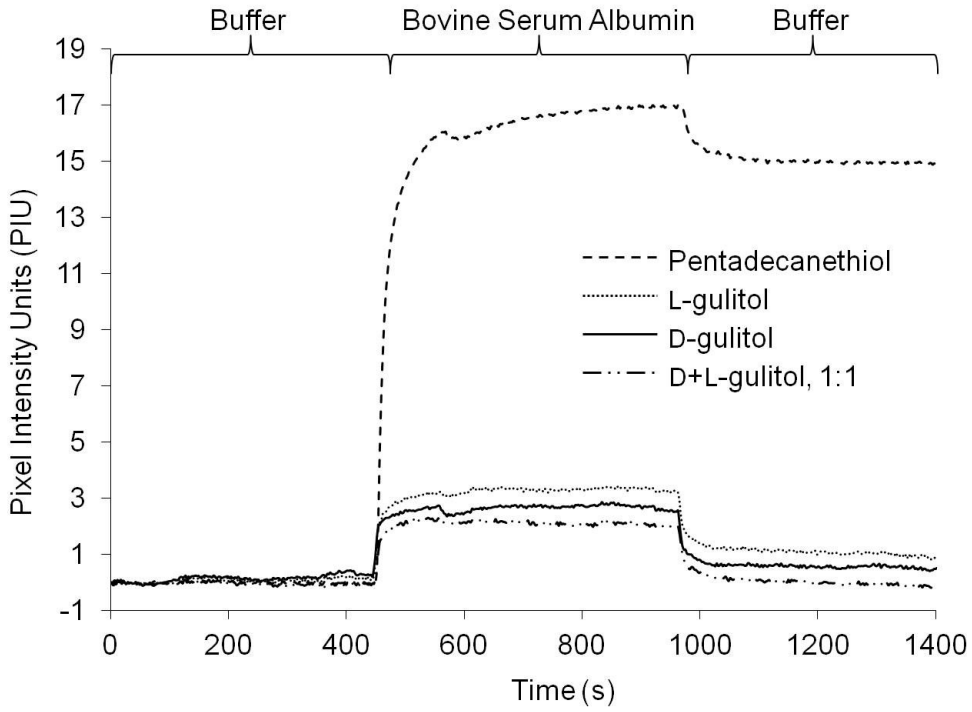

Figure 2.3 Intensity of surface plasmon resonance (SPR) for adsorption of bovine serum albumin (0.5 mg/mL in 1× PBS, pH 7.42) over time on four SAMs presenting methyl groups, D-gulitol; L-gulitol; or a racemic mixture of D- and L-gulitol-terminated alkanethiols. Figure adapted from the work by Luk and co-workers.[68]

Similar results were obtained for fibrinogen and lysozyme (Figure 2.4). Particularly, the monolayers of racemic polyols were highly effective at resisting fibrinogen (m.w. 340 kDa), one of the most sticky proteins, whereas the monolayers of enantiomeric polyols were not as effective at resisting fibrinogen (Figure 2.4).

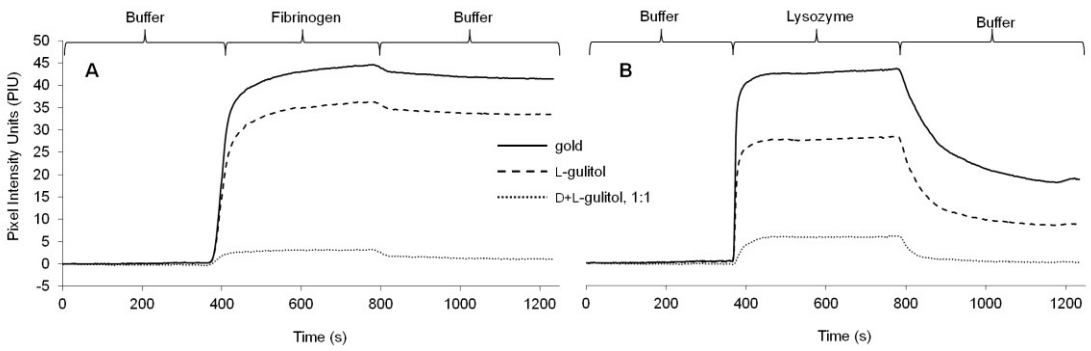

Figure 2.4 Intensity of surface plasmon resonance (SPR) for adsorption of (**A**) Fibrinogen (0.5 mg/mL in 1× PBS, pH 7.42) and (**B**) Lysozyme (0.5 mg/mL in 1× PBS, pH 7.42), over time on bare gold and two SAMs presenting L-gulitol and racemic mixture of D- and L-gulitol-terminated alkanethiols. Figure adapted from the work by Luk and co-workers.[68]

Figure 2.5 shows the data for adsorption of bovine serum albumin (BSA) on SAMs formed by $CH_3(CH_2)_{14}SH$, D-mannonamide-terminated alkanethiol (**2**), L-mannonamide-terminated alkanethiol (**2′**), or the racemic mixture of the two enantiomers (**2** and **2′**) on a SPR array chip (16 spots per chip). Buffer (1× PBS, pH 7.42) was first introduced to the SAMs, followed by PBS containing BSA (0.5 mg/mL). Pure PBS was introduced again to observe the irreversibly adsorbed protein on SAMs. The percentage of the monolayer covered by the adsorbed proteins (%ML) was compared to the amount of protein adsorbed on the methyl-terminated SAMs, and was estimated by $\%ML = (\Delta PIU_{mannonamide}/\Delta PIU_{methyl})\times 100$, for which ΔPIU is the difference in the pixel intensity units before and after the surface were exposed to the protein solution.[91, 95]

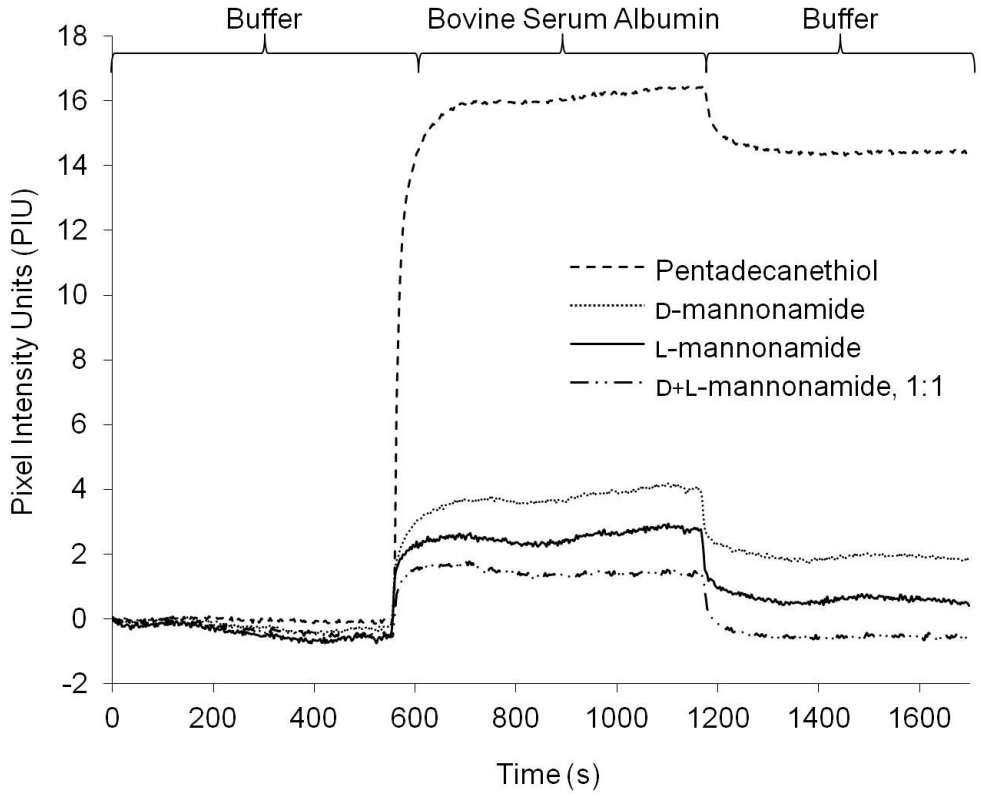

Figure 2.5 Intensity of surface plasmon resonance (SPR) for adsorption of bovine serum albumin (0.5 mg/mL in 1× PBS, pH 7.42) over time on four SAMs presenting methyl groups, D-mannonamide; L-mannonamide; or a racemic mixture of D- and L-mannonamide alkanethiols. Figure adapated from the work by Luk and co-workers[†]

Self-assembled monolayers (SAMs) presenting D-mannonamide and L-mannonamide were both protein-resistant, supporting about 21.18 ± 7.13% and 6.95 ± 0.71% of monolayer (%ML), respectively. Interestingly, SAMs presenting the racemic mixture of the two enantiomers again exhibited little protein adsorption (%ML= 1.11 ± 0.42) that was within the

[†] *Stereochemical Effects of Chiral Monolayers on Enhancing the Resistance to Mammalian Cell Adhesion* Debjyoti Bandyopadhyay, Deepali Prashar and Yan-Yeung Luk* *Chem. Commun.*, **2011**, 47, 6165-6167-Reproduced in part by permission of The Royal Society of Chemistry. Verbatim text in Arial font size 10 and identical figures are indicated in the legend.

noise of the SPR signals.

Collectively, these result suggests that SAMs presenting racemic mixture of enantiomeric alkanethiols is likely more resistant to protein adsorption than SAMs presenting either of the enantiomers.

2.3 Conclusions

The results on resisting protein adsorption indicate that chiral polyol-terminated SAMs have different ability to resist the adsorption of proteins. While, D-gulitol SAMs were slightly more resistant to protein adsorption than the L-gulitol SAMs, the D-mannonamide SAMs were comparatively less resistant to protein adsorption than the L-mannonamide SAMs. But for both gulitol and mannonamide SAMs, the SAMs presenting the racemic mixture of the alkanethiols were more resistant to protein adsorption than the SAMs presenting the ennantiomers alone. Collectively, the results presented here suggest that SAMs presenting racemic mixture of enantiomeric alkanethiols is more resistant to protein adsorption than SAMs presenting either enantiomer. Considering that the racemic and enantiomeric SAMs have the same chemical composition, the major difference in the ability of these two surfaces to resist the adsorption of proteins likely resides in the water solvation at the interface.[97, 108-111] This observation opens new explorations for studying surface-biologic interactions.

2.4 Experimental Section

Chemicals. 1-Pentadecanethiol and chemicals used for synthesizing all other alkanethiols were purchased from Aldrich Chemicals (Milwaukee, WI) and used as received. Ethanol was used as a solvent for preparing all alkanethiol solutions and for washing SAMs on gold films. Minimum amount of DMSO was mixed with ethanol for solubilizing polyol-terminated alkanethiols, which were poorly soluble in pure ethanol. Bovine serum albumin, lysozyme and fibrinogen were

purchased from Sigma-Aldrich (St. Louis, MO). Phosphate buffered saline, 1× PBS (2.7 mM potassium chloride, 137 mM sodium chloride, 8 mM sodium phosphate dibasic, 1.48 mM potassium phosphate monobasic, pH 7.42) was prepared by dissolving 5 PBS tablets (SIGMA, Allentown, PA) in 1000 mL of deionized water with a resistivity of 18 MΩ cm (Millipore, Billerica, MA).

General Information for Synthesis of Alkanethiols. The processes involving reactants sensitive to moisture or air were carried out under an atmosphere of argon using oven-dried glassware. Reagents and solvents were reagent grade and used as supplied unless otherwise mentioned. THF was distilled from sodium benzophenone. Solvents were removed under reduced pressure using rotary evaporator below 40 ºC. Silica Gel 60 F_{254} precoated plates (0.25-mm thickness, EMD) were used for TLC and a solution of phosphomolybdic acid/ceric sulfate/sulfuric acid (10g : 1.25 g : 8% 250 mL), followed by charring at ~ 150 ºC, was used for visualization. Flash column chromatography was performed using SILICYCLE, Silica-P Flash Silica Gel with 40-63μ mesh size. NMR spectra (^{1}H, ^{13}C) were recorded on 300 MHz Bruker instrument. ^{1}H chemical shifts are reported in ppm relative to $CDCl_3$ δ 7.26 and DMSO-d_6 δ 2.50. ^{13}C chemical shifts are reported relative to $CDCl_3$ δ 77.23 and DMSO-d_6 δ 39.51. High Resolution Mass Spectra (HRMS) was recorded by positive ion electrospray on a Bruker 12 Tesla APEX – Qe FTICR-MS with Apollo II ion source.

Synthesis of chiral alditol-terminated alkanethiols. The synthesis of D-gulitol-terminated alkanethiol, **1** is shown in Scheme 2.2. Briefly, **1a** was synthesized from D-gulono-1,4-lactone using literature reported procedures.[112] Nucleophilic displacement with 11-bromo-1-undecene afforded the alkene **1b.** Reaction of **1b** with thiolacetic acid using catalytic amount of azobisisobutyronitrile (AIBN) under UV irradiation afforded the thio ester **1c.** Hydrolysis of **1c** in methanolic HCl afforded alkanethiol **1**. L-Gulitol-terminated alkanethiol, **1′** was synthesized similarly. Synthesis for **2** and **2′** is described in Scheme 2.3.

Scheme 2.2

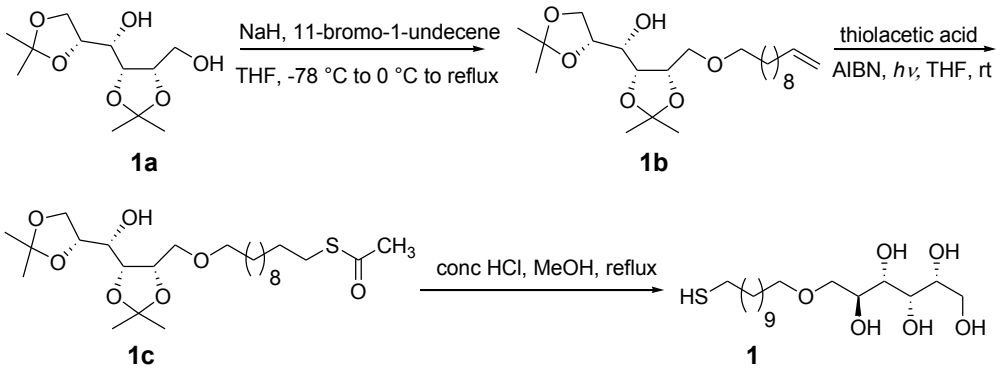

Synthesis of Compound, 1b. Compound **1a**[112] (0.252 g, 0.962 mmol) was dissolved in THF (15 mL). The solution was cooled to -78 ºC and charged with NaH (0.077 g, 60% by wt in mineral oil, 0.783 mmol). The mixture was warmed up to 0 °C and allowed to stir at 0 °C for 60 min. 11-bromo-1-undecene (0.42 mL, 1.923 mmol) was added to the reaction mixture at 0 °C and the reaction was warmed up to ambient temperature subsequently. The reaction mixture was stirred at ambient temperature for 20 min and then refluxed for 48 h. The reaction mixture was cooled down, quenched with brine and extracted with EtOAc. The organic phase was dried over anhydrous Na_2SO_4 and the crude product was obtained as yellow oil after evaporation of solvent. The crude product was purified using flash silica gel column (10% EtOAc in Hexanes) to obtain **1b** (0.132 g, 46 %, calculated from recovered **1a**) as colorless oil after evaporation of solvents. R_f = 0.62, (30% EtOAc in Hexanes). ^{1}H NMR (300 MHz, $CDCl_3$): δ 5.88-5.75 (m,1H), 5.03-4.91 (m, 2H), 4.35-4.24 (m, 2H), 4.13-4.03 (m, 2H), 3.85 (t, J_{H-H} = 8.0 Hz, 1H), 3.75-3.69 (m, 2H), 3.61 (dd, J_{H-H} = 10.1 Hz, 4.6 Hz, 1H), 3.53-3.41 (m, 2H), 2.95 (d, 1H, J_{H-H} = 6.4 Hz), 2.07-2.00 (m, 2H), 1.59-1.53 (m, 2H), 1.51 (s, 3H), 1.46 (s, 3H), 1.39 (s, 3H),1.37 (s, 3H), 1.28 (br s, 12H). ^{13}C NMR (75 MHz, $CDCl_3$): δ 139.4, 114.3, 109.7, 108.9, 77.0, 76.8, 75.9, 72.1, 69.8, 69.4, 66.2, 33.9, 29.7, 29.6, 29.3, 29.1, 27.2, 26.7, 26.2, 25.5, 25.3. HRMS: found = 437.2864 $[M+Na]^+$, calcd for $[C_{23}H_{42}O_6+ Na]^+$ 437.2873.

Synthesis of Compound, 1c. Recrystallized azobisisobutyronitrile (AIBN) (20 mg) and thiolacetic acid (0.11 mL, 1.493 mmol) were added to a solution of compound **1b** (0.155 g, 0.373

mmol) in anhydrous THF (5.0 mL). The reaction mixture was stirred under UV source for 18 h. The solvent was removed under vacuum to yield the crude product as yellow oil. The crude product was purified using flash silica gel column (10% EtOAc in Hexanes) to obtain **1c** (0.109g, 60%) as a yellow oil after evaporation of solvent. R_f **=** 0.73, (30% EtOAc in Hexanes). ^{1}H NMR (300 MHz, $CDCl_3$): δ 4.35-4.24 (m, 2H), 4.13-4.03 (m, 2H), 3.85 (t, 1H, J_{H-H} = 7.94 Hz), 3.75-3.70 (m, 2H), 3.61 (dd, J_{H-H} = 10.15 Hz, 4.64 Hz, 1H), 3.53-3.41 (m, 2H), 2.94 (d, J_{H-H} = 6.31 Hz, 1H), 2.87 (t, J_{H-H} = 7.38 Hz, 2H), 2.33 (s, 3H), 1.61-1.54 (m, 4H), 1.51 (s, 3H), 1.46 (s, 3H), 1.34 (s, 3H), 1.26 (br s, 14H). ^{13}C NMR (75 MHz, $CDCl_3$): δ 196.2, 109.7, 108.9, 77.0, 75.9, 72.2, 69.8, 69.4, 66.2, 30.8, 29.7, 29.6, 29.3, 29.2, 28.9, 27.2, 26.7, 26.2, 25.6, 25.3. HRMS: found = 513.2847 $[M+Na]^+$, calcd for $[C_{25}H_{46}O_7S+ Na]^+$ 513.2856.

Synthesis of Compound, 1. Compound **1c** (0.064 g, 0.131 mmol) was dissolved in MeOH (5 mL). The solution was degassed by bubbling argon for 10 min. Concentrated HCl (37%, 0.5 mL) was added to this solution and the mixture was refluxed for 2 h. The solvent was evaporated and **1** (0.047g, 97%) was obtained as a white solid after drying under vacuum. ^{1}H NMR (300 MHz, DMSO-d_6): δ 4.53-4.34 (br m, 4H), 4.06 (br s, 1H), 3.66-3.27 (m, 10H), 2.44 (q, J_{H-H} = 7.31 Hz, 2H), 2.19 (t, 7.56 Hz, 1H), 1.53-1.45 (br m, 4H), 1.24 (br s, 14H). ^{13}C NMR (75 MHz, DMSO-d_6): δ 73.6, 72.8, 72.2, 70.5, 69.8, 68.6, 62.5, 33.4, 29.3, 29.0, 28.9, 28.5, 27.7, 25.6, 23.7. HRMS: found = 391.2137 $[M+Na]^+$, calcd for $[C_{17}H_{36}O_6S+ Na]^+$ 391.2124.

Scheme 2.3

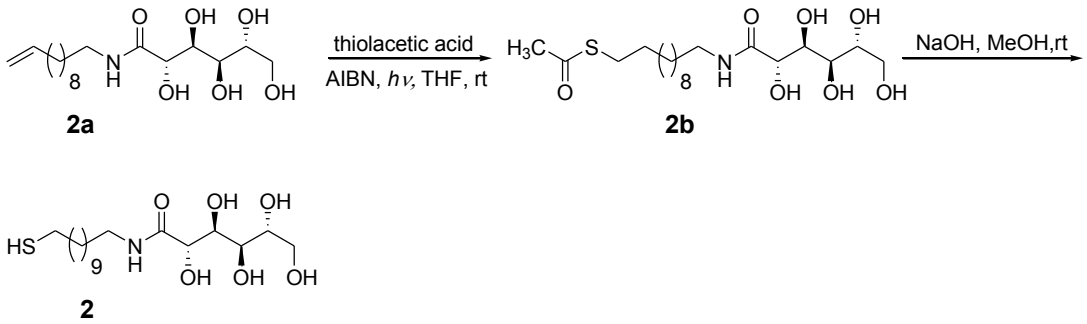

Synthesis of Compound, 2b. Compound **2a** (0.050 g, 0.144 mmol) was suspended in THF (6 mL) and to it was added thiolacetic acid (0.04 mL, 0.576 mmol) and recrystallized AIBN (10 mg).

The vessel was evacuated and purged with argon. The reaction mixture was stirred under U.V source at rt for 12 h. Silica gel slurry was prepared of the crude material and loaded onto a silica gel column (DCM → 1% DCM in MeOH → 10% DCM in MeOH). The pure compound **2b** (0.0351 g, 58%) was obtained as a white solid after evaporation of solvent. ^{1}H NMR (300 MHz, DMSO-d_6): δ 7.89-7.85 (t, J_{H-H} = 6.04 Hz, 1H), 5.47 (d, J_{H-H} = 6.32 Hz, 1H), 4.50-4.43 (m, 4H), 4.28 (t, J_{H-H} = 5.79 Hz, 1H), 3.86 (t, J_{H-H} = 13.78 Hz, 1H), 3.75 (t, J_{H-H} = 12.73 Hz, 1H), 3.62-3.56 (m, 1H), 3.44-3.43 (m, 2H), 3.10-3.02 (m, 2H), 2.80 (t, J_{H-H} = 7.12 Hz, 2H), 2.30 (s, 3H), 1.50-1.39 (m, 4H), 1.22 (br s, 14H).^{13}C NMR (75 MHz, DMSO-d_6): δ 195.4, 173.6, 71.9, 70.9, 70.5, 70.3, 63.8, 55.3, 30.6, 29.1, 29.09, 29.01, 28.97, 28.9, 28.8, 28.5, 28.3, 28.1, 26.4. HRMS: found = 446.2182 $[M + Na]^+$, calcd for $[C_{19}H_{37}NO_7S + Na]^+$ 446.2183.

Synthesis of Compound, 2. Compound **2b** (0.011 g, 0.029 mmol) was suspended in 29.8 μL of 1 N NaOH prepared in methanol. The mixture was stirred under argon at rt for 1 h and then neutralized by adding 29.8 μL of 1 N HCl prepared in methanol. The solvent was evaporated and the crude residue washed with cold methanol to obtain the desired compound **2** (0.007 g, 59%) as a white solid. ^{1}H NMR (300 MHz, DMSO-d_6): δ 7.87 (br s, 1H), 5.47 (br s, 1H), 4.47-4.28 (br m, 4H), 3.86-3.43 (br m, 7H), 3.06 (br s, 2H), 1.62-1.23 (br s, 18H). ^{13}C NMR (75 MHz, DMSO-d_6): δ 173.2, 73.3, 72.9, 71.8, 69.5, 62.5, 38.3, 29.1, 28.8, 28.6, 28.5, 27.7, 26.4. HRMS: found = 404.2076 $[M + Na]^+$, calcd for $[C_{17}H_{35}NO_6S + Na]^+$ 404.2077.

Compound **2′** was synthesized using procedures similar to those used for the synthesis compound **2**.

Surface Plasmon Resonance. All surface plasmon resonance (SPR) experiments were performed on a SPRimagerII Array System (GWC Technologies, Madison, WI). Solutions of the alkanethiols (1 μL) and solutions containing 1:1 mixture of the enantiomers **1** and **1′** or **2** and **2′** (1 μL) were spotted with a micropipette on SpotReady 16 chips (GWC Technologies, Madison, WI). The chips were placed in a tightly covered Petri dish, containing swabs of Kimwipes saturated with ethanol to prevent evaporation of ethanol from the spotted solutions. After 15 h the chips

were rinsed with ethanol and blow dried with a stream of nitrogen gas. The chips were then given a final rinse with water, gently blow dried with a stream of nitrogen gas and mounted in a standard flow cell (GWC Technologies, Madison, WI) for the SPR experiment. Phosphate buffered saline, 1× PBS (2.7 mM potassium chloride, 137 mM sodium chloride, 8 mM sodium phosphate dibasic, 1.48 mM potassium phosphate monobasic, pH 7.42) was used as buffer and for preparing the protein solutions. The protein solutions were filtered through a 0.25-μm filter before use. The percentage of the monolayer covered by the adsorbed proteins (%ML) was compared to the amount of protein adsorbed on methyl-terminated SAMs, and was estimated by the equation $\%ML = (\Delta PIU_{gulitol\ or\ mannonamide}/\Delta PIU_{methyl})\times 100$ and the standard deviation in the %ML was determined over three replicates

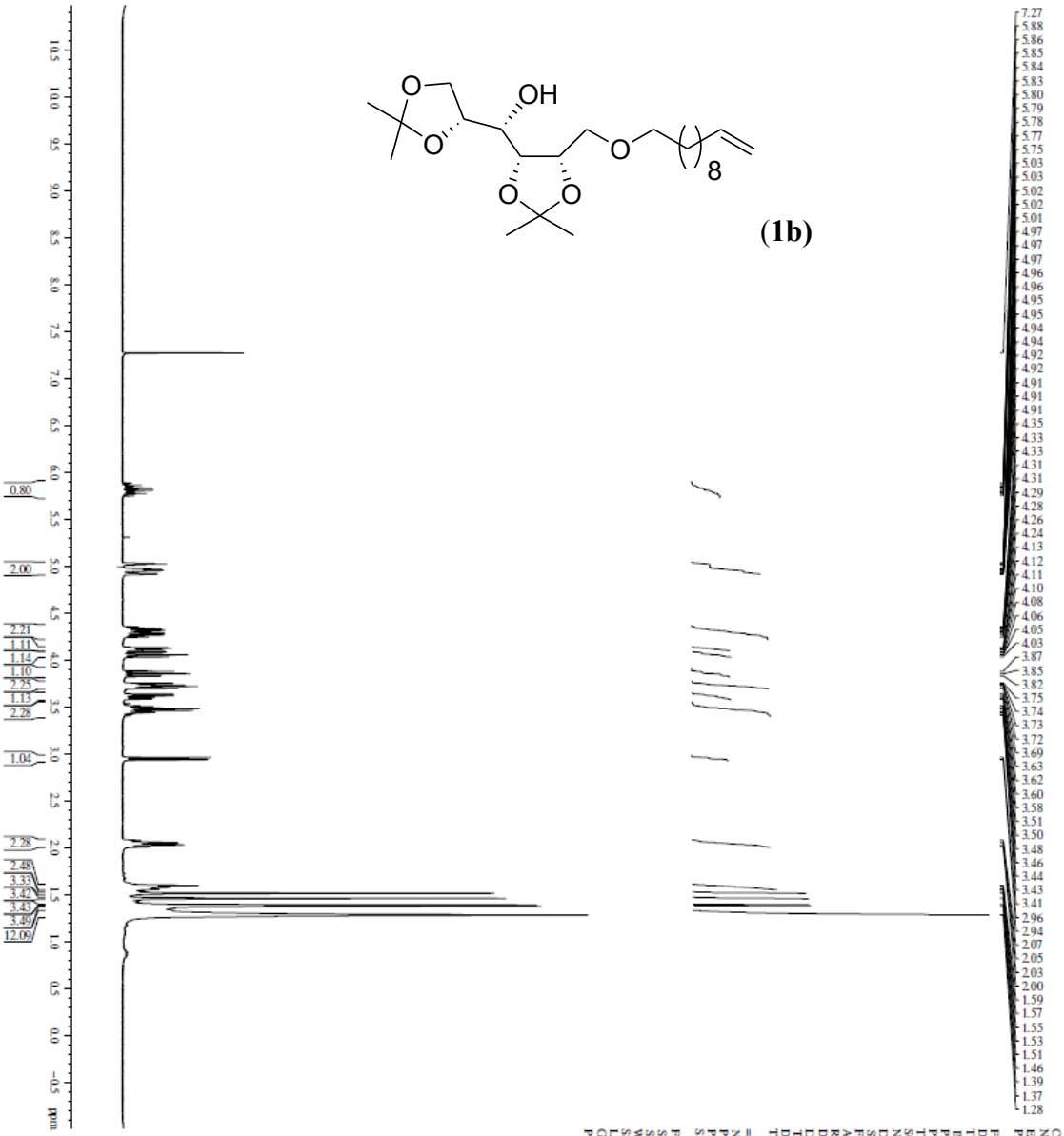
OH
O
O
O
O
O
8
(1b)
Current Data Parameters
NAME DB 3-47 HNMR
EXPNO 1
PROCNO 1
F2 - Acquisition Parameters
Date_ 20081105
Time 11.10
INSTRUM spect
PROBHD 5 mm QNP 1H1
PULPROG zg
TD 32768
SOLVENT CDCl3
NS 16
DS 0
SWH 3591.954 Hz
FIDRES 0.109618 Hz
AQ 4.56133556 sec
RG 322.5
DW 139.200 usec
DE 54.00 usec
TE 299.2 K
D1 1.00000000 sec
TD0 1
====== CHANNEL f1 ======
NUC1 1H
P1 9.75 usec
PL1 0.00 dB
SFO1 300.1315007 MHz
F2 - Processing parameters
SI 32768
SF 300.1300039 MHz
WDW no
SSB 0
LB 0.00 Hz
GB 0
PC 1.00
0.80
2.00
2.21
1.11
1.14
1.10
2.25
1.13
2.28
1.04
2.28
2.48
3.33
3.41
3.42
3.43
3.49
12.09
ppm

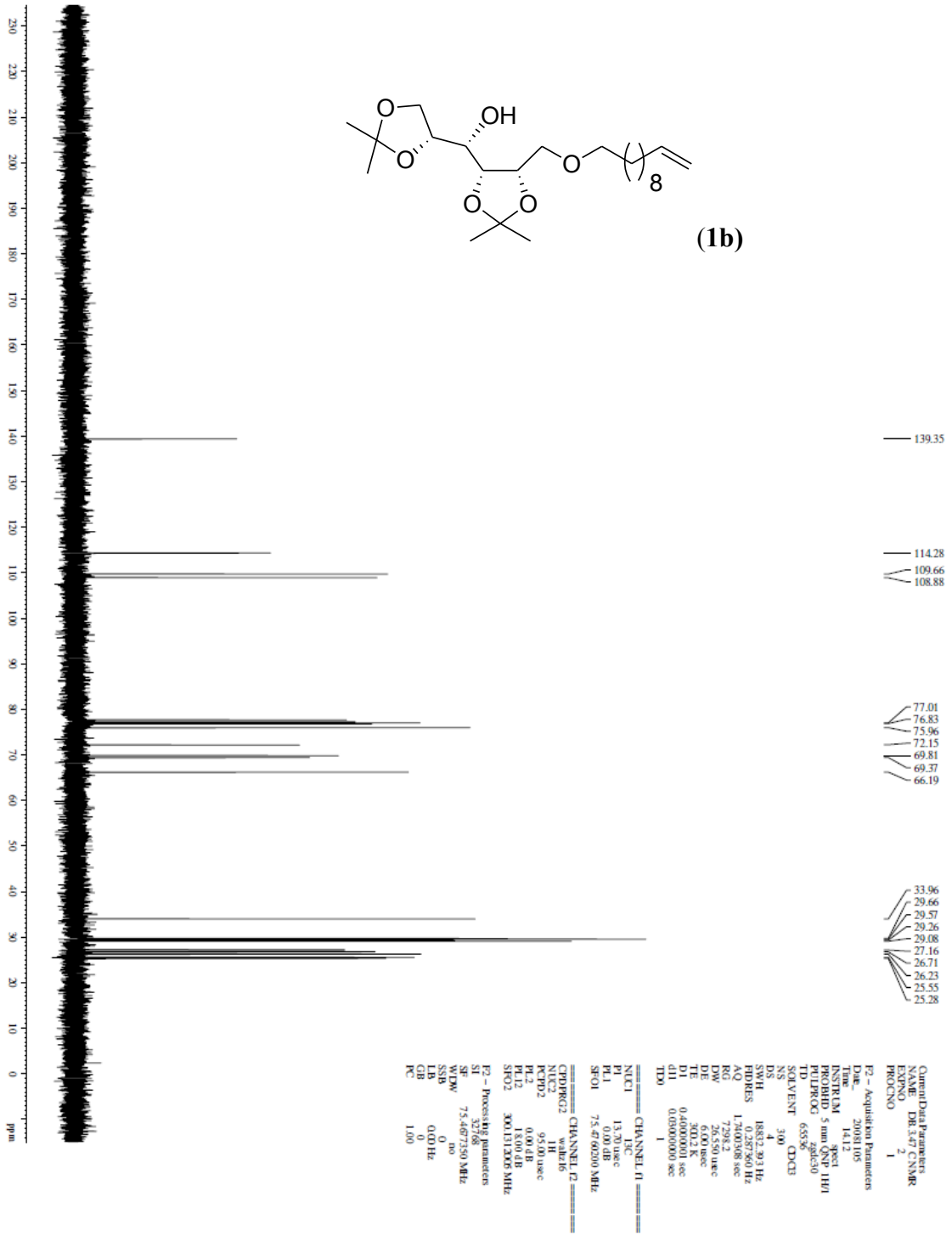
OH
O
O
O
O
O
8
(1b)
139.35
114.28
109.66
108.88
77.01
76.83
75.96
72.15
69.81
69.37
66.19
33.96
29.66
29.57
29.26
29.08
27.16
26.71
26.23
25.55
25.28
ppm

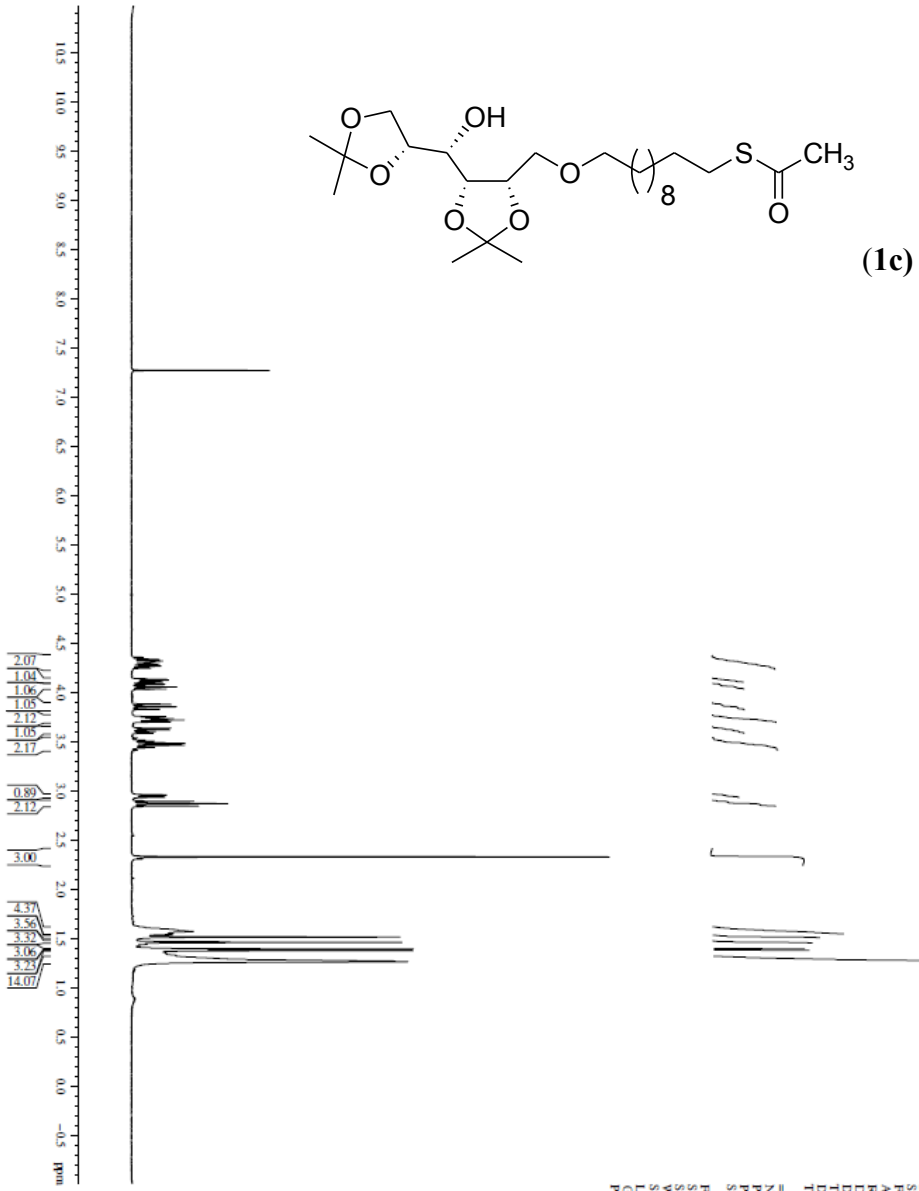
OH
O
O
O
O
O
8
S
CH3
O
(1c)
7.27
4.35
4.34
4.33
4.31
4.31
4.29
4.28
4.26
4.26
4.24
4.13
4.12
4.11
4.10
4.08
4.06
4.05
4.03
3.88
3.85
3.82
3.75
3.74
3.73
3.72
3.70
3.63
3.62
3.60
3.58
3.53
3.51
3.50
3.48
3.46
3.44
3.43
3.41
2.95
2.93
2.89
2.87
2.84
2.33
1.61
1.59
1.57
1.54
1.51
1.46
1.39
1.37
1.26
2.07
1.04
1.06
1.05
2.12
1.05
2.17
0.89
2.12
3.00
4.37
3.56
3.32
3.06
3.23
14.07
ppm
Current Data Parameters
NAME DR 3.49 H NMR
EXPNO 1
PROCNO 1
F2 - Acquisition Parameters
Date_ 20081112
Time 10.32
INSTRUM spect
PROBHD 5 mm QNP 1H/1
PULPROG zg
TD 32768
SOLVENT CDCl3
NS 16
DS 0
SWH 3591.954 Hz
FIDRES 0.109618 Hz
AQ 4.561556 sec
RG 256
DW 139.200 usec
DE 54.00 usec
TE 300.2 K
D1 1.00000000 sec
TD0 1
======== CHANNEL f1 ========
NUC1 1H
P1 9.75 usec
PL1 0.00 dB
SFO1 300.1315007 MHz
F2 - Processing parameters
SI 32768
SF 300.1300039 MHz
WDW no
SSB 0
LB 0.00 Hz
GB 0
PC 1.00

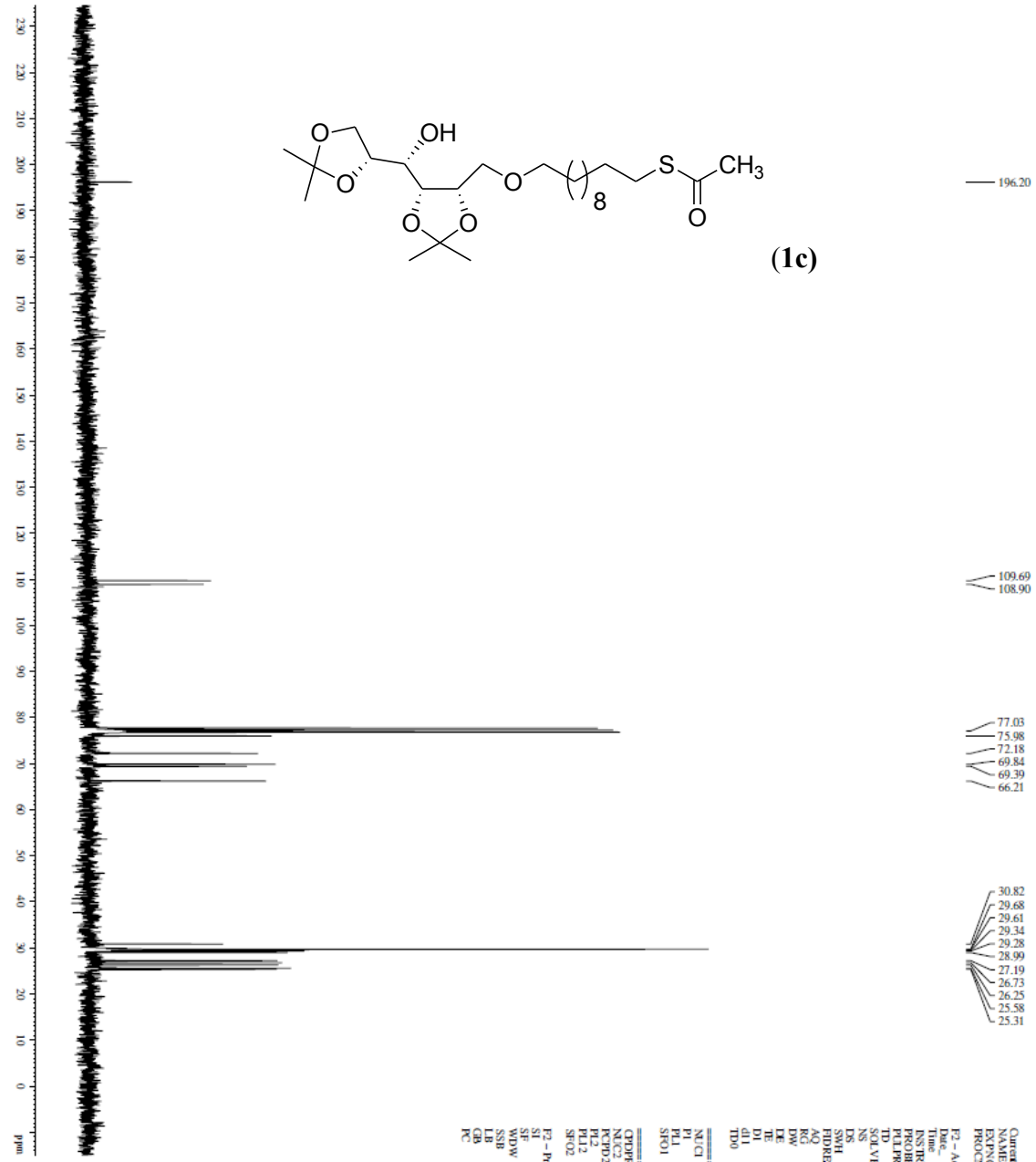
OH
O
O
O
O
O
8
S
CH3
O
(1c)
196.20
109.69
108.90
77.03
75.98
72.18
69.84
69.39
66.21
30.82
29.68
29.61
29.34
29.28
28.99
27.19
26.73
26.25
25.58
25.31
ppm

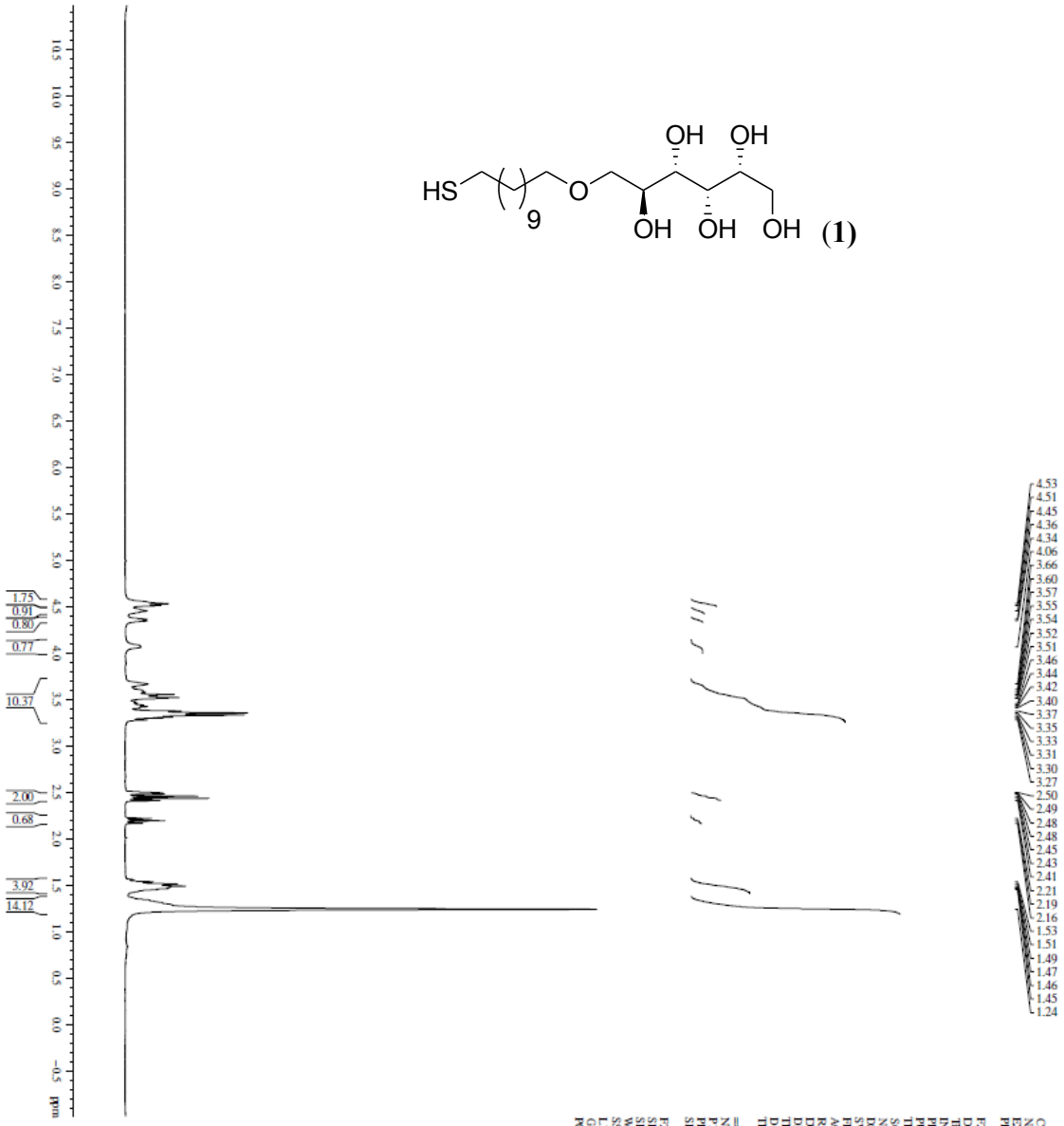
HS
9
O
OH
OH
OH
OH
OH
(1)
1.75
0.91
0.80
0.77
10.37
2.00
0.68
3.92
14.12
ppm

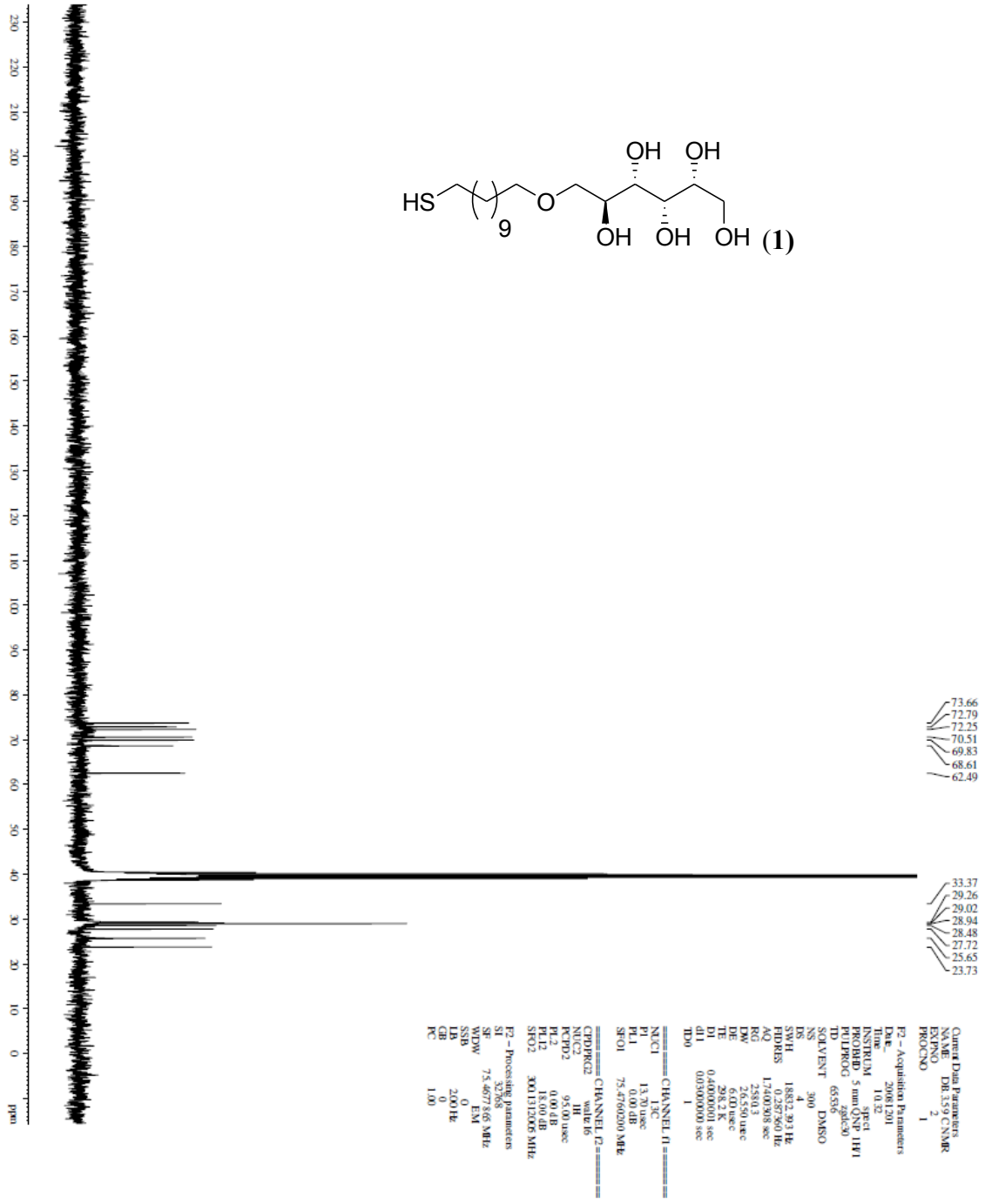
HS
9
O
OH
OH
OH
OH
OH
(1)
73.66
72.79
72.25
70.51
69.83
68.61
62.49
33.37
29.26
29.02
28.94
28.48
27.72
25.65
23.73
ppm

Chapter 3

Stereochemical Effects and Enhancement of Resisting Mammalian Cell Adhesion on Chiral Monolayers[‡]

Summary

Among different bioinert surfaces, sugar and sugar derivatized self-assembled monolayers (SAMs) have been shown to be highly effective in resisting all aspects of biofouling such as protein adsorption, mammalian cell adhesion and biofilm formation. The rich stereochemistry of sugar derivatives and the mechanism of their antifouling chemistry remain relatively unexplored. This section of the dissertation describes chiral effects observed during mammalian cell adhesion on chiral monolayers of polyol-terminated alkanethiols surrounding micrometer sized patterned monolayers of methyl-terminated alkanethiols on gold. This work demonstrates that the resistance of mammalian cell (Swiss 3T3 albino fibroblasts) adhesion is different on monolayers of enantiomeric alkanethiols on gold films, and this anti-biofouling chemistry can be enhanced by using monolayers formed by a racemic mixture of the enantiomeric alkanethiols. While SAMs presenting the enantiomers D-mannonamide or L-mannonamide could not resist cell adhesion, SAMs presenting D-gulitol could resist cell adhesion longer than SAMs presenting its enantiomer L-gulitol. Interestingly, racemic

---

[‡]*Stereochemical Effects of Chiral Monolayers on Enhancing the Resistance to Mammalian Cell Adhesion* Debjyoti Bandyopadhyay, Deepali Prashar and Yan-Yeung Luk* *Chem. Commun.*, **2011**, 47, 6165-6167-Reproduced in part by permission of The Royal Society of Chemistry. Verbatim in Arial font size 10 and identical figures are indicated in the legend.

monolayers for both gulitol and mannonamide were found to be more resistant to cell adhesion than monolayers presenting the corresponding enantiomers alone. These results are consistent with the kosmotrope theory, which states that molecules that can stabilize native protein folding when immobilized on surfaces, can also resist protein adsorption and other biofoulings.

3.1 Background and Significance

Most mammalian cells are adherent and need to adhere and spread on an underlying matrix for normal growth and development. *In vivo*, mammalian cells adhere and spread on the extra cellular matrix (ECM) which comprises of a collection of insoluble proteins and glycoaminoglycans.[78] Adhesion is mediated by specific binding of cell surface receptors with cell adhesion molecules provided by the ECM and those secreted by the cells.[78] Fibronectin mediates cell adhesion on ECM and *in vitro* via specific interaction with the cell surface receptor integrin. The αβ subunit of integrin recognizes the specific amino acid sequence Arg-Gly-Asp (RGD) in fibronectin.[77] If cells are not allowed to adhere, they initiate a program of apoptosis leading to their death. Cell death may be accompanied by release of the cellular constituents including cytoplasmic and membrane proteins. The proteins can then non-specifically adsorb onto the surface and mediate cell adhesion and proliferation.

A material intended to be used as a biomaterial, prosthesis or medical device, when implanted in a living tissue leads to sequence of host reactions including injury, blood-material interactions, provisional matrix formation, acute inflammation, chronic inflammation, granulation tissue formation, foreign body reaction, fibrosis or fibrous capsule development.[4] While all these events are naturally expected to occur in response

to implantation of a medical device or prosthesis, in the worst case, the implant needs to be surgically removed due to device failure or infection. One of the first events, which occur on implantation of a biomaterial, is that the biomaterial is coated by naturally occurring serum factors called opsonins. The two major opsonins are IgG and the complement activated-fragment C3b, which are plasma-derived proteins capable of coating an implanted biomaterial.[4] The immune cells such as neutrophils and macrophages have the corresponding receptors for these opsonization proteins and hence are able to recognize the foreign material on implantation. These receptors sometimes help in the activation of the adhered neutrophils[113] and macrophages.[114-115] Hence, non-specific adsorption of the serum proteins aids in the identification of an implanted biomaterial by the immune cells causing implant rejection or life threatening infections.

Resisting mammalian cell adhesion is a more stringent test for bioinertness of a surface. Mammalian cell adhesion will generally last longer (over weeks) while proteins tend to adsorb on surfaces and the surface is covered with a monolayer of protein within minutes.[74] Self-assembled monolayers (SAMs) formed by the enantiomeric polyol-terminated alkanethiols D-gulitol, **1**, L-gulitol, **1′** and D-mannonamide, **2**, L-mannonamide, **2′**, together with their racemic mixtures have been shown to resist the adsorption of proteins (Chapter 2). Here, the effectiveness of these SAMs to resist the adhesion of mammalian cells (Swiss 3T3 albino fibroblasts) has been evaluated. The synthesis of two diastereomeric polyol-terminated alkanethiols, D-gulonamide, **5**, D-gluconamide, **6** (Scheme 3.1) is also reported and the ability of the SAMs formed by the diastereomeric, enantiomeric and racemic polyol-terminated alkanethiols to confine

adhered mammalian cells within micrometer sized cell-adhesive patterns of methyl-terminated SAMs has been evaluated.

3.2 Results and Discussion

3.2.1 Enantiomeric and racemic effects during mammalian cell adhesion on monolayers of alditol-terminated alkanethiols

Patterned monolayers were created by microcontact printing, where circular regions of pentadecanethiol (135 μm in diameter) are surrounded by SAMs formed by **1**, **1′** or SAMs formed by racemic mixture of the enantiomers (Figure 3.1). The patterned SAMs were cultured with Swiss albino 3T3 fibroblasts, and monitored using optical microscopy.

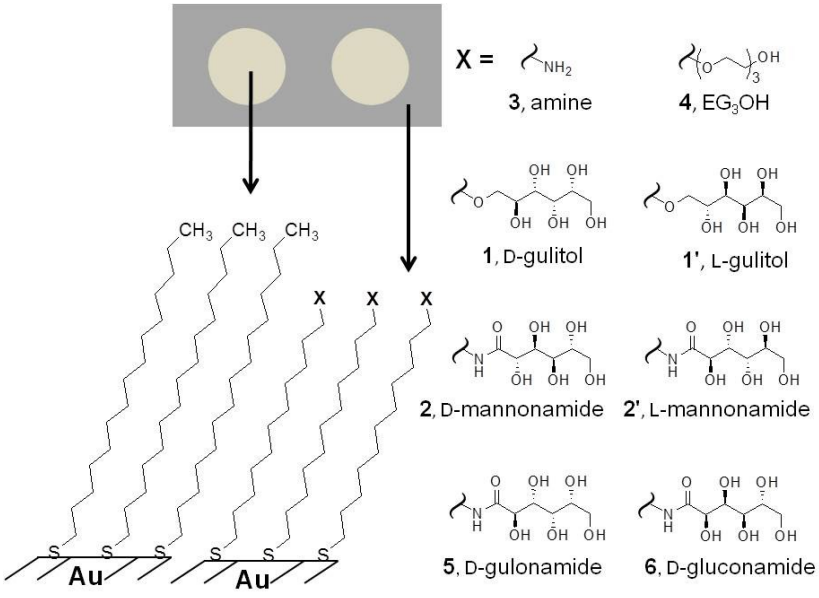

Figure 3.1 Schematic representation of patterned SAMs of $HS(CH_2)_{14}CH_3$, surrounded by the chiral polyol- or amine- or EG_3OH-terminated SAMs on gold films. Figure adapted from the work by Luk and co-workers.[69]

Cell adhesion confined to circular patterns was observed for SAMs presenting the enantiomeric alkanethiols, **1** and **1′**, and the racemic mixture of the enantiomers. Surprisingly,

the D-gulitol-terminated monolayers were more resistant to cell adhesion than the L-gulitol-terminated monolayers. While D-gulitol-terminated monolayers confined cell adhesion in circular patterns up to 19 days, L-gulitol-terminated monolayers failed at 13 days. This observation demonstrated that mammalian cells have a higher propensity to overcome the bioinertness of surface formed by one enantiomer over the other. Interestingly, SAMs formed by the racemic mixture of the enantiomers, **1** and **1′**, confined cell adhesion up to 23 days, longer than SAMs formed by either of the enantiomers (Figure 3.2). This result suggests an enhanced anti-fouling surface chemistry by using racemic mixture of chiral molecules that can form bioinert monolayers.

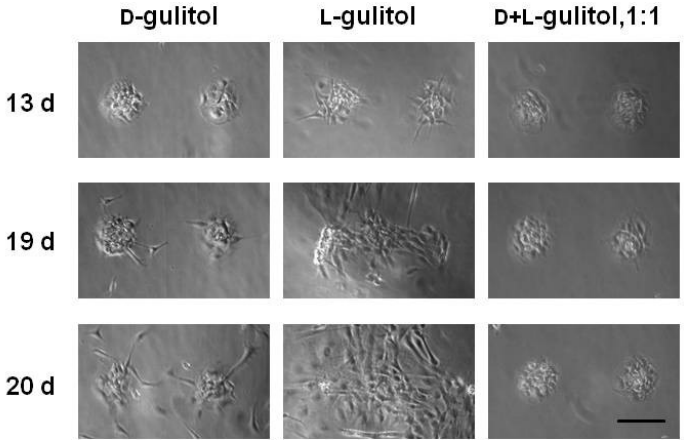

Figure 3.2 Optical micrographs for the adhesion of Swiss albino 3T3 fibroblast on circular patterns (135 μm in diameter) of $HS(CH_2)_{14}CH_3$, surrounded by alditol-terminated SAMs on gold films. The number of days the substrates were in the culture is indicated to the left. Optical micrographs are representative of ten replicates of 135 μm circular patterns (only two are shown). Scale bar = 152 μm. Figure adapted from the work by Luk and co-workers.[69]

Mammalian cell adhesion on surface is mediated by selective molecular binding including cell surface receptor integrin binding to a small tripeptide Arg-Gly-Asp (RGD) on extra cellular matrix (ECM) proteins fibronectin or vitronectin,[77] which is the key event for initiating vital cell activities.[78] Interestingly, Addadi and co-workers have shown that adhesion of epithelial cells

(A6 *Xenopus Laevis*) on (S, S)-tartrate tetrahydrate crystal was slow and mediated by RGD containing adhesive proteins, but attachment and spreading on the (R, R) crystal was fast, RGD-independent and led to cell death.[84] Recently, macrophages were reported to have reduced adhesion with round morphology on monolayer of *N*-Isobutyryl-D-cysteine on gold surface, but with larger number of cells and well-spread morphology on monolayer of *N*-Isobutyryl-L-cysteine.[85] In contrast to these findings, the different ability of enantiomeric monolayers to resist cell adhesion suggests that cells can distinguish chirality of the surface, even when the surface chemistry is resistant to cell adhesion.

3.2.2 Diastereomeric and racemic effects during mammalian cell adhesion on monolayers of aldonamide-terminated alkanethiols

The diastereomeric polyol-terminated monolayers, for which the polyols are linked by amide bonds instead of ether bonds were also examined. The mannonamide-terminated monolayers, **2** and **2′** failed to resist cell adhesion, but D-gulonamide, **5**, and D-gluconamide, **6**, confined cell adhesion upto 2 days and 5 days, respectively (Figure 3.3). Interestingly, while monolayers presenting either D-mannonamide, **2** or L-mannonamide, **2′** were not adhesion-resistant, monolayers formed by a racemic mixture of the enantiomers (50/50 : **2**/**2′**) were adhesion-resistant and confined adhered cell up to 10 days (Figure 3.4). These results enforce the observed racemic enhancement effect on bioinertness.

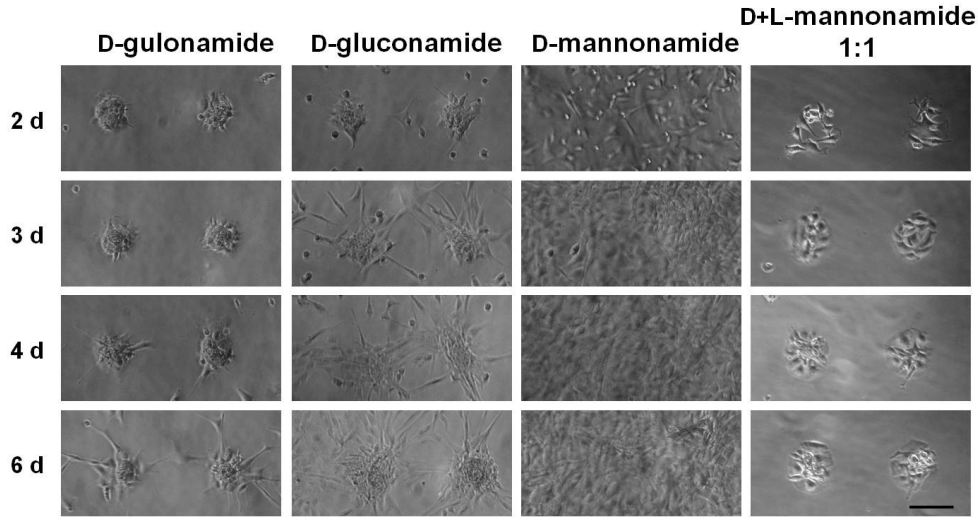

Figure 3.3 Optical micrographs for the adhesion of Swiss albino 3T3 fibroblast on circular patterns (135 μm in diameter) of $HS(CH_2)_{14}CH_3$, surrounded by aldonamide-terminated SAMs on gold films. The number of days the substrates were in the culture is indicated to the left. Optical micrographs are representative of ten replicates of 135 μm circular patterns (only two are shown).Scale bar = 152 μm. Figure adapted from the work by Luk and co-workers.[69]

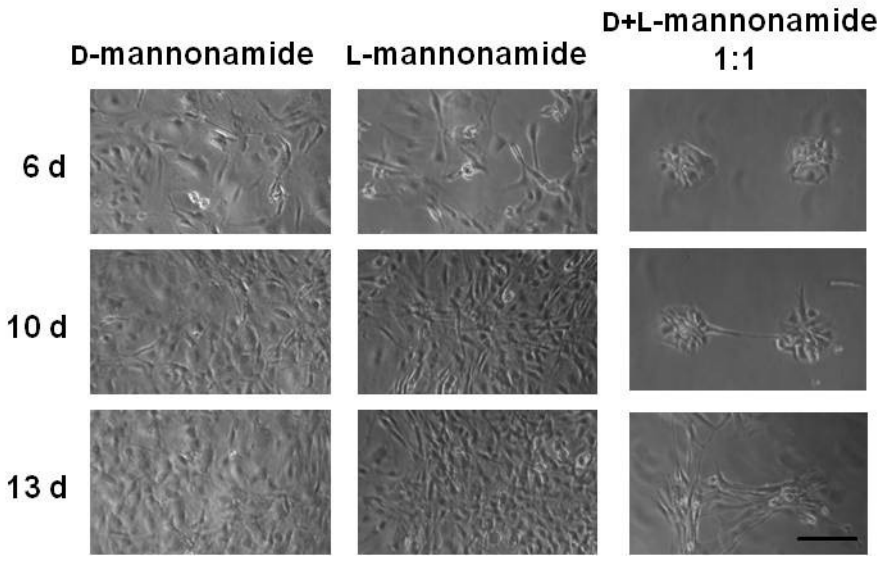

Figure 3.4 Optical micrographs for the adhesion of Swiss albino 3T3 fibroblast on circular patterns (135 μm in diameter) of $HS(CH_2)_{14}CH_3$, surrounded by mannonamide-terminated SAMs on gold films. The number of days the substrates were in the culture is indicated to the left. Optical micrographs are representative of ten replicates of 135 μm circular patterns (only two are shown). Scale bar = 152 μm. Figure adapted from the work by Luk and co-workers.[69]

3.2.3 Hydrophilic surfaces are not necessarily bioinert

The mechanism of an antifouling chemistry is not trivial; hydrophilic surfaces are not necessarily beneficial for achieving bioinertness. Proteins are known to adsorb on surfaces presenting hydrophilic amine groups.[93] An interesting theoretical study by Sharp and co-workers suggests that similar water organization is induced by methyl and amino moieties.[116] To examine the effect of potentially protein-denaturing, yet hydrophilic surface on mammalian cell adhesion, patterned squares (600 μm-wide) of $HS(CH_2)_{14}CH_3$ surrounded by amine-[117] and tri(ethylene glycol)-terminated[118] SAMs, **3** and **4** were prepared. At the early stage, cell adhesion was only seen on amine-terminated SAMs, and little cells were seen inside the methyl-terminated squares, giving a "reversed" pattern (Figure 3.5A). Over short period of 3 days, a confluent monolayer of cells was observed covering the entire monolayer (Figure

3.5B). In contrast, tri(ethylene glycol)-terminated monolayer resisted cell adhesion from the beginning of cell culture (Figure 3.5C). These results support the notion that amine groups are likely chaotropic in nature, and supported rapid cell adhesion.

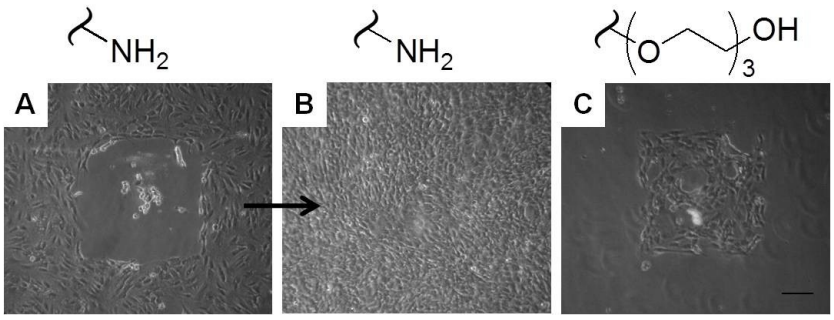

Figure 3.5 Optical micrographs for the adhesion of Swiss albino 3T3 fibroblast on 600 *μ*m-wide squares of pentadecanethiols, surrounded by (A) amine-terminated monolayer, **3**, for 1 day, (B) for 3 day, and (C) EG_3OH-terminated monolayer, **4**, for 1 day. Optical micrographs are representative of ten replicates of 600 *μ*m square patterns (only one is shown). Scale bar = 152 *μ*m. Figure adapted from the work by Luk and co-workers.[69]

3.2.4 Resisting biofouling by surfaces presenting kosmotropic polyols

Several theories exist for bioinert chemistries that resist adsorption of proteins.[74, 89-92, 94-95, 108] To explore the understanding of bioinert surface chemistry, we note that polyols are similar in structure to glycerol and sucrose that are known to stabilize protein structure.[104-106] Other small molecules such as urea and guanidinium are known to denature proteins.[98, 119-123] While the stabilizing or destabilizing effects of added ions or molecules on protein folding may due to direct[98-100, 102-103] or indirect[98, 123] interactions between the additives and the proteins, the stabilizing effect by kosmotropic organic osmolytes on protein structure is likely indirect.[98] Together, these results are consistent with the notion that kosmotropic organic molecules that stabilize protein structure can also resist biofouling when immobilized on surface.[74, 92, 96] One plausible mechanism for such anti-fouling chemistry is an extensively

hydrogen bonded water network on the monolayer, which prevents biological entities from contacting or attaching to the surface.[74, 92, 96, 110, 124]

3.3 Conclusions

Self-assembled monolayers (SAMs) presenting chiral polyols that have the same chemical composition have different ability to resist mammalian cell adhesion. While cells can distinguish chiral surfaces that support adhesion,[84-85] the results presented here show that cells can also distinguish chirality of the surface when the surface chemistry is to resist cell adhesion. Enhanced bioinertness on monolayer formed by racemic mixtures of both gulitol- and mannonamide-terminated alkanethiols was observed, suggesting that this racemic effect on bioinertness is likely general for other bioinert chiral monolayers. These results suggest an approach for potentially enhancing antifouling chemistry on materials beyond gold films. This bioinert chemistry is believed to be strongly influenced by the water solvation and organization at the interface.[108, 125]

3.4 Experimental Section

Chemicals. 1-Pentadecanethiol and chemicals used for synthesizing all other alkanethiols were purchased from Aldrich Chemicals (Milwaukee, WI) and used as received. Ethanol was used as a solvent for preparing all alkanethiol solutions and for washing the SAM modified gold substrates. A minimum amount of DMSO was mixed with ethanol for solubilizing polyol-terminated alkanethiols, which were poorly soluble in pure ethanol. Water used had a resistivity of 18 MΩ cm (Millipore, Billerica, MA).

General Information for Synthesis of Alkanethiols. The processes involving reactants sensitive to moisture or air were executed under an atmosphere of argon using oven-dried glassware. Reagents and solvents were reagent grade and used as supplied unless otherwise mentioned. THF was distilled from sodium benzophenone ketyl. Solvents were removed under reduced pressure using rotary evaporator below 40 ºC. EMD Silica Gel 60 F_{254} precoated plates (0.25-mm thickness) were used for TLC and a solution of phosphomolybdic acid/ ceric sulfate/ sulfuric acid (10g : 1.25 g : 8% 250 mL), followed by charring at ~ 150 ºC, was used for

visualization. Flash column chromatography was performed using SILICYCLE, Silica-P Flash Silica Gel with 40-63μ mesh size. NMR spectra (^1H, ^{13}C) were recorded on 300 MHz Bruker instrument. ^1H chemical shifts are reported in ppm relative to $CDCl_3$ δ 7.26 and DMSO-d_6 δ 2.50. ^{13}C chemical shifts are reported relative to $CDCl_3$ δ 77.23 and DMSO-d_6 δ 39.51. (High Resolution Mass Spectra) HRMS samples were analyzed by positive ion electrospray or electron impact.

Scheme 3.1

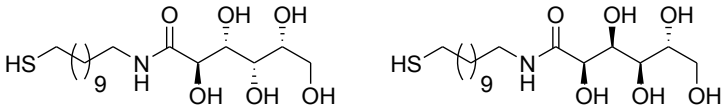

5 (D-gulonamide) **6 (D-gluconamide)**

Scheme 3.2

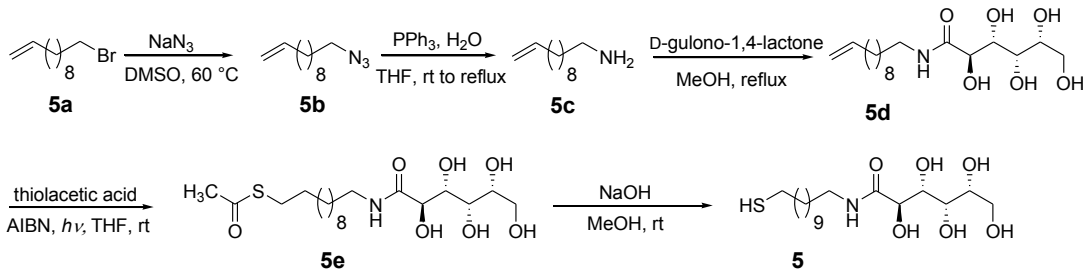

The synthesis for **5** is shown in Scheme 3.2. Briefly, the alkene, **5d** was obtained by aminolysis,[126] of D-gulono-1,4-lactone in refluxing methanol. Reaction of **5d** with thiolacetic acid using catalytic amount of AIBN (azobisisobutyronitrile) under UV light afforded the thioester **5e**. Base hydrolysis of the thioester **5e** with methanolic NaOH followed by acidification afforded alkanethiol **5**. Compound **6** was synthesized similarly.

Synthesis of Compound 5b. NaN_3 (1.115 g, 17.153 mmol) was added to a solution of 11-bromo-1-undecene, **5a** (2.000 g, 8.576 mmol) in DMSO (20.0 mL) and the mixture was stirred at rt for 10 min followed by heating at 60 ºC for 2 h. The mixture was cooled to rt followed by addition of 20 mL of brine. The organic layer was extracted with DCM and the combined organic

extracts were dried over anhydrous Na_2SO_4. Evaporation of solvent yielded the crude product as yellow oil. The crude product was purified using silica gel column (Hexanes → 5% EtOAc in Hexanes) to obtain pure compound, **5b** (1.028 g, 61%) as a colorless oil after evaporation of solvent. R_f = 0.41, (Hexanes). ^{1}H NMR (300 MHz, $CDCl_3$): δ 5.89-5.75 (m, 1H), 5.04-4.92 (m, 2H), 3.26 (t, J_{H-H} = 6.9 Hz, 2H), 2.04 (q, J_{H-H} = 6.3 Hz, 2H), 1.65-1.56 (m, 2H), 1.39-1.36 (m, 2H), 1.30 (br s, 10H). ^{13}C NMR (75 MHz, $CDCl_3$): δ 139.6, 114.5, 51.9, 34.2, 29.82, 29.8, 29.54, 29.5, 29.3, 29.2, 27.1. HRMS: found = 194.1649 [M - H] , calcd for [$C_{11}H_{21}N_3$ - H] 194.1652.

Synthesis of Compound 5c. PPh_3 (0.793 g, 3.023 mmol) was added to a solution of compound, **5b** (0.531 g, 2.748 mmol) in THF (15.0 mL) and the reaction mixture was stirred at rt for 2 h. 55 *μ*L (~1 eq) of water was then added to the reaction mixture which was stirred at rt for another 30 min. The reaction mixture was then refluxed till no more starting material was seen on TLC. The reaction mixture was allowed to cool to rt, solvent was evaporated and the residue was directly loaded on to the silica gel column (EtOAc → DCM → 3:3:1 DCM : MeOH : Et_3N). Pure compound, **5c** (0.429 g, 92 %) was obtained as colorless viscous oil after evaporation of solvent. ^{1}H NMR (300 MHz, $CDCl_3$): δ 5.83-5.72 (m, 1H), 5.00-4.88 (m, 2H), 2.67 (t, J_{H-H} = 6.8 Hz, 2H), 2.05 (br s, 2H), 2.01 (q, J_{H-H} = 6.7 Hz, 2H), 1.45-1.32 (m, 4H), 1.26 (br s, 10H). ^{13}C NMR (75 MHz, $CDCl_3$): δ 138.5, 113.7, 41.5, 33.4, 29.2, 29.09, 29.06, 28.7, 28.5, 26.5. HRMS: found = 170.1905 $[M + H]^+$, calcd for $[C_{11}H_{23}N + H]^+$ 170.1909.

Synthesis of Compound 5d. D-gulono-1,4-lactone (0.103 g, 0.579 mmol) was added to a solution of compound, **5c** (0.098 g, 0.579 mmol) in MeOH (5.0 mL) and the mixture was refluxed for 20 h. The mixture was allowed to cool to to rt and then in an ice bath, which led to precipitation of the crude product as a white solid. The solid was washed with ice cold methanol and any residual solvent was evaporated to yield the pure compound, **5d** (0.106 g, 53%) as a white solid. R_f = 0.61, (20% MeOH in DCM). ^{1}H NMR (300 MHz, DMSO-d_6): δ 7.83-7.79 (m, 1H), 5.83-5.70 (m, 1H), 5.44 (br s, 1H), 4.99-4.89 (m, 2H), 4.66 (br s, 1H), 4.46-4.37 (m, 3H), 3.88 (br s, 1H), 3.60-3.29 (m, 5H), 3.07-3.01 (m, 2H), 1.98 (q, J_{H-H} = 6.7 Hz, 2H), 1.38-1.31 (m, 4H), 1.22 (br s, 10

H). ^{13}C NMR (75 MHz, DMSO-d_6): δ 173.2, 138.9, 114.7, 73.3, 72.9, 71.9, 69.5, 62.5, 38.3, 33.2, 29.1, 29.0, 28.9, 28.8, 28.6, 28.3, 26.4. HRMS: found = 370.2197 $[M + Na]^+$, calcd for $[C_{17}H_{33}NO_6 + Na]^+$ 370.2206.

Synthesis of Compound 5e. Recrystallized azobisisobutyronitrile (AIBN) (5 mg) and thiolacetic acid (0.026 g, 0.344 mmol) were added to a solution of compound, **5d** (0.030 g ,0.086 mmol) in MeOH (6.0 mL). The reaction mixture was stirred under UV source for 18 h. The solvent was removed under vacuum to yield the crude product as white solid. The solid was washed with ice cold methanol and any residual solvent evaporated to give pure compound, **5e** (0.030 g, 82%) as a white solid. R_f = 0.48, (20% MeOH in DCM). ^{1}H NMR (300 MHz, DMSO-d_6): δ 7.84-7.80 (m, 1H), 5.47 (br s, 1H), 4.67 (br s, 1H), 4.48-4.41 (m, 3H), 3.88-3.83 (m, 1H), 3.60-3.33 (m, 5H), 3.18 (br s, 1H), 3.08-3.02 (m, 2H), 2.82-2.77 (m, 1H), 2.29 (s, 3H), 1.47-1.38 (m, 4H), 1.22 (br s, 14 H). ^{13}C NMR (75 MHz, DMSO-d_6): δ 195.7, 173.2, 73.3, 72.9, 71.8, 69.5, 68.9, 62.5, 52.5, 38.3, 35.9, 35.8, 30.6, 29.0, 28.8, 28.3, 28.1, 26.4, 25.1. HRMS: found = 446.2168 $[M + Na]^+$, calcd for $[C_{19}H_{37}NO_7S + Na]^+$ 446.2188.

Synthesis of Compound 5. Argon gas was bubbled through a solution of compound, **5e** (0.031 g, 0.072 mmol) in MeOH (2.0 mL) for 10 min followed by addition of 80.5 µL solution of 1N NaOH in MeOH. The reaction mixture was stirred at rt till TLC (20% MeOH in DCM) indicated complete consumption of the starting material. The reaction mixture was cooled to 0 ºC in an ice bath and to it was added 80.5 µL solution of 1N HCl in MeOH. The mixture was stirred at 0 ºC for 20 min and then kept undisturbed at 0 ºC to allow precipitation of solid product. The supernatant was carefully decanted and compound, **5** (0.029 g, quantitative) was obtained as a white solid after evaporation of any residual solvent. ^{1}H NMR (300 MHz, DMSO-d_6): δ 7.81 (br s, 1H), 5.46 (br s, 1H), 4.66 (br s, 1H), 4.47-4.38 (m, 3H), 3.88 (br s, 1H), 3.60-3.32 (m, 5H), 3.04 (m, 2H), 2.68-2.64 (m, 1H), 1.58-1.38 (m, 4H), 1.22 (br s, 14H). ^{13}C NMR (75 MHz, DMSO-d_6): δ 173.2, 73.3, 72.8, 69.5, 62.5, 38.4, 29.1, 28.8, 28.6, 28.5, 27.7, 26.4. HRMS: found = 404.2068 $[M + Na]^+$, calcd for $[C_{17}H_{35}NO_6S + Na]^+$ 404.2083.

Cleaning of Glass Substrates. Substrates for the gold films were Fisher's finest premium microscope slides (Fisher Scientific, Pittsburgh, PA). Prior to gold deposition, the slides were cleaned with piranha solution. The slides were soaked in piranha solution (3 parts of 35% H_2O_2 in water and 7 parts of concentrated H_2SO_4) at 70 °C for 45 min. Warning! *Piranha solution is extremely corrosive and has the potential for detonation if contaminated with a significant amount of oxidizable material.* After cooling, the piranha solution was poured off and the slides were rinsed 20 times with water having a resistivity of 18 MΩ cm (Millipore, Billerica, MA), followed by 10 rinses of ethanol and 10 rinses of methanol. The slides were then dried individually with a stream of nitrogen gas and stored in an 80 °C oven overnight.

Gold Deposition on Glass Substrates. Semitransparent gold film of approximately 280 Å thickness were deposited onto the piranha cleaned glass substrates with an electron beam evaporation system from Thermionics (Port Townsend, WA). A layer of titanium (approximately 70 Å thick) was applied first for adhesion of the gold film. Films were deposited at an oblique angle of 45° to the normal of the substrate. The rates of deposition were set at 0.2 Å/s for both gold and titanium. Pressure was maintained at or below 2×10^{-6} Torr throughout the deposition.

Microcontact Printing. Microcontact printing was done using polydimethylsiloxane (PDMS) stamps using slight modifications of literature reported procedures.[39] Briefly, gold slides were cut into approximately 1.0 cm × 1.0 cm pieces (gold substrates), rinsed with ethanol and then dried with a stream of nitrogen gas. PDMS stamps were dabbed with 2.0 mM solution of 1-pentadecanethiol, dried with a stream of nitrogen gas and placed on the gold substrates to allow conformal contact for 20 seconds. The substrates were then rinsed with ethanol, dried with a stream of nitrogen gas and placed in 1.0 mM solutions of alkanethiols **3**, **4**, **5**, **6**; 0.2 mM solutions of alkanethiols **1**, **1′**and 0.2 mM solution containing 1:1 mixture of the enantiomers **1** and **1′**; 1.0 mM solutions of alkanethiols **2**, **2′** and 1.0 mM solution containing 1:1 mixture of the enantiomers **2** and **2′** for 15 h. The substrates were then taken out of the solution, rinsed with ethanol and dried with a stream of nitrogen gas before using them in mammalian cell or bacterial cell culture.

Mammalian Cell Culture. Swiss 3T3 Albino fibroblasts were cultured using general culture procedures.[127] Briefly, Swiss 3T3 Albino cells purchased from ATCC (Rockville, MD) were cultured in Dulbecco's modified Eagle's medium (DMEM; pH 7.4) supplemented with 10% fetal bovine serum (FBS) (Sigma-Aldrich, St. Louis, MO), 10 μL/mL Penicillin-Streptomycin (Sigma-Aldrich, St. Louis, MO) and 24 μL/mL Nystatin (Sigma-Aldrich, St. Louis, MO) in a 25 mL Falcon tissue culture flask (Becton Dickson, Franklin Lakes, NJ). All cultures were kept in an incubator at 37 °C supplemented with 5% CO_2. The media was changed every 3 d. Confluent layer of 3T3 fibroblast cells were detached from culture flask by incubating with 2 mL 0.25% trypsin/0.5 mM EDTA solution for 5-10 min followed by addition of 8 mL of serum containing media.

Mammalian Cell Culture on SAM Modified Gold Substrates. SAM modified gold substrates were placed in a fresh 25 mL Falcon tissue culture flask and incubated in 7.5 mL of serum containing media supplemented with 1.0 μL Penicillin-Streptomycin (Sigma-Aldrich, St. Louis, MO) and 2.4 μL Nystatin (Sigma-Aldrich, St. Louis, MO) for 20 min. 2.5 mL of the cell suspension was introduced in the flask and incubated for 24 h. Media was changed after 24 h of incubation. Pictures of cell attachment and growth on the plate were taken daily using Cannon C-5060 Wide Zoom camera and viewed from AE31 trinocular inverted microscope (Motic, British Columbia, Canada). Culture media was changed every 3 d.

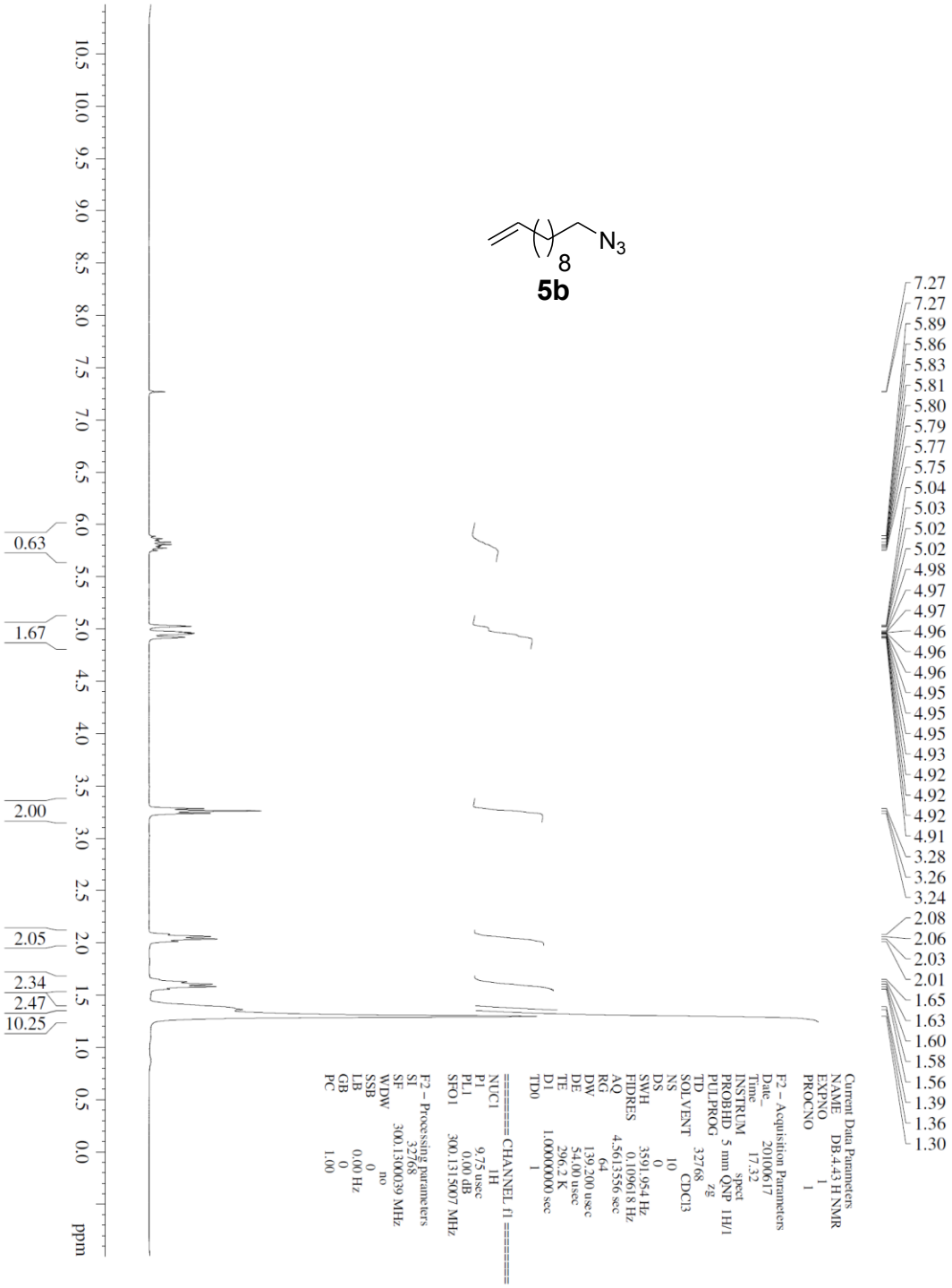
N3
8
5b
7.27
7.27
5.89
5.86
5.83
5.81
5.80
5.79
5.77
5.75
5.04
5.03
5.02
5.02
4.98
4.97
4.97
4.96
4.96
4.96
4.95
4.95
4.95
4.93
4.92
4.92
4.92
4.91
3.28
3.26
3.24
2.08
2.06
2.03
2.01
1.65
1.63
1.60
1.58
1.56
1.39
1.36
1.30
Current Data Parameters
NAME DB.4.43 H NMR
EXPNO 1
PROCNO 1
F2 – Acquisition Parameters
Date_ 20100617
Time 17.32
INSTRUM spect
PROBHD 5 mm QNP 1H/1
PULPROG zg
TD 32768
SOLVENT CDCl3
NS 10
DS 0
SWH 3591.954 Hz
FIDRES 0.109618 Hz
AQ 4.5613556 sec
RG 64
DW 139.200 usec
DE 54.00 usec
TE 296.2 K
D1 1.00000000 sec
TD0 1
======== CHANNEL f1 ========
NUC1 1H
P1 9.75 usec
PL1 0.00 dB
SFO1 300.1315007 MHz
F2 – Processing parameters
SI 32768
SF 300.1300039 MHz
WDW no
SSB 0
LB 0.00 Hz
GB 0
PC 1.00
0.63
1.67
2.00
2.05
2.34
2.47
10.25
10.5 10.0 9.5 9.0 8.5 8.0 7.5 7.0 6.5 6.0 5.5 5.0 4.5 4.0 3.5 3.0 2.5 2.0 1.5 1.0 0.5 0.0
ppm

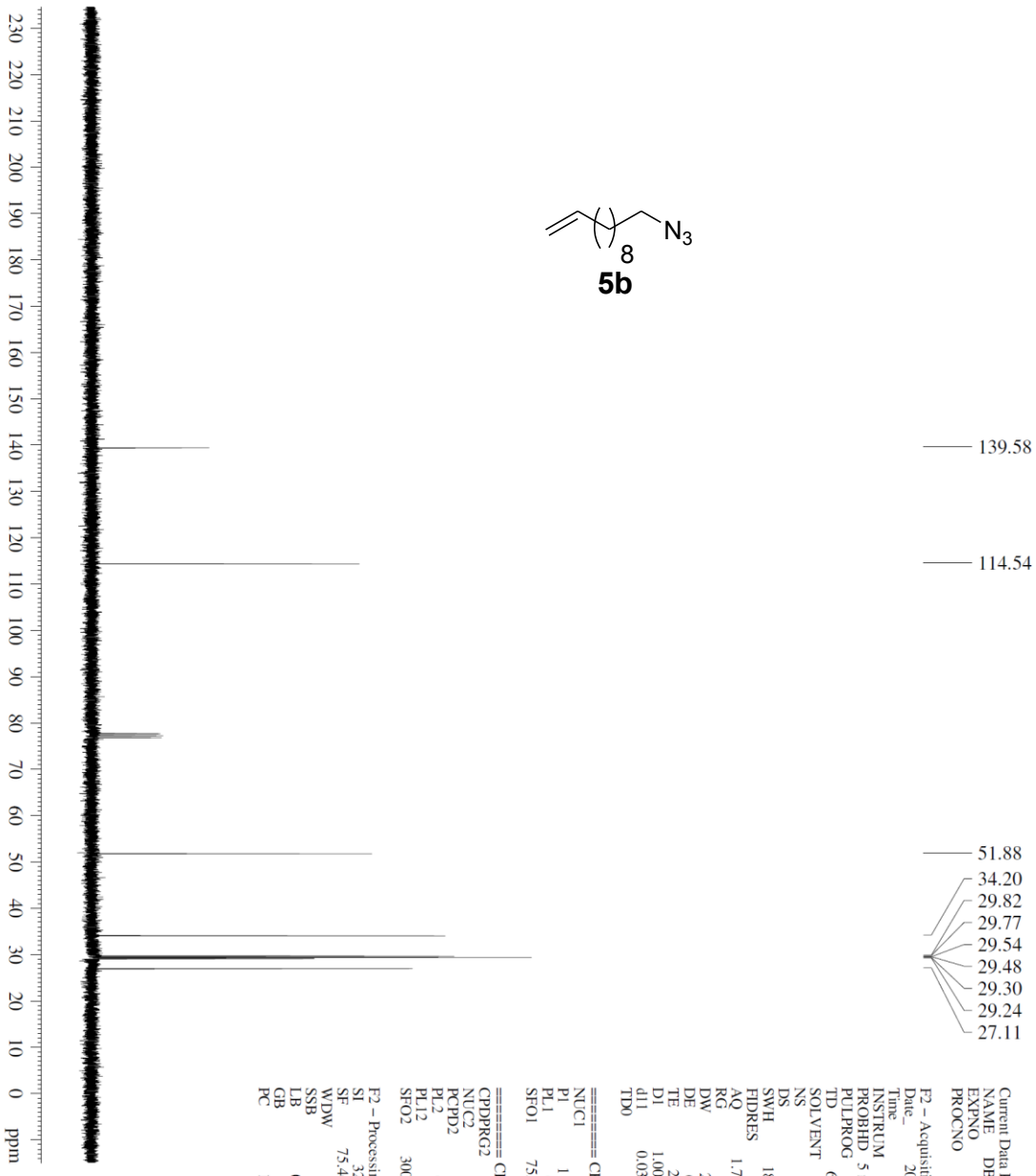
N3
8
5b
139.58
114.54
51.88
34.20
29.82
29.77
29.54
29.48
29.30
29.24
27.11
Current Data Parameters
NAME DB.4.43 C NMR
EXPNO 2
PROCNO 1
F2 – Acquisition Parameters
Date_ 20100617
Time 17.49
INSTRUM spect
PROBHD 5 mm QNP 1H/1
PULPROG zgdc
TD 65536
SOLVENT CDCl3
NS 250
DS 0
SWH 18832.393 Hz
FIDRES 0.287360 Hz
AQ 1.7400308 sec
RG 2048
DW 26.550 usec
DE 6.00 usec
TE 296.2 K
D1 1.00000000 sec
d11 0.03000000 sec
TD0 1
======== CHANNEL f1 ========
NUC1 13C
P1 11.80 usec
PL1 0.00 dB
SFO1 75.4760200 MHz
======== CHANNEL f2 ========
CPDPRG2 waltz16
NUC2 1H
PCPD2 95.00 usec
PL2 0.00 dB
PL12 18.00 dB
SFO2 300.1312005 MHz
F2 – Processing parameters
SI 32768
SF 75.4677345 MHz
WDW no
SSB 0
LB 0.00 Hz
GB 0
PC 1.40
230 220 210 200 190 180 170 160 150 140 130 120 110 100 90 80 70 60 50 40 30 20 10 0 ppm

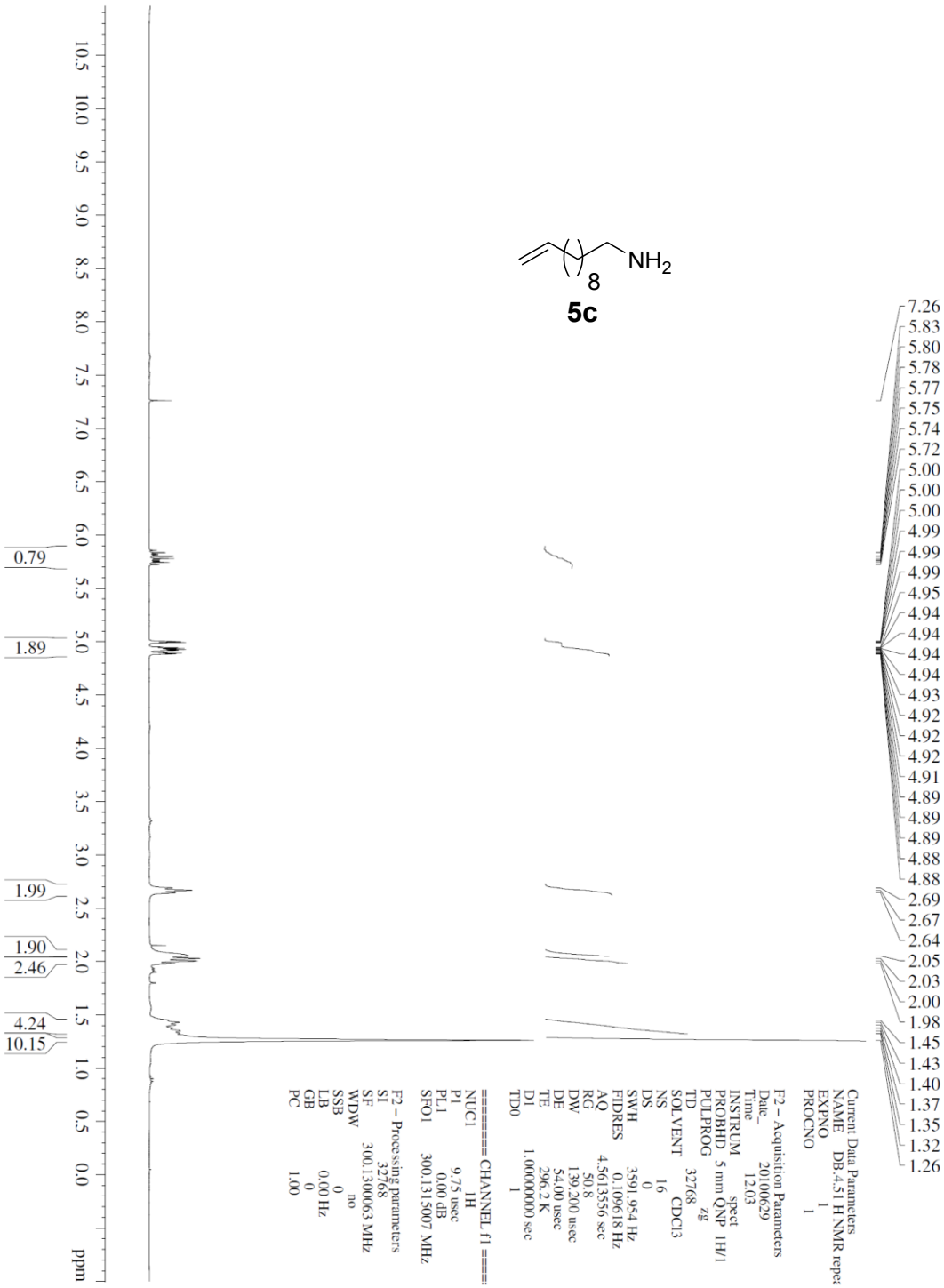
NH2
8
5c
7.26
5.83
5.80
5.78
5.77
5.75
5.74
5.72
5.00
5.00
5.00
4.99
4.99
4.99
4.95
4.94
4.94
4.94
4.94
4.93
4.92
4.92
4.92
4.91
4.89
4.89
4.89
4.88
4.88
2.69
2.67
2.64
2.05
2.03
2.00
1.98
1.45
1.43
1.40
1.37
1.35
1.32
1.26
Current Data Parameters
NAME DB.4.51 H NMR repea
EXPNO 1
PROCNO 1
F2 – Acquisition Parameters
Date_ 20100629
Time 12.03
INSTRUM spect
PROBHD 5 mm QNP 1H/1
PULPROG zg
TD 32768
SOLVENT CDCl3
NS 16
DS 0
SWH 3591.954 Hz
FIDRES 0.109618 Hz
AQ 4.5613556 sec
RG 50.8
DW 139.200 usec
DE 54.00 usec
TE 296.2 K
D1 1.00000000 sec
TD0 1
======== CHANNEL f1 ========
NUC1 1H
P1 9.75 usec
PL1 0.00 dB
SFO1 300.1315007 MHz
F2 – Processing parameters
SI 32768
SF 300.1300063 MHz
WDW no
SSB 0
LB 0.00 Hz
GB 0
PC 1.00
0.79
1.89
1.99
1.90
2.46
4.24
10.15
10.5 10.0 9.5 9.0 8.5 8.0 7.5 7.0 6.5 6.0 5.5 5.0 4.5 4.0 3.5 3.0 2.5 2.0 1.5 1.0 0.5 0.0
ppm

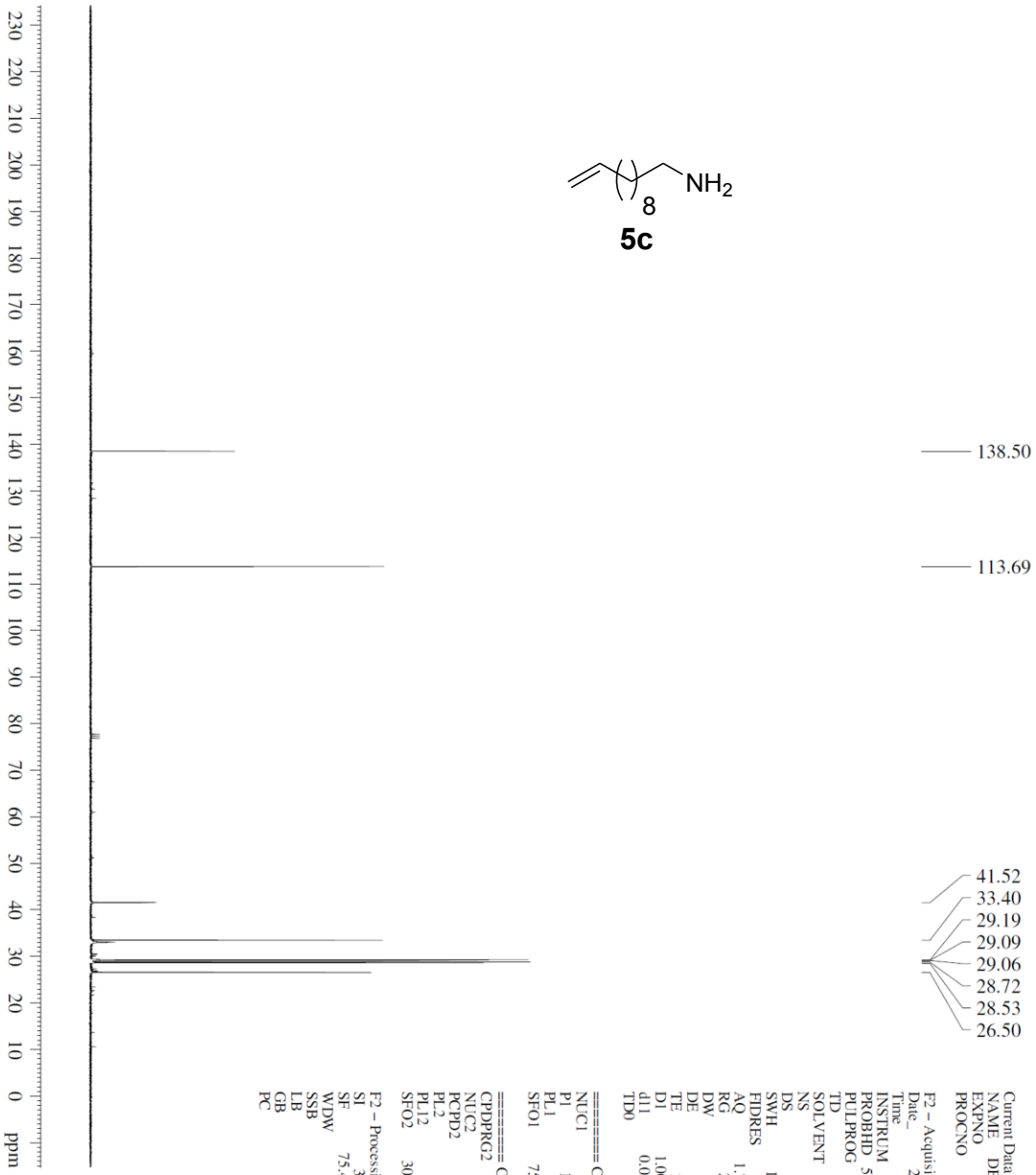

Current Data Parameters
NAME DB-4.51 C NMR repeat
EXPNO 2
PROCNO 1

F2 – Acquisition Parameters
Date_ 20100629
Time 12.20
INSTRUM spect
PROBHD 5 mm QNP 1H/1
PULPROG zgdc
TD 65536
SOLVENT CDCl3
NS 200
DS 0
SWH 18832.393 Hz
FIDRES 0.287360 Hz
AQ 1.7400308 sec
RG 2896.3
DW 26.550 usec
DE 6.00 usec
TE 296.2 K
D1 1.00000000 sec
d11 0.03000000 sec
TD0 1

======== CHANNEL f1 ========
NUC1 13C
P1 11.80 usec
PL1 0.00 dB
SFO1 75.4760200 MHz

======== CHANNEL f2 ========
CPDPRG2 waltz16
NUC2 1H
PCPD2 95.00 usec
PL2 0.00 dB
PL12 18.00 dB
SFO2 300.1312005 MHz

F2 – Processing parameters
SI 32768
SF 75.4677602 MHz
WDW EM
SSB 0
LB 0.00 Hz
GB 0
PC 1.40

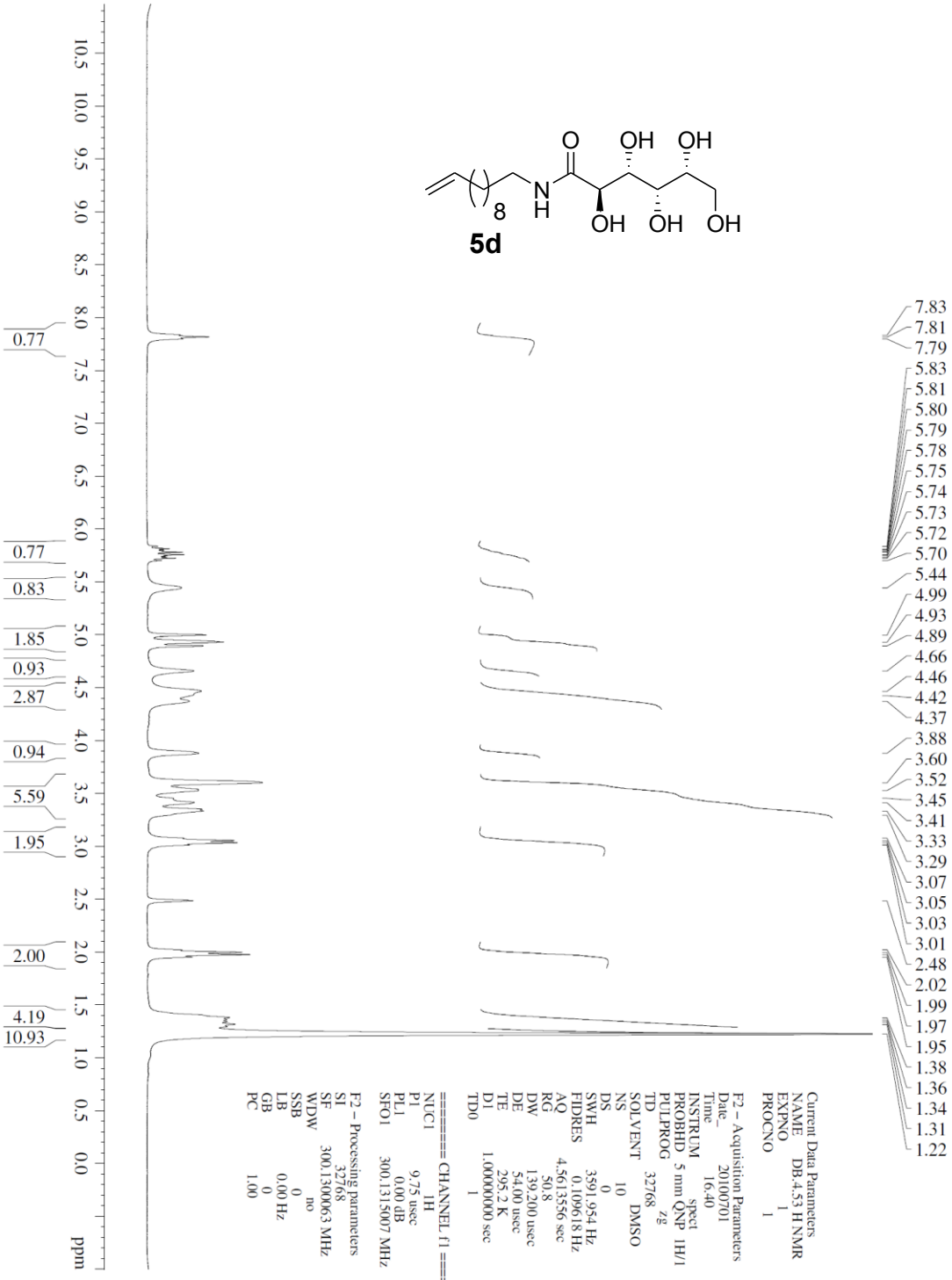
5d
7.83
7.81
7.79
5.83
5.81
5.80
5.79
5.78
5.75
5.74
5.73
5.72
5.70
5.44
4.99
4.93
4.89
4.66
4.46
4.42
4.37
3.88
3.60
3.52
3.45
3.41
3.33
3.29
3.07
3.05
3.03
3.01
2.48
2.02
1.99
1.97
1.95
1.38
1.36
1.34
1.31
1.22
0.77
0.77
0.83
1.85
0.93
2.87
0.94
5.59
1.95
2.00
4.19
10.93
ppm

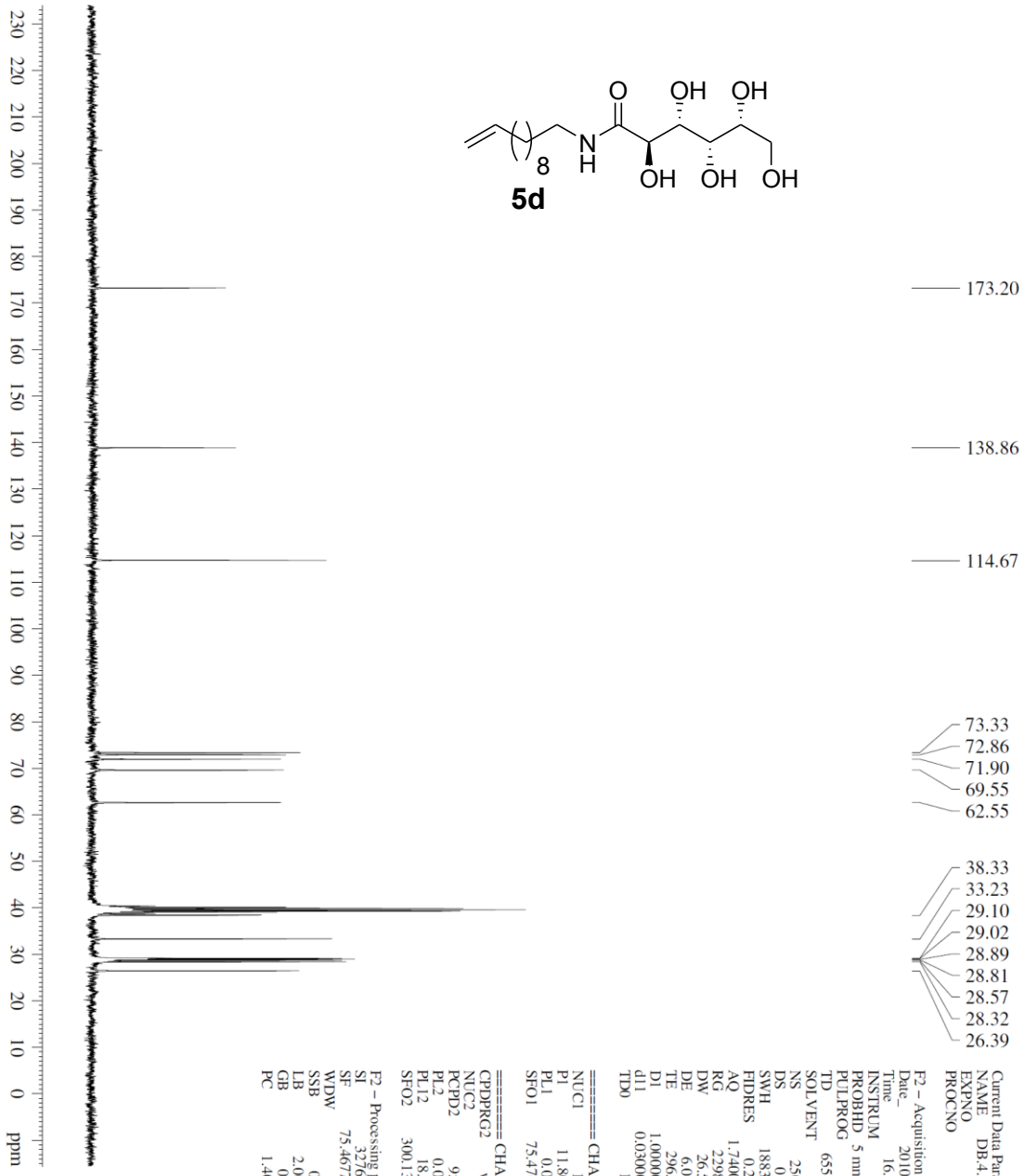
5d
173.20
138.86
114.67
73.33
72.86
71.90
69.55
62.55
38.33
33.23
29.10
29.02
28.89
28.81
28.57
28.32
26.39
Current Data Parameters
NAME DB-4.53 C NMR
EXPNO 2
PROCNO 1
F2 – Acquisition Parameters
Date_ 20100701
Time 16.57
INSTRUM spect
PROBHD 5 mm QNP 1H/1
PULPROG zgdc
TD 65536
SOLVENT DMSO
NS 250
DS 0
SWH 18832.393 Hz
FIDRES 0.287360 Hz
AQ 1.7400308 sec
RG 2298.8
DW 26.550 usec
DE 6.00 usec
TE 296.2 K
D1 1.00000000 sec
d11 0.03000000 sec
TD0 1
======== CHANNEL f1 ========
NUC1 13C
P1 11.80 usec
PL1 0.00 dB
SFO1 75.4760200 MHz
======== CHANNEL f2 ========
CPDPRG2 waltz16
NUC2 1H
PCPD2 95.00 usec
PL2 0.00 dB
PL12 18.00 dB
SFO2 300.1312005 MHz
F2 – Processing parameters
SI 32768
SF 75.4677808 MHz
WDW EM
SSB 0
LB 2.00 Hz
GB 0
PC 1.40
230 220 210 200 190 180 170 160 150 140 130 120 110 100 90 80 70 60 50 40 30 20 10 0 ppm

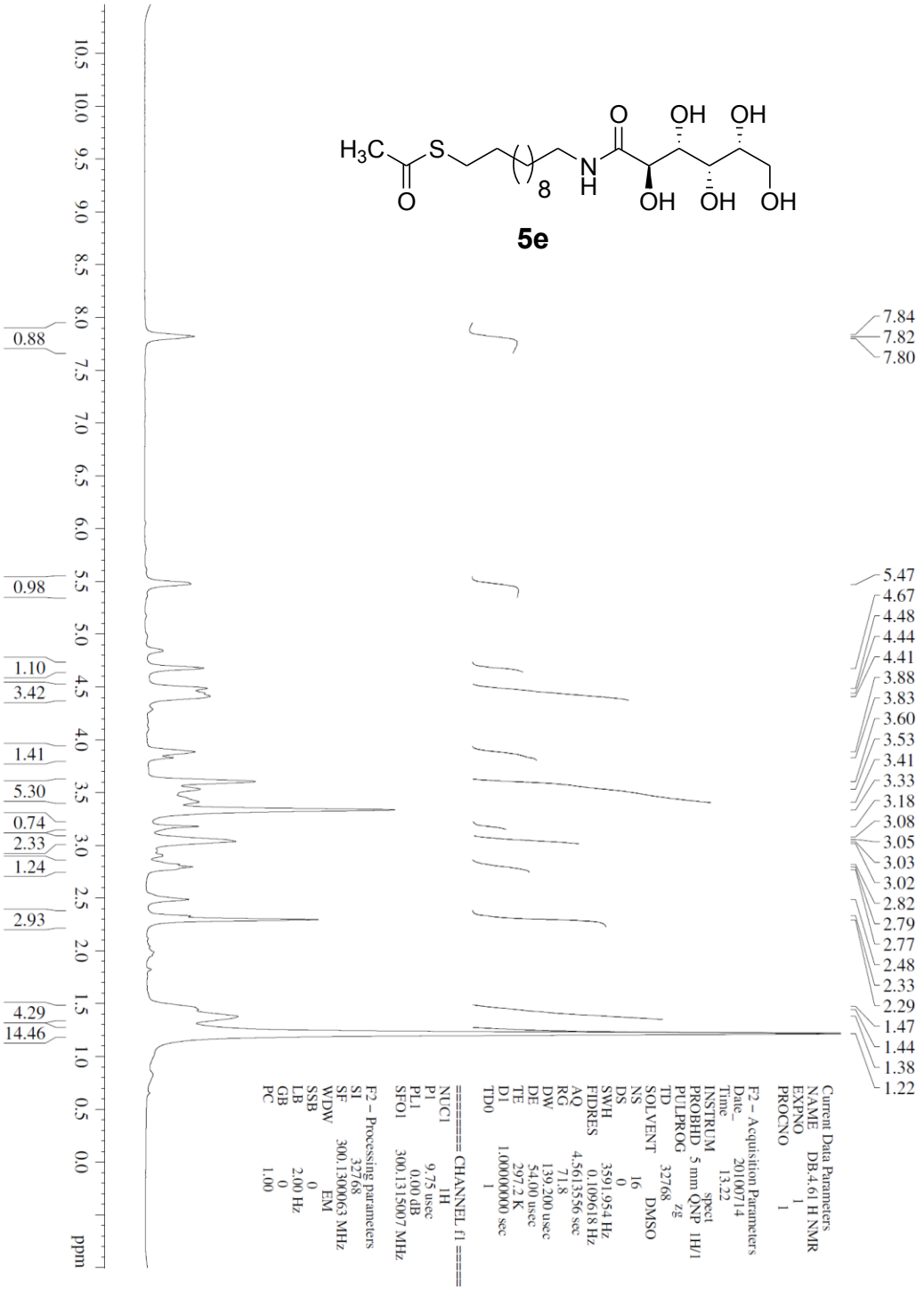
H3C
S
O
8
N
H
O
OH
OH
OH
OH
OH
5e
7.84
7.82
7.80
5.47
4.67
4.48
4.44
4.41
3.88
3.83
3.60
3.53
3.41
3.33
3.18
3.08
3.05
3.03
3.02
2.82
2.79
2.77
2.48
2.33
2.29
1.47
1.44
1.38
1.22
0.88
0.98
1.10
3.42
1.41
5.30
0.74
2.33
1.24
2.93
4.29
14.46
ppm

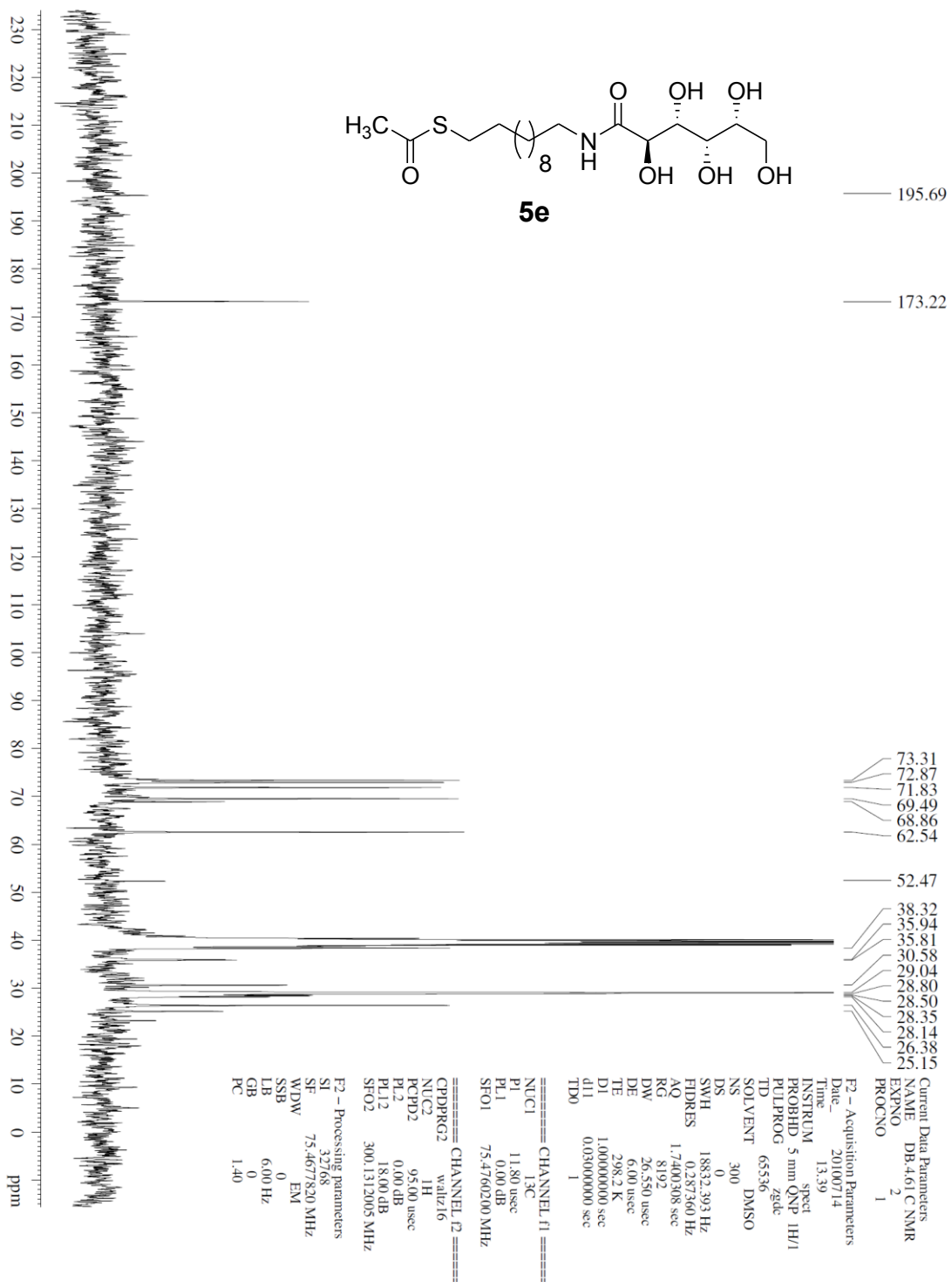
5e
195.69
173.22
73.31
72.87
71.83
69.49
68.86
62.54
52.47
38.32
35.94
35.81
30.58
29.04
28.80
28.50
28.35
28.14
26.38
25.15
ppm

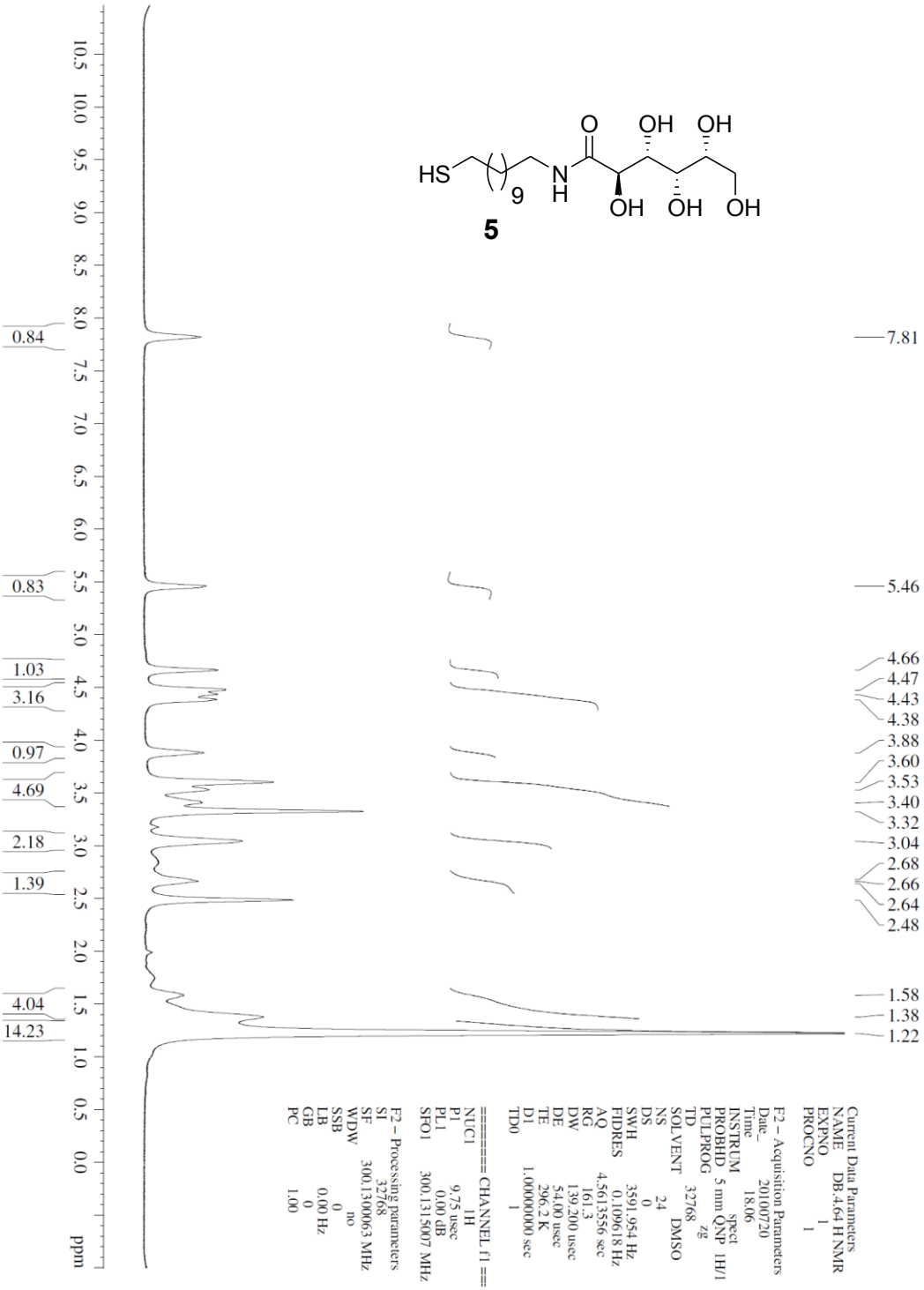
HS
9
N
H
O
OH
OH
OH
OH
OH
5
7.81
5.46
4.66
4.47
4.43
4.38
3.88
3.60
3.53
3.40
3.32
3.04
2.68
2.66
2.64
2.48
1.58
1.38
1.22
0.84
0.83
1.03
3.16
0.97
4.69
2.18
1.39
4.04
14.23
ppm
Current Data Parameters
NAME DB.4.64 H NMR
EXPNO 1
PROCNO 1
F2 – Acquisition Parameters
Date_ 20100720
Time 18.06
INSTRUM spect
PROBHD 5 mm QNP 1H/1
PULPROG zg
TD 32768
SOLVENT DMSO
NS 24
DS 0
SWH 3591.954 Hz
FIDRES 0.109618 Hz
AQ 4.5613556 sec
RG 161.3
DW 139.200 usec
DE 54.00 usec
TE 296.2 K
D1 1.00000000 sec
TD0 1
======== CHANNEL f1 ========
NUC1 1H
P1 9.75 usec
PL1 0.00 dB
SFO1 300.1315007 MHz
F2 – Processing parameters
SI 32768
SF 300.1300063 MHz
WDW no
SSB 0
LB 0.00 Hz
GB 0
PC 1.00

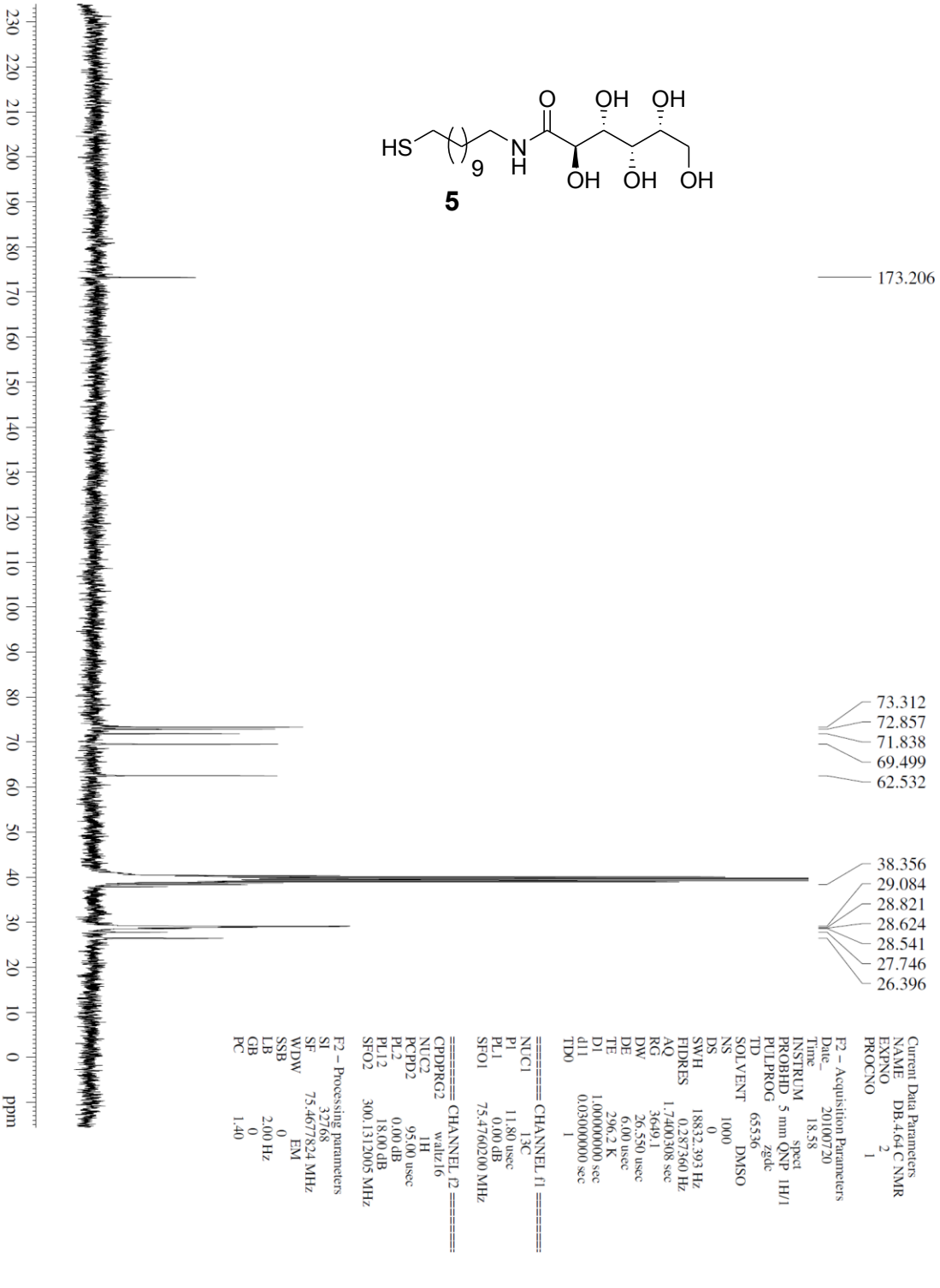
HS
9
N
H
O
OH
OH
OH
OH
OH
5
173.206
73.312
72.857
71.838
69.499
62.532
38.356
29.084
28.821
28.624
28.541
27.746
26.396
Current Data Parameters
NAME DB.4.64 C NMR
EXPNO 2
PROCNO 1
F2 – Acquisition Parameters
Date_ 20100720
Time 18.58
INSTRUM spect
PROBHD 5 mm QNP 1H/1
PULPROG zgdc
TD 65536
SOLVENT DMSO
NS 1000
DS 0
SWH 18832.393 Hz
FIDRES 0.287360 Hz
AQ 1.7400308 sec
RG 3649.1
DW 26.550 usec
DE 6.00 usec
TE 296.2 K
D1 1.00000000 sec
d11 0.03000000 sec
TD0 1
======== CHANNEL f1 ========
NUC1 13C
P1 11.80 usec
PL1 0.00 dB
SFO1 75.4760200 MHz
======== CHANNEL f2 ========
CPDPRG2 waltz16
NUC2 1H
PCPD2 95.00 usec
PL2 0.00 dB
PL12 18.00 dB
SFO2 300.1312005 MHz
F2 – Processing parameters
SI 32768
SF 75.4677824 MHz
WDW EM
SSB 0
LB 2.00 Hz
GB 0
PC 1.40
230 220 210 200 190 180 170 160 150 140 130 120 110 100 90 80 70 60 50 40 30 20 10 0 ppm

Chapter 4

Anti-Biofouling Chemistry of Chiral Polyol Monolayers: Enhancement of Biofilm Resistance on Racemic Surface[§]

Summary

Among the many approaches for controlling biofilm formation including the inhibition of quorum sensing or dispersing an already formed biofilm, one approach is to modify the surface chemistry to resist bacteria attachment and/or biofilm formation directly. Here, the synthesis of enantiomerically pure alkanethiols that terminate with different stereoisomer's of sugar alcohols, and the effect of chirality of these polyol-terminated SAMs on resisting biofilm formation is reported. Patterned SAMs of pentadecanethiol, surrounded by SAMs formed by alkanethiols terminated in D-gulitol, L-gulitol, D-mannonamide, L-mannonamide and racemic mixture of these alkanethiols, were presented to bacterial cell culture. Biofilm experiments were conducted in a flow cell using a red fluorescent *Escherichia coli* strain. The SAMs formed by racemic mixture of the polyol-terminated alkanethiols, were found to be more bioinert towards biofilm formation than the SAMs presenting the enantiomers alone. Biofilm formation on these patterned substrates was found to exhibit a well-resolved two-phase process. During the first phase of biofilm formation, the polyol-terminated SAMs allowed weak attachment of bacteria (probably though non-specific hydrogen bonds), while the hydrophobic

[§]Reproduced in part with permission from *Anti-Fouling Chemistry of Chiral Monolayers: Enhancing Biofilm Resistance on Racemic Surface* Debjyoti Bandyopadhyay, Deepali Prashar and Yan-Yeung Luk* *Langmuir*, **2011**, 27 (10), 6124–6131. Copyright 2011 American Chemical Society. Verbatim text in Arial font size 10 and identical figures are indicated in the legend.

pentadecanethiol SAMs were rendered temporarily bioinert, due to presence of adsorbed biomolecules (peptide and proteins). During the second phase of biofilm formation, the weakly attached bacteria migrated to, modified and attached on the hydrophobic pentadecanthiol SAMs, followed by growth and vertical development of biofilm. These results reveal the different chemistries that separate the different stages of biofilm formation, and the stereochemical influence on resisting biofoulings at a molecular-level.

4.1 Background and Significance

4.1.1 Biofilm formation is one consequence of quorum sensing

Since the discovery of bacteria by Antonie van Leeuwenhoek in 1676,[128] the scientific community has believed that bacteria can only exists as a unicellular organism and is not capable of showing any form of multicellular behavior. This view has changed significantly over the last ~40 years, since the discovery by Nealson, Platt and Hastings in 1970 that the marine bacterium *Vibrio fischeri* was capable of modulating its light producing ability based on its population density.[129] Later in 1981, Eberhard and co-workers discovered that *V. fischeri* was able to sense its population density, by secreting an extracellular signaling molecule identified as an acylated homoserine lactone (AHL).[130] Bacteria use small molecule signaling pathways to coordinate population wide gene expression through processes called quorum sensing and hence quorum sensing confers a form of multicellularity to the otherwise unicellular bacterium.[87] Quorum sensing initiates a number of processes including virulence factor production, antibiotic production, biofilm formation, swarming motility, bioluminescence, root nodulation, sporulation and conjugation.[131]

4.1.2 Different stages of biofilm formation

Biofilm formation is believed to occur in five stages, including initial reversible adhesion of planktonic microorganism, secretion of polymer matrix by the microorganism that leads to biofilm formation, biofilm maturation and eventual dispersion of biofilms.[18] The initial attachment can result from specific molecular recognitions such as that between pili proteins on the bacterial cell surface and mannose groups,[132] or between the adhesive matrix molecules and the adsorbed proteins on the host.[133-137] In the absence of specific recognition, bacteria can also attach to surfaces through nonspecific molecular interactions and proceed to form biofilms. In case of nonspecific adhesion, the amount of bacteria attached to the surface appears to be linearly proportion to the surface adhesiveness.[138]

Pseudomonas aeruginosa is an opportunistic pathogen, which can cause serious and sometimes life-threatening infection in patients suffering from cystic fibrosis (CF) or persons with a compromised immune system.[139] Psl, Pel and alginate are the major exopolysaccharides constituents of *P. aeruginosa* biofilm.[140-141] The polysaccharide synthesis locus (PA2235-2245) codes for the exopolysaccharide Psl, which allows the bacterium to attach to a surface and helps in maintaining the biofilm structure.[142-145] Wozniak and co-workers have used confocal laser scanning microscopy (CLSM) to visualize the Psl exopolysachharide, during the different stages of biofilm formation by *P. aeruginosa*.[146]

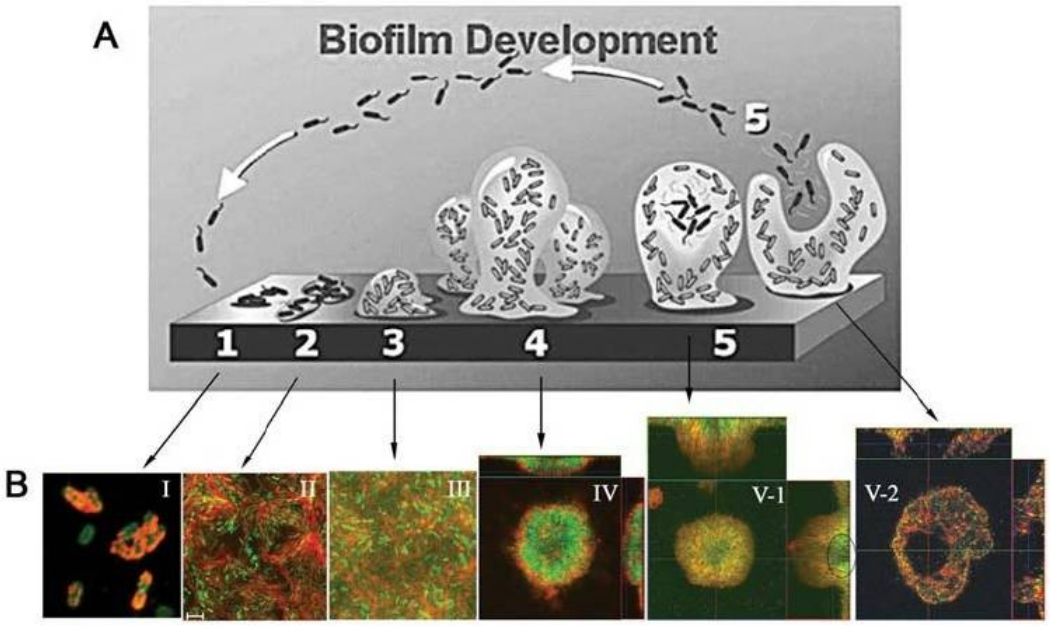

Figure 4.1 (A) Schematic representation of the five stages of biofilm formation. (B) Fluorescent micrographs of stained Psl matrix (red fluorescent) and *P. aeruginosa* (green fluorescent), during the different stages of *P. aeruginosa* biofilm formation. The black circle in image V-1 refers to the Psl matrix-free cavity. Figure adapted and modified.[18, 146] [Citation: Ma L, Conover M, Lu H, Parsek MR, Bayles K, et al. (2009) Assembly and Development of the *Pseudomonas aeruginosa* Biofilm Matrix. PLoS Pathog 5(3): e1000354. doi:10.1371/journal.ppat.1000354. Copyright: © 2009 Ma et al. This is an open-access article distributed under the terms of the Creative Commons Attribution License, which permits unrestricted use, distribution, and reproduction in any medium, provided the original author and source are credited].

During the initial stages, the Psl forms a helical coat around the bacterium, which helps the bacterium to attach to the surface, neighboring cells and to the biofilm matrix. During biofilm maturation, the Psl accumulates on the periphery of the 3-dimensional

microcolonies, which causes a Psl matrix-free cavity in the centre of the microcolony. During the dispersal stage, freely swimming cells, dead cells, cell lysis products such as enzymes and extracellular DNA appear in the Psl matrix-free cavity.[146] Figure 4.1 gives a schematic representation of the different stages of biofilm formation. Although the observations made by Wozniak and co-workers are specific to biofilms formed by *P. aeruginosa*, a similar set of events may be expected during biofilm formation by other bacteria. Quorum sensing plays a very important role during the development and maturation of bacterial biofilms.[147] lasI-lasR and rhlR-rhlI are the two cell-cell signaling systems identified in *P. aeruginosa*.[148-152] The lasI gene codes for a protein responsible for the synthesis of the extracellular diffusible signal, N-(3-oxododecanoyl)-L-homoserinelactone.[153] When the signaling molecules reach sufficient levels, it binds to the lasR protein, which leads to activation of a number of virulence genes including lasI and rhlR-rhlI.[153-156] Greenberg and co-workers have shown that while the wild-type *P. aeruginosa* PAO1 forms a mature and differentiated biofilm marked with lot of intervening space between the cells, the lasI-rhlI double mutant forms a thin and undifferentiated biofilm containing a high density of tightly packed cells.[147] Hence, quorum-sensing signals are involved during the maturation and differentiation of *P. aeruginosa* biofilms, but not necessarily during the initial stages of biofilm formation, attachment and proliferation.

4.1.3 Problems associated with biofilm formation

Unlike planktonic bacterial cells, sessile bacterial cells in a biofilm are resistant to antibiotic treatment and host defenses. Although antibiotics are able to treat the infection

caused by planktonic bacteria, antibiotics fail to eradicate the biofilm, which is the root cause of a persistent infection.[157] Even the antibodies produced in response to the antigens specific to the bacterial cells are unable to kill bacterial cells within a biofilm and instead cause damage to the surrounding host tissue.[158] Greenberg and co-workers have proposed three mechanisms by which bacterial cells within a biofilm resist antimicrobial treatment.[6] The first mechanism is that the extracellular polymeric substance (EPS) might be impermeable to antibiotics and hence protects the bacterial cells within a biofilm. The second mechanism is that the bacterial cells in the biofilm are in a starved and metabolically less active state. The metabolically less active bacterial cells in a biofilm will be less susceptible to antibacterial treatment than the planktonic bacterial cells. The third mechanism is that the bacterial cells within a biofilm have varying genetic makeup. While some bacteria might be susceptible to antibiotics, others might be genetically resistant to antibiotics and other antimicrobial agents.

Here, the use of enantiomerically pure alkanethiols that terminate with different stereoisomer's of sugar alcohol, and the effect of chirality of these polyol-terminated SAMs on resisting formation of biofilm by the bacterium *E. coli* is reported. We also report the enhancement of anti-fouling chemistry by using monolayers that consists of a racemic mixture of alkanethiols.

4.2 Results and Discussion

4.2.1 Patterning bacterial biofilms

While inhibiting quorum sensing[7, 159-162] or dispersing already formed biofilms by chemicals is one viable approach to reduce or eliminate the biofilms,[163-164] the other approach is to directly modify the surface chemistry to resist bacteria attachment and/or biofilm formation.[75-76, 138, 165-166]

To examine the bioinertness of monolayers formed by alditol-terminated alkanethiols (D-gulitol, **1** and L-gulitol, **1′**) and aldonamide-terminated alkanethiols (D-mannonamide, **2** and L-mannonamide, **2′**) (Scheme 4.1), circular patches (135 *μ*m in diameter) of pentadecanethiols surrounded by alkanethiols either **1**, **1′**, **2**, **2′**, or racemic mixtures of these enantiomers were prepared by microcontact printing (Figure 4.2).

Scheme 4.1

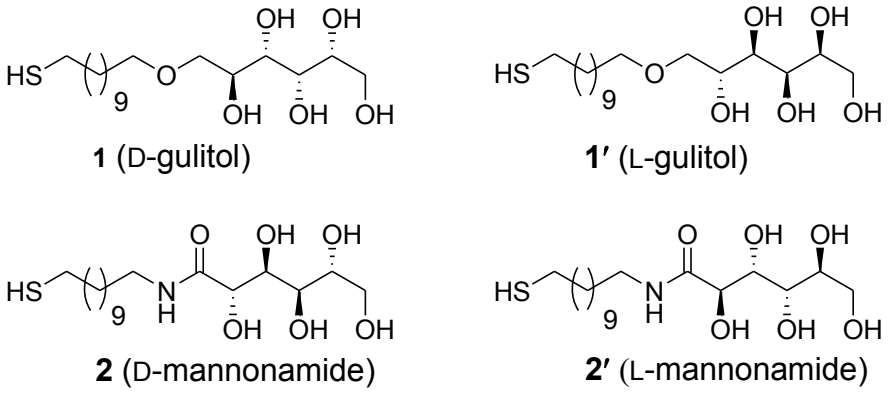

To measure the ability of these polyol-terminated monolayers at resisting the formation of biofilms by *E.coli* (RP437 engineered to express the Ds-Red-Express fluorescent protein),[76, 167] the patterned SAMs were placed in a flow cell and were inoculated with a bacteria-containing broth (OD_{600} = 0.05) for 1 h to allow the bacteria to attach to the surface. Culture media was then continuously flown through the channels and the formation of biofilm on the patterned SAMs was monitored by fluorescence microscopy.

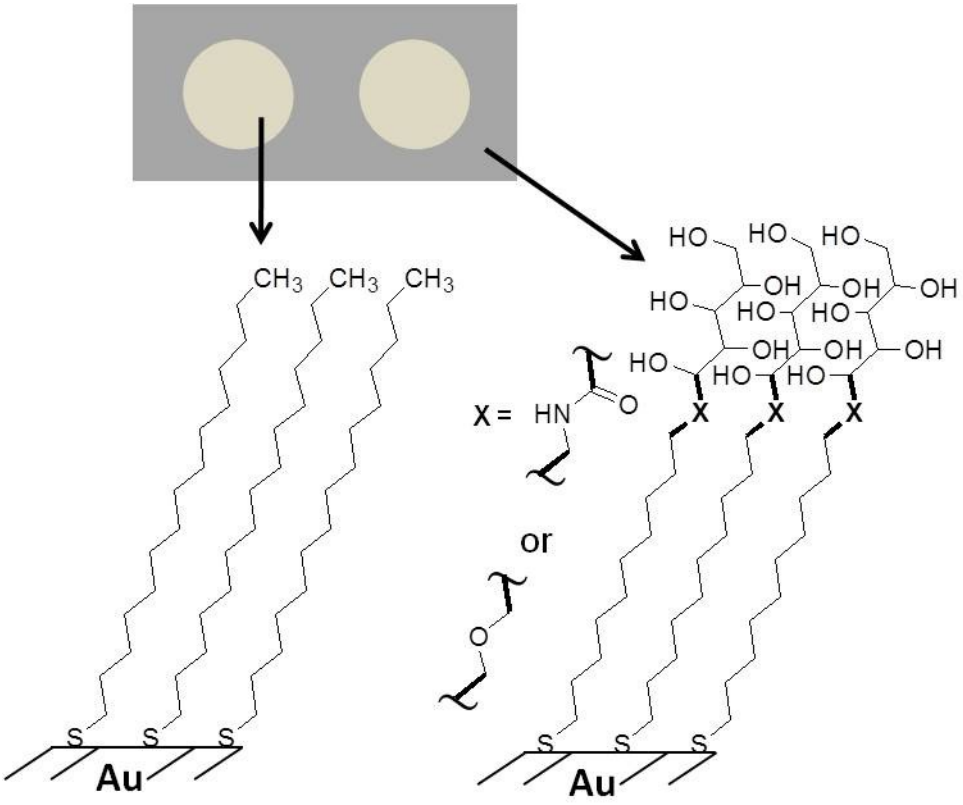

Figure 4.2 Schematic representation of patterned SAMs of pentadecanethiol, $HS(CH_2)_{14}CH_3$, surrounded by the alditol- or aldonamide-terminated SAMs on gold films. Figure adapted from the work by Luk and co-workers.[68]

4.2.2 Patterned substrates identify two-phase process of biofilm formation

The formation of biofilm on the patterned SAMs exhibited a well-resolved two-phase process. In the first phase, fluorescent signals started to appear over the first 6 hours mainly outside the circular patterns (135 *μ*m in diameter) on both the bare gold (Figure 4.3A) and polyol-terminated monolayers (Figure 4.3B); with visibly weaker fluorescent signal in the circular patterns. The fluorescent signal was weaker on the polyol-terminated monolayers than on bare gold. On smaller patches (95 *μ*m in diameter), this circular patterns of weaker fluorescence was not readily visible. In the second phase, beginning after about two days in the first phase, the patterns of the fluorescent signals started to reverse as the media continuously flowed through the channels.

The fluorescent signals outside the circular patterns disappeared (Figure 4.3C), and fluorescent signals emerged in and persisted over the circular patterns for rather long period of time (~ 20 days) in this phase (Figure 4.4). The circular patterns of biofilms were observed on SAMs presenting all four enantiomers of polyols (gulitols **1** and **1′**, and mannonamides **2** and **2′**), and on SAMs formed by a racemic mixture of each pair of enantiomers of the alkanethiols (Figure 4.4 and Figure 4.5). Surfaces presenting enantiomers are known to cause different levels of mammalian cell adhesion.[84-85] Here, the stronger resistance of biofilm formation by racemic monolayers suggest that the resistance of a chiral surface to biological entities (bacteria and biofilm formation) is also sensitive to the chirality of the molecules immobilized on the surface.

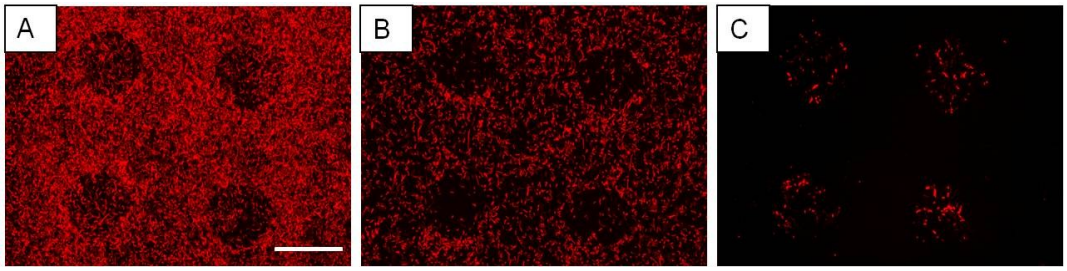

Figure 4.3 Fluorescent micrographs of biofilm formed by *E.coli* on patterned gold films. The patterned monolayers consist of circular regions of pentadecanethiolates surrounded by (A) bare gold at 6 hours, (B) by alkanethiol **1** at 6 hours and (C) at 3 days of bacteria culture. Fluorescent micrographs are representative of ten replicates of 135 *μ*m circular patterns (only four are shown). Scale bar = 152 *μ*m. Figure adapted from the work by Luk and co-workers.[68]

4.2.3 Polyol-terminated SAMs only allow initial reversible attachment of bacteria but resist long-term biofilm formation

The results here suggest that polyol-terminated SAMs supported initial and reversible attachment of bacteria (Figure 4.3B) in the first phase of the experiment, but resisted the subsequent biofilm formation in the second phase, which included the secretion, attachment and vertical development of biopolymer matrix. As a result, the reversibly attached bacteria detached

over time, and the biofilm only forms on the patterned regions (Figure 4.3C). As time progresses, both the gulitol- and mannonamide-terminated monolayers exhibited resistance to biofilm formation. Interestingly, at 20 days (Figure 4.4 and Figure 4.5), fluorescent signals on the bio-inert SAMs presenting the racemic mixture of enantiomers were considerably lower than that on bio-inert SAMs presenting just the enantiomers alone. This observation suggests that SAMs presenting racemic mixture of enantiomeric alkanethiols (gulitol or mannonamide) is more resistant to biofilm formation than SAMs presenting a single enantiomeric alkanethiol. These two phases of experimental observations match the two distinct stages of the metabolic activities modeled for nonspecific bacterial adhesion. First stage involves the reversible contacts of planktonic bacterial cells, and the second stage involves the synthesis and secretion of adhesive polymers that lead to irreversible attachment and biofilm formation.[165, 168-172] These results indicate that both stages are observed on different locations of the same patterned surface due to the bioinertness of chiral monolayers at resisting biofilm formation (second stage) but not reversible attachment (first stage).

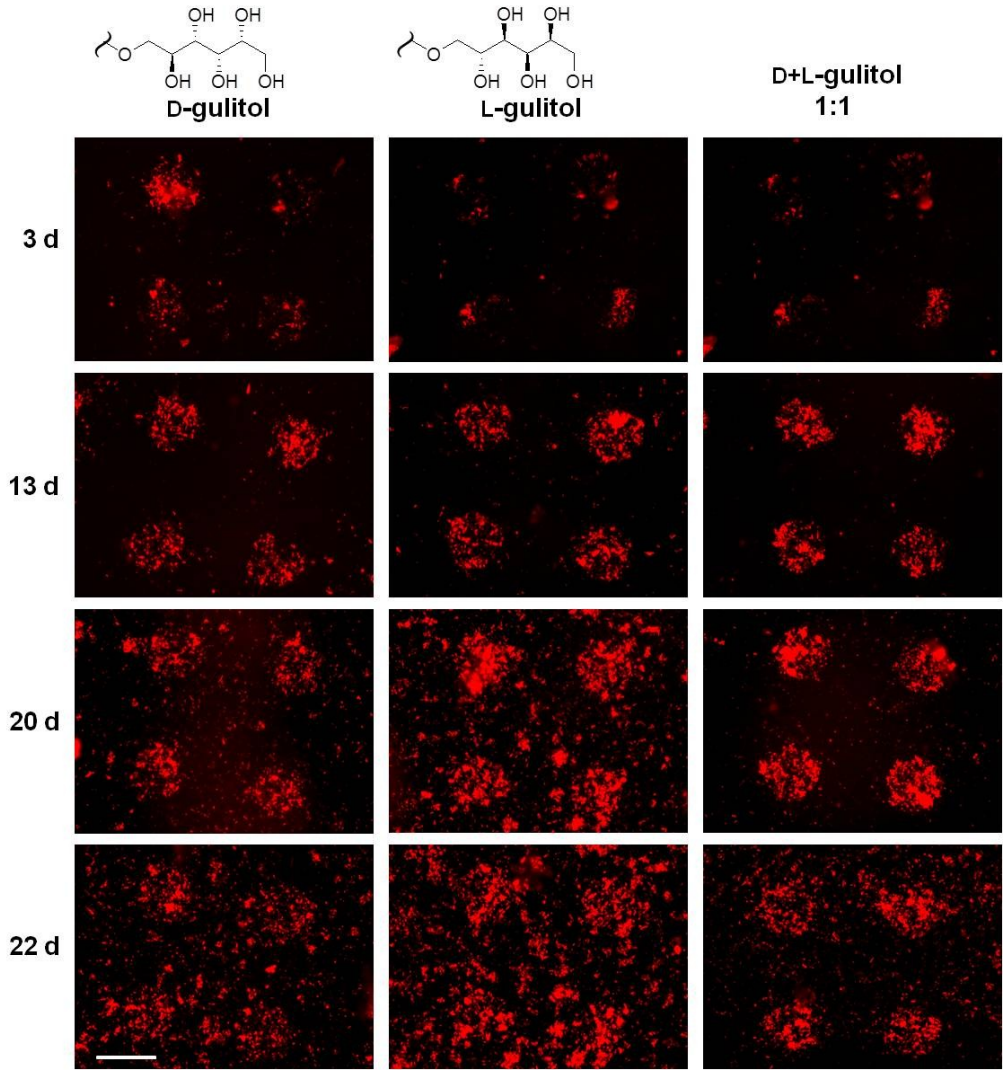

Figure 4.4 Fluorescent signal of biofilm formed by *E.coli* on patterned SAMs on gold films. The patterned chemistry consists of circular regions of pentanedecanethiolates surrounded by SAMs formed by **1**, **1′**, or their racemic mixture. The stereochemistry of the polyols is shown above the fluorescent micrographs. The number of days in the culture is shown to the left. Fluorescent micrographs are representative of ten replicates of 135 *μ*m circular patterns (only four are shown). Scale bar = 152 *μ*m. Figure adapted from the work by Luk and co-workers.[68]

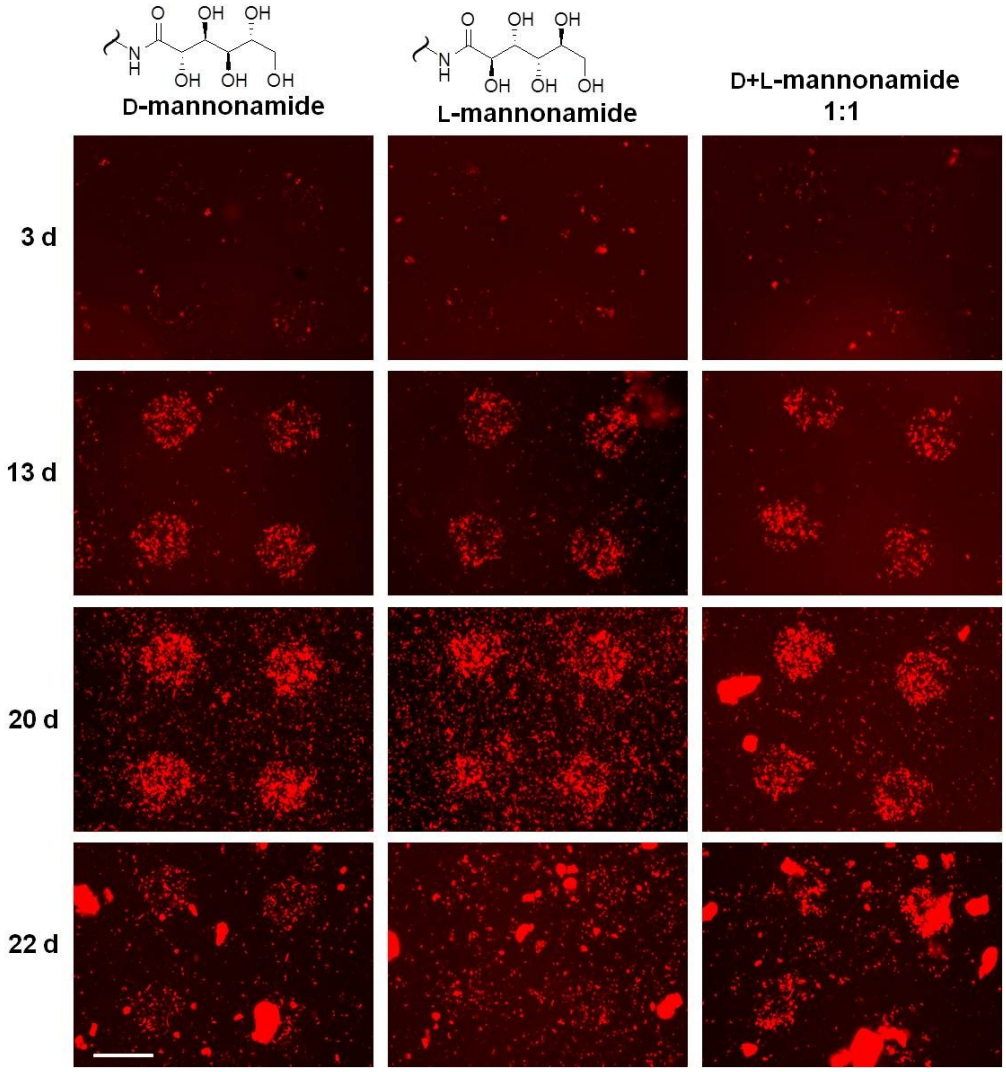

Figure 4.5 Fluorescent micrographs of biofilm formed by *E.coli* on patterned SAMs on gold films. The patterned chemistry consist of circular regions of pentanedecanethiolates surrounded by SAMs formed by **2** (D-mannonamide), **2′** (L-mannonamide), or their racemic mixture. The stereochemistry of the polyols is shown above the fluorescent micrographs. The number of days in the culture is shown to the left. Fluorescent micrographs are representative of ten replicates of 135 μm circular patterns (only four are shown). Scale bar = 152 μm. Figure adapted from the work by Luk and co-workers.[68]

4.2.4 Rationale behind observing two-phase process of biofilm formation on patterned substrates

Protein adsorption on surfaces is known to render surfaces bioinert, usually for a rather short period. For instance, bovine serum albumin (BSA) is used as a blocking agent for many surface-based bioassays.[173] The adsorbed proteins on the surface go through structural changes over time. During the early stages of protein adsorption, a hydrated layer of water will likely be formed due to the presence of adsorbed proteins, regardless of the degree of protein denaturation. Over time, protein denaturation on surface will allow bacteria and their secreted biopolymers to further modify the surface, which results in losses of the initial temporary bioinertness. At the first phase of biofilm formation (Figure 4.6A) on these surfaces, adsorbed biomolecules (proteins and peptides) on the methyl-terminated surfaces in the micro-contact printed patterns prevented bacteria attachment and biofilm formation temporarily, whereas the polyol-terminated monolayers allowed some weak, reversible attachment of bacteria possibly through non-specific hydrogen bonds. Furthermore, the bioinertness of the polyol SAMs may be more easily impaired at location where there were defects in the polycrystalline gold films than that by oligo(ethylene glycol)-terminated SAMs. Thus, another important parameter is the study of the influence of topography and polycrystallinity on the antifouling chemistry. The preconditioning of the hydrophobic surface was overcome by the increase in population of bacteria over time. Assisted by the flow of the media, the weakly attached bacteria may detach and migrate, modify and attach to the hydrophobic patterns of methyl-terminated SAMs, which further supported the attachment and development of the secreted biopolymer matrix, and the vertical development of biofilm formation (Figure 4.6B).

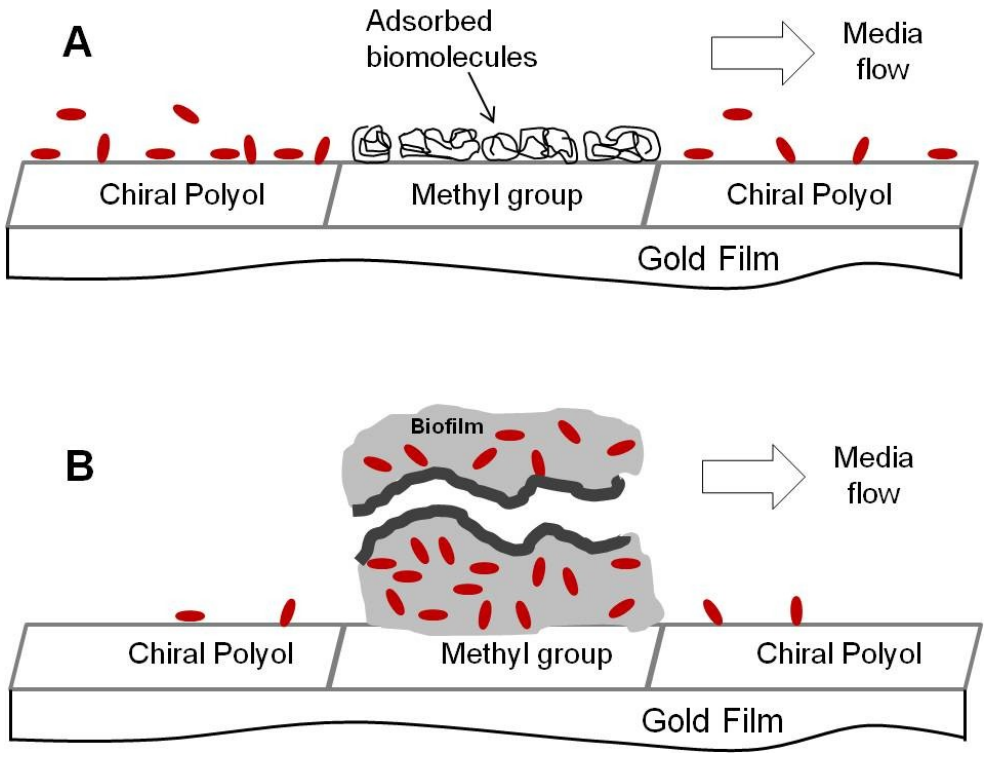

Figure 4.6 Proposed two phases, (A) and (B), of biofilm formation on chiral monolayers of polyol-terminated alkanethiolates surrounding micrometer sized patterns of methyl-terminated monolayers on gold film. Red ovals represent *E.coli* expressing red fluorescent protein. Figure adapted from the work by Luk and co-workers.[68]

4.2.5 Amine SAMs prevents bacterial attachment during initial period of biofilm formation.

Formation of biofilm in a flow cell was studied on patterned substrates where amine-terminated SAMs (Chapter 3) or D-gulitol-terminated SAMs surrounded circular patterns of methyl-terminated SAMs. Fluorescent signals started to appear outside the circular patterns on the D-gulitol SAMs over the first 6 h, with visibly weaker fluorescent signals within the circular patterns (Figure 4.7 A). Interestingly, the fluorescent signal outside the circular patterns on the amine SAMs were weaker over the first 6 h, with visibly stronger

fluorescent signals within the circular patterns (Figure 4.7 B). Based on results presented earlier, the pattern of fluorescent signal observed on for the D-gulitol SAMs matched the pattern expected for polyol SAMs, where the D-gulitol SAMs allowed temporary reversible attachment of bacteria probably via hydrogen bonds, while the methyl SAMs were probably rendered temporarily bioinert due to the presence of a hydrated layer of protein. The chaotropic character of amine SAMs was demonstrated in Chapter 3, where amine SAM supported rapid mammalian cell adhesion. On patterned substrates where amine SAMs surrounded patterned squares of methyl SAMs, adhered mammalian cells were only observed on regions presenting amine SAMs on day 1of mammalian cell culture. Over a short period of 3 days, a complete monolayer of adhered mammalian cells covered the entire surface. Hence, the chaotropic nature of the amine groups probably caused rapid adsorption of a layer of proteins or other biomolecules on the amine SAMs and was thus rendered temporarily bioinert. These results further prove the chaotropic nature of amines on surfaces.

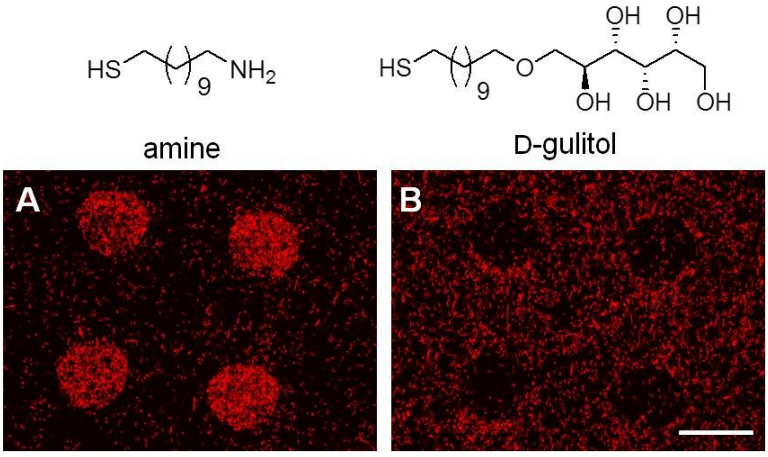

Figure 4.7 Fluorescent micrographs at 6 h from bacterial culture with *E.coli* on patterned SAMs on gold films where circular patterns of methyl-terminated SAMs are surrounded by (A) amine-terminated SAMs and D-gulitol-terminated SAMs. Fluorescent micrographs are representative of ten replicates of 135 μm circular patterns (only four are shown). Scale bar = 152 μm.

4.2.6 Kosmotropic character of polyols is the basis for the resistance towards biofilm formation of surface presenting polyols

As kosmotropes that stabilize native protein folding have been believed to be preferentially excluded from proteins due to the water organization in their solvation shells,[103-106] one possible mechanism for the antifouling chemistry of polyol-terminated monolayers is that these kosmotrope-coated surfaces create an interfacial solvation layer that exclude the secreted polymers required for biofilm formation. Proteins, bacterial and mammalian cells have different ability to penetrate the solvation layer for surface attachment. Bacteria and mammalian cells themselves involve secretion of proteins and biopolymers, which further complicates and increases the challenges for designing a single surface chemistry that can resist all different kind of biofouling processes. Consistent with this information, this study reveals that chemistry that resists biofilm formation may not resist bacterial cell attachment. However, based on this and past studies,[74, 76] it might be correct to say that a surface chemistry capable of long-term resistance to

biofilm formation and mammalian cell adhesion should be on a gross scale resistant to protein adsorption. Collectively, these studies support a "kosmotrope" theory,[74, 96] which suggest that molecules that can stabilize the native folding of protein, when immobilized on a surface, can also resist protein adsorption. Particularly, what contributes to the stability of a folded protein has also been a daunting problem, and among many theories or arguments, the nature of the water solvation shells of the solutes is considered to be of primary importance.[174] It should be noted that the optimal chain length of alkanethiol for bioinertness is likely different between oligo(ethylene glycol) and polyols on monolayers. Thus, the number of methylene units in the alkanethiols is another parameter for optimization when developing specific applications.

4.2.7 A hypothesis for the enhanced resistance of racemic SAMs towards biofilm formation

Interestingly, when two enantiomers are mixed, there are three possible modes of assemblies or aggregates. These assembly structures include conglomerate, racemic compound and solid solution.[175] These three forms of assemblies have different properties including solubility in water. For SAMs consisting of a racemic mixture of enantiomeric alkanethiols, it is not clear which assembly exists in the polyol head groups of the monolayer. However, the hydration of surface of the "racemic monolayer" will be different from that of surface of "enantiomeric monolayer". The packing of racemic polyol groups, and the more rigid conformation of the polyol may provide a different hydration than that by oligo(ethylene glycols). Because monolayers formed by both pairs of enantiomers exhibited enhancement of bioinertness when racemic mixtures are used, this racemic enhancement effect is likely a general phenomenon.

4.2.8 The Bioinert Bowl: Studying bacterial behavior in a completely bioinert environment

Biofilm formation has five stages, including initial reversible adhesion of planktonic bacteria, secretion of polymer matrix by bacteria that leads to biofilm formation, biofilm maturation and eventual dispersion of biofilms.[18] Although the different stages of biofilm formation are well described in the literature, the literature is only limited to a specific species of bacteria such as *P. aeruginosa*.[146] Although the process of biofilm formation may be similar for different bacteria, biofilm formation may be fundamentally different (at least at the molecular level) for different bacterial species. Moreover, it is questionable if bacterial surface attachment is a prerequisite for bioflm formation or not. It is important to find the answers to some intriguing questions: what happens when you deny bacteria a surface for attachment? Over production of the extracellular polymeric substance (EPS) in mutant strains of *Pseudomonas fluorescens*, is reported to enable the bacterium to form biofilms at the air-liquid interface.[176] So, if we deny bacteria a surface for attachment, can biofilm form in solution or at the air-liquid interface? It is possible that the mechanism of biofilm formation in solution or at the air-liquid interface is fundamentally different from that on a surface.

D-mannitol-terminated alkanethiol,[74, 92] was used to form bioinert SAMs on a gold-coated glass bowl, named the "bioinert bowl". The "bioinert bowl" can allow us to control bacterial behavior, by denying the bacteria a surface for attachment (Figure 4.8). In a flow cell or static culture containing gold substrates modified with D-mannitol or any other bioinert SAM, bacteria can go elsewhere for attachment (Figure 4.8), which is not possible in case of the "bioinert bowl". It would be interesting if biofilm formation (if

any) in the "bioinert bowl" is associated with a fundamentally different mechanism of biofilm formation or a genetically altered form of bacteria. Environmental stress is known to initiate biofilm formation and the biofilm further protects the bacteria within it from stress.[5, 18] It is possible that the absence of a surface for attachment can also be perceived by the bacterium as stress.

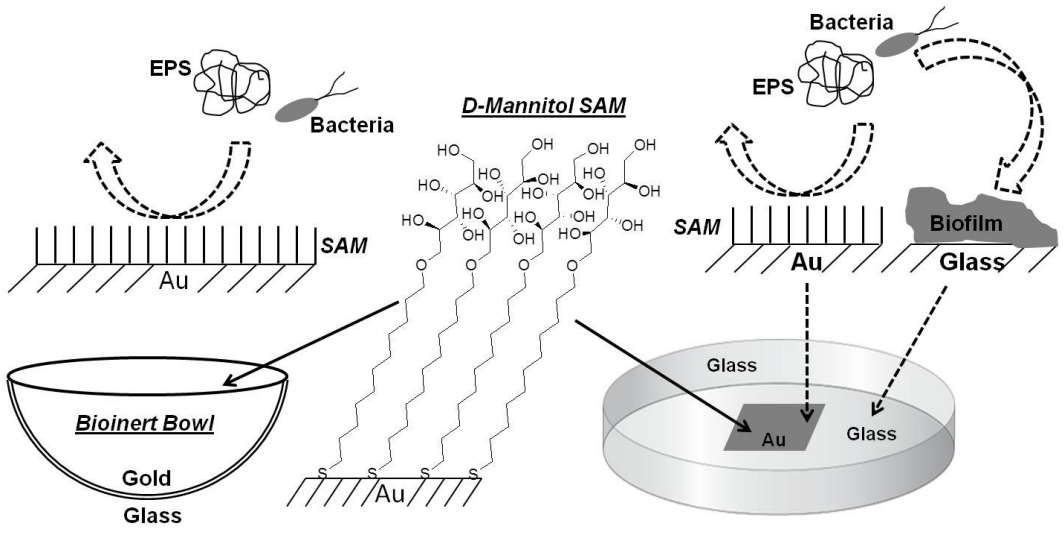

Figure 4.8 (Left) Gold-coated glass bowl modified with bioinert D-mannitol-terminated alkanethiolate self-assembled monolayers (D-mannitol SAM) (Bioinert Bowl), which denies surface attachment of bacteria or attachment of extracellular polymeric substance (EPS) secreted by the bacteria. (Right) A glass petridish containing a gold substrate modified with D-mannitol SAM. Here, although the SAM modified gold substrate resists the attachment of bacteria or EPS and subsequent biofilm formation, the bacteria can go elsewhere such as the base and wall of the glass petridish, which allow attachment of bacteria or EPS and subsequent biofilm formation.

The bacteria *E. coli* RP437 was grown under static conditions at 37 °C in the bioinert bowl and a glass bowl for 24 h. After 24 h, both the bioinert bowl (Figure 4.9 A1) and

glass bowl (Figure 4.9 A3) had the presence of surface unattached biomass settled at the bottom of the bowls. This surface *unattached* "biomass" is referred to as "bio-aggregate", to differentiate it from surface *attached* biofilm. Interestingly, biofilm was not clearly visible in case of the bioinert bowl (Figure 4.9 A2), but was clearly visible in case of the glass bowl (Figure 4.9 A4). In order to stain the biofilm present in the bowls, the bacterial culture and bio-aggregate was removed from the bowls and the bowls were treated with aqueous 0.1% crystal violet.[177] Crystal violet staining revealed that the amount of biofilm was much less in case of the bioinert bowl (Figure 4.9 B1), as compared to the amount of biofilm in the glass bowl (Figure 4.9 B2).

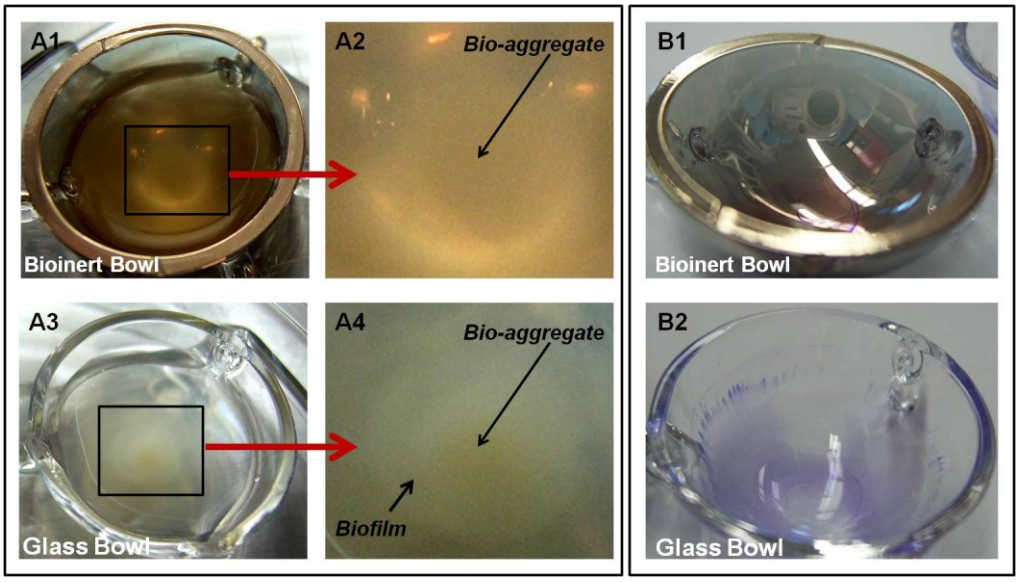

Figure 4.9 The bioinert bowl (A1) and the glass bowl (A3) after 24 h of bacterial culture. The enlarged view of the bioinert bowl (A2) showing the presence of surface unattached bio-aggregate and enlarged view of the glass bowl (A4) showing the presence of both surface unattached bio-aggregate and surface attached biofilm. Crystal violet stained bioinert bowl (B1) and glass bowl (B2), after 24 h of bacterial culture.

Although bio-aggregate formation can occur in both the bioinert bowl and glass bowl, the bioinert bowl can resist biofilm formation. It is possible that the bacteria associated with the bio-aggregate in the bioinert bowl, has a different genetic makeup than the bacteria associated with the bio-aggregate in the glass bowl. The stress which the complete bioinert environment of the bioinert bowl presents to the bacteria (in the form of denying a surface for attachment), might cause the bacteria to develop mutations against the stress and hence alter its genetic makeup.

Since the bioinert and glass bowls were approximately of the same size and surface area, the amount of biofilm present in bowls could be estimated by crystal violet staining.[177] The bowls were stained with crystal violet dye and the optical density at 600 nm (OD_{600}) of the solution containing the dissolved crystal violet dye in 95% ethanol was measured after 6 h and 24 h of bacterial culture. After 6 h, the OD_{600} value for both the bioinert bowl and glass bowl were found to be similar, although the OD_{600} value for the glass bowl was slightly higher than that for the bioinert bowl. After 24 h, the OD_{600} value for the bioinert bowl was approximately 50% of the OD_{600} value for the glass bowl (Table 4.1).

Table 4.1 OD_{600} values from crystal violet stained biofilm in the bioinert bowl and glass bowl after 6 h and 24 h.

Entry	Time (h)	OD_{600} Values from Crystal Violet Stained Biofilm	
		Bioinert Bowl	Glass Bowl
1.	6 h	0.123	0.170
2.	24 h	0.209	0.411

Since negligible amount of biofilm was formed in the bioinert and glass bowl after 6 h of bacterial culture (images not shown), the OD_{600} values at 6 h is probably due to background staining of the bowls by the crystal violet dye. Moreover, since the OD_{600} values at 6 h were similar for the bioinert and gold bowl, the background staining is approximately same for both the bioinert and glass bowl. Hence, it can be concluded that after 24 h, the amount of biofilm present in the bioinert bowl is much less than the amount of biofilm present in the glass bowl (after adjusting for any background staining).

These observations agree with the results from the formation of biofilm on patterned substrates in a flow cell, where polyol-terminated bioinert SAMs surrounded circular patterns of methyl-terminated (pentadecanethiol) SAMs. Within 6 h of bacterial culture on these patterned substrates, the fluorescent signal was significantly higher on the regions presenting the polyol SAMs than on methyl-terminated SAMs. After two days, the patterns of the fluorescent signals started to reverse as the media continuously flowed through the channels. The fluorescent signals outside the circular patterns disappeared, and fluorescent signals emerged and persisted over the circular patterns for rather long period. This observation was rationalized based on the initial temporary bioinertness of the methyl-terminated SAMs, due to the presence of a hydrated layer of adsorbed proteins that can prevent bacterial attachment, whereas the polyol-terminated SAMs allowed temporary bacterial attachment possibly via to non-specific hydrogen bonding between the polyol SAMs and the bacterial cell surface. During the initial 6 h period, the bioinert bowl and glass bowl might allow temporary attachment of bacterial cells or adhesion of proteins and contribute to the background OD_{600} values of 0.123 and 0.170 respectively (Table 4.1). After 24 h, while the bacterial cells could form biofilm on the surface of the glass bowl ($OD_{600} = 0.411$), the bioinert bowl could resist formation of biofilm ($OD_{600} = 0.209$) (Table 4.1).

4.3 Conclusions

The molecular interactions governing the different stages of biofilm formation are likely different. The results presented here on resisting biofilm formation indicate that the polyol-terminated SAMs can distinguish interactions between the first two and the rest of the stages of biofilm formation. These findings suggest a powerful and potentially general antifouling approach

by integrating multiple surface chemistries that resist different stages of biofilm formation. In addition, the monolayers formed from a racemic mixture of enantiomeric polyol-terminated alkanethiols are more resistant to biofilm formation than monolayers consisting of either of the single enantiomers.

4.4 Experimental Section

Chemicals. 1-Pentadecanethiol was purchased from Aldrich Chemicals (Milwaukee, WI) and used as received. Ethanol was used as a solvent for preparing all alkanethiol solutions and for washing SAMs on gold films. Minimum amount of DMSO was mixed with ethanol for solubilizing polyol-terminated alkanethiols, which were poorly soluble in pure ethanol. Water used had a resistivity of 18 MΩ cm (Millipore, Billerica, MA).

Cleaning of Glass Substrates. Substrates for the gold films were Fisher's finest premium microscope slides (Fisher Scientific, Pittsburgh, PA). Prior to gold deposition, the slides were cleaned with piranha solution. The slides were soaked in piranha solution (3 parts of 35% H_2O_2 in water and 7 parts of concentrated H_2SO_4) at 70 °C for 45 min. **Warning!** *Piranha solution is extremely corrosive and also has the potential for detonation if contaminated with a significant amount of oxidizable material.* After cooling, the piranha solution was poured off and the slides were rinsed 20 times with water having a resistivity of 18 MΩ cm (Millipore, Billerica, MA), followed by 10 rinses of ethanol and 10 rinses of methanol. The slides were then dried individually with a stream of nitrogen gas and stored in an 80 °C oven overnight.

Gold Deposition on Glass Substrates. Semitransparent gold film of approximately 280 Å thickness were deposited onto the piranha-cleaned glass substrates with an electron beam evaporation system from Thermionics (Port Townsend, WA). A layer of titanium (approximately 70 Å thick) was applied first for adhesion of the gold film. Films were deposited at an oblique angle of 45° to the normal of the substrate. The rates of deposition were set at 0.2 Å/s for both gold and titanium. Pressure was maintained at or below 2×10^{-6} Torr throughout the deposition.

Microcontact Printing. Microcontact printing was done using polydimethylsiloxane (PDMS) stamps using slight modifications of literature reported procedures.[39] Briefly, gold slides were cut into approximately 1.0 cm × 1.0 cm pieces (gold substrates), rinsed with ethanol and then dried with a stream of nitrogen gas. PDMS stamps were dabbed with 2.0 mM solution of pentadecanethiol, dried with a stream of nitrogen gas and placed on the gold substrates to allow conformal contact for 20 seconds. The substrates were then rinsed with ethanol, dried with a stream of nitrogen gas and placed in 0.2 mM solutions of alkanethiols **1**, **1′** and 0.2 mM solution containing 1:1 mixture of the enantiomers **1** and **1′**; 1 mM solutions of alkanethiols **2**, **2′** and 1 mM solution containing 1:1 mixture of the enantiomers **2** and **2′** for 15 h. The substrates were then taken out of the solution rinsed with ethanol and dried with a stream of nitrogen gas before using them in bacterial cell culture.

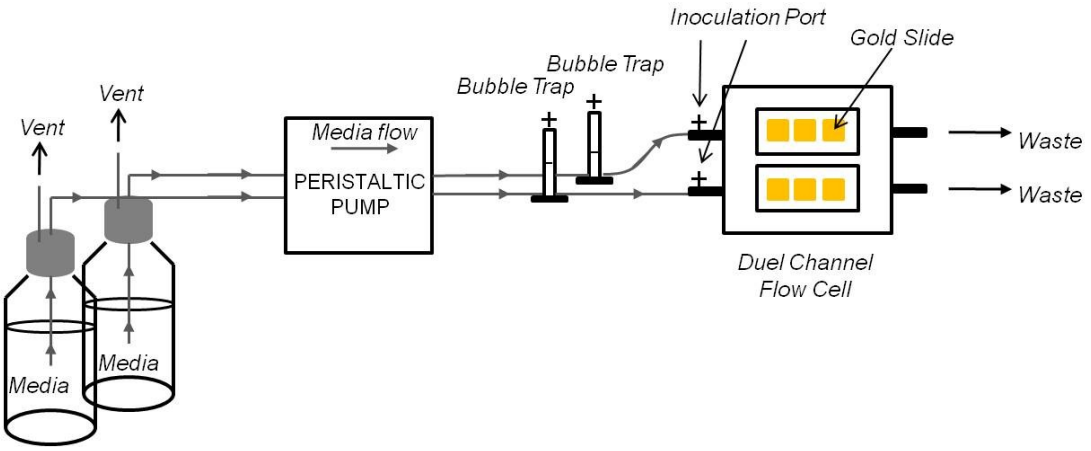

Figure 4.10 Set up of the flow cell experiment. Figure adapted from the work by Luk and co-workers.[68]

Bacterial Cell Culture on SAMs in a Flow Cell. Overnight culture of *E.coli* RP437 engineered to express the Ds-Red-Express fluorescent protein[76, 167] was grown in Luria-Bertini broth supplemented with 10 *μ*g/mL of Tetracycline and diluted to an optical density of 0.05 at 600 nm (OD_{600} = 0.05) measured by a Genesis 5 spectrophotometer (Spectronic Instruments, Rochester, NY). SAM modified gold substrates were placed in a dual channel flow cell (anodized aluminum

FC 281, BioSurface Technologies Corporation, Bozeman, MT). The slides were incubated in 5× diluted Luria-Bertini broth supplemented with 10 μg/mL of Tetracycline flowing at a rate of 10 mL/hour using a Masterflex L/S variable-speed economy drive peristaltic pump (Cole-Parmer, Vernon Hills, IL) for 20 min at ambient temperature. After stopping the flow of media, each channel was inoculated by injecting into the channels 20.0 mL of bacteria-containing broth (OD_{600} = 0.05). The flow of media (10 mL/h) was reintroduced after 1 h of inoculation to allow the bacteria to attach (Figure 4.10 shows the set up of the flow cell experiment). The formation of biofilm was monitored using an Axio Imager M1 microscope (Carl Zeiss MicroImaging GmbH, Göttingen, Germany). Fluorescent images were captured every day using an AxioCamMR3 camera and processed with AxioVision Release 4.6 digital imaging software (Carl Zeiss). Fluorescent micrographs presented are representative of ten replicates of 135 μm circular patterns.

Bacterial Culture in Bioinert and Glass Bowl. 1.5 mL of 1 mM solution of D-mannitol-terminated alkanethiol in EtOH was poured into a gold-coated glass bowl and the glass bowl was placed in chamber saturated with vapors of EtOH overnight. Overnight culture of *E.coli* RP437 was grown in Luria-Bertini broth supplemented with 20 μg/mL of streptomycin and diluted to an optical density of 0.05 at 600 nm (OD_{600} = 0.05) measured by a Genesis 5 spectrophotometer (Spectronic Instruments, Rochester, NY). The D-mannitol-terminated SAM modified bioinert bowl and an unmodified glass bowl was rinsed with EtOH, blow dried with a stream of N_2(g) and placed in a sterile chamber, saturated with water vapor. The bowls were hydrated by adding 1 mL of sterile water for 1 h, the water was then removed and replaced with 1 mL of the bacterial culture with OD_{600} = 0.05. The bowls were then incubated at 37 °C for the next 24 h. After 6 h, any biofilm formed in the bowls was stained with crystal violet dye. Briefly, the bacterial

broth was removed from the bowls and the bowls were air dried for 20 min. The bowls were then rinsed with water (1 mL × 3) and then air dried again for 20 min. 1 mL of 1% CV solution in water was then added to the bowls which were then placed at rt for 30 min. After 30 min, the crystal violet solution was removed and the bowls were washed with water (1 mL × 3) and then air dried for 20 min. 1 mL of 95% EtOH was then added to the bowls and the bowls were placed at rt for 30 min. The 95% EtOH solution containing the dissolved CV dye was then gently mixed and then the OD of the solution was measured at 600 nm. The same steps of staining the biofilm with CV dye were repeated for another set of bionert and glass bowls after 24 h. Images of the bowls were also acquired before and after staining with CV.

Chapter 5

Evaluating the Ability of Self-Assembled Monolayers of Polyol-Terminated Alkanephosponic Acids on Titanium oxide (TiO_2) to Resist the Adhesion of Mammalian Cells and as Water-Soluble Coatings for Magnetite (Fe_3O_4) Nanoparticles

Summary

The synthesis and use of end-functionalized alkanephosphonic acids terminated in the sugar alcohols D-mannitol, L-mannitol and D-gulitol to form chiral polyol-terminated self-assembled monolayers (SAMs) on metal oxide thin films or nanoparticles is reported. A facile and efficient synthesis of D-gulitol modified Fe_3O_4 (magnetite) nanoparticles (D-GPA MNPs) is also reported. The D-GPA MNPs were synthesized by treating magnetite nanoparticles (MNPs) with a solution of D-gulitol-terminated alkanephosphonic acid in dimethyl sulfoxide (DMSO) under ambient conditions. The D-GPA MNPs were soluble in water and the dispersion of D-GPA MNPs remained stable in water for long periods. Although the D-GPA MNPs were found to precipitate out of solution over time, the D-GPA MNPs could be readily dispersed back into solution by simply agitating the solution. These water-soluble D-GPA MNPs have potential applications in the field of magnetic resonance imaging (MRI) contrast agents, drug delivery and hyperthermia.

5.1 Background and Significance

Self-assembled monolayers (SAMs) are a convenient system for tailoring the surface properties of metal and metal oxide thin films and nanoparticles. Controlling the surface

and interfacial properties of metal or metal oxide thin films and nanoparticles is imperative for integration of these materials for wide variety of applications.[39, 178] On thin films, SAMs are used as etch resists, templates for crystallization and model surfaces for biological and electrochemical studies.[39] The properties of nanoparticles are strongly dependent on their size and shape. To obtain highly monodispersed particles, it is desirable to achieve rapid nucleation, followed by controlled growth to achieve monodispersity.[179] During the synthesis of nanoparticles, surfactants are added to control the growth and prevent aggregation of the nanoparticles. The surfactants form SAMs on the surface of the nanoparticles and act as physical[178] or electrostatic barrier[180] to prevent aggregation of the nanoparticles.

Commonly used SAMs are based either on the interaction of reactive silanes[181] with OH-terminated oxide surfaces or chemisorption of alkanethiols on gold.[39] While silanes may lead to formation of films thicker than a monolayer, due to uncontrolled polymerization, alkanethiols involve the use of expensive materials such as gold or silver. The siloxane products of silanization are also hydrolytically unstable and this limits their use under aqueous conditions.[182] Gold is also undesirable for studies involving fluorescence microscopy since gold has a tendency to quench fluorescence signals.

Self-assembled monolayers (SAMs) of alkanethiolates on gold have been widely used as model substrates for studying biofouling due to protein adsorption,[28, 68-69, 74] mammalian cell adhesion[29, 69, 74] and biofilm formation,[68, 75-76] but alkanethiolate SAMs on gold and silver substrates are not stable for long periods due to oxidation of the thiol head group.[183] Hence, it is highly desirable to have a new surface chemistry, which can form robust SAMs on technologically more relevant but less expensive substrates.

Alkanephosphonic acids are common coatings for surface of native metal oxide or alloys such as iron,[44] steel,[45] aluminum,[45-46] copper[45] and even mica.[48] Raven and co-workers have reported that dense and highly ordered monolayers can be prepared by the adsorption of octadecylphosphonic acid onto nonporous ZrO_2, TiO_2 and zirconated silica powders.[46] As a substrate, titanium is highly desirable because it combines the strength of steel and lightweight of aluminum. Titanium is also resistant to corrosion under ambient conditions and has wide application in industry, medical implants and devices.[184-185] The exposure of the bare surface of titanium metal or its alloys to oxygen results in spontaneous formation of an oxide layer,[186-188] which protects the metal against corrosion. Schwartz and co-workers have reported that assembling alkanephosphonic acids from solution onto TiO_2 followed by gentle heating, provides an alkanephosphonate monolayer which is strongly surface-bound, unlike the monolayers formed without this heat treatment which can be easily washed away by solvent rinse.[47] Titanium is also a desirable material for medical implants.[189] While mammalian cell adhesion is undesirable for certain titanium based medical implants, such a cardiovascular implants,[190] it is desirable for titanium based bone implants for better osseointegration.[191] Schwartz and co-workers reported that the bonding of the tripeptide arginine-glycine-aspartic acid (RGD), on a monolayer of 11-hydroxyundecylphosphonate on titanium or titanium alloy Ti-6Al-4V, facilitates attachment and spreading of human osteoblasts.[192] Self-assembled monolayers (SAMs) of polyol-terminated alkanethiol on gold have been reported to resist different biofouling processes such as protein adsorption,[68-69, 74] mammalian cell adhesion[69, 74] and biofilm formation[68, 75-76] but it is highly desirable to transfer the bioinert

chemistry of the polyol SAMs on gold to a technologically more relevant material such as titanium.

Magnetic iron oxide nanoparticles are desirable in medical applications for targeted drug delivery, magnetic resonance imaging (MRI) contrast agents, detoxification of biological fluids, hyperthermia and cell separation.[178] Gedanken and co-workers have reported the synthesis of alkanesulfonic and octadecanephosphonic acid functionalized amorphous Fe_2O_3 nanoparticles.[193] Markovich and co-workers have also reported the synthesis of fatty acid and alkanephosphonic acid functionalized magnetite nanoparticles.[194] Zhang and co-workers have reported the synthesis of iron oxide nanoparticles, conjugated with an amine-functionalized poly(ethylene glycol) silane and the peptide chlorotoxin to target and inhibit the invasion of tumor-cells.[195-197] Lartigue et al. have reported the synthesis of water-soluble and biocompatible rhamnose-coated Fe_3O_4 nanoparticles by covalently linking rhamnose on the nanoparticles through a phosphonate linker.[198] Huang and co-workers have reported the synthesis of water-soluble, magnetic Fe_3O_4 glyco-nanoparticles for detecting and differentiating cancer cells, based on specific binding between receptors on the cancer cell surface and sugar groups presented on the nanoparticles.[199] Lartigue et al. have also reported the use of phosphonate chemistry to synthesize water-soluble sugar-coated Fe_3O_4 nanoparticles and evaluated their magnetic relaxometric and hyperthermia properties.[200]

Here, the synthesis of chiral polyol-terminated alkanephosphonic acids **1** (D-mannitol), **2** (L-mannitol), **3** (D-gulitol) and hydroxyl-terminated alkanephosphonic acid **4** (hydroxyl) (Scheme 5.1) is reported for fabricating SAMs on TiO_2 thin films, to evaluate the resistance of these SAMs towards mammalian cell (Swiss albino 3T3 fibroblasts)

adhesion. A facile synthesis of D-gulitol modified Fe_3O_4 nanoparticles is reported to provide an example of how polyol-terminated alkanephosphonic acids can be used to synthesize water-soluble metal oxide nanoparticles.

5.2 Results and Discussion

Polyol- and hydroxyl-terminated alkanephosphonic acids were synthesized to form SAMs on TiO_2 and the resistance of these SAMs towards mammalian cell adhesion was studied. Two enantiomeric polyol-terminated alkanephsophonic acids **1** (D-mannitol), **2** (L-mannitol), one diastereomeric polyol-terminated alkanephosphonic acid **3** (D-gulitol) and a hydroxyl-terminated alkanephosphonic acid **4** (hydroxyl) were synthesized, for studying the effect of stereochemistry and the number of hydroxyl groups on the ability of these SAMs to resist the adhesion of mammalian cells on TiO_2.

The D-gulitol-terminated alkanephosphonic acid was then used to synthesize D-gulitol modified magnetite nanoparticles, to study the solubility and stability of these modified nanoparticles in water.

Scheme 5.1

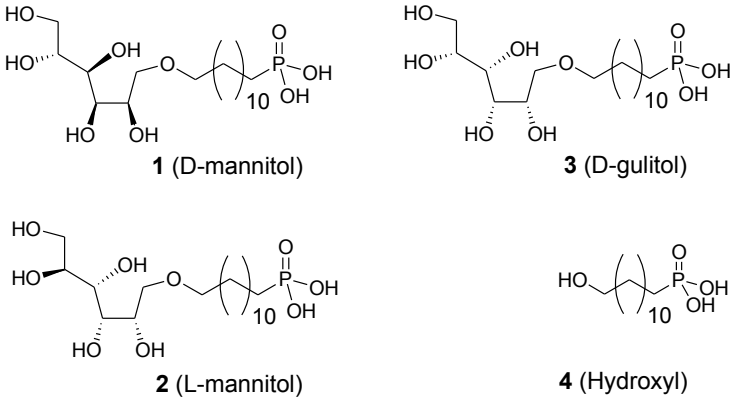

5.2.1 Synthesis of mannitol-terminated alkanephosphonic acids

The first attempt at synthesizing **1** is illustrated in Scheme 5.2. Compound **1a** was synthesized using literature reported procedures.[201-202] Nucleophilic substitution using excess of 1,12-dibromododecane, afforded the bromide **1b** with a yield of 31%. Arbuzov rearrangement[203-204] on the bromide **1a** using triethylphosphite ($P(OEt)_3$) as solvent afforded **1c**, together with a byproduct, which was the major product in this reaction. Detailed ^{1}H, ^{31}P NMR and mass spectral analysis revealed that the byproduct formed was the phosphonate **1c′**. The byproduct **1c′** resulted from reaction of the free secondary hydroxyl group in **1c** with triethylphosphite during the Arbuzov rearrangement step. If the byproduct was indeed the phosphonate **1c′**, I speculated that acid hydrolysis of **1c′** should yield the phosphonate ester **1d**. Interestingly, the hydrolysis of **1c′** in 1N HCl afforded compound **1d** in quantitative yield. The formation of **1d** further proved that the byproduct in the Arbuzov rearrangement step was indeed **1c′**. Compound **1d** was further treated with bromotrimethylsilane (Me_3SiBr) and subsequent methanolysis of the intermediate disilyl ester,[205] was expected to afford **1**, but instead afforded the corresponding dimethyl ester, **1′**. Compound **1′** was formed instead of **1**, due to the trans-esterification reaction in the presence of methanol as solvent and Me_3SiBr as the Lewis acid catalyst.

Scheme 5.2

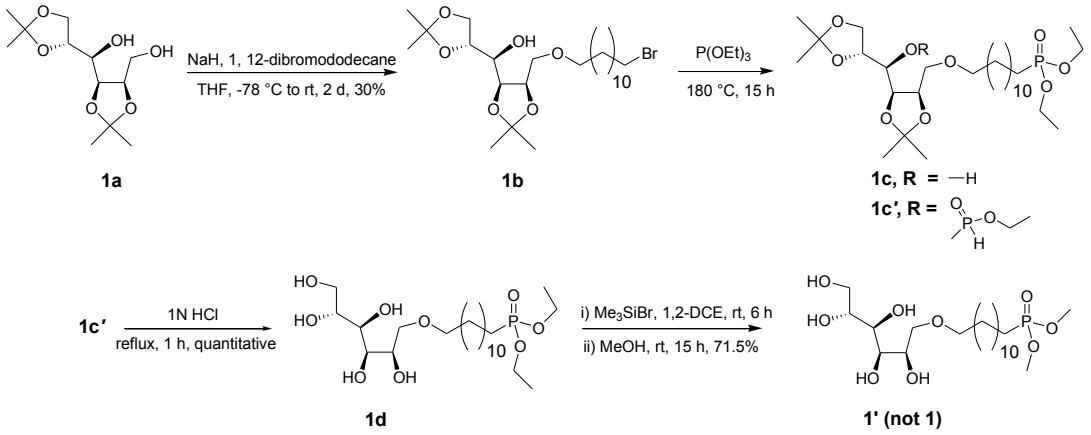

Since reaction of triethylphosphite with the hydroxyl group in **1b** decreased the yield of the desired phosphonate ester **1c**, the secondary hydroxyl group was protected as the *tert*-butyldimethylsilyl (TBS) ether. The TBS protection of the secondary hydroxyl in **1b** resulted in higher in the Arbuzov rearrangement step, providing an efficient route for synthesizing compound **1**. The optimized synthesis for **1** is illustrated in Scheme 5.3. The secondary hydroxyl group in compound **1b** was protected as the TBS ether by reacting compound **1b** with *tert*-butyldimethylsilyl triflate (TBS-OTf) as the silylating agent and 2,6-lutidine as base, to yield **1e** with a relatively low yield of 48%. Arbuzov rearrangement reaction on TBS protected **1e** provided the phosphonate ester **1f** with a yield of 92%. Finally, hydrolysis of **1f** in 1,2-dichloroethane (1,2-DCE), using Me_3SiBr as the Lewis acid catalyst, followed by an aqueous workup provided the desired phosphonic acid **1** with a yield of 94%. Based on our previous experience with chiral polyol-terminated alkanethiols, the enantiomeric compound **2** was also synthesized for studying the effect stereochemistry of the polyol-fragment on the bioinert properties of

the polyol SAMs. Compound **2** was synthesized following similar synthetic procedures as outlined for compound **1** and is illustrated in Scheme 5.3.

Scheme 5.3

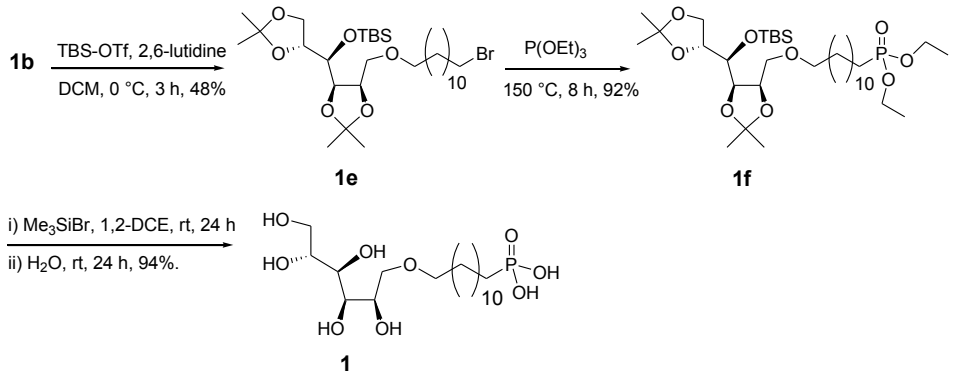

5.2.2 Synthesis of D-gulitol-terminated alkanephosphonic acid

A single diasteromeric phosphonic acid **3** (D-gulitol) was also synthesized by following synthetic procedures similar to those outlined for compounds **1** and **2**. The synthesis of compound **3** is illustrated in Scheme 5.4. Briefly, compound **3a** was synthesized following literature reported procedures.[112] Nucleophilic substitution using excess of 1,12-dibromododecane, afforded the bromide **3b** with a yield of 46%. Protection of the secondary hydroxyl group in **3b** as the TBS ether afforded compound **3c** with a yield of 34%. Reaction of **3c** with $P(OEt)_3$ under Arbuzov rearrangement conditions afforded the phosphonate ester **3d** with a yield of 91%. Hydrolysis of the phosphonate ester **3d** in 1,2-DCE with Me_3SiBr as the Lewis acid catalyst afforded the desired compound **3** with a yield of 95%.

Scheme 5.4

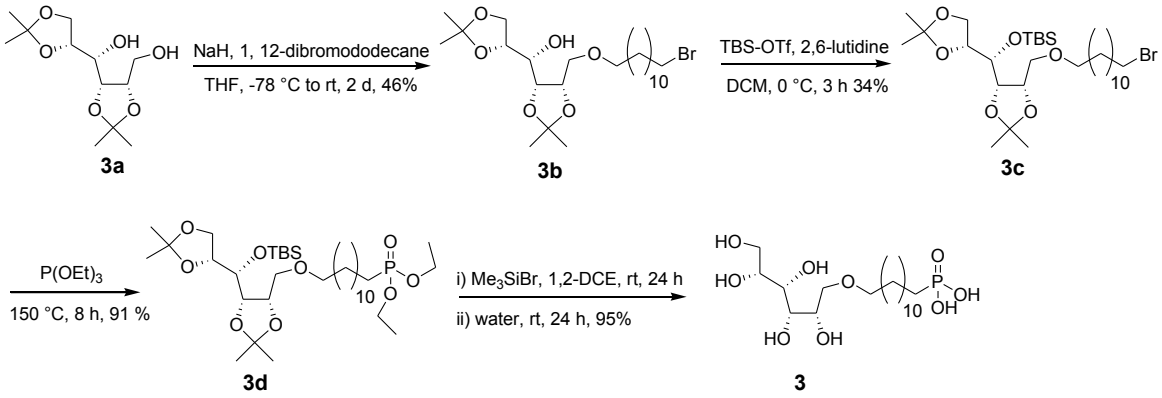

5.2.3 Synthesis of hydroxyl-terminated alkanephosphonic acid

The hydroxyl-terminated alkanephosphonic acid **4** (hydroxyl) was also synthesized, to study the effect of the number of hydroxyl groups on the bioinert properties of the polyol SAMs. The synthesis of compound **4**, is described in scheme 5.5. Briefly, the primary hydroxyl group of 12-bromo-1-dodecanol, **4a** was protected as the TBS ether using TBS-Cl as the silylating agent and imidazole as base, to afford the bromide **4b** with a yield of 88%. Compound **4b** was treated with $P(OEt)_3$ under the condition of Arbuzov rearrangement to afford the phosphonate ester **4c**. Finally, hydrolysis of **4c** with Me_3SiBr followed by aqueous workup afforded the hydroxyl-terminated phosphonic acid **4**.

Scheme 5.5

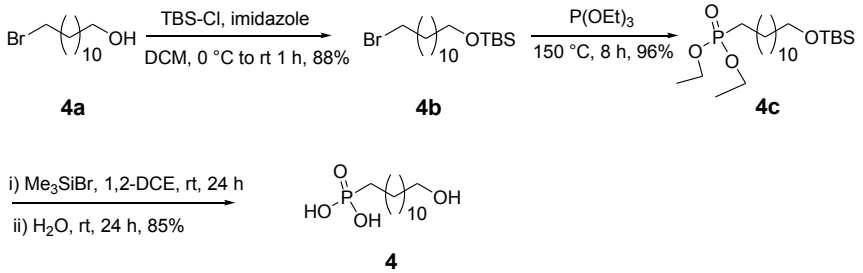

5.2.4 Synthesis of D-gulitol modified magnetite nanoparticles (D-GPA MNP)

D-gulitol-terminated alkanephosphonic acid, **3** was used to synthesize water-soluble Fe_3O_4 (magnetite) nanoparticles (MNP). Magnetite nanoparticles were synthesized using the co-precipitation method reported by Markovich and co-workers.[194] In order to coat the nanoparticles with **3**, the nanoparticles were stirred for 24 h in a solution of compound **3** in DMSO. A separate batch of nanoparticles was also stirred in DMSO alone. A short magnetic separation of the large particles (30 min), followed by decantation of the supernatant afforded a clear solution of the D-gulitol modified magnetite nanoparticles (D-GPA MNPs) or unmodified nanoparticles (MNPs). The supernatant was further subjected to prolonged magnetic decantation (24 h), which resulted in the modified or unmodified nanoparticles to settle at the bottom of the vial (Figure 5.1). During the prolonged magnetic decantation, it was interesting to note that the D-GPA MNPs remained in solution longer than the MNPs. Even after 24 h, the DMSO suspension of D-GPA MNPs was slightly darker in color than the DMSO suspension of the unmodified nanoparticles.

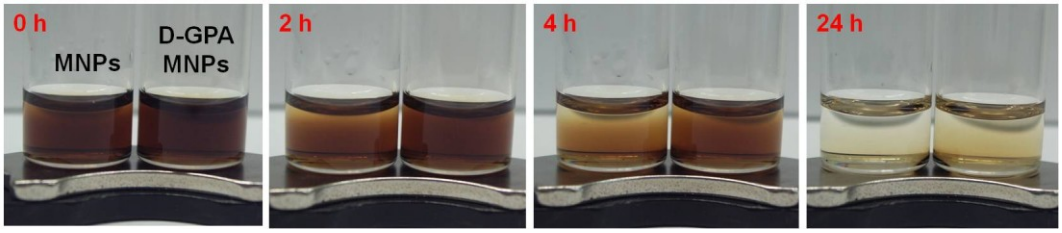

Figure 5.1 Magnetic decantation of a DMSO suspension of magnetite nanoparticles (MNPs) and D-gulitol modified magnetite nanoparticles (D-GPA MNPs) over time (hours). The modified and unmodified nanoparticles are seen to collect at the bottom of the vial after 24 h.

The supernatant was discarded and the particles were washed with DMSO and suspended in water. While the dispersion of the D-GPA MNPs in water was clear, the dispersion of the MNPs showed signs of precipitation, immediately after addition of water. Within 8 h, while the dispersion of the D-GPA MNPs in water was still clear, the dispersion of MNPs precipitated out completely (Figure 5.2, 8 h). Even after 24 h, the sample containing the dispersion of D-GPA MNPs was stable and only showed small amount of precipitate formation (Figure 5.2, 24 h). Over time, D-GPA MNPs were seen to settle down to the bottom of the vial under gravity (Figure 5.2, 96 h), but could be dispersed back into solution by simply agitating the vial (Figure 5.2, 12 d).

Figure 5.2 Stability of dispersion of magnetite nanoparticles (MNPs) and D-gultiol modified magnetite nanoparticles (D-GPA MNPs) in water over time.

5.2.5 Size determination of D-GPA MNPs using dynamic light scattering (DLS) and transmission electron microscopy (TEM)

Dynamic light scattering (DLS) on the sample of D-GPA MNPs in water revealed a narrow distribution of hydrodynamic size of the particles. The average hydrodynamic diameter of the nanoparticles was found to be to be 36.21 ± 4.01 nm (Figure 5.3).

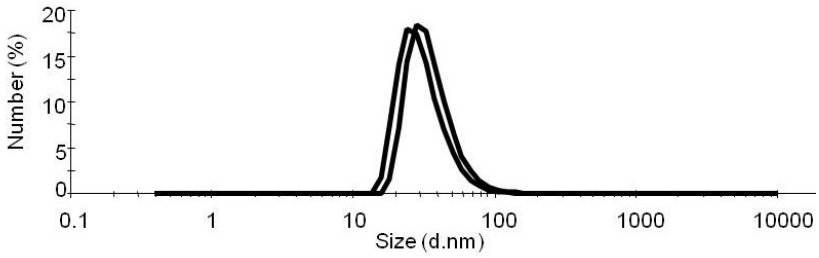

Figure 5.3 Number density from DLS showing two replicates for D-gulitol modified magnetite nanoparticles.

The D-GPA MNPs sample was also analyzed using TEM. Transmission electron microscopy (TEM) also revealed a narrow size distribution and a roughly spherical morphology for the D-GPA MNPs. The average size of the D-GPA MNPs was estimated to be 9.37 ± 3.05 nm from the TEM image (Figure 5.4).

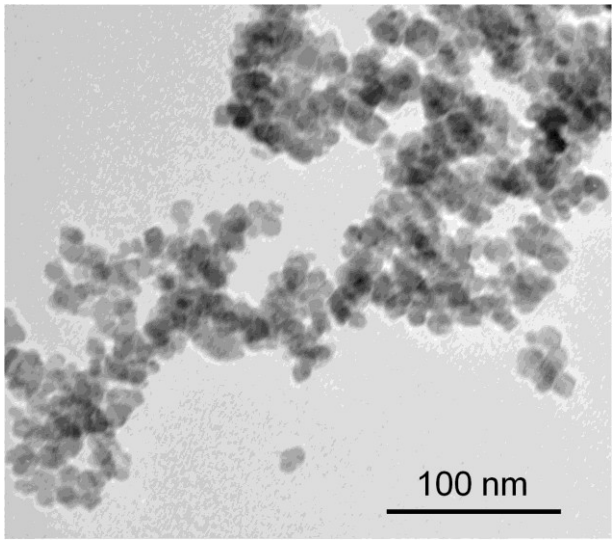

Figure 5.4 Transmission electron micrograph of D-gulitol modified magnetite nanoparticles (D-GPA MNPs).

5.3 Conclusions and Perspectives

This study reports the synthesis of polyol-terminated alkanephsophonic acids **1** (D-mannitol), **2** (L-mannitol), **3** (D-gulitol) and a hydroxyl-terminated alkanephosphonic acid **4** (hydroxyl).

The D-gulitol-terminated alkanephosphonic acid was further used to synthesize D-gulitol modified magnetite nanoparticles (D-GPA MNPs), to study the solubility and stability of these modified nanoparticles in water. The D-gulitol modified magnetite nanoparticles (D-GPA MNPs) were found to be soluble and stable towards agglomeration in water as compared to the unmodified magnetite nanoparticles (MNPs).Water-soluble magnetite nanoparticles have applications in magnetic resonance imaging (MRI), drug delivery and hyperthermia. These water-soluble D-GPA MNPs can be functionalized with targeting ligands or antibodies and can have potential application in targeted drug delivery and magnetic resonance imaging.

Further characterization of the D-GPA MNPs using thermo gravimetric analysis (TGA), infrared (IR) analysis can be conducted to confirm the presence of the polyol-terminated alkanephosphonate SAMs on the surface of these nanoparticles.

5.4 Experimental Section

Chemicals. Chemicals used for synthesizing all alkanephosphonic acids were purchased from Aldrich Chemicals (Milwaukee, WI) and used as received. DMSO was used as a solvent for preparing all the alkanephosphonic acid solutions. Water used had a resistivity of 18 MΩ cm (Millipore, Billerica, MA).

Synthesis of D-Gulitol Modified Magnetite Nanoparticles. Magnetite nanoparticles were synthesized following procedures reported by Markovich and co-workers.[194] The synthesized magnetite nanoparticles (2 mg) were suspended in 1 mL of a 0.5% solution of compound **3** in DMSO. The suspension was sonicated at high power for 10 min followed by shaking at rt for 24 h. After 24 h, the undispersed magnetite nanoparticles were removed by short magnetic decantation (30 min). The supernatant was then subjected to prolonged magnetic decantation (24 h) in a vial. After 24 h, the supernatant was carefully removed while the vial was placed on a strong permanent magnet to keep the nanoparticles undisturbed at the base of the vial. The nanoparticles were rinsed 3 times with 100 μL of DMSO (to remove unreacted **3**) while the vial was placed on the magnet. During the rinsing step, the vial was gently moved across the surface of the magnet to enable efficient rinsing of the nanoparticles with DMSO. Finally, after removing the DMSO, the nanoparticles were re-suspended in water. The same treatment was applied to the unmodified magnetite nanoparticles except that the nanoparticles were not treated with any alkanephosphonic acid.

Dynamic Light Scattering (DLS). DLS experiments were performed on a MALVERN zetasizer nanoseries (MALVERN Instruments Ltd. Worcestershire, U.K.) instrument at a scattering angle of 173°. A solution of the D-gulitol modified magnetite nanoparticles in water was used for DLS measurements.

Transmission Electron Microscopy (TEM). TEM measurements were performed on a JEOL 2000 EX instrument operated at 120 kV with tungsten filament (SUNY-ESF, N.C Brown Center for Untrastructure Studies). A dilute solution of D-gulitol modified

magnetite nanoparticles in water was drop casted on a carbon coated copper grid and directly visualized under the transmission electron microscope. Particle size was analyzed manually using CorelDRAW X5 image processing software, by modeling each particle as a sphere and the standard deviation in the size of the particles was determined over 20 particles.

Details for the Synthesis of Alkanephosphonic Acids

General Information for Synthesis of Alkanephosphonic Acids. The processes involving reactants sensitive to moisture or air were carried out under an atmosphere of argon using oven-dried glassware. Reagents and solvents were reagent grade and used as supplied unless otherwise mentioned. THF was distilled from sodium benzophenone. Solvents were removed under reduced pressure using rotary evaporator below 40 ºC. Silica Gel 60 F_{254} precoated plates (0.25-mm thickness, EMD) were used for TLC and a solution of phosphomolybdic acid/ceric sulfate/sulfuric acid (10g : 1.25 g : 8% 250 mL), followed by charring at ~ 150 ºC, was used for visualization. Flash column chromatography was performed using SILICYCLE, Silica-P Flash Silica Gel with 40-63µ mesh size. NMR spectra (^{1}H, ^{13}C) were recorded on 300 MHz Bruker instrument. ^{1}H, ^{13}C NMR spectra were recorded on 300 MHz and ^{31}P NMR spectra recorded on 500 MHz Bruker instrument. ^{1}H chemical shifts are reported in ppm relative to $CDCl_3$ δ 7.26. ^{13}C chemical shifts are reported relative to $CDCl_3$ δ 77.23 and ^{31}P chemical shifts relative to H_3PO_4 set at δ 0.0. (High Resolution Mass Spectra) HRMS was recorded by positive ion electrospray on a Bruker 12 Tesla APEX –Qe FTICR-MS with Apollo II ion source. ESI-MS obtained on Shimadzu 2010 instrument.

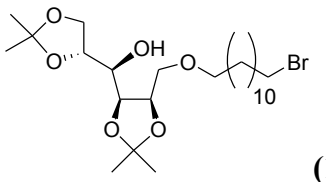

(1b)

NaH (0.031 g, 60% by wt in mineral oil, 0.783 mmol) was added to a solution of compound **1a**[201-202] (0.158 g, 0.602 mmol) in THF (2 mL) at -78 °C. The reaction mixture was warmed up to 0 °C and was stirred at 0 °C for 90 min. A solution of 1,12-dibromododecane (0.791 g, 2.411 mmol) in THF (3 mL) was drop wise via a cannula to the reaction mixture at 0 °C. The reaction mixture was stirred at rt for 2 d and then quenched with water. The aqueous phase was extracted with EtOAc and the combined organic phase was dried over anhydrous Na_2SO_4. The crude product was obtained as colorless oil after evaporation of solvent. The crude product was purified using flash silica gel column (20% EtOAc in Hexane) to obtain **1b** (0.097 g, 30%) as white solid after evaporation of solvent. R_f = 0.37 (20% EtOAc in Hexane). ^{1}H NMR (300 MHz, $CDCl_3$): δ 4.38-4.32 (m, 2H), 4.12-3.98 (m, 3H), 3.79-3.65 (m, 2H), 3.52-3.46 (m, 3H), 3.55 (t, J_{H-H} = 6.8 Hz, 2H), 1.88-1.78 (m, 2H), 1.51(s, 3H), 1.42 (s, 3H), 1.41 (s, 3H), 1.35 (s, 3H), 1.25 (br s, 18H). ^{13}C NMR (75 MHz, $CDCl_3$): 109.4, 108.6, 76.0, 75.9, 75.9, 72.3, 70.8, 69.14, 67.5, 34.2, 33.0, 29.7, 29.6, 28.9, 28.3, 27.1, 26.7, 26.2, 25.5, 25.0. HRMS: found 531.2296 $[M + Na]^+$, calcd for $[C_{24}H_{45}BrO_6 + Na]^+$ 531.2292.

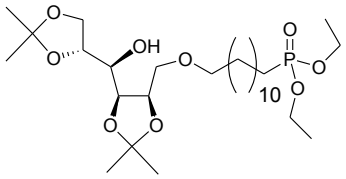

(1c)

A solution of compound **1b** (0.057g, 0.112 mmol) in freshly distilled $P(OEt)_3$ (7 mL) was heated at 180 °C overnight. Concentration of the reaction mixture under high vacuum gave a colorless oily residue. Preparative TLC (80% EtOAc in Hexane) of the colorless residue provided **1c′** and desired **1c** (0.016g, 25.4%).

Data for **1c′:**

R_f = 0.11 (80% EtOAc in Hexane). ^{1}H NMR (300 MHz, $CDCl_3$): δ 8.16 (d, J = 34.7 Hz, 0.5H), 5.76 (d, J = 28.9 Hz, 0.5H), 4.77-4.54 (m, 0.5H), 4.33-3.92 (m, 11H), 3.74-3.70 (m, 1H), 3.59-3.38 (m, 3H), 1.40 (s, 3H), 1.36 (s, 3H), 1.32 (br s, 13H), 1.31 (br s, 5H), 1.30 (s, 3H), 1.28-1.19 (br s, 16H). ^{13}C NMR (75 MHz, $CDCl_3$): δ 110.9, 110.2, 77.5, 77.4, 77.2, 73.4, 69.7, 66.3, 63.1, 62.8, 62.7, 32.0, 31.2, 31.1, 31.0, 28.8, 27.9, 27.6, 27.0, 26.6, 23.9, 18.0, 17.9, 17.7. ^{31}P NMR (200 MHz, $CDCl_3$): δ 35.81, 34.78, 12.19, 11.62, 8.65, 8.04. HRMS: found 681.3492 $[M + Na]^+$, calcd for $[C_{30}H_{60}O_{11}P_2 + Na]^+$ 681.3503.

Data for **1c:**

R_f = 0.19 (80% EtOAc in Hexane). ^{1}H NMR (300 MHz, $CDCl_3$): δ 4.38 (br, s, 2H), 4.12-4.00 (m, 7H), 3.81-3.66 (m, 2H), 3.54-3.48 (m, 3H), 3.15 (d, $J_{H\text{-}H}$ = 6.1 Hz, 1H), 1.52 (s, 3H), 1.41 (s, 3H), 1.39 (s, 3H), 1.35 (s, 3H), 1.25 (br, s, 18H). ^{13}C NMR (75 MHz, $CDCl_3$): δ 109.6, 108.7, 76.0, 75.9, 75.9, 72.4, 70.9, 69.2, 67.6, 61.6, 61.6, 30.9, 29.8,

29.6, 29.3, 27.1, 26.8, 26.2, 25.1, 16.7, 16.6. ^{31}P NMR (200 MHz, $CDCl_3$): δ 34.78. HRMS: found 589.3465 $[M + Na]^+$, calcd for $[C_{28}H_{55}O_9P + Na]^+$ 589.3476.

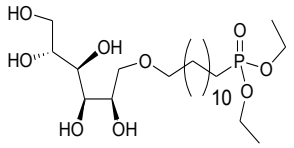

(1d)

Compound **1c′** (0.117 g, 0.177 mmol) was suspended in 15 mL of 1N HCl and refluxed for 1h. The reaction mixture was brought to room temperature and neutralized by drop wise addition of aq 1N NaOH. Water was evaporated under reduced pressure to yield a white residue. The residue was washed with THF and the washings were filtered through a pad of celite. The filtrate was concentrated to yield **1d** (0.082 g, quantitative) as a colorless sticky solid. ^{1}H NMR (300 MHz, MeOD): δ 4.06 (br d, 4H), 3.73 (br d, 7H), 3.49 (br s, 3H), 1.55 (br s, 4H), 1.30 (br s, 24H) . ^{13}C NMR (75 MHz, MeOD): δ 74.2, 72.9, 72.8, 71.6, 71.4, 71.1, 65.1, 63.2, 63.2, 31.7, 31.5, 30.8, 30.8, 30.6, 30.3, 27.3, 26.8, 24.9, 23.5, 23.5, 16.9, 16.8. ^{31}P NMR (200 MHz, $CDCl_3$): δ 34.73. HRMS: found 509.2831$[M + Na]^+$, calcd for $[C_{22}H_{47}O_9P + Na]^+$ 509.2849.

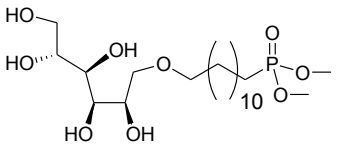

(1′)

To a dry solution of **1d** (0.0739g, 0.152 mmol) in 1,2-DCE was added Me_3SiBr (0.06 mL, 0.456 mmol) drop wise. The reaction mixture was stirred at rt for the next 6 h. The solvent was evaporated and 10 mL of MeOH was added to the residue and the mixture

was stirred at rt for 15 h. The solvent was evaporated and the residue obtained was dissolved in MeOH and the product **1′** (0.0498 g, 71.51%) was precipitated out as a white solid by adding diethyl ether. ^{1}H NMR (300 MHz, MeOD): δ 4.08-3.99 (m, 1H), 3.78-3.70 (br m, 3H), 3.68-3.61 (m, 3H), 3.57-3.47 (m, 3H), 1.77-1.57 (m, 5H), 1.30 (br s, 17H). ^{13}C NMR (75MHz, MeOD): δ 74.1, 73.01, 72.8, 71.7, 71.3, 65.2, 31.9, 31.6, 30.8, 30.6, 30.4, 27.3, 26.1, 23.8, 16.9. ^{31}P NMR (200 MHz, MeOD) δ 33.68. HRMS: found 481.2537 $[M + Na]^+$, calcd for $[C_{20}H_{43}O_9P + Na]^+$ 481.2537.

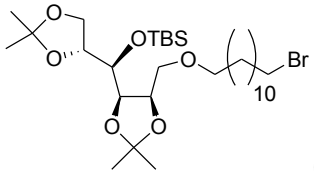

(1e)

To a solution of compound **1b** (0.300 g, 0.590 mmol) in DCM (15 mL) was added 2,6-lutidine (0.13 mL, 1.151 mmol) at 0 °C followed by drop wise addition of TBS-OTf (0.54 mL, 2.361 mmol) over 5 min. The reaction mixture was stirred at 0 °C for 3 h and then quenched by adding saturated solution of $NaHCO_3$. The aqueous phase was extracted with DCM and the combined organic phase was dried over anhydrous Na_2SO_4. Evaporation of solvent afforded the crude product as colorless oil. The crude product was purified using silica gel column (20% EtOAc in Hexane) to obtain **1e** (0.146 g, 48%) as a yellow oil after evaporation of solvent. R_f = 0.43 (15% EtOAc in Hexane). ^{1}H NMR (300 MHz, $CDCl_3$): δ 4.17-3.84 (m, 6H), 3.57-3.52 (m, 1H), 3.40-3.36 (br m, 5H), 1.88-1.78 (m, 2H), 1.59-1.51 (br m, 2H), 1.43 (s, 3H), 1.39(s, 3H), 1.30 (s, 6H), 1.25 (br s, 16H), 0.87 (s, 9H), 0.10 (s, 3H), 0.09 (s, 3H) . ^{13}C NMR (75 MHz, $CDCl_3$): δ 109.1, 107.9, 79.5, 77.0, 76.2, 71.9, 71.1, 70.4, 66.5, 34.1, 33.0, 29.8, 29.74, 29.70, 29.65, 29.60, 28.9,

28.35, 28.26, 26.5, 26.3, 26.1, 25.9, 25.4, 18.7, -3.8, -4.3. HRMS: found 645.3143 [M + Na]$^+$, calcd for [$C_{30}H_{59}BrO_6Si$ + Na]$^+$ 645.3156.

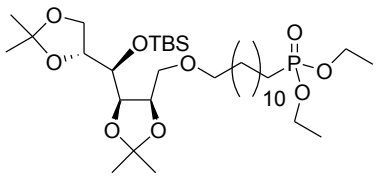

(1f)

To compound **1e** (0.138 g, 0.220 mmol) was added freshly distilled $P(OEt)_3$ (0.18 mL, 1.103 mmol) and the mixture was heated at 150 °C for 8 h. The reaction mixture was cooled to rt and the loaded directly on to the silica gel column (50 % EtOAc in Hexane) to obtain pure product **1f** (0.138 g, 92%) as a yellow oil after evaporation of solvent. R_f= 0.28 (80% EtOAc in Hexane). ^{1}H NMR (300 MHz, $CDCl_3$): δ 4.17-3.82 (m, 10 H), 3.55-3.50 (m, 1H), 3.44-3.33 (br m, 3H), 1.74-1.49 (m, 6H), 1.49 (s, 3H), 1.42 (s, 3H), 1.37(s, 3H), 1.31 (br s 8H), 1.28 (s, 3H), 1.26 (br s 14H), 0.86 (s, 9H), 0.08 (s, 3H), 0.07 (s, 3H). ^{13}C NMR (75 MHz, $CDCl_3$): δ 109.1, 107.9, 79.5, 77.0, 76.2, 71.9, 71.1, 70.4, 66.4, 61.6, 61.5, 30.9, 30.7, 29.8, 29.7, 29.6, 29.5, 29.4, 29.3, 29.2, 28.2, 26.8, 26.5, 26.3, 26.1, 25.9, 25.4, 24.9, 22.6, 22.5, 18.6, 16.7, 16.6, -3.8, -4.3. ^{31}P NMR (200MHz, $CDCl_3$) δ 34.68.HRMS: found 703.4338 [M + Na]$^+$, calcd for [$C_{34}H_{69}O_9PSi$ + Na]$^+$ 703.4341.

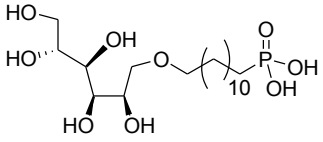

(1)

Me_3SiBr (0.13 mL, 1.010 mmol) was added drop wise to a solution of compound **1f** (0.138 g, 0.203 mmol) in freshly distilled1,2-DCE (3 mL) at rt and the reaction mixture was stirred at rt for the next 24 h. The solvent was evaporated and to the residue was

added water (3 mL) at rt and the mixture was stirred at rt for the next 24 h. The water was evaporated and the residue was washed with Et_2O (5 mL × 5) and DCM (5 mL × 5) to obtain pure compound **1** (0.081 g, 94%) as a white solid on drying. ^{1}H NMR (300 MHz, DMSO-d_6): δ 5.83 (br s, 5H), 3.61-3.42 (m, 5H), 3.41-3.28 (m, 5H), 1.47-1.44 (br m, 4H), 1.23 (br s, 18H). ^{13}C NMR (75 MHz, DMSO-d_6): δ 73.3, 71.3, 70.6, 69.7, 69.5, 63.9, 30.2, 30.0, 29.3, 29.0, 28.9, 28.7, 28.4, 26.6, 25.7, 22.74, 22.69. ^{31}P NMR (200MHz, DMSO-d_6) δ 28.55. HRMS: found 453.2230 $[M + Na]^+$, calcd for $[C_{18}H_{39}O_9P + Na]^+$ 453.2224.

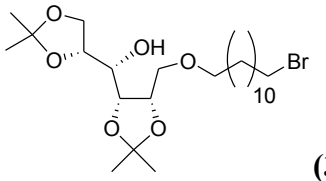

(3b)

NaH (0.1888 g, 60% by wt in mineral oil, 4.719 mmol) was added to a solution of compound **3a**[112] (0.618 g, 2.359 mmol) in THF (10 mL) at -78 °C. The reaction mixture was warmed up to 0 °C and was stirred at 0 °C for 90 min. A solution of 1,12-dibromododecane (3.097 g, 9.438 mmol) in THF (10 mL) was added drop wise to the above reaction mixture via a cannula at 0 °C and the reaction mixture was stirred at rt for 2 d. The reaction was quenched by addition of water and the aqueous phase extracted with EtOAc. The combined organic phase was dried over anhydrous Na_2SO_4 and the crude product was obtained as colorless oil after evaporation of solvent. The crude product was purified using flash silica gel column (20% EtOAc in Hexane) to obtain **3b** (0.249 g, 46%, calculated from recovered **3a**) as a yellow oil after evaporation of solvent. R_f = 0.25, (20% EtOAc in Hexane). ^{1}H NMR (300 MHz, $CDCl_3$): δ 4.34-4.23 (m 2H),

4.21-4.02 (dd, J_{H-H} = 6.5 Hz, 3.2 Hz, 1H), 4.04 (dt, J_{H-H} = 7.3 Hz, 1.5 Hz, 1H), 3.84 (t, J_{H-H} = 7.3 Hz, 1H), 3.74-3.69 (m, 2H), 3.60 (dd, J_{H-H} = 10.1 Hz, 4.6 Hz, 1H), 3.50-3.38 (m, 4H), 2.94 (d, J_{H-H} = 6.3 Hz, 1H), 1.90-1.80 (m, 2H), 1.59-1.54 (m, 2H), 1.50 (s, 3H), 1.45 (s, 3H), 1.38 (s, 3H), 1.37 (s, 3H), 1.27 (br s, 6H). ^{13}C NMR (75 MHz, $CDCl_3$): δ 109.6, 108.8, 76.8, 75.9, 72.1, 69.7, 69.3, 66.1, 34.1, 33.0, 29.7, 29.6, 29.5, 28.9, 28.3, 27.1, 26.7, 26.2, 25.9, 25.5, 25.2. HRMS found = 531.1196 $[M + Na]^+$, calcd for $[C_{24}H_{45}BrO_6 + Na]^+$ = 531.2292.

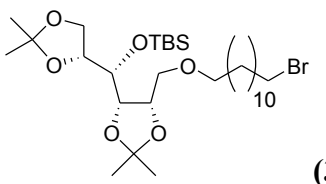

(3c)

To a solution of compound **3b** (0.242 g, 0.477 mmol) in DCM (10 mL) was added 2,6-lutidine (0.11 mL, 0.930 mmol) at 0 °C, followed by drop wise addition of TBS-OTf (0.44 mL, 1.908 mmol) over 5 min. The reaction mixture was stirred at 0 °C for 3 h and then quenched by adding saturated solution of $NaHCO_3$. The aqueous phase was extracted with DCM and the combined organic phase was dried over anhydrous Na_2SO_4 to afforded the crude product as colorless oil after evaporation of solvent. The crude product was purified using silica gel column (100% Hexane → 2% EtOAc in Hexane) to obtain **3c** (0.223 g, 75%) as a yellow oil after evaporation of solvent. R_f = 0.43 (15% EtOAc in Hexane). ^{1}H NMR (300 MHz, $CDCl_3$): δ 4.26-4.19 (m, 3H), 3.95-3.87 (m, 3H), 3.57-3.55 (m, 1H), 3.44-3.37 (m, 5H), 1.89-1.80 (m, 2H), 1.54-1.52 (m, 2H), 1.43 (s, 3H), 1.42 (s, 3H), 1.33 (s, 6H), 1.26 (br s, 16H), 0.90 (s, 9H), 0.11 (s, 3H), 0.10 (s, 3H). ^{13}C NMR (75 MHz, $CDCl_3$): δ 109.5, 108.1, 77.9, 76.8, 76.0, 71.8, 70.6, 70.3, 66.0, 34.2,

33.0, 29.9, 29.80, 29.76, 29.72, 29.7, 29.6, 29.0, 28.4, 28.0, 26.5, 26.4, 26.3, 25.75, 25.70,18.8,-3.8,-4.2. HRMS: found 645.3159 $[M + Na]^+$, calcd for $[C_{30}H_{59}BrO_6Si + Na]^+$ 645.3156.

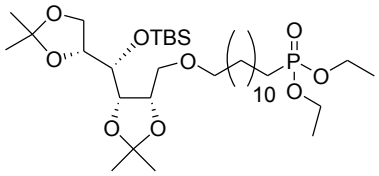

(3d)

To compound **3c** (0.067 g, 0.108 mmol) was added freshly distilled $P(OEt)_3$ (0.09 mL, 0.534 mmol) and the reaction mixture was heated at 150 °C for 8 h. The reaction mixture was cooled down to rt and loaded directly onto silica gel column (80% EtOAc in Hexane) to obtain pure compound **3d** (0.067 g, 91%) as yellow oil after evaporation of solvent. R_f = 0.28 (80% EtOAc in Hexane). ^1H NMR (300 MHz, $CDCl_3$): δ 4.24-3.84 (m, 10H), 3.58-3.53 (m, 1H), 3.47-3.32 (m, 3H), 1.76-1.53 (m, 6H), 1.42 (s, 3H), 1.40 (s, 3H), 1.32-1.28 (m, 14H), 1.24 (s, 14H), 0.88 (s, 9H), 0.10 (s, 3H), 0.08 (s, 3H). ^{13}C NMR (75 MHz, $CDCl_3$): 109.5, 108.1, 77.9, 76.7, 76.0, 71.8, 70.6, 70.2, 65.9, 61.6, 61.5, 51.5, 30.9, 30.7, 29.9, 29.82, 29.79, 29.7, 29.65, 29.57, 29.3, 28.0, 26.8, 26.5, 26.4, 26.3, 25.72, 25.66, 24.9, 22.6, 22.5, 18.7, 18.2, 16.7, 16.6, 10.3, -4.2, -3.9. ^{31}P NMR (200 MHz, $CDCl_3$) δ 34.61. HRMS: found 703.4325 $[M + Na]^+$, calcd for $[C_{34}H_{69}O_9PSi + Na]^+$ 703.4341.

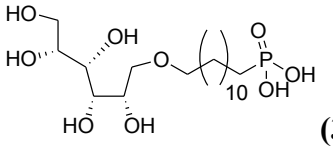

(3)

Me_3SiBr (0.21 mL, 1.628 mmol) was added drop wise to a solution of compound **3d** (0.222 g, 0.326 mmol) in freshly distilled1,2-DCE (5 mL) at rt and the reaction mixture

was stirred at rt for the next 24 h. The solvent was evaporated and to the residue was added water (5 mL) and the mixture was stirred for the next 24 h. Water was evaporated and the residue was washed with Et_2O (5 mL × 5) and DCM (5 mL × 5) to obtain pure compound **3** (0.133 g, 95%) as a white solid on drying. ^{1}H NMR (300 MHz, DMSO-d_6): δ 5.35 (br s, 5H), 3.65-3.27 (m, 10H), 1.46-1.44 (br m, 4H), 1.22 (br s, 18H). ^{13}C NMR (75 MHz, DMSO-d_6): δ 73.7, 72.8, 72.3, 70.6, 69.9, 68.7, 62.5, 30.2, 30.0, 29.3, 29.1, 29.04, 28.98, 28.7, 28.4, 26.6, 25.7, 22.74, 22.69. ^{31}P NMR (200MHz, DMSO-d_6) δ 28.55. HRMS: found 453.2228 $[M + Na]^+$, calcd for $[C_{18}H_{39}O_9P + Na]^+$ 453.2224.

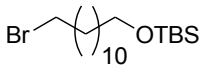

(4b)

Imidazole (0.443 g, 6.504 mmol) was added to a solution of 12-bromododecanol, **4a** (0.519 g, 1.959 mmol) in DCM (20 mL) at 0 °C. TBS-Cl (0.443 g, 2.938 mmol) was added to the reaction mixture portion wise at 0 °C and the reaction mixture was stirred at 0 °C for a while and then warmed up to rt. The reaction was quenched by adding saturated solution of $NaHCO_3$ and the aqueous layer extracted with DCM. The combined organic phase were dried over anhydrous Na_2SO_4 and evaporation of solvent gave the crude product as colorless oil. The crude product was purified with silica gel column (1%→5% EtOAc in Hexane) to yield the pure product **4b** (0.656 g, 88%) as a yellow oil after evaporation of solvent. R_f = 0.40 (4% EtOAc in Hexane). ^{1}H NMR (300 MHz, $CDCl_3$): δ 3.59 (t, $J_{H\text{-}H}$ = 6.6 Hz, 2H), 3.41 (t, $J_{H\text{-}H}$ = 6.9 Hz, 2H), 1.90-1.80 (m, 2H), 1.54-1.39 (m, 4H), 1.27 (br s, 16H), 0.89 (s, 9H), 0.05 (s, 6H). ^{13}C NMR (75 MHz, $CDCl_3$): δ 63.5, 34.2, 33.11, 33.07, 29.83, 29.77, 29.74, 29.6, 29.0, 28.4, 26.2, 26.0, 18.6, -5.0. HRMS: found 401.1847 $[M + Na]^+$, calcd for $[C_{18}H_{39}BrOSi + Na]^+$ 401.1846.

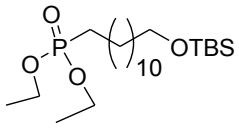

(4c)

To compound **4b** (0.400 g, 1.054 mmol) was added freshly distilled $P(OEt)_3$ (0.18 mL, 1.054 mmol) and the reaction mixture was heated at 150 °C for 8 h. The reaction mixture was cooled to rt and directly loaded onto silica gel column (80% EtOAc in Hexane) to obtain pure compound **4c** (0.443 g, 96%) as yellow oil after evaporation of solvent. R_f = 0.28 (80% EtOAc in Hexane). ^{1}H NMR (300 MHz, $CDCl_3$): δ 4.15-4.02 (m, 4H), 3.59 (t, $J_{H\text{-}H}$ = 6.6 Hz, 2H), 1.78-1.45 (m, 6H), 1.34-1.29 (m, 8H), 1.26 (br s, 14H), 0.89 (s, 9H), 0.04 (s, 6H). ^{13}C NMR (75 MHz, $CDCl_3$): δ 63.5, 61.6, 61.5, 33.1, 30.9, 30.7, 29.83, 29.77, 29.65, 29.59, 29.3, 26.8, 26.2, 26.0, 25.0, 22.64, 22.58, 18.6, 16.7, 16.6, -5.0.^{31}P NMR (200 MHz, $CDCl_3$) δ 34.68. HRMS: found 459.3022 $[M + Na]^+$, calcd for $[C_{22}H_{49}O_4PSi + Na]^+$ 459.3029.

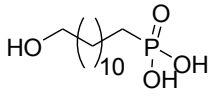

(4)

Me_3SiBr (0.45 mL, 3.435 mmol) was added drop wise to a solution of compound **4c** (0.300 g, 0.687 mmol) in freshly distilled 1,2-DCE (7 mL) at rt and the reaction mixture was stirred at rt for the next 24 h. The solvent was evaporated and to the residue was added water (7 mL) and the mixture was allowed to stir at rt for the next 24 h. The water was evaporated and the residue was washed with Et_2O (5 mL × 5) and DCM (5 mL × 5) to obtain pure compound **4** (0.156 g, 85%) as a white solid after drying. ^{1}H NMR (300 MHz, DMSO-d_6): δ 8.10 (br s, 2H), 3.36 (t, $J_{H\text{-}H}$ = 6.0 Hz), 1.45-1.39 (m, 4H), 1.24 (br s,

18H). ^{13}C NMR (75 MHz, DMSO-d_6): δ 60.7, 32.6, 30.2, 30.0, 29.1, 29.05, 29.0, 28.9, 28.7, 28.4, 26.6, 25.5, 22.7. ^{31}P NMR (200 MHz, DMSO-d_6) δ 28.48. HRMS: found 289.1540 $[M + Na]^+$, calcd for $[C_{12}H_{27}O_4P + Na]^+$ 289.1539.

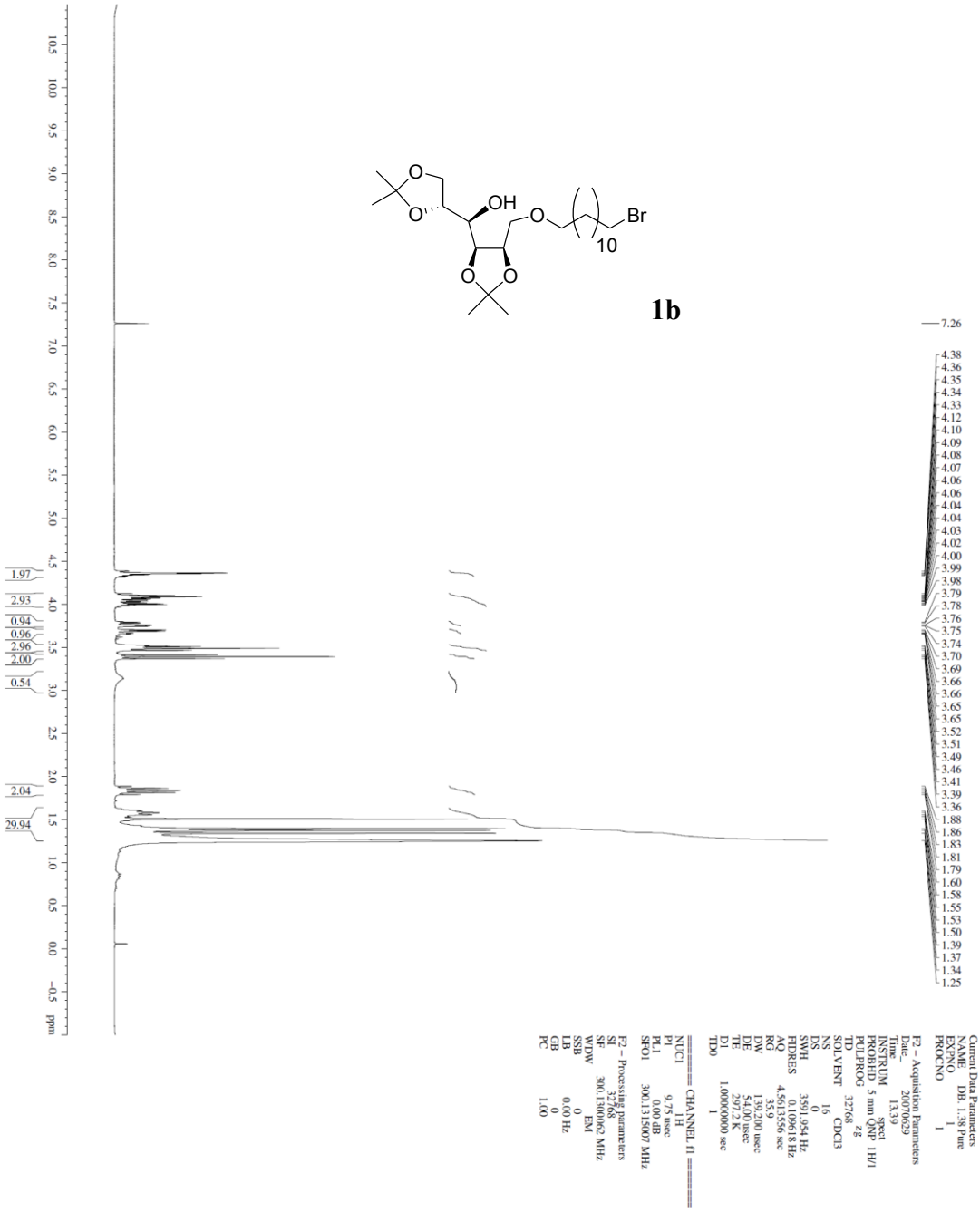
1b
OH
O
Br
10
7.26
1.97
2.93
0.94
0.96
2.96
2.00
0.54
2.04
29.94
ppm

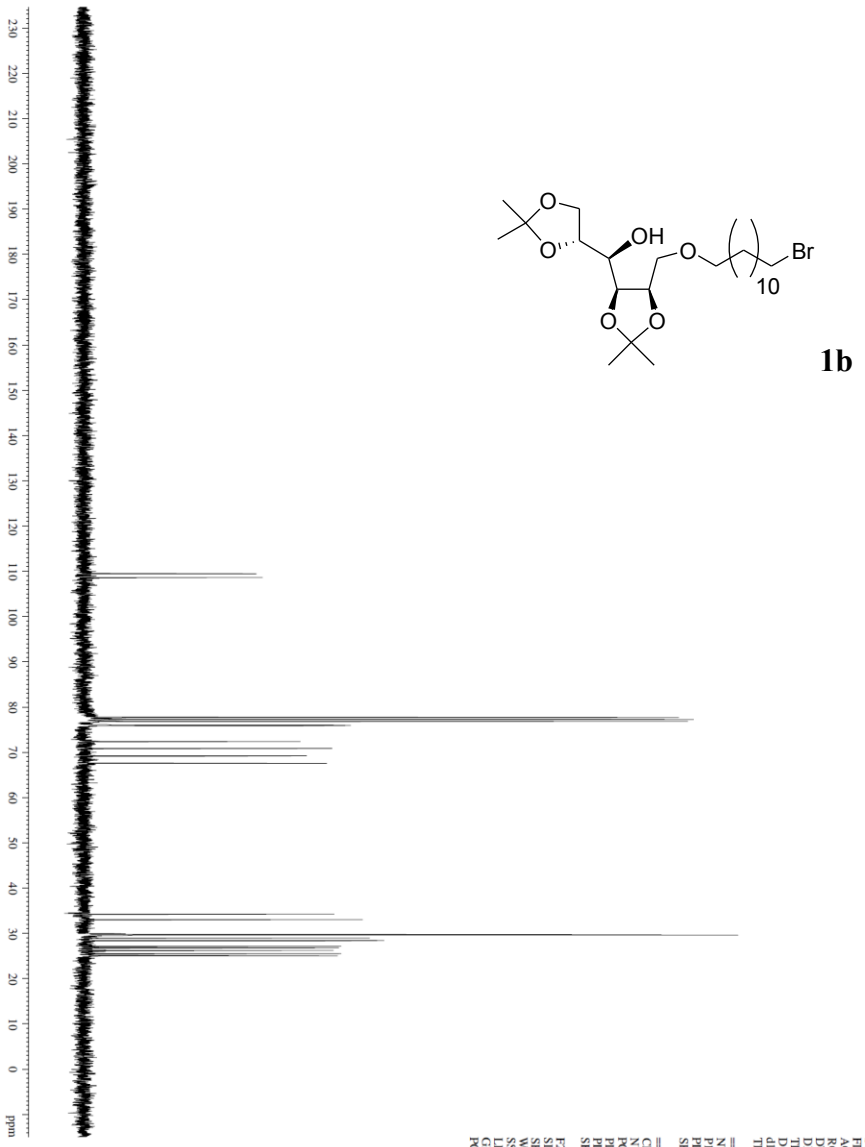
OH
O
O
O
O
O
O
Br
10

1b

230 220 210 200 190 180 170 160 150 140 130 120 110 100 90 80 70 60 50 40 30 20 10 0 ppm
109.43
108.60
76.01
75.94
75.87
72.35
70.81
69.15
67.55
34.21
33.01
29.69
29.59
28.94
28.35
27.10
26.74
26.19
25.47
25.04
Current Data Parameters
NAME DB.1.38.pure cnmr
EXPNO 2
PROCNO 1
F2 - Acquisition Parameters
Date_ 20070629
Time 18.13
INSTRUM spect
PROBHD 5 mm QNP 1H/1
PULPROG 65536,cpd,30
SOLVENT CDCl3
NS 250
DS 4
SWH 18832.393 Hz
FIDRES 0.287360 Hz
AQ 1.7400308 sec
RG 7298.2
DW 26.550 usec
DE 6.00 usec
TE 298.2 K
D1 0.40000000 sec
d11 0.03000000 sec
TD0 1
======== CHANNEL f1 ========
NUC1 13C
P1 13.70 usec
PL1 0.00 dB
SFO1 75.4760200 MHz
======== CHANNEL f2 ========
CPDPRG2 waltz16
NUC2 1H
PCPD2 95.00 usec
PL2 0.00 dB
PL12 18.00 dB
SFO2 300.1312005 MHz
F2 - Processing parameters
SI 32768
SF 75.4677349 MHz
WDW EM
SSB 0
LB 1.00 Hz
GB 0
PC 1.00

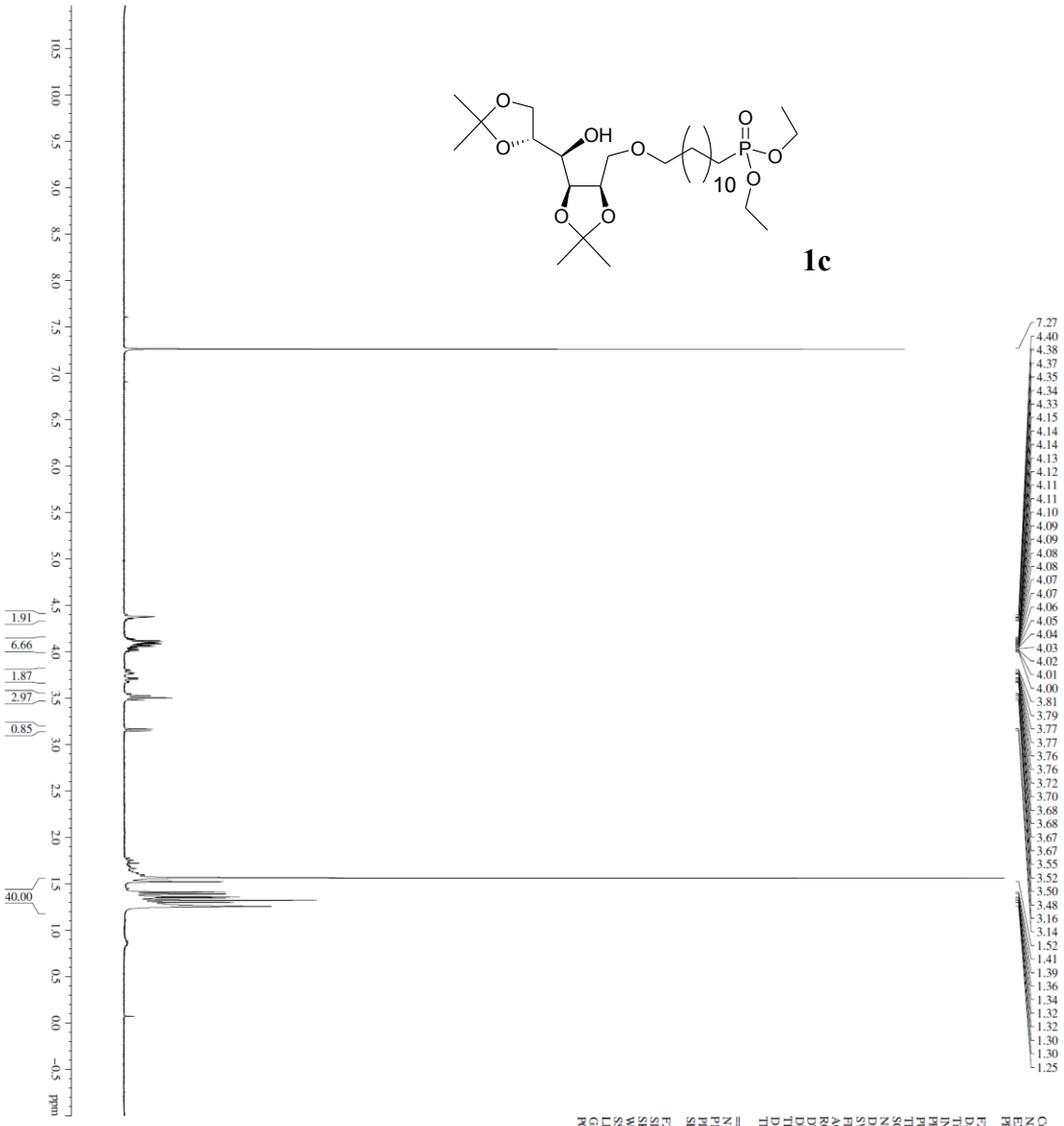
1.91
6.66
1.87
2.97
0.85
40.00
ppm
1c
Current Data Parameters
NAME DB.178 T second prep
EXPNO 1
PROCNO 1
F2 - Acquisition Parameters
Date_ 20100815
Time 13:47
INSTRUM spect
PROBHD 5 mm QNP 1H/1
PULPROG zg
TD 32768
SOLVENT CDCl3
NS 50
DS 0
SWH 3591.954 Hz
FIDRES 0.109618 Hz
AQ 4.561556 sec
RG 1024
DW 139.200 usec
DE 54.00 usec
TE 299.2 K
D1 1.00000000 sec
TD0 1
======== CHANNEL f1 ========
NUC1 1H
P1 9.75 usec
PL1 0.00 dB
SFO1 300.1315007 MHz
F2 - Processing parameters
SI 32768
SF 300.1300062 MHz
WDW no
SSB 0
LB 0.00 Hz
GB 0
PC 1.00

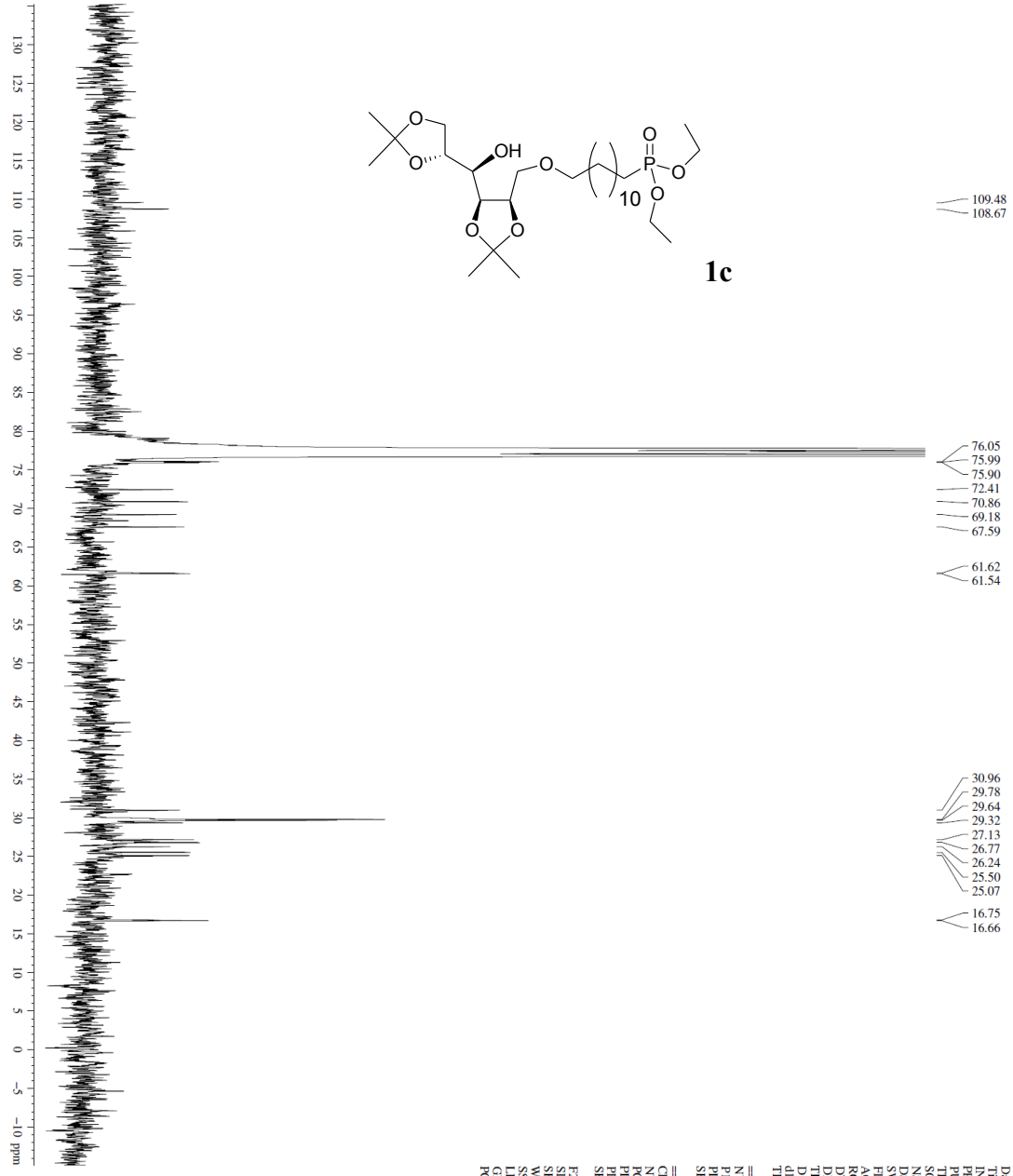

Current Data Parameters
NAME DB.1.78 top pure cmnr
EXPNO 2
PROCNO 1

F2 – Acquisition Parameters
Date_ 20070819
Time 5.57
INSTRUM spect
PROBHD 5 mm QNP 1H/1
PULPROG zgdc30
TD 65536
SOLVENT CDCl3
NS 13000
DS 4
SWH 18832.393 Hz
FIDRES 0.287360 Hz
AQ 1.7400308 sec
RG 7298.2
DW 26.550 usec
DE 6.00 usec
TE 298.2 K
D1 0.40000001 sec
d11 0.03000000 sec
TD0 1

======== CHANNEL f1 ========
NUC1 13C
P1 13.70 usec
PL1 0.00 dB
SFO1 75.4760200 MHz

======== CHANNEL f2 ========
CPDPRG2 waltz16
NUC2 1H
PCPD2 95.00 usec
PL2 0.00 dB
PL12 18.00 dB
SFO2 300.1312005 MHz

F2 – Processing parameters
SI 32768
SF 75.4677326 MHz
WDW EM
SSB 0
LB 3.00 Hz
GB 0
PC 1.00

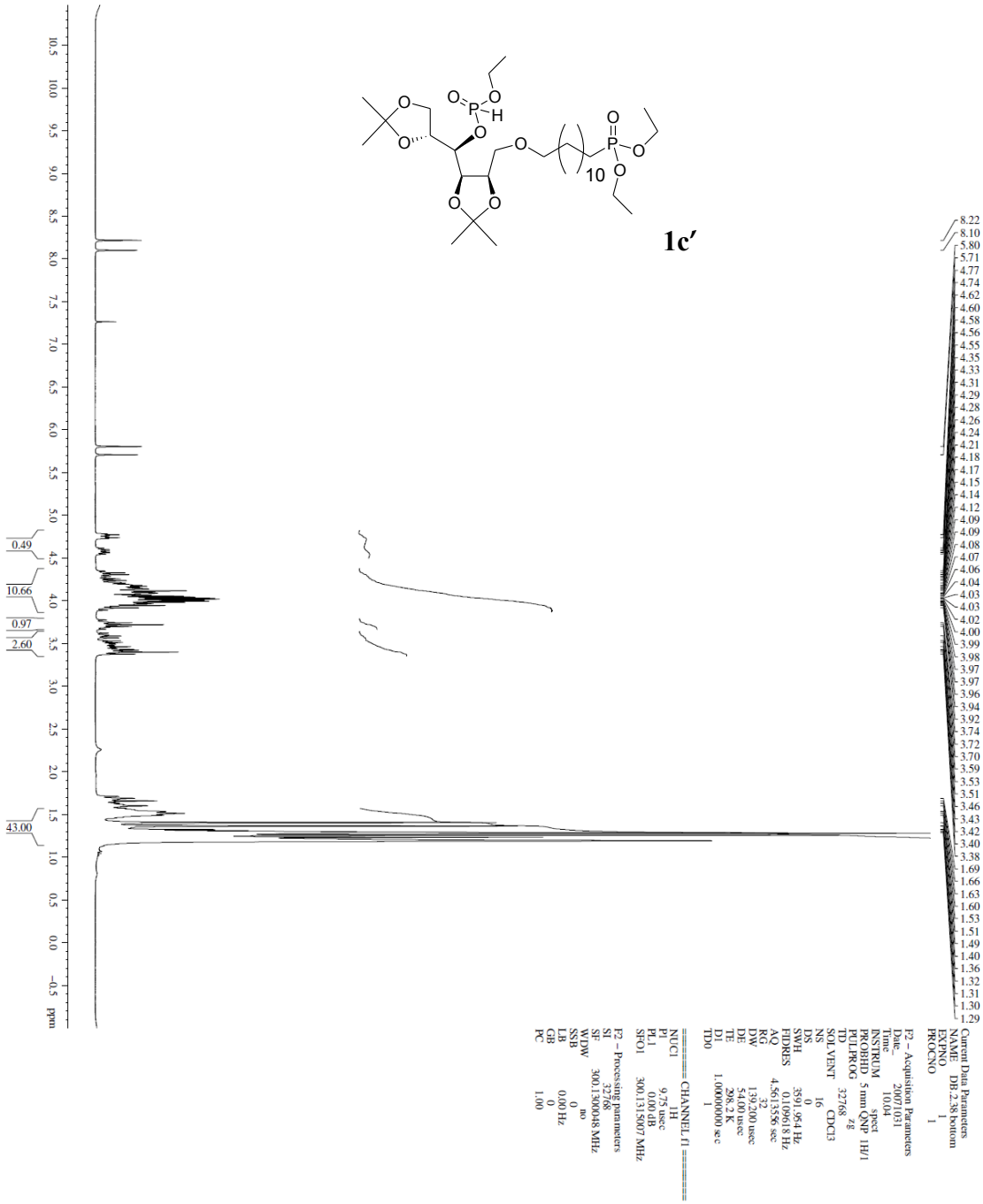
1c′
0.49
10.66
0.97
2.60
43.00
ppm

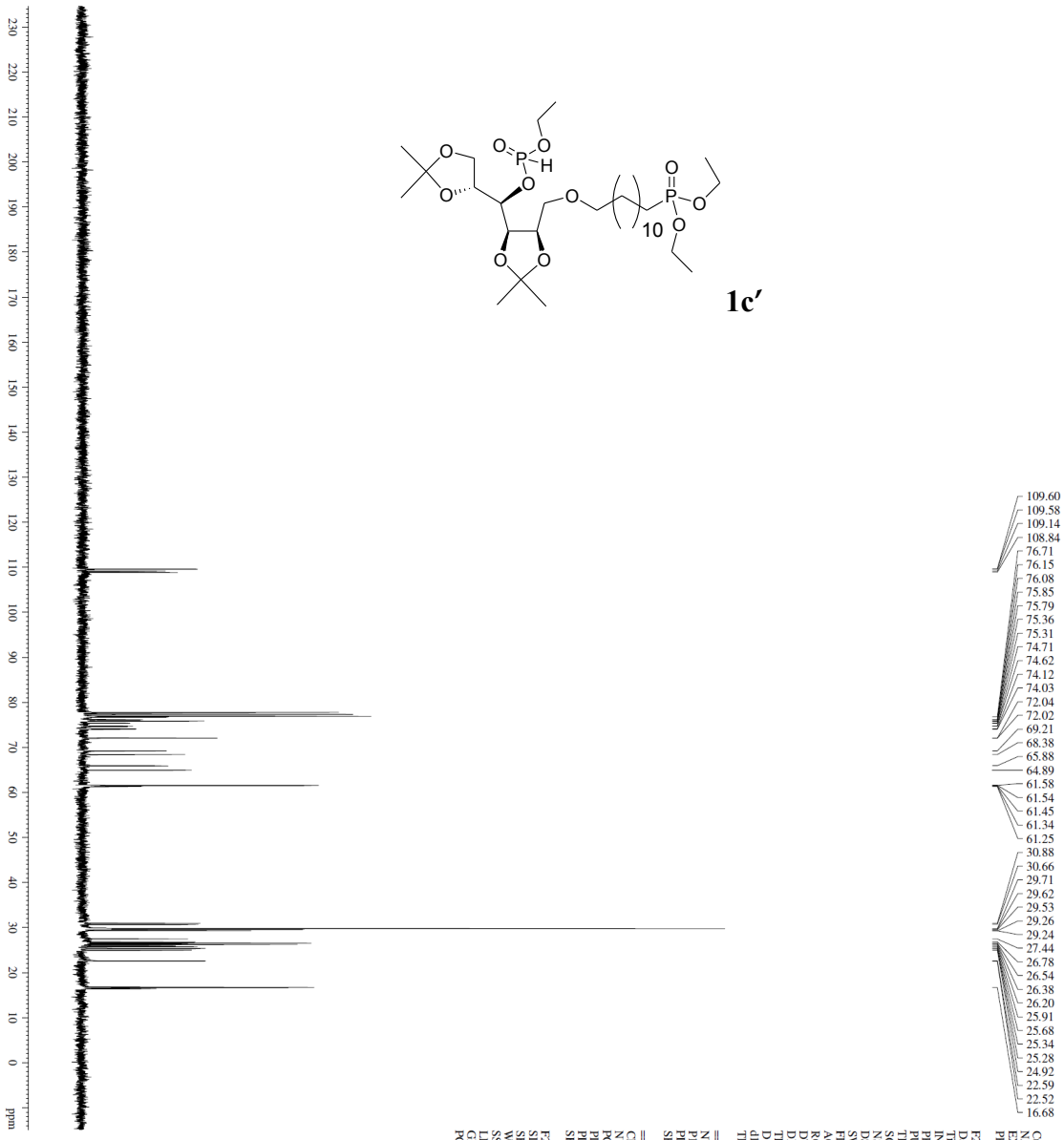
109.60
109.58
109.14
108.84
76.71
76.15
76.08
75.85
75.79
75.36
75.31
74.71
74.62
74.12
74.03
72.04
72.02
69.21
68.38
65.88
64.89
61.58
61.54
61.45
61.34
61.25
30.88
30.66
29.71
29.62
29.53
29.26
29.24
27.44
26.78
26.54
26.38
26.20
25.91
25.68
25.34
25.28
24.92
22.59
22.52
16.68
Current Data Parameters
NAME DB-2.38 bottom cnmr
EXPNO 2
PROCNO 1
F2 - Acquisition Parameters
Date_ 20071031
Time 17:45
INSTRUM spect
PROBHD 5 mm QNP 1H/1
PULPROG zgdc30
TD 65536
SOLVENT CDCl3
NS 300
DS 4
SWH 18832.393 Hz
FIDRES 0.287360 Hz
AQ 1.7400308 sec
RG 11585.2
DW 26.550 usec
DE 6.00000 usec
TE 298.2 K
D1 0.40000001 sec
d11 0.03000000 sec
TD0 1
======== CHANNEL f1 ========
NUC1 13C
P1 13.70 usec
PL1 0.00 dB
SFO1 75.4762200 MHz
======== CHANNEL f2 ========
CPDPRG2 waltz16
NUC2 1H
PCPD2 95.00 usec
PL2 0.00 dB
PL12 18.00 dB
SFO2 300.1312005 MHz
F2 - Processing parameters
SI 32768
SF 75.4677328 MHz
WDW EM
SSB 0
LB 1.00 Hz
GB 0
PC 1.00
230 220 210 200 190 180 170 160 150 140 130 120 110 100 90 80 70 60 50 40 30 20 10 0 ppm

O
O
P
H
O
O
O
O
O
O
O
10
P
O
O
O

1c′

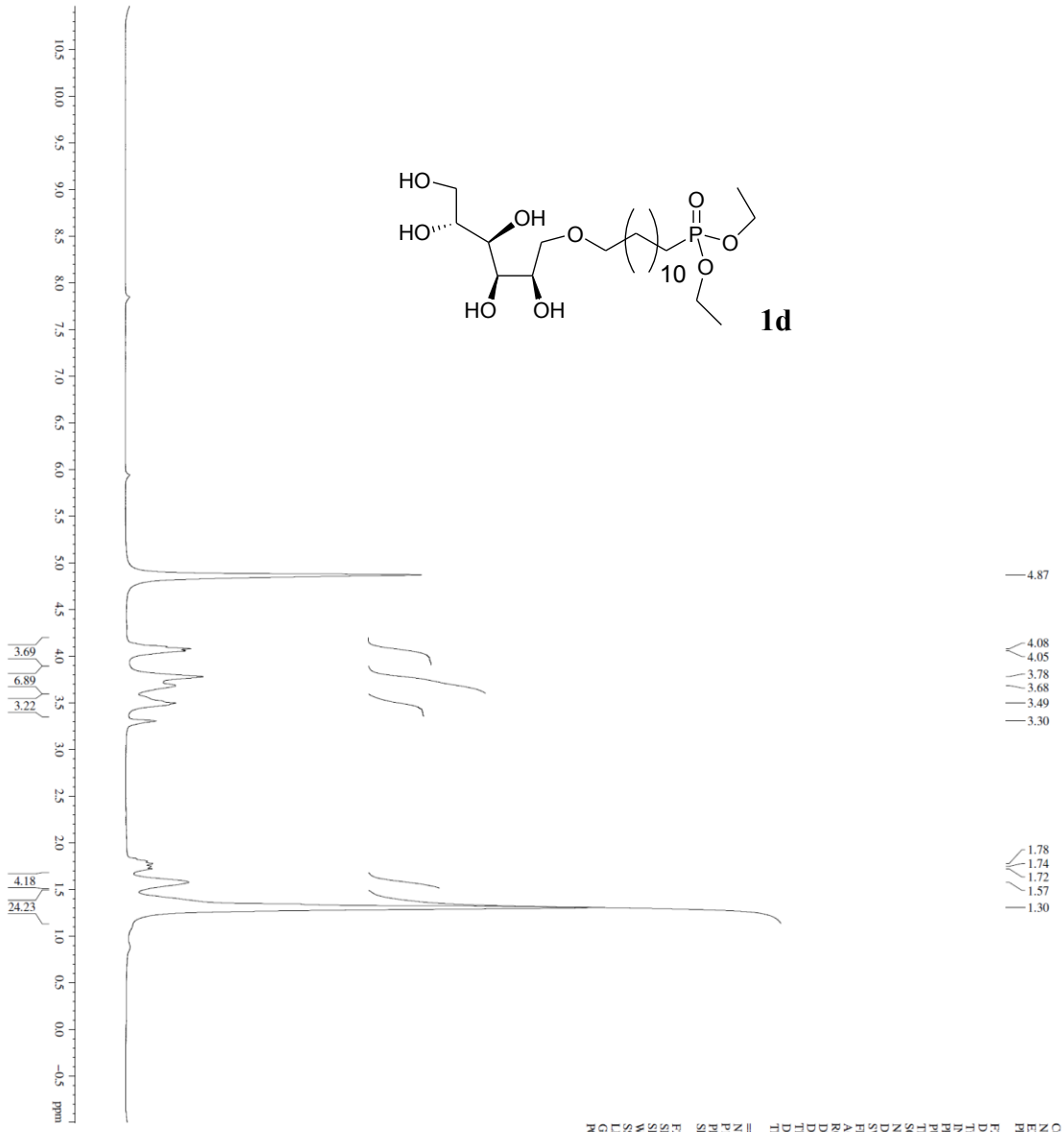
HO
HO
OH
HO
OH
O
10
P
O
O
O
O
1d
4.87
4.08
4.05
3.78
3.68
3.49
3.30
1.78
1.74
1.72
1.57
1.30
3.69
6.89
3.22
4.18
24.23
10.5 10.0 9.5 9.0 8.5 8.0 7.5 7.0 6.5 6.0 5.5 5.0 4.5 4.0 3.5 3.0 2.5 2.0 1.5 1.0 0.5 0.0 –0.5 ppm
Current Data Parameters
NAME DB.acid hydrolysis of 2.38B H NMR MeOD
EXPNO 1
PROCNO 1
F2 – Acquisition Parameters
Date_ 20080308
Time 16.53
INSTRUM spect
PROBHD 5 mm QNP 1H/1
PULPROG zg
TD 32768
SOLVENT MeOH
NS 24
DS 0
SWH 3591.954 Hz
FIDRES 0.109618 Hz
AQ 4.5613556 sec
RG 57
DW 139.200 usec
DE 54.00 usec
TE 299.2 K
D1 1.00000000 sec
TD0 1
======== CHANNEL f1 ========
NUC1 1H
P1 9.75 usec
PL1 0.00 dB
SFO1 300.1315007 MHz
F2 – Processing parameters
SI 32768
SF 300.1300063 MHz
WDW no
SSB 0
LB 0.00 Hz
GB 0
PC 1.00

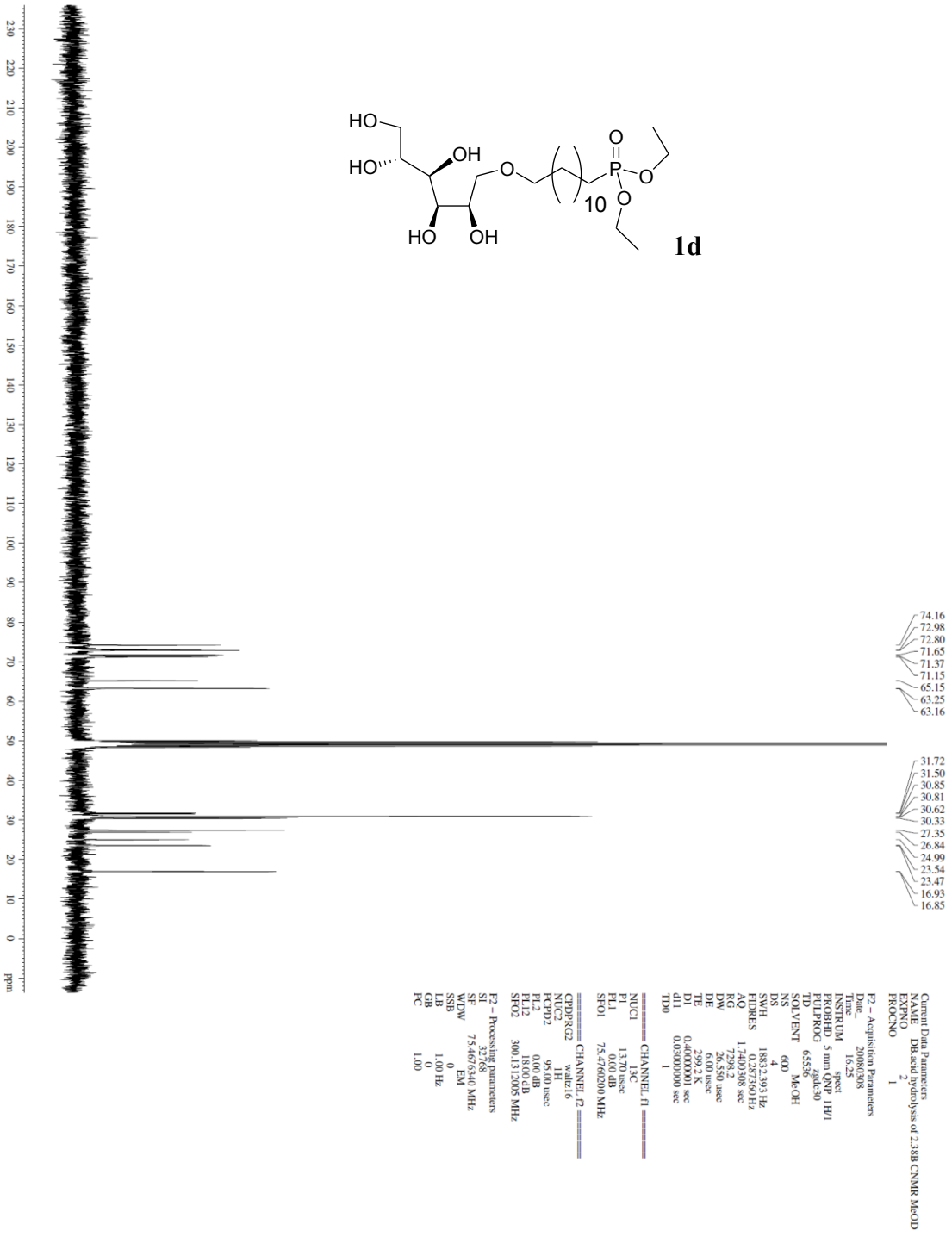
HO
HO
OH
HO
OH
O
10
O
P
O
O
O
1d
74.16
72.98
72.80
71.65
71.37
71.15
65.15
63.25
63.16
31.72
31.50
30.85
30.81
30.62
30.33
27.35
26.84
24.99
23.54
23.47
16.93
16.85
230 220 210 200 190 180 170 160 150 140 130 120 110 100 90 80 70 60 50 40 30 20 10 0 ppm
Current Data Parameters
NAME DB.acid hydrolysis of 2.38B CNMR MeOD
EXPNO 2
PROCNO 1
F2 - Acquisition Parameters
Date_ 20080308
Time 16.25
INSTRUM spect
PROBHD 5 mm QNP 1H/1
PULPROG zgdc30
TD 65536
SOLVENT MeOH
NS 600
DS 4
SWH 18832.393 Hz
FIDRES 0.287360 Hz
AQ 1.7400308 sec
RG 7298.2
DW 26.550 usec
DE 6.00 usec
TE 299.2 K
D1 0.40000001 sec
D11 0.03000000 sec
TD0 1
======== CHANNEL f1 ========
NUC1 13C
P1 13.70 usec
PL1 0.00 dB
SFO1 75.4760200 MHz
======== CHANNEL f2 ========
CPDPRG2 waltz16
NUC2 1H
PCPD2 95.00 usec
PL2 0.00 dB
PL12 18.00 dB
SFO2 300.1312005 MHz
F2 - Processing parameters
SI 32768
SF 75.4676540 MHz
WDW EM
SSB 0
LB 1.00 Hz
GB 0
PC 1.00

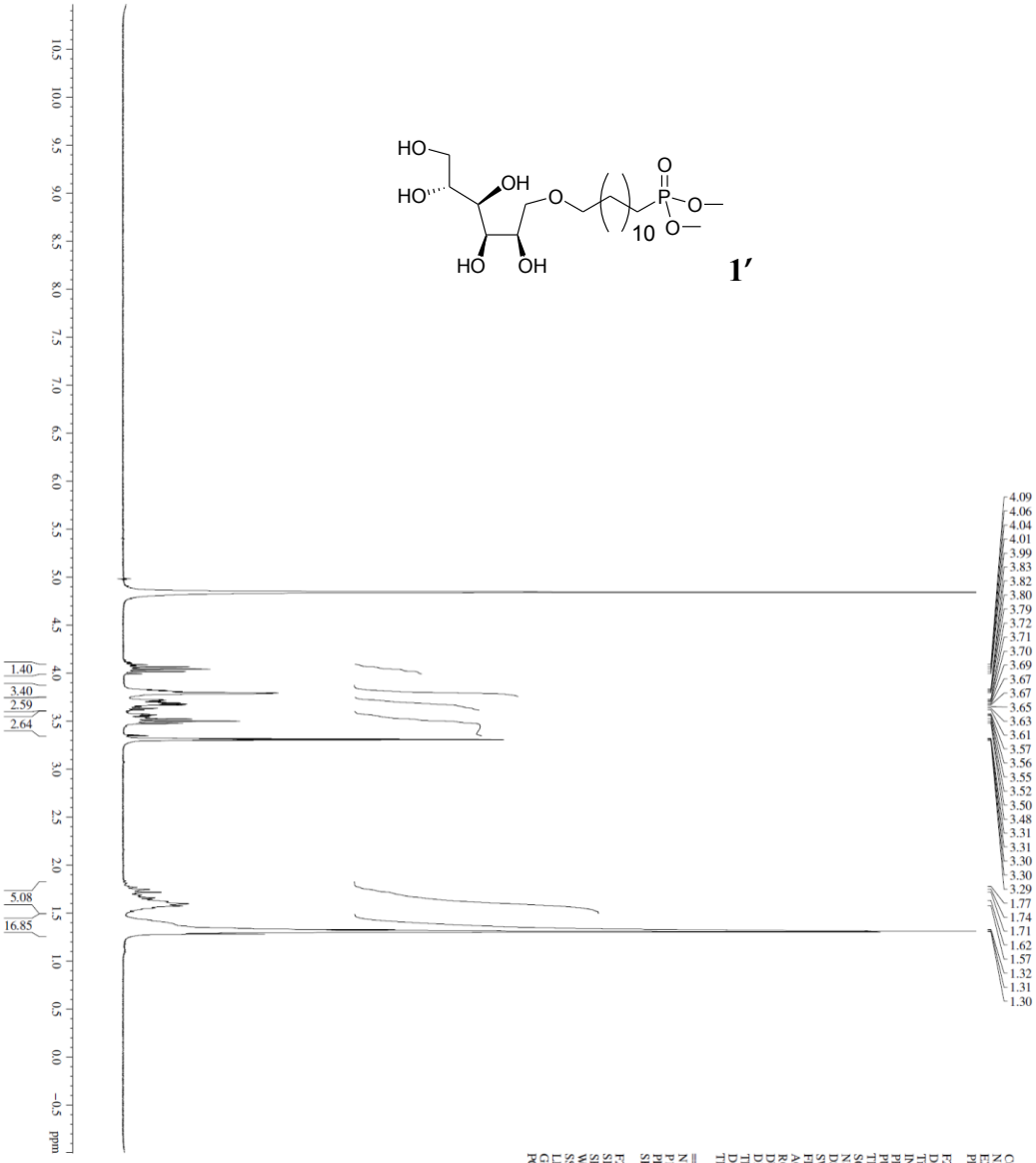
HO
HO
OH
HO
OH
O
10
O
P
O
O
1′
4.09
4.06
4.04
4.01
3.99
3.83
3.82
3.80
3.79
3.72
3.71
3.70
3.69
3.67
3.67
3.65
3.63
3.61
3.57
3.56
3.55
3.52
3.50
3.48
3.31
3.31
3.30
3.30
3.29
1.77
1.74
1.71
1.62
1.57
1.32
1.31
1.30
1.40
3.40
2.59
2.64
5.08
16.85
10.5 10.0 9.5 9.0 8.5 8.0 7.5 7.0 6.5 6.0 5.5 5.0 4.5 4.0 3.5 3.0 2.5 2.0 1.5 1.0 0.5 0.0 −0.5 ppm
Current Data Parameters
NAME DB-2-77 H NMR
EXPNO 1
PROCNO 1
F2 – Acquisition Parameters
Date_ 20080313
Time 18.12
INSTRUM spect
PROBHD 5 mm QNP 1H/1
PULPROG zg
TD 32768
SOLVENT D2O
NS 24
DS 0
SWH 3591.954 Hz
FIDRES 0.109618 Hz
AQ 4.561356 sec
RG 161.3
DW 139.200 usec
DE 54.00 usec
TE 299.2 K
D1 1.00000000 sec
TD0 1
CHANNEL f1
NUC1 1H
P1 9.75 usec
PL1 0.00 dB
SFO1 300.1315097 MHz
F2 – Processing parameters
SI 32768
SF 300.1300063 MHz
WDW no
SSB 0
LB 0.00 Hz
GB 0
PC 1.00

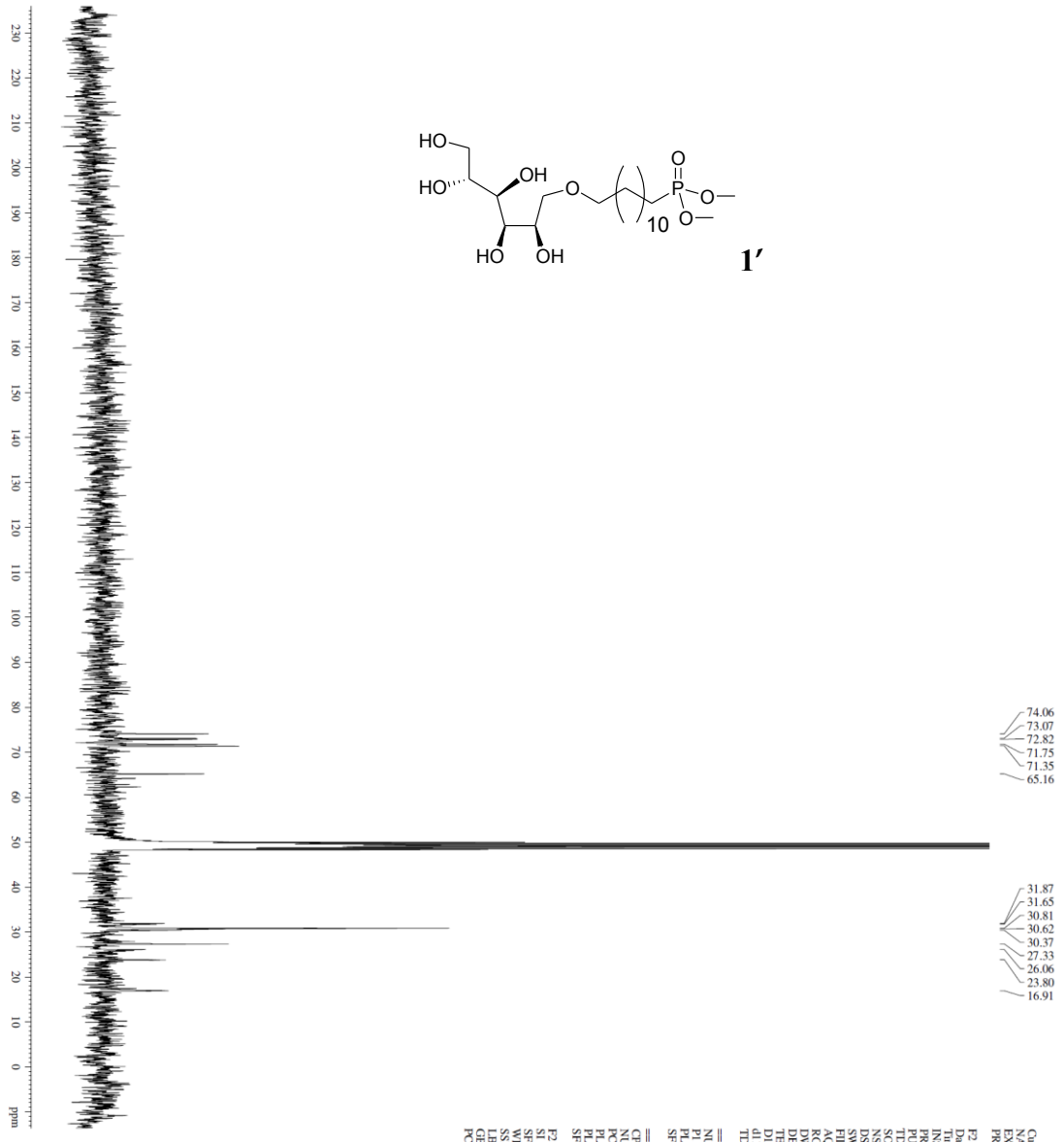

Current Data Parameters
NAME DB.2.77.C.NMR
EXPNO 2
PROCNO 1

F2 – Acquisition Parameters
Date_ 20080313
Time 18.38
INSTRUM spect
PROBHD 5 mm QNP 1H/1
PULPROG zgdc30
TD 65536
SOLVENT D2O
NS 600
DS 4
SWH 18832.393 Hz
FIDRES 0.287340 Hz
AQ 1.7400308 sec
RG 7298.2
DW 26.550 usec
DE 6.00 usec
TE 299.2 K
D1 0.40000001 sec
d11 0.03000000 sec
TD0 1

======== CHANNEL f1 ========
NUC1 13C
P1 13.70 usec
PL1 0.00 dB
SFO1 75.4760200 MHz

======== CHANNEL f2 ========
CPDPRG2 waltz16
NUC2 1H
PCPD2 95.00 usec
PL2 0.00 dB
PL12 18.00 dB
SFO2 300.1312005 MHz

F2 – Processing parameters
SI 32768
SF 75.4676440 MHz
WDW EM
SSB 0
LB 4.00 Hz
GB 0
PC 1.00

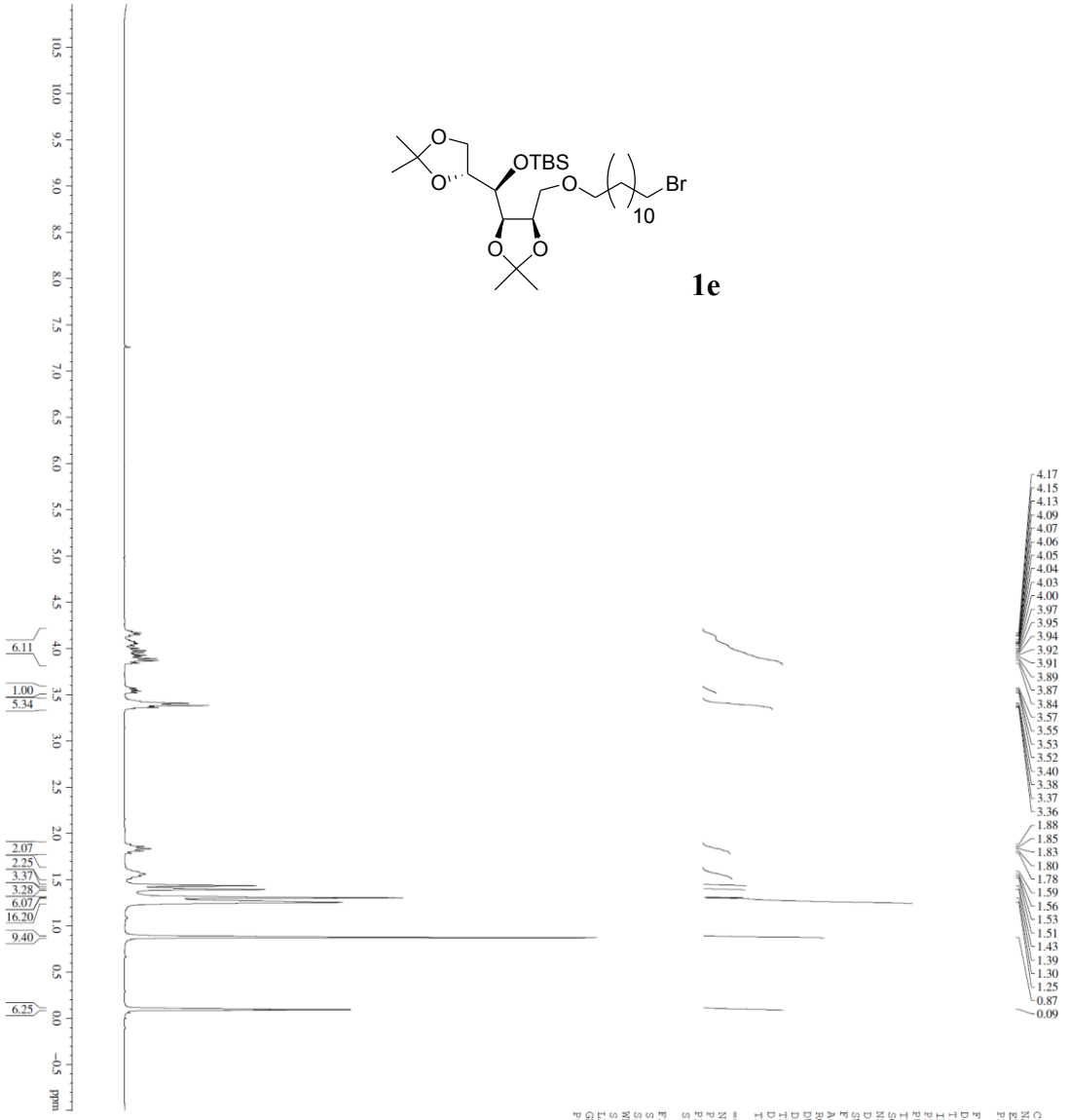
OTBS
O
Br
10
1e
6.11
1.00
5.34
2.07
2.25
3.37
3.28
6.07
16.20
9.40
6.25
ppm

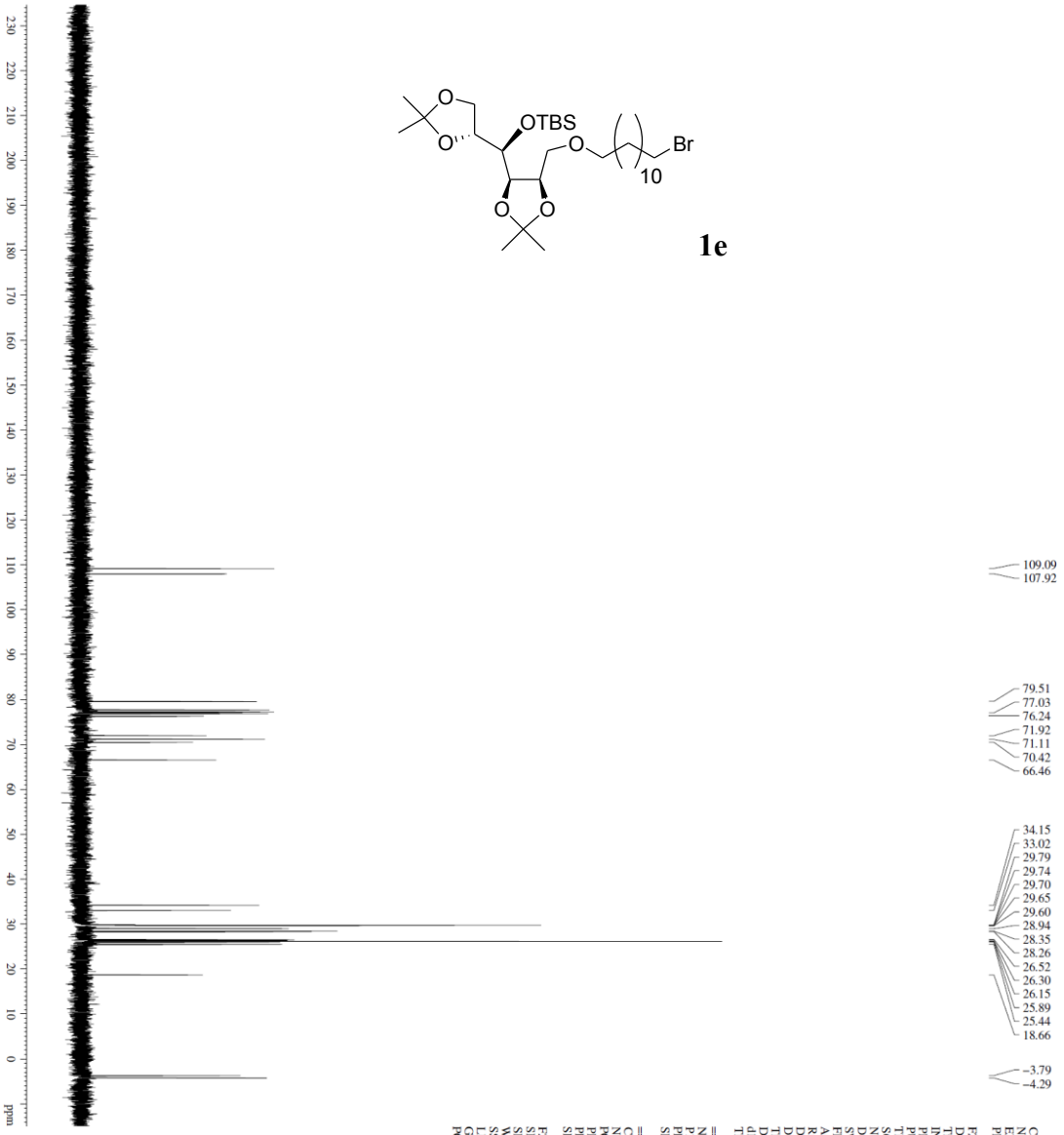
OTBS
Br
10
O
O
O
O
O
O
1e
109.09
107.92
79.51
77.03
76.24
71.92
71.11
70.42
66.46
34.15
33.02
29.79
29.74
29.70
29.65
29.60
28.94
28.35
28.26
26.52
26.30
26.15
25.89
25.44
18.66
-3.79
-4.29
Current Data Parameters
NAME DB-2.85 C NMR
EXPNO 2
PROCNO 1
F2 - Acquisition Parameters
Date_ 20080515
Time 18.47
INSTRUM spect
PROBHD 5 mm QNP 1H/1
PULPROG zgdc30
TD 65536
SOLVENT D2O
NS 300
DS 4
SWH 18832.393 Hz
FIDRES 0.287360 Hz
AQ 1.7400308 sec
RG 51600
DW 26.550 usec
DE 6.00 usec
TE 298.2 K
D1 0.40000001 sec
d11 0.03000000 sec
TD0 1
======== CHANNEL f1 ========
NUC1 13C
P1 13.70 usec
PL1 0.00 dB
SFO1 75.4760200 MHz
======== CHANNEL f2 ========
CPDPRG2 waltz16
NUC2 1H
PCPD2 95.00 usec
PL2 0.00 dB
PL12 18.00 dB
SFO2 300.1312005 MHz
F2 - Processing parameters
SI 32768
SF 75.4677347 MHz
WDW no
SSB 0
LB 0.00 Hz
GB 0
PC 1.00
230 220 210 200 190 180 170 160 150 140 130 120 110 100 90 80 70 60 50 40 30 20 10 0 ppm

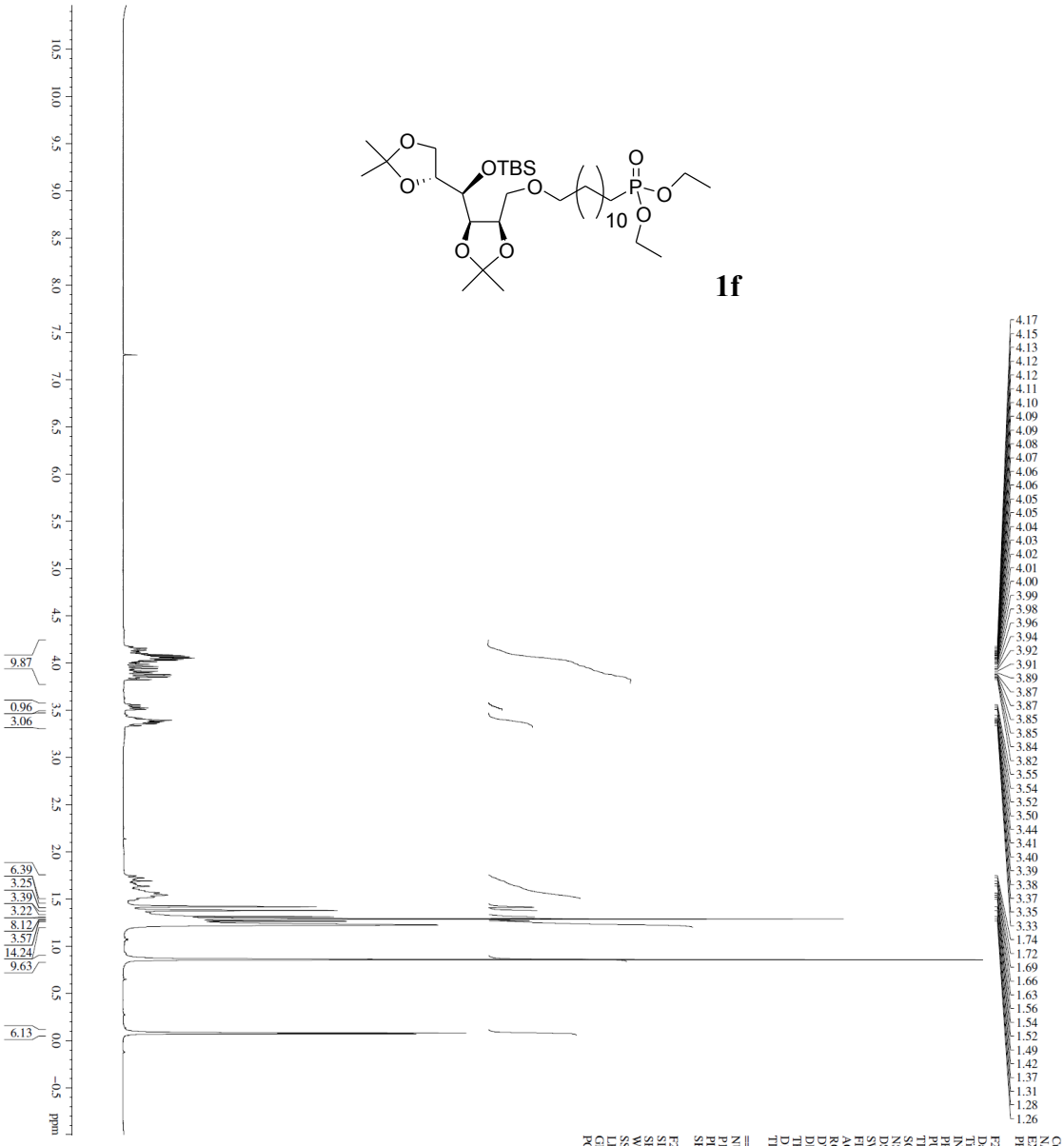
OTBS
O
O
O
O
O
O
P
O
O
10
O
1f
9.87
0.96
3.06
6.39
3.25
3.39
3.22
8.12
3.57
14.24
9.63
6.13
ppm
Current Data Parameters
NAME DB.2.88 H NMR
EXPNO 1
PROCNO 1
F2 – Acquisition Parameters
Date_ 20180528
Time 11.43
INSTRUM spect
PROBHD 5 mm QNP 1H/1
PULPROG zg
TD 32768
SOLVENT CDCl3
NS 16
DS 0
SWH 3591.954 Hz
FIDRES 0.109618 Hz
AQ 4.5613556 sec
RG 128.4
DW 139.200 usec
DE 54.00 usec
TE 298.2 K
D1 1.00000000 sec
TD0 1
CHANNEL f1
NUC1 1H
P1 9.75 usec
PL1 0.00 dB
SFO1 300.1315007 MHz
F2 – Processing parameters
SI 32768
SF 300.1300063 MHz
WDW no
SSB 0
LB 0.00 Hz
GB 0
PC 1.00

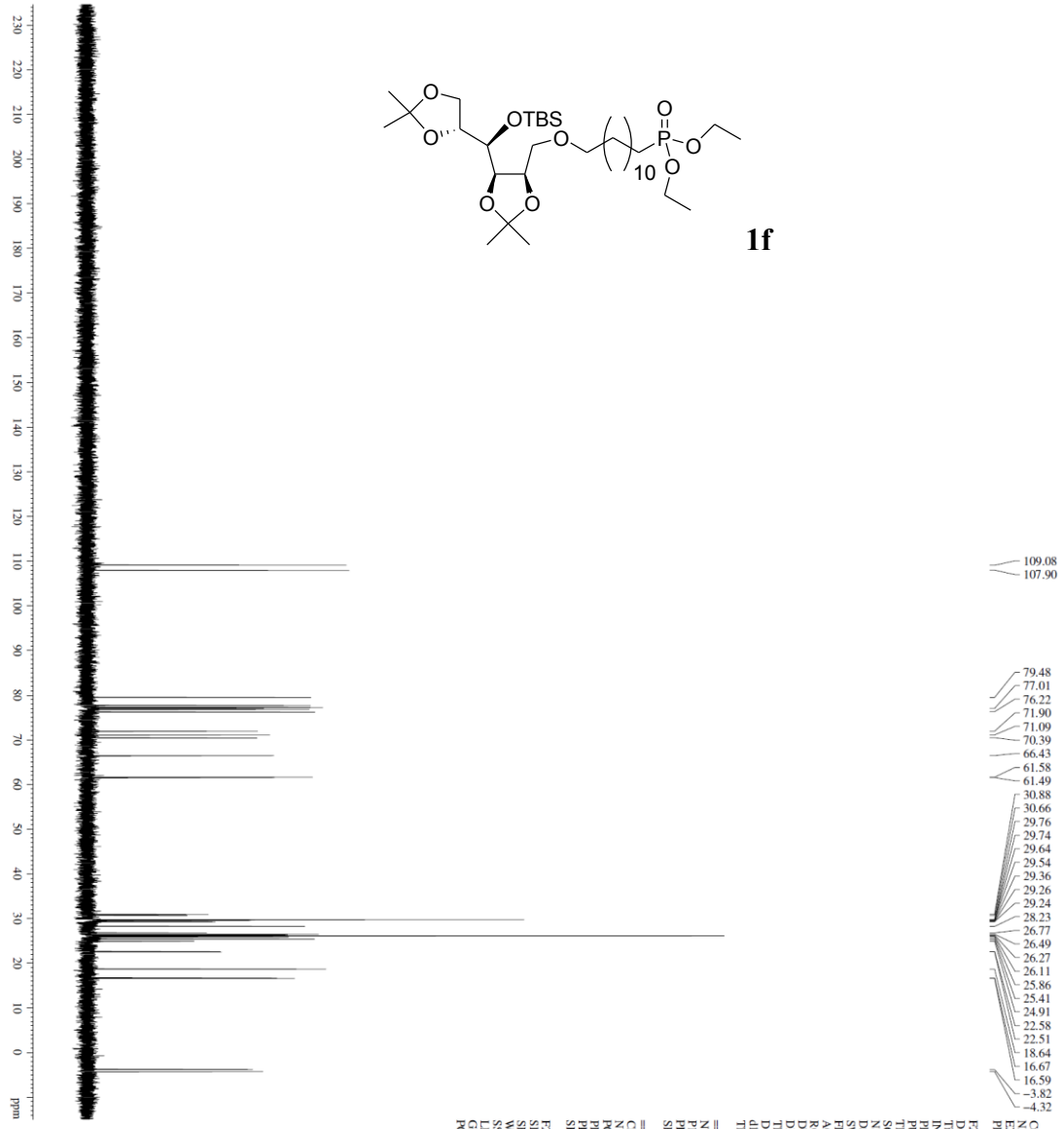
OTBS
O
O
O
O
O
O
O
O
P
O
10
1f
109.08
107.90
79.48
77.01
76.22
71.90
71.09
70.39
66.43
61.58
61.49
30.88
30.66
29.76
29.74
29.64
29.54
29.36
29.26
29.24
28.23
26.77
26.49
26.27
26.11
25.86
25.41
24.91
22.58
22.51
18.64
16.67
16.59
−3.82
−4.32
Current Data Parameters
NAME DB2.88 C NMR
EXPNO 2
PROCNO 1
F2 – Acquisition Parameters
Date_ 20080528
Time 12.04
INSTRUM spect
PROBHD 5 mm QNP 1H/1
PULPROG zgdc30
TD 65536
SOLVENT CDCl3
NS 500
DS 4
SWH 18832.393 Hz
FIDRES 0.287360 Hz
AQ 1.7400308 sec
RG 1149.4
DW 26.550 usec
DE 6.00 usec
TE 298.2 K
D1 0.40000001 sec
d11 0.03000000 sec
TD0 1
CHANNEL f1
NUC1 13C
P1 13.70 usec
PL1 0.00 dB
SFO1 75.4760200 MHz
CHANNEL f2
CPDPRG2 waltz16
NUC2 1H
PCPD2 95.00 usec
PL2 0.00 dB
PL12 18.00 dB
SFO2 300.1312005 MHz
F2 – Processing parameters
SI 32768
SF 75.4677354 MHz
WDW no
SSB 0
LB 0.00 Hz
GB 0
PC 1.00
230
220
210
200
190
180
170
160
150
140
130
120
110
100
90
80
70
60
50
40
30
20
10
0
ppm

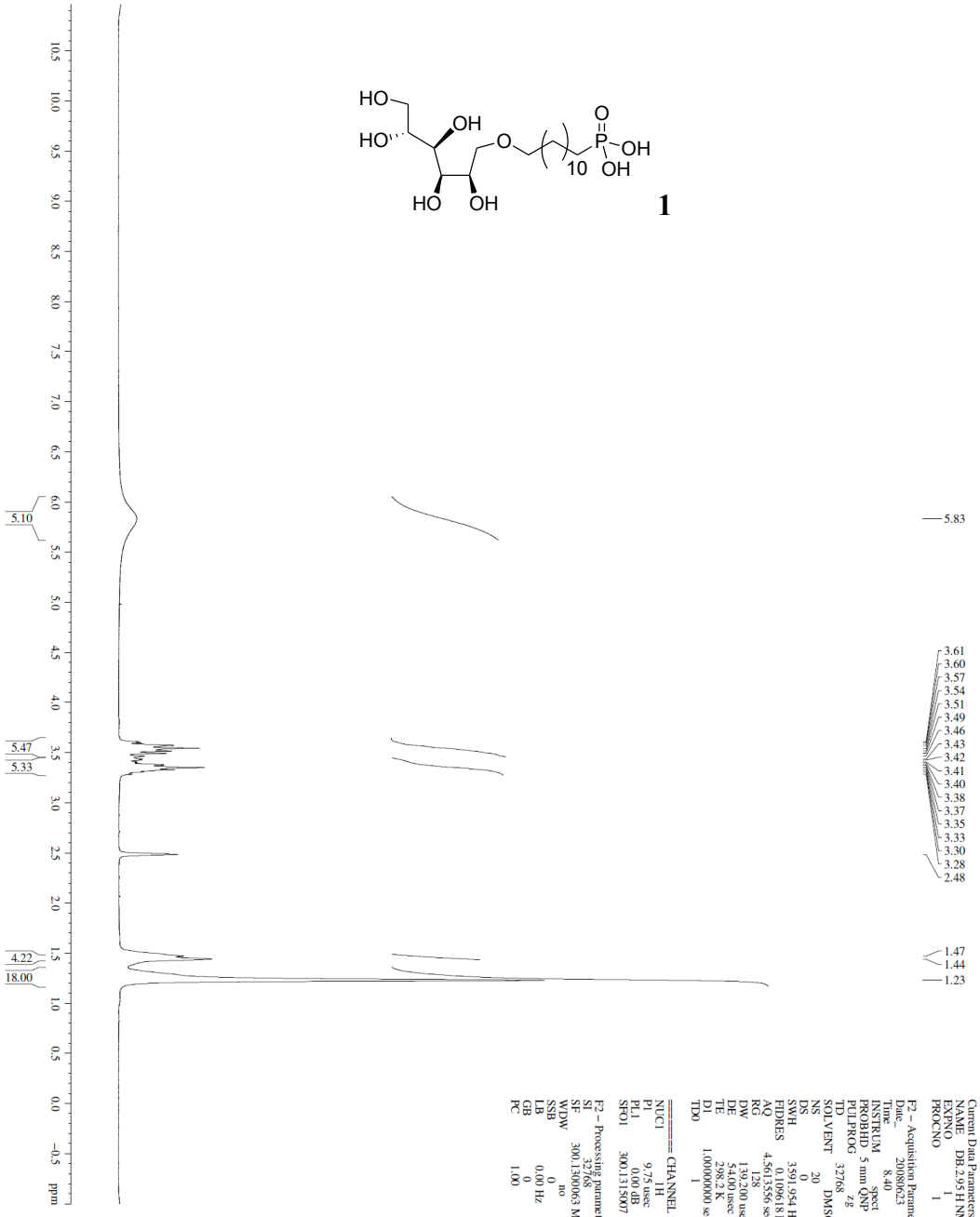
HO
HO
OH
HO
OH
O
O
P
OH
OH
10
1
5.10
5.47
5.33
4.22
18.00
5.83
3.61
3.60
3.57
3.54
3.51
3.49
3.46
3.43
3.42
3.41
3.40
3.38
3.37
3.35
3.33
3.30
3.28
2.48
1.47
1.44
1.23
10.5
10.0
9.5
9.0
8.5
8.0
7.5
7.0
6.5
6.0
5.5
5.0
4.5
4.0
3.5
3.0
2.5
2.0
1.5
1.0
0.5
0.0
−0.5
ppm
Current Data Parameters
NAME DB.2.95.H NMR in DMSO final
EXPNO 1
PROCNO 1
F2 – Acquisition Parameters
Date_ 20080623
Time 8.40
INSTRUM spect
PROBHD 5 mm QNP 1H/1
PULPROG zg
TD 32768
SOLVENT DMSO
NS 20
DS 0
SWH 3591.954 Hz
FIDRES 0.109618 Hz
AQ 4.5613556 sec
RG 128
DW 139.200 usec
DE 54.00 usec
TE 298.2 K
D1 1.00000000 sec
TD0 1
======== CHANNEL f1 ========
NUC1 1H
P1 9.75 usec
PL1 0.00 dB
SFO1 300.1315007 MHz
F2 – Processing parameters
SI 32768
SF 300.1300063 MHz
WDW no
SSB 0
LB 0.00 Hz
GB 0
PC 1.00

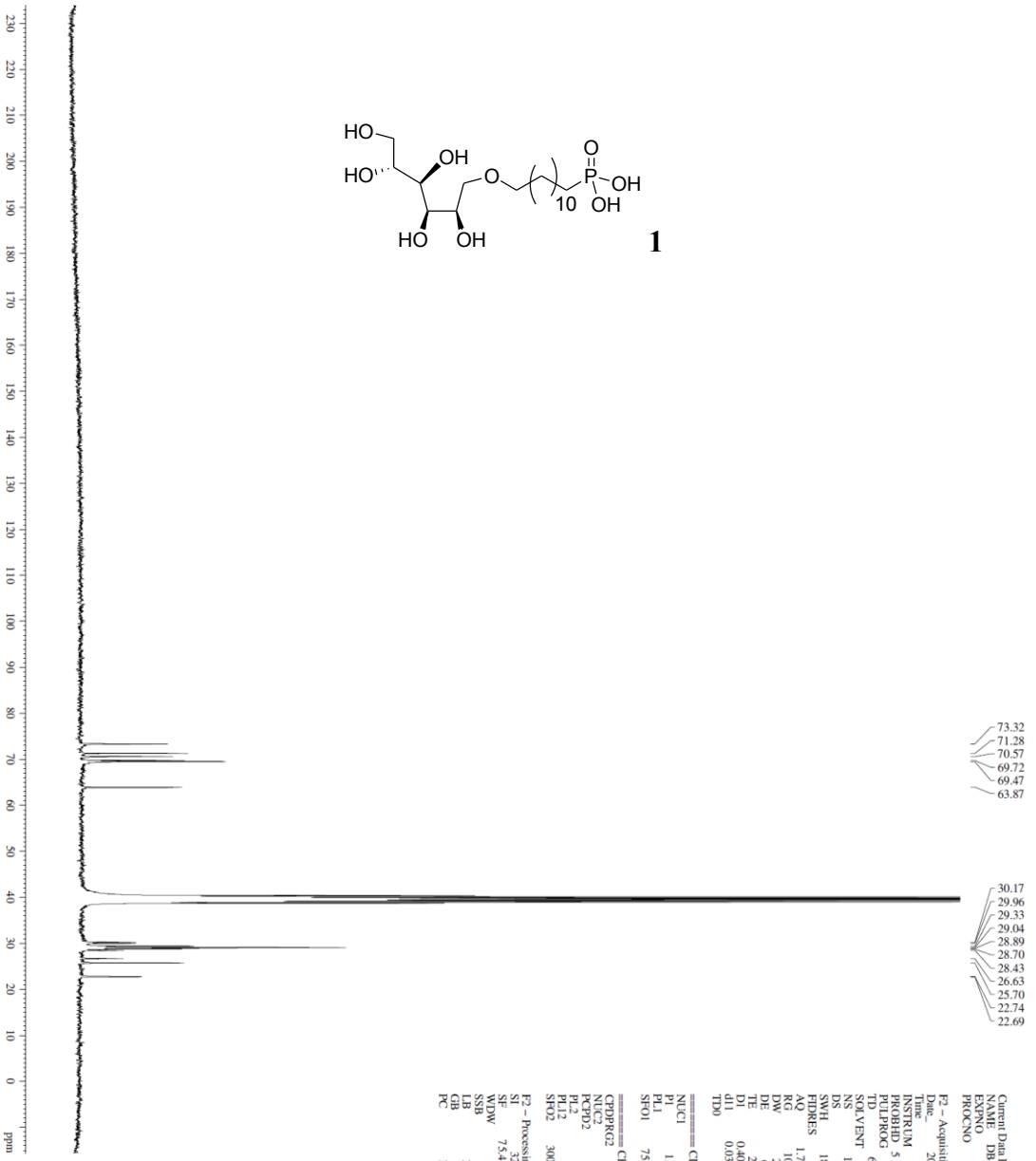

1

Current Data Parameters
NAME DB-295 C NMR in DMSO final
EXPNO 2
PROCNO 1

F2 – Acquisition Parameters
Date_ 20080623
Time 4.59
INSTRUM spect
PROBHD 5 mm QNP 1H/1
PULPROG zgdc30
TD 65536
SOLVENT DMSO
NS 10000
DS 4
SWH 18832.393 Hz
FIDRES 0.287360 Hz
AQ 1.7400308 sec
RG 10321.3
DW 26.550 usec
DE 6.00 usec
TE 298.2 K
D1 0.40000001 sec
d11 0.03000000 sec
TD0 1

======== CHANNEL f1 ========
NUC1 13C
P1 13.70 usec
PL1 0.00 dB
SFO1 75.4766200 MHz

======== CHANNEL f2 ========
CPDPRG2 waltz16
NUC2 1H
PCPD2 95.00 usec
PL2 0.00 dB
PL12 18.00 dB
SFO2 300.1312005 MHz

F2 – Processing parameters
SI 32768
SF 75.4677833 MHz
WDW EM
SSB 0
LB 3.00 Hz
GB 0
PC 1.00

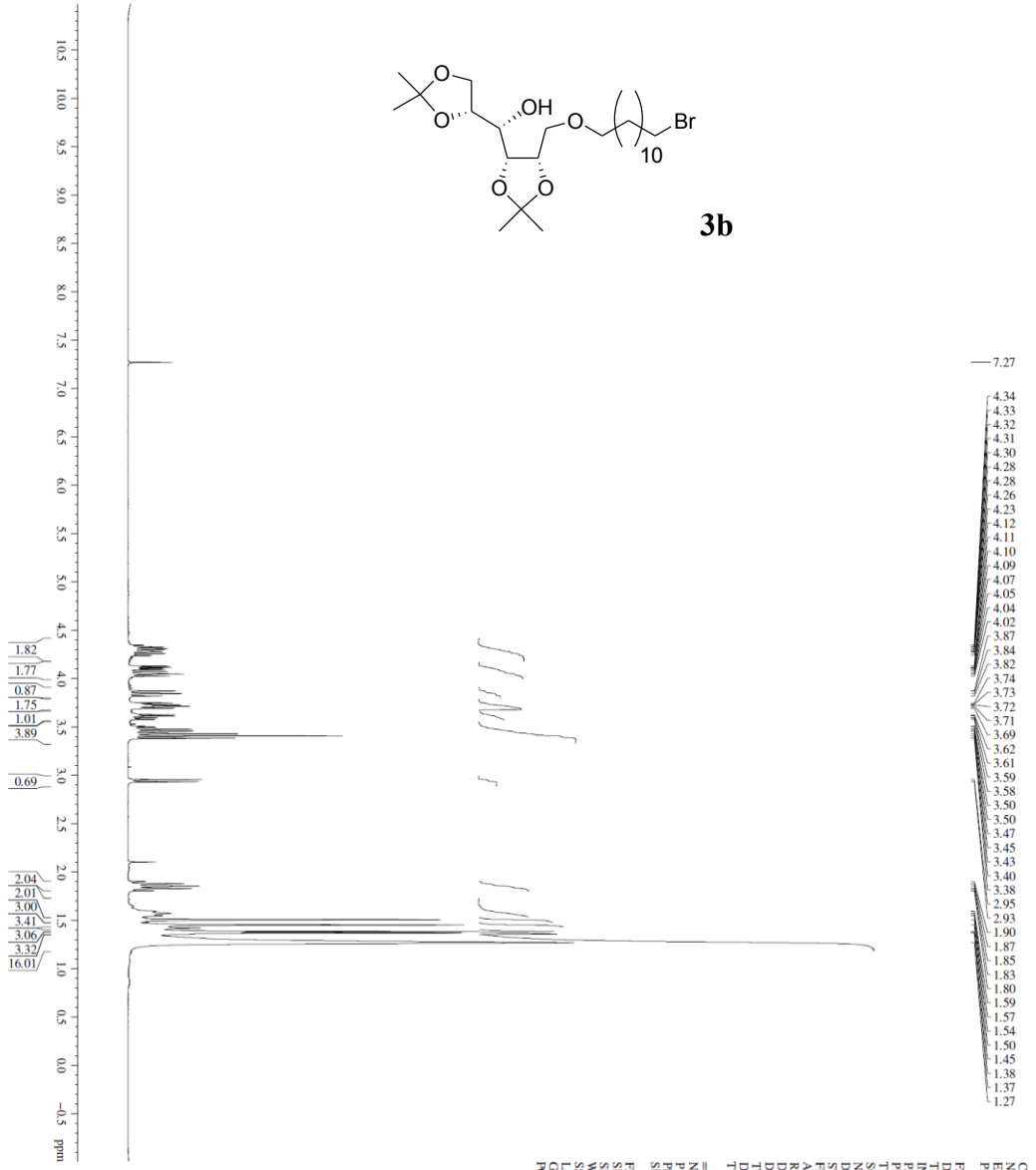
OH
O
Br
10
3b
7.27
4.34
4.33
4.32
4.31
4.30
4.28
4.28
4.26
4.23
4.12
4.11
4.10
4.09
4.07
4.05
4.04
4.02
3.87
3.84
3.82
3.74
3.73
3.72
3.71
3.69
3.62
3.61
3.59
3.58
3.50
3.50
3.47
3.45
3.43
3.40
3.38
2.95
2.93
1.90
1.87
1.85
1.83
1.80
1.59
1.57
1.54
1.50
1.45
1.38
1.37
1.27
1.82
1.77
0.87
1.75
1.01
3.89
0.69
2.04
2.01
3.00
3.41
3.06
3.32
16.01
10.5
10.0
9.5
9.0
8.5
8.0
7.5
7.0
6.5
6.0
5.5
5.0
4.5
4.0
3.5
3.0
2.5
2.0
1.5
1.0
0.5
0.0
−0.5
ppm
Current Data Parameters
NAME DB-3.23 HNMR
EXPNO 1
PROCNO 1
F2 – Acquisition Parameters
20081103
Time 15.44
INSTRUM spect
PROBHD 5 mm QNP 1H/1
PULPROG zg
TD 32768
SOLVENT CDCl3
NS 16
DS 0
SWH 3594.954 Hz
FIDRES 0.109618 Hz
AQ 4.5613556 sec
RG 71.8
DW 139.200 usec
DE 54.00 usec
TE 300.2 K
D1 1.00000000 sec
TD0 1
CHANNEL f1
NUCI 1H
P1 9.75 usec
PL1 0.00 dB
SFO1 300.1315007 MHz
F2 – Processing parameters
SI 32768
SF 300.1300039 MHz
WDW no
SSB 0
LB 0.00 Hz
GB 0
PC 1.00

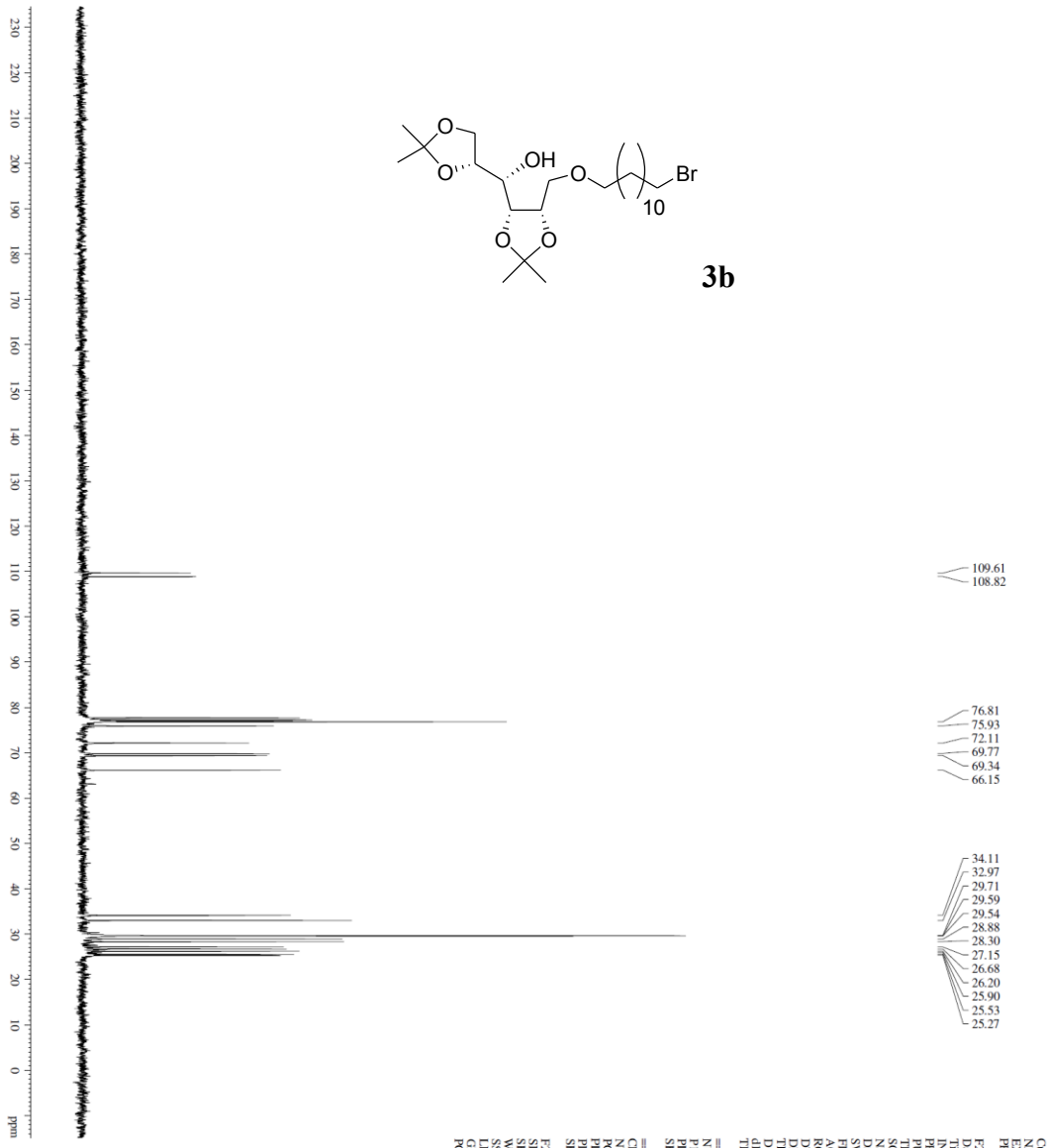
O
O
OH
O
Br
10
O
O
3b
109.61
108.82
76.81
75.93
72.11
69.77
69.34
66.15
34.11
32.97
29.71
29.59
29.54
28.88
28.30
27.15
26.68
26.20
25.90
25.53
25.27
Current Data Parameters
NAME DB-3.25 C NMR
EXPNO 2
PROCNO 1
F2 – Acquisition Parameters
Date_ 20081103
Time 16.02
INSTRUM spect
PROBHD 5 mm QNP 1H/1
PULPROG zgdc30
TD 65536
SOLVENT CDCl3
NS 300
DS 4
SWH 18832.393 Hz
FIDRES 0.287360 Hz
AQ 1.7400308 sec
RG 7298.2
DW 26.550 usec
DE 6.00 usec
TE 300.2 K
D1 0.40000001 sec
d11 0.03000000 sec
TD0 1
======== CHANNEL f1 ========
NUC1 13C
P1 13.70 usec
PL1 0.00 dB
SFO1 75.4760200 MHz
======== CHANNEL f2 ========
CPDPRG2 waltz16
NUC2 1H
PCPD2 95.00 usec
PL2 0.00 dB
PL12 18.00 dB
SFO2 300.1312005 MHz
F2 – Processing parameters
SI 32768
SF 75.4677368 MHz
WDW EM
SSB 0
LB 2.00 Hz
GB 0
PC 1.00
230 220 210 200 190 180 170 160 150 140 130 120 110 100 90 80 70 60 50 40 30 20 10 0 ppm

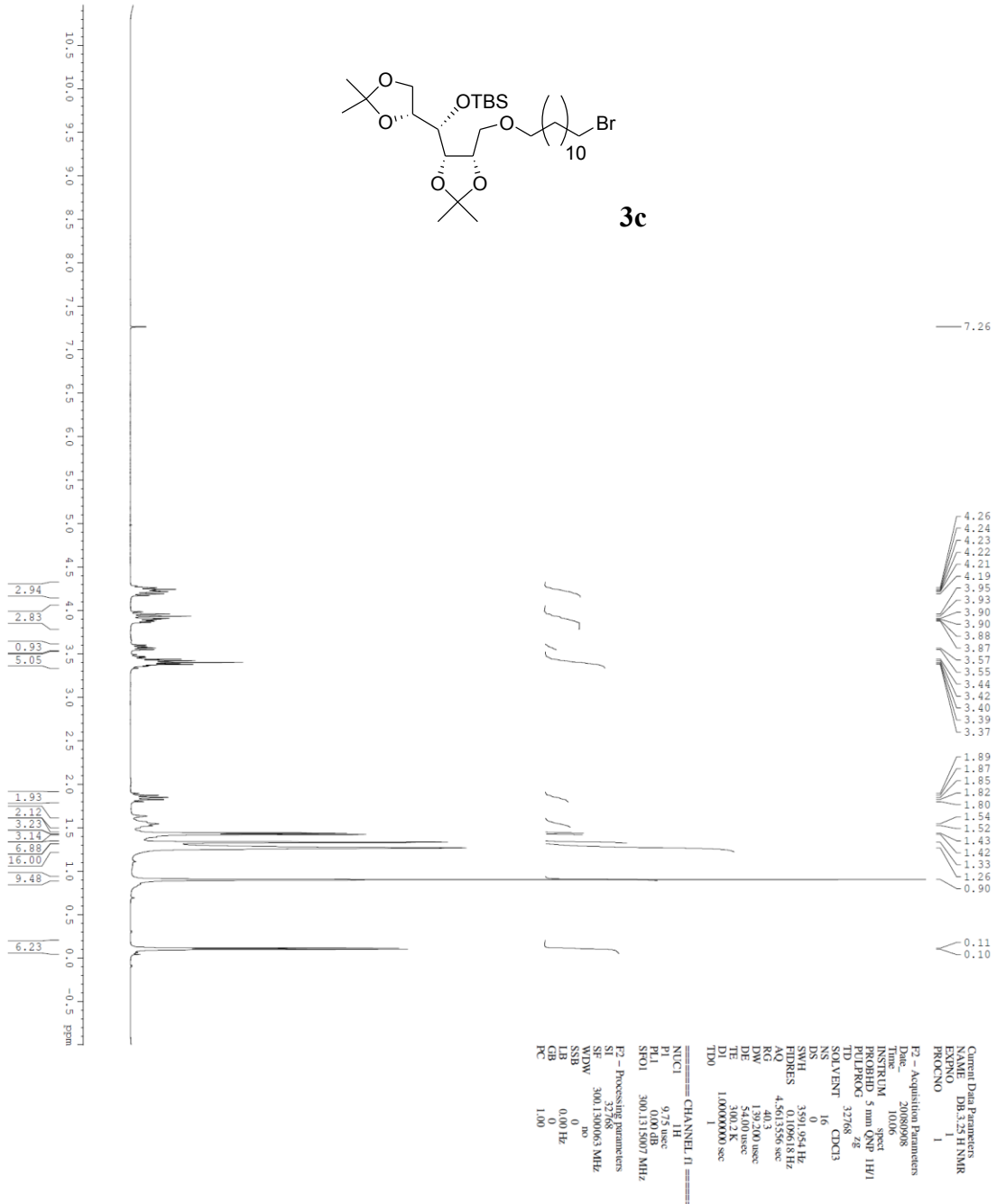
OTBS
O
O
O
O
O
Br
10
3c
7.26
4.26
4.24
4.23
4.22
4.21
4.19
3.95
3.93
3.90
3.90
3.88
3.87
3.57
3.55
3.44
3.42
3.40
3.39
3.37
1.89
1.87
1.85
1.82
1.80
1.54
1.52
1.43
1.42
1.33
1.26
0.90
0.11
0.10
2.94
2.83
0.93
5.05
1.93
2.12
3.23
3.14
6.88
16.00
9.48
6.23
10.5 10.0 9.5 9.0 8.5 8.0 7.5 7.0 6.5 6.0 5.5 5.0 4.5 4.0 3.5 3.0 2.5 2.0 1.5 1.0 0.5 0.0 -0.5 ppm
Current Data Parameters
NAME DB-3-25 H NMR
EXPNO 1
PROCNO 1
F2 - Acquisition Parameters
Date_ 20080908
Time 10.06
INSTRUM spect
PROBHD 5 mm QNP 1H/1
PULPROG zg
TD 32768
SOLVENT CDCl3
NS 16
DS 0
SWH 3591.954 Hz
FIDRES 0.109618 Hz
AQ 4.561556 sec
RG 40.3
DW 139.200 usec
DE 5.00 usec
TE 300.2 K
D1 1.00000000 sec
TD0 1
======== CHANNEL f1 ========
NUC1 1H
P1 9.75 usec
PL1 0.00 dB
SFO1 300.1315007 MHz
F2 - Processing parameters
SI 32768
SF 300.1300063 MHz
WDW no
SSB 0
LB 0.00 Hz
GB 0
PC 1.00

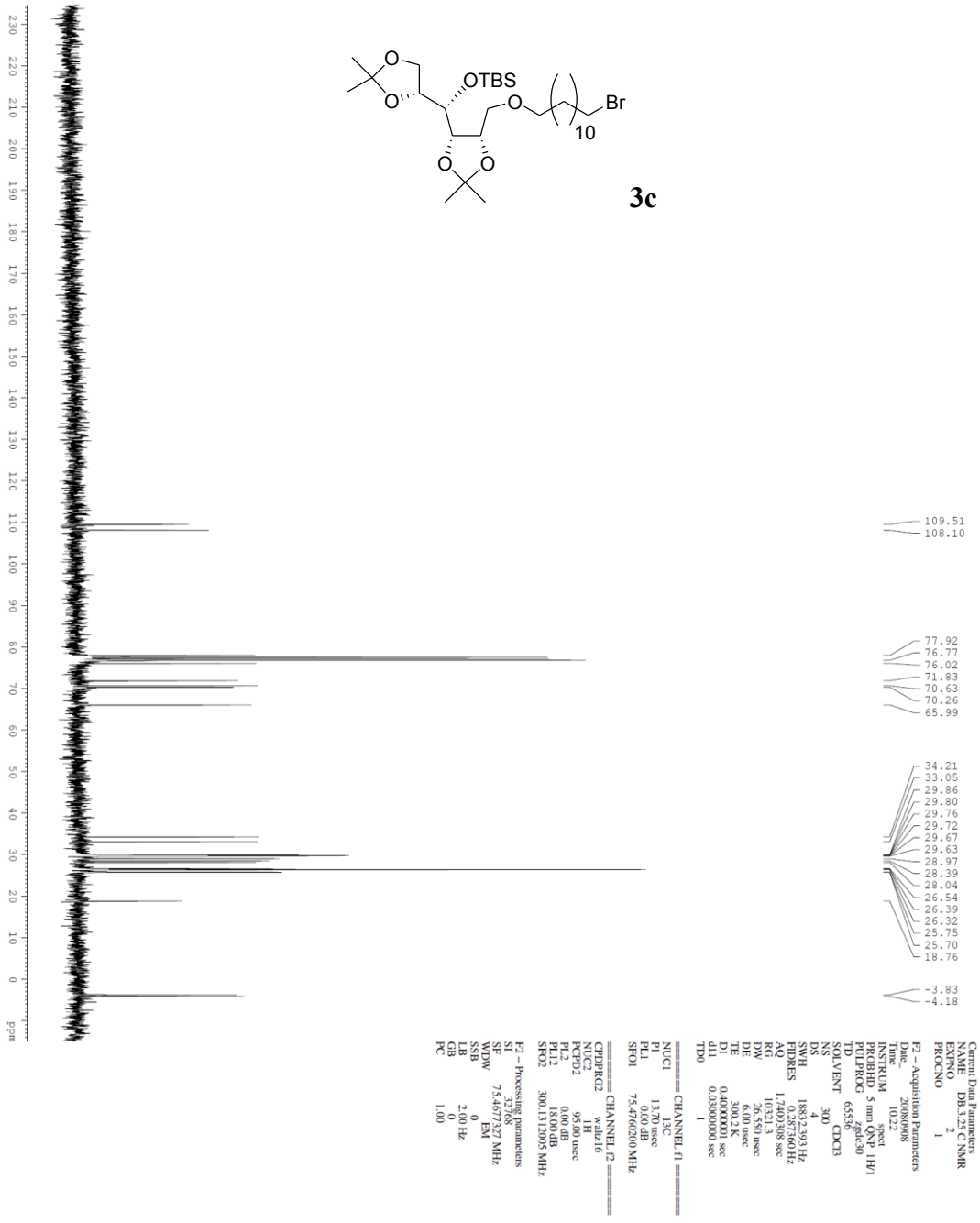
OTBS
Br
10
3c
109.51
108.10
77.92
76.77
76.02
71.83
70.63
70.26
65.99
34.21
33.05
29.86
29.80
29.76
29.72
29.67
29.63
28.97
28.39
28.04
26.54
26.39
26.32
25.75
25.70
18.76
-3.83
-4.18
ppm

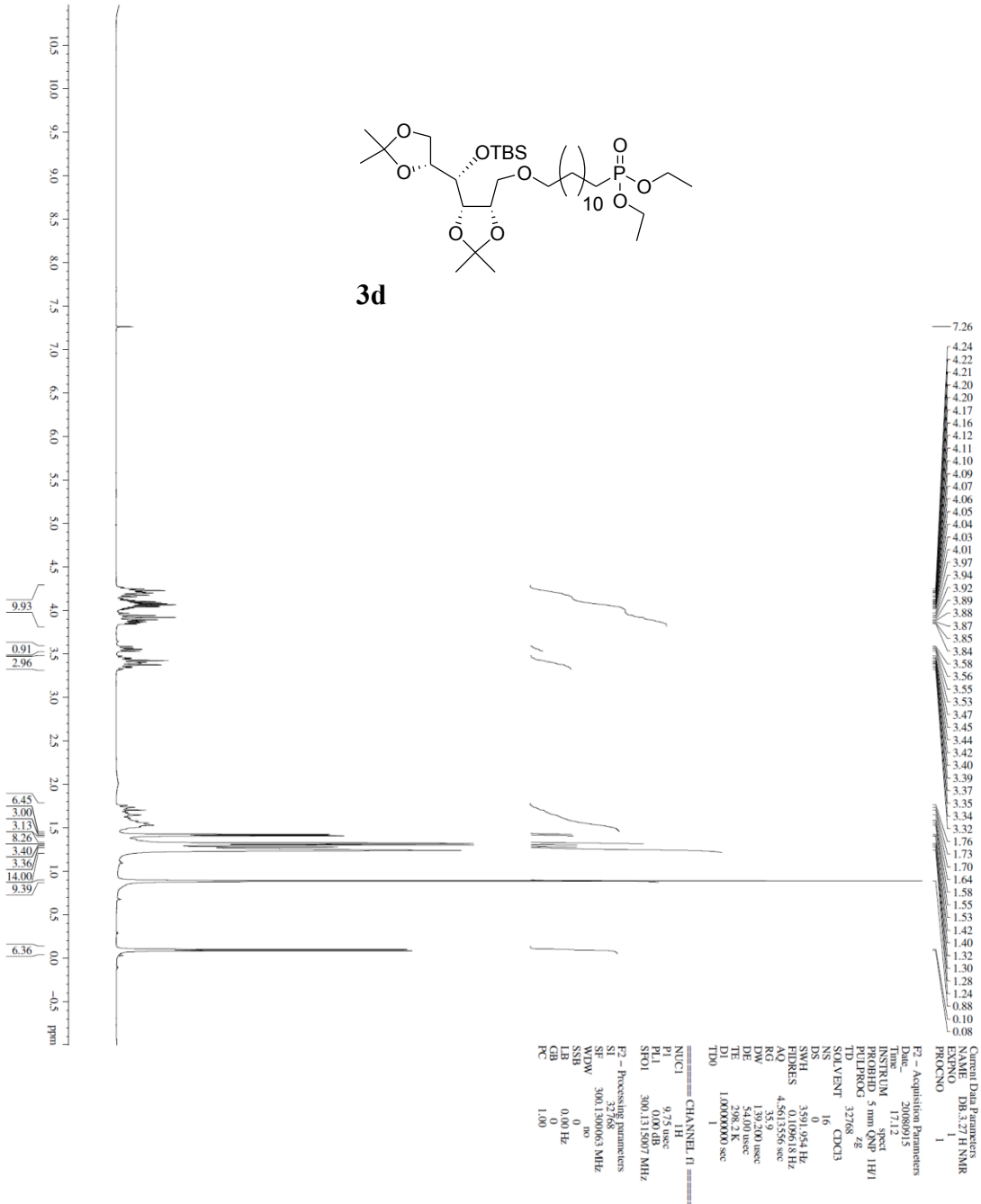
OTBS
O
O
O
O
O
O
O
P
O
O
10
3d
9.93
0.91
2.96
6.45
3.00
3.13
8.26
3.40
3.36
14.00
9.39
6.36
ppm
7.26
4.24
4.22
4.21
4.20
4.20
4.17
4.16
4.12
4.11
4.10
4.09
4.07
4.06
4.05
4.04
4.03
4.01
3.97
3.94
3.92
3.89
3.88
3.87
3.85
3.84
3.58
3.56
3.55
3.53
3.47
3.45
3.44
3.42
3.40
3.39
3.37
3.35
3.34
3.32
1.76
1.73
1.70
1.64
1.58
1.55
1.53
1.42
1.40
1.32
1.30
1.28
1.24
0.88
0.10
0.08
Current Data Parameters
NAME DB-3-27-H NMR
EXPNO 1
PROCNO 1
F2 – Acquisition Parameters
Date_ 20080915
Time 17.12
INSTRUM spect
PROBHD 5 mm QNP 1H/1
PULPROG zg
TD 32768
SOLVENT CDCl3
NS 16
DS 0
SWH 3591.954 Hz
FIDRES 0.109618 Hz
AQ 4.5613556 sec
RG 35.9
DW 139.200 usec
DE 54.00 usec
TE 296.2 K
D1 1.0000000 sec
TD0 1
======== CHANNEL f1 ========
NUC1 1H
P1 9.75 usec
PL1 0.00 dB
SFO1 300.1315007 MHz
F2 – Processing parameters
SI 32768
SF 300.1300063 MHz
WDW no
SSB 0
LB 0.00 Hz
GB 0
PC 1.00

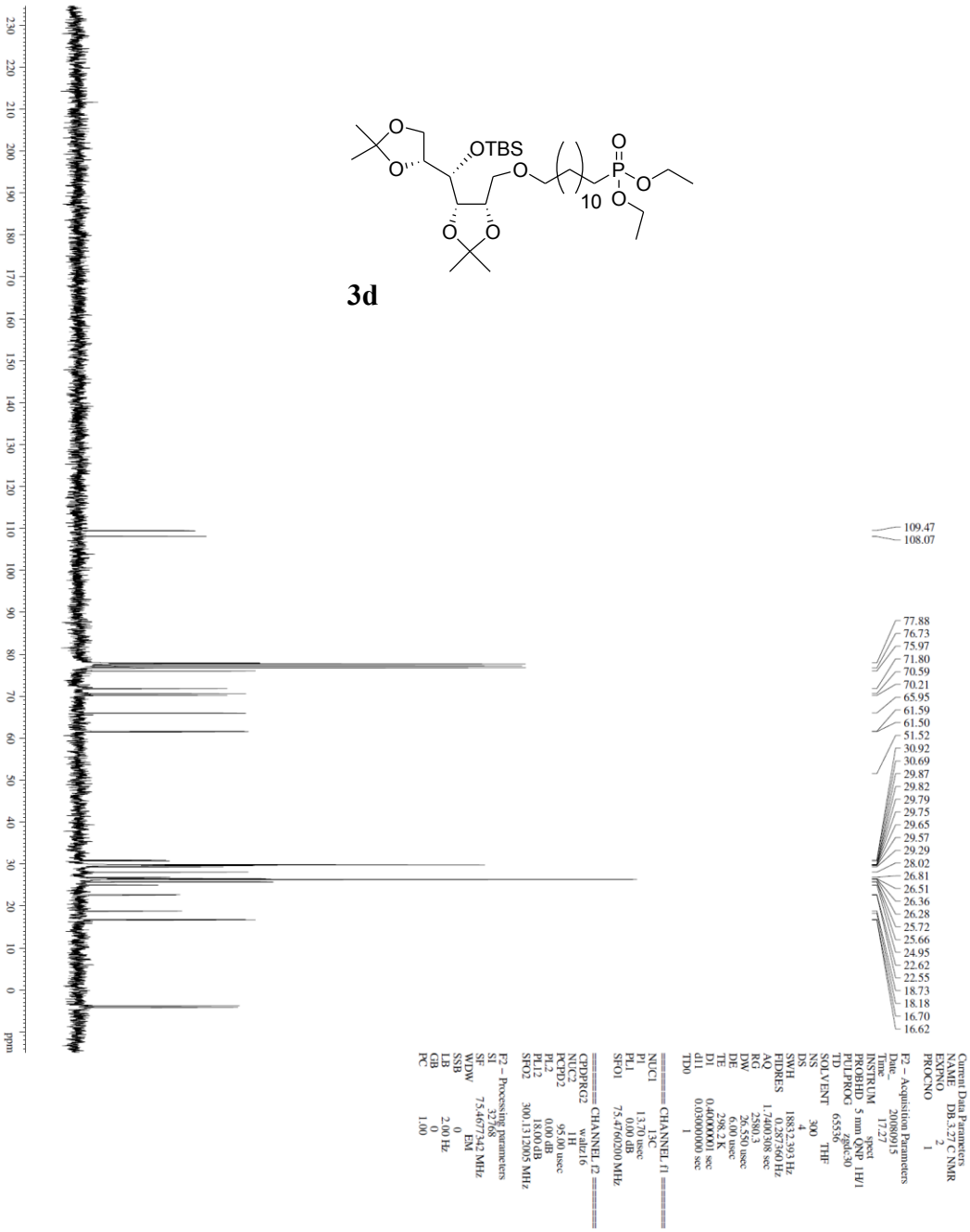
OTBS
O
O
O
O
O
O
O
P
O
O
10
3d
109.47
108.07
77.88
76.73
75.97
71.80
70.59
70.21
65.95
61.59
61.50
51.52
30.92
30.69
29.87
29.82
29.79
29.75
29.65
29.57
29.29
28.02
26.81
26.51
26.36
26.28
25.72
25.66
24.95
22.62
22.55
18.73
18.18
16.70
16.62
Current Data Parameters
NAME DB.3.27.C.NMR
EXPNO 2
PROCNO 1
F2 - Acquisition Parameters
Date_ 20080915
Time 17.27
INSTRUM spect
PROBHD 5 mm QNP 1H/1
PULPROG zgdc30
TD 65536
SOLVENT THF
NS 300
DS 4
SWH 18832.393 Hz
FIDRES 0.287280 Hz
AQ 1.7401568 sec
RG 2580.3
DW 26.550 usec
DE 6.00 usec
TE 298.2 K
D1 0.40000001 sec
d11 0.03000000 sec
TD0 1
====== CHANNEL f1 ======
NUC1 13C
P1 13.70 usec
PL1 0.00 dB
SFO1 75.4760200 MHz
====== CHANNEL f2 ======
CPDPRG2 waltz16
NUC2 1H
PCPD2 95.00 usec
PL2 0.00 dB
PL12 18.00 dB
SFO2 300.1312005 MHz
F2 - Processing parameters
SI 32768
SF 75.4677342 MHz
WDW EM
SSB 0
LB 2.00 Hz
GB 0
PC 1.00
230 220 210 200 190 180 170 160 150 140 130 120 110 100 90 80 70 60 50 40 30 20 10 0 ppm

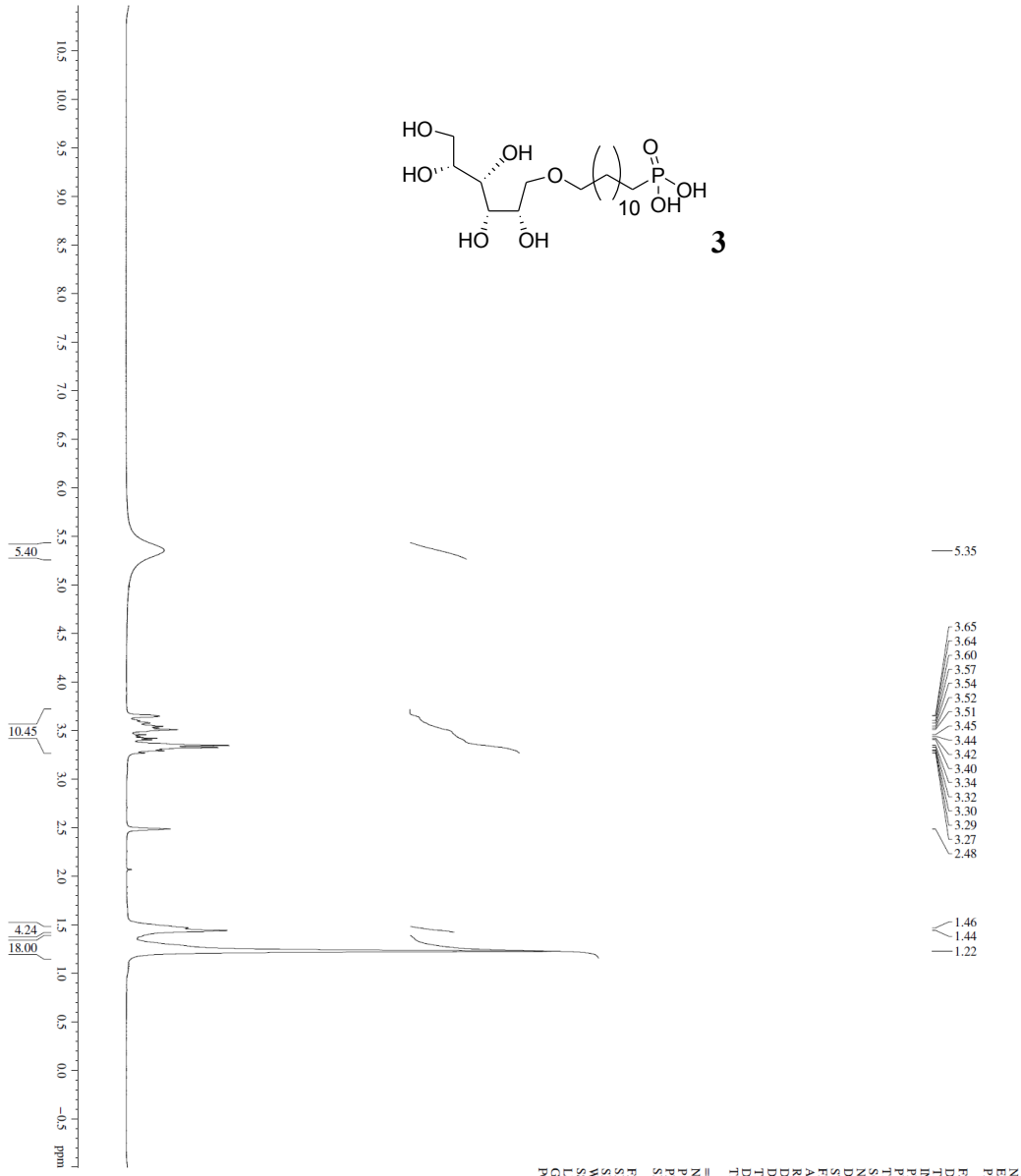
HO
HO
OH
HO
OH
O
O
P
OH
OH
10
3
5.40
10.45
4.24
18.00
ppm
5.35
3.65
3.64
3.60
3.57
3.54
3.52
3.51
3.45
3.44
3.42
3.40
3.34
3.32
3.30
3.29
3.27
2.48
1.46
1.44
1.22
Current Data Parameters
NAME DB-3-35 H NMR in DMSO
EXPNO 1
PROCNO 1
F2 - Acquisition Parameters
Date_ 20080930
Time 23.12
INSTRUM spect
PROBHD 5 mm QNP 1H/1
PULPROG zg
TD 32768
SOLVENT DMSO
NS 16
DS 0
SWH 3591.954 Hz
FIDRES 0.109618 Hz
AQ 4.5613556 sec
RG 11.4
DW 139.200 usec
DE 54.00 usec
TE 298.2 K
D1 1.00000000 sec
TD0 1
======== CHANNEL f1 ========
NUC1 1H
P1 9.75 usec
PL1 0.00 dB
SFO1 300.1315007 MHz
F2 - Processing parameters
SI 32768
SF 300.1300063 MHz
WDW no
SSB 0
LB 0.00 Hz
GB 0
PC 1.00


HO
OH
HO
O
O
P
OH
10
OH
HO
OH
3
73.73
72.84
72.30
70.56
69.88
68.68
62.54
30.18
29.97
29.31
29.08
29.04
28.98
28.90
28.71
28.42
26.61
25.70
22.74
22.68
230 220 210 200 190 180 170 160 150 140 130 120 110 100 90 80 70 60 50 40 30 20 10 0 ppm
Current Data Parameters
NAME DB.3.35 C NMR in DMSO
EXPNO 2
PROCNO 1
F2 – Acquisition Parameters
Date_ 20081001
Time 5.23
INSTRUM spect
PROBHD 5 mm QNP 1H/1
PULPROG zgdc30
TD 65536
SOLVENT DMSO
NS 10000
DS 4
SWH 18832.393 Hz
FIDRES 0.287560 Hz
AQ 1.7400308 sec
RG 2298.8
DW 26.550 usec
DE 6.00 usec
TE 299.2 K
D1 0.40000001 sec
d11 0.03000000 sec
TD0 1
======== CHANNEL f1 ========
NUC1 13C
P1 13.70 usec
PL1 0.00 dB
SFO1 75.4760200 MHz
======== CHANNEL f2 ========
CPDPRG2 waltz16
NUC2 1H
PCPD2 95.00 usec
PL2 0.00 dB
PL12 18.00 dB
SFO2 300.1312005 MHz
F2 – Processing parameters
SI 32768
SF 75.4677837 MHz
WDW EM
SSB 0
LB 1.00 Hz
GB 0
PC 1.00

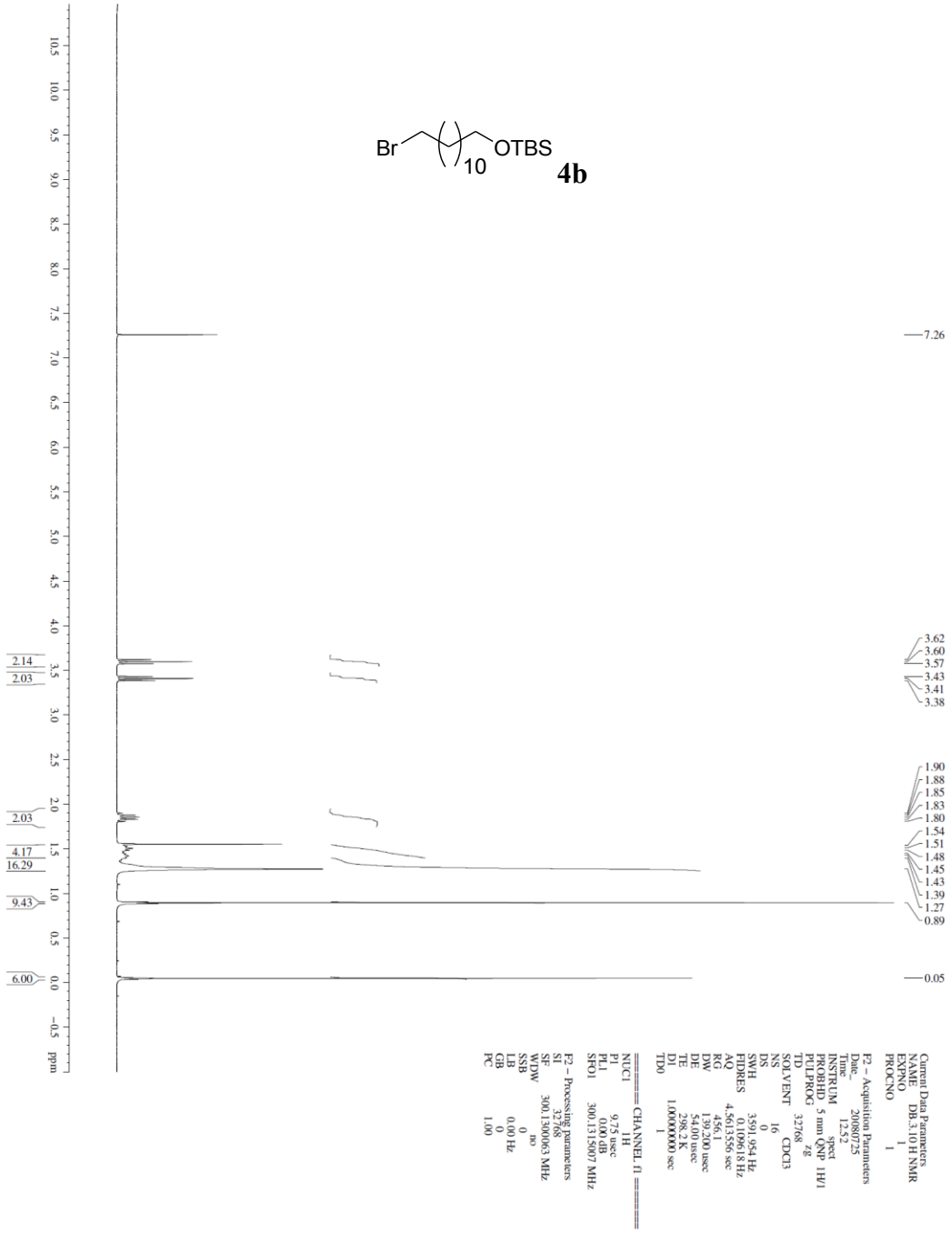

4b

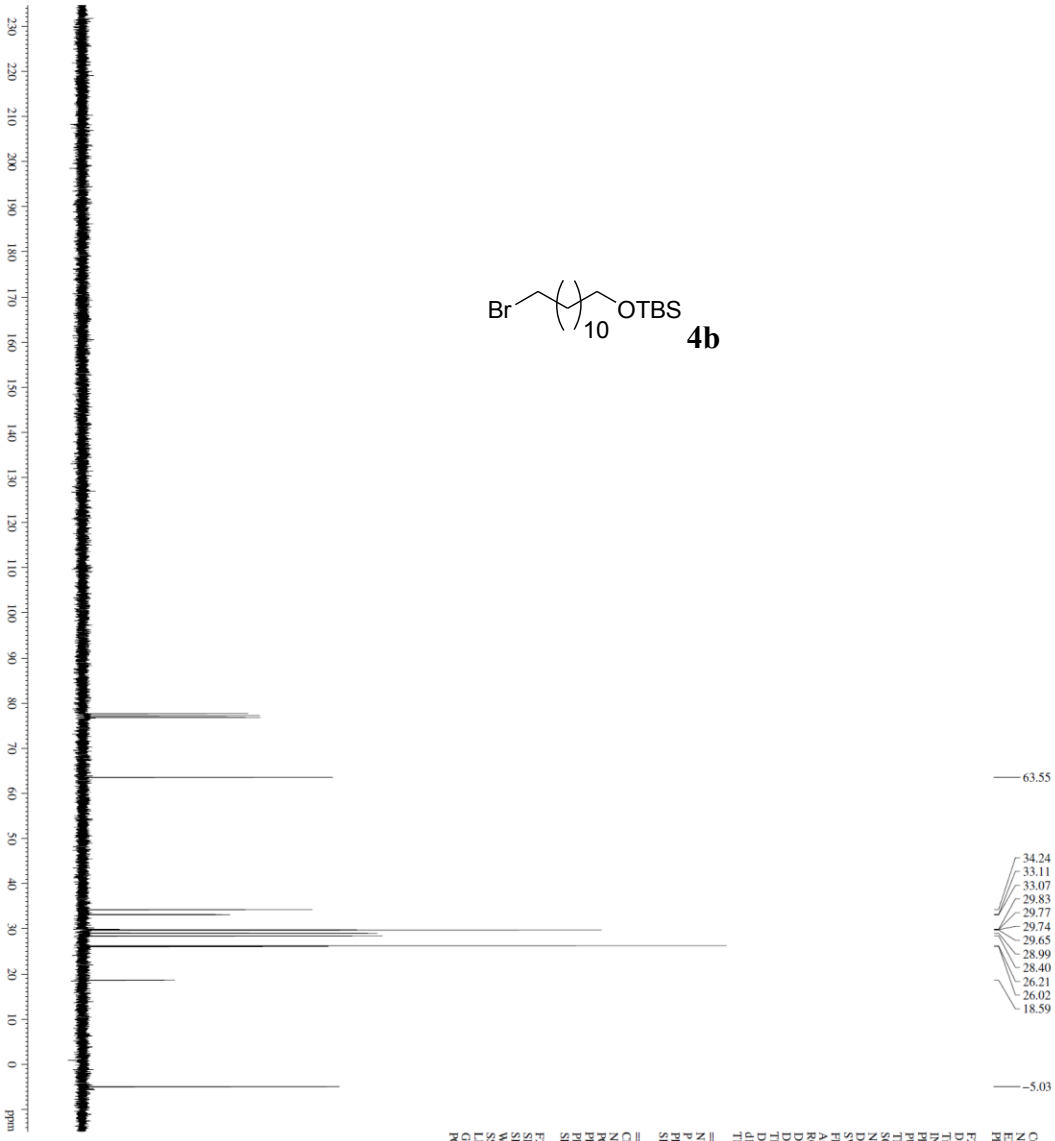
Br
10
OTBS
4b
63.55
34.24
33.11
33.07
29.83
29.77
29.74
29.65
28.99
28.40
26.21
26.02
18.59
-5.03
ppm

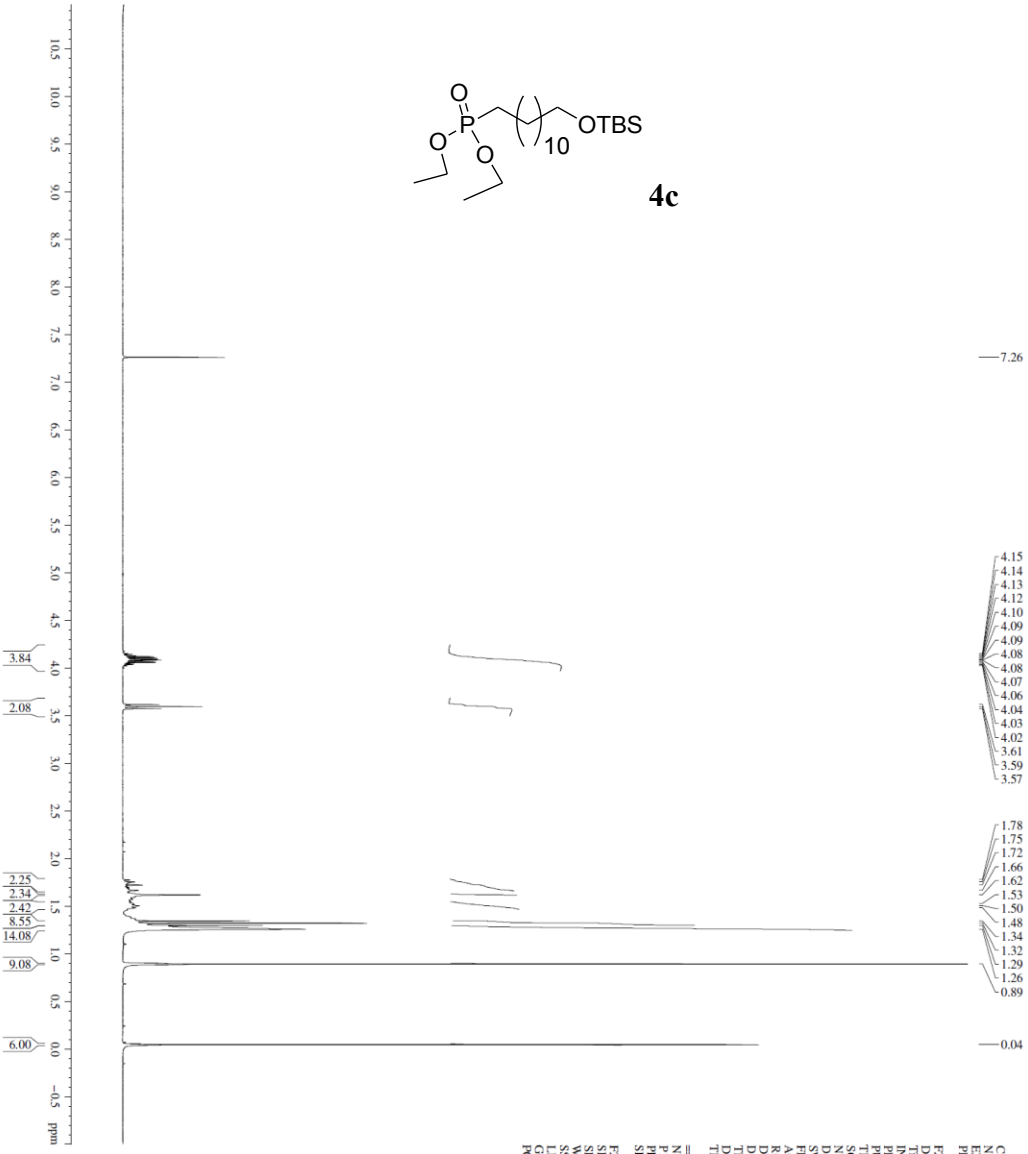

4c

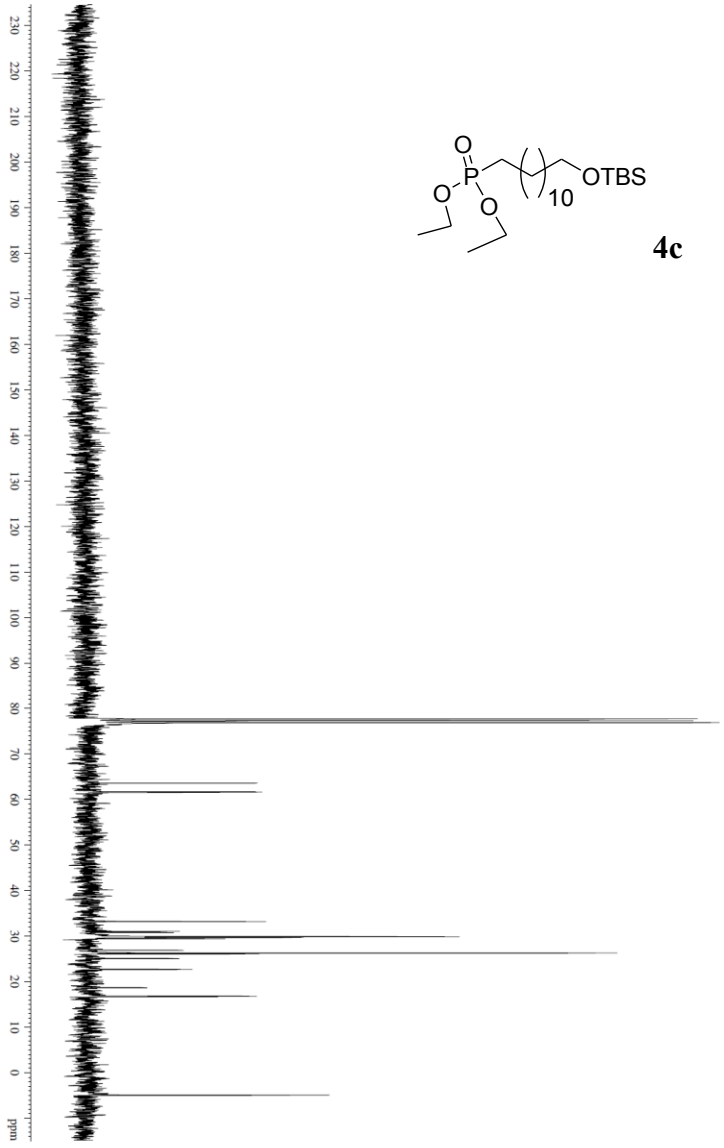

4c

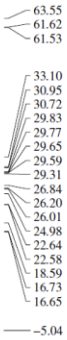

Current Data Parameters
NAME DB.3.11.C NMR
EXPNO 2
PROCNO 1

F2 – Acquisition Parameters
Date_ 20080730
Time 16.44
INSTRUM spect
PROBHD 5 mm QNP 1H/1
PULPROG zgdc30
TD 65536
SOLVENT CDCl3
NS 300
DS 4
SWH 18832.393 Hz
FIDRES 0.287360 Hz
AQ 1.7400308 sec
RG 11585.2
DW 26.550 usec
DE 6.00 usec
TE 298.2 K
D1 0.40000001 sec
d11 0.03000000 sec
TD0 1

======== CHANNEL f1 ========
NUC1 13C
P1 13.70 usec
PL1 0.00 dB
SFO1 75.4760200 MHz

======== CHANNEL f2 ========
CPDPRG2 waltz16
NUC2 1H
PCPD2 95.00 usec
PL2 0.00 dB
PL12 18.00 dB
SFO2 300.1312005 MHz

F2 – Processing parameters
SI 32768
SF 75.4677351 MHz
WDW EM
SSB 0
LB 2.00 Hz
GB 0
PC 1.00

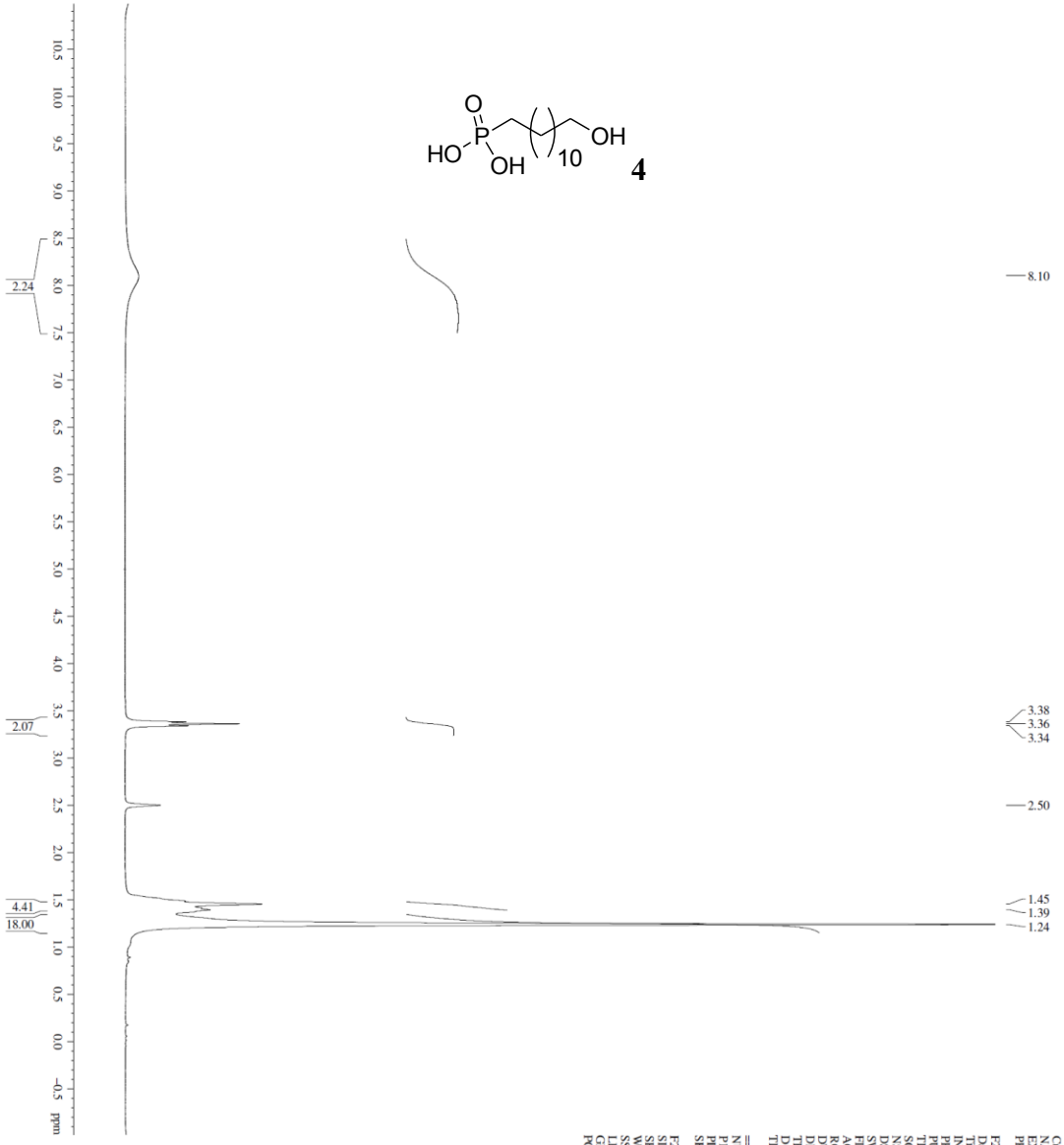
O
HO
P
OH
10
OH
4
8.10
3.38
3.36
3.34
2.50
1.45
1.39
1.24
2.24
2.07
4.41
18.00
ppm
Current Data Parameters
NAME DR-3-13 1H NMR in DMSO
EXPNO 1
PROCNO 1
F2 – Acquisition Parameters
Date_ 20080804
Time 11.55
INSTRUM spect
PROBHD 5 mm QNP 1H/1
PULPROG zg
TD 32768
SOLVENT DMSO
NS 16
DS 0
SWH 3591.954 Hz
FIDRES 0.109618 Hz
AQ 4.5613556 sec
RG 114
DW 139.200 usec
DE 5.50 usec
TE 298.2 K
D1 1.00000000 sec
TD0 1
======== CHANNEL f1 ========
NUC1 1H
P1 9.75 usec
PL1 0.00 dB
SFO1 300.1315007 MHz
F2 – Processing parameters
SI 32768
SF 300.1300010 MHz
WDW no
SSB 0
LB 0.00 Hz
GB 0
PC 1.00

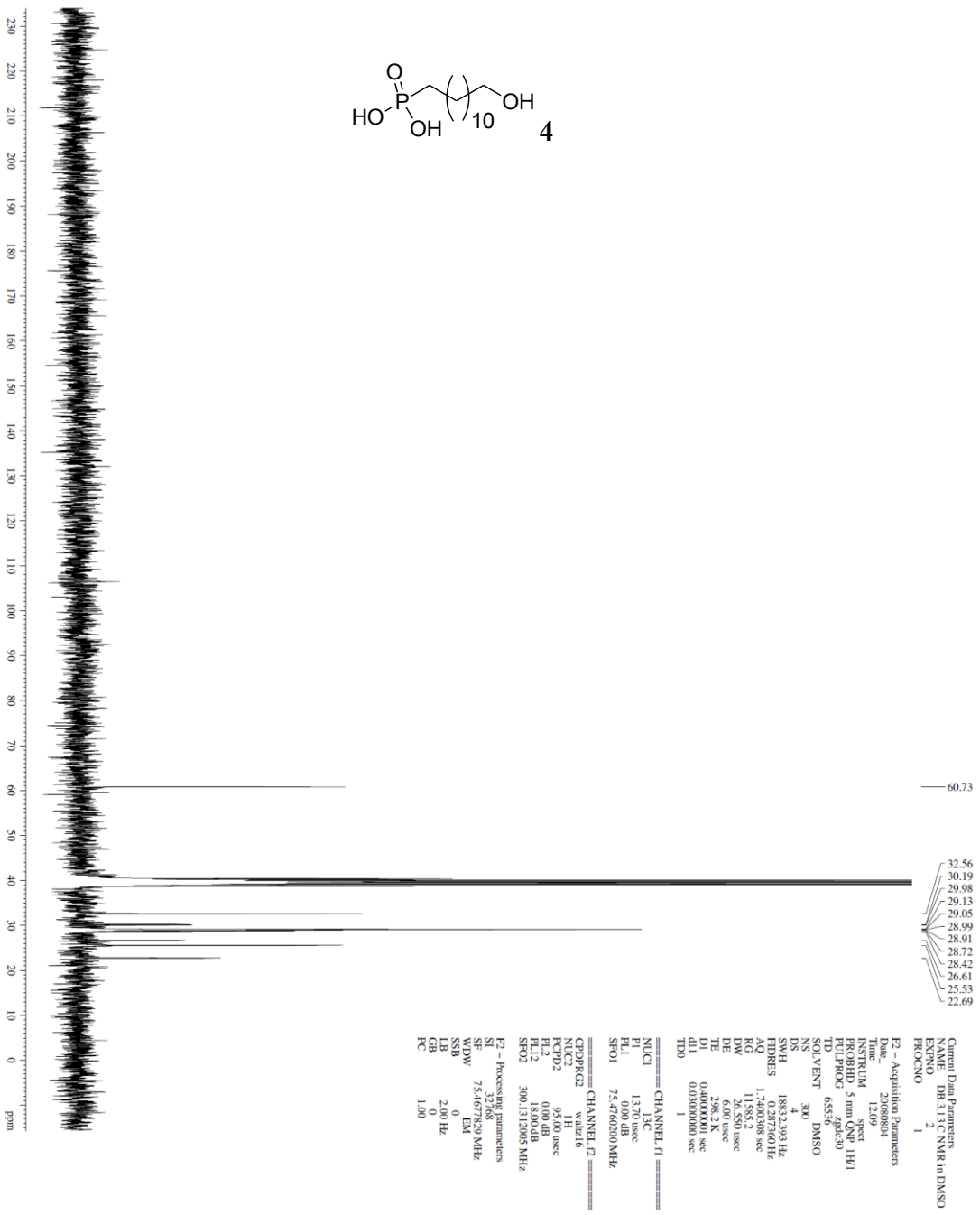
O
P
HO
OH
OH
10
OH
4
60.73
32.56
30.19
29.98
29.13
29.05
28.99
28.91
28.72
28.42
26.61
25.53
22.69
Current Data Parameters
NAME DB.3.13 C NMR in DMSO
EXPNO 2
PROCNO 1
F2 - Acquisition Parameters
Date_ 20080804
Time 12.09
INSTRUM spect
PROBHD 5 mm QNP 1H/1
PULPROG zgdc30
TD 65536
SOLVENT DMSO
NS 300
DS 4
SWH 18832.393 Hz
FIDRES 0.287360 Hz
AQ 1.7400308 sec
RG 11585.2
DW 26.550 usec
DE 6.00 usec
TE 298.2 K
D1 0.40000000 sec
d11 0.03000000 sec
TD0 1
CHANNEL f1
NUC1 13C
P1 13.70 usec
PL1 0.00 dB
SFO1 75.4760200 MHz
CHANNEL f2
CPDPRG2 waltz16
NUC2 1H
PCPD2 95.00 usec
PL2 0.00 dB
PL12 18.00 dB
SFO2 300.1312005 MHz
F2 - Processing parameters
SI 32768
SF 75.4677829 MHz
WDW EM
SSB 0
LB 2.00 Hz
GB 0
PC 1.00
230
220
210
200
190
180
170
160
150
140
130
120
110
100
90
80
70
60
50
40
30
20
10
0
ppm

Chapter 6

Adamantane Tethered Brominated Furanones - *Towards a Multifunctional Interface for Controlling Biofilm Formation*

Summary

Using antibiotic agents is one viable approach for controlling the root cause of biofilm formation. Antibiotics generally target cellular processes essential for bacterial survival and hence their long-term use stimulates bacterial evolution by creating selective pressure for antibiotic resistant mutations. Biofilm formation is one consequence of bacterial cell-cell communication called quorum sensing. Inhibiting quorum sensing is a promising approach to control biofilm formation or biofilm related infections. Quorum sensing inhibitors do not target cellular processes that are vital for bacterial survival; hence, bacterial cells are less likely to develop mutations against quorum sensing modulators. While surfaces can be engineered to resist the attachment of bacteria or biofilm, such surfaces are compromised due to chemical degradation or are overpowered due to excessive biofilm formation. Covalent immobilization of quorum-sensing inhibitors on surfaces has been reported, however immobilization chemistries are either ambiguous or can lead to alteration of the active structure of the inhibitors. Another viable approach is *non-covalent* immobilization of the quorum sensing inhibitors in a suitable synthetic matrix on the surface, to modulate their release and uptake. Moreover, such a surface has the potential for regeneration by simple treatment of the surface with more inhibitor in time. Using a porous hydrogel material as the synthetic matrix can provide a large surface area for non-covalent immobilization of the inhibitors and a larger surface area for the

bacteria to tackle. Some natural and synthetic brominated furanones are known to inhibit biofilm formation. Here, the synthesis of adamantane tethered brominated furanones is reported, which will be non-covalently encapsulated in a beta-cylclodextrin (βCD) functionalized porous hydrogel material. This non-covalent immobilization chemistry will utilize the interactions between the hydrophobic adamantane moiety and hydrophobic annular cavity of βCD. The present work reports the effect of the adamantane tethered brominated furanones alone on the growth of *Escherichia coli* and their ability to inhibit biofilm by the bacterium. The synthesized adamantane tethered brominated furanones were found to be non-toxic to *E. coli* and were able to reduce biofilm formation by ~40% at 200 μM.

6.1 Introduction and Goal

6.1.1 Molecular inhibition of biofilm formation

While one approach for controlling bacterial biofilm formation and related infections on surfaces is to design surfaces which can resist the attachment of bacteria or biofilm,[68, 75-76] the other approach is to use molecules which can inhibit the formation of biofilm.[8] While conventional antibiotics are able to kill planktonic bacterial cells and eradicate the root cause of bacterial infections, antibiotics fail when it comes to killing bacterial cells within a biofilm. Antibiotics are unable to kill the metabolically dormant bacterial cells within a biofilm that is also generally impermeable to antibiotics.[6, 157] Antibiotics generally target cellular processes essential for bacterial survival and hence their long-term use stimulates bacterial evolution by creating selective pressure for antibiotic resistant mutations.[206-207] Once the bacterial cells develop resistance to antibiotics, even high doses of the antibiotics are unable to treat bacterial infections. Another approach to

control biofilm and biofilm related infection is to inhibit biofilm formation with agents, which are not bactericidal and do not give way to drug-resistant mutations.

6.1.2 Biofilm formation is one consequence of quorum sensing

Biofilm formation is once consequence of bacterial cell-cell signaling called "quorum sensing". Bacteria use small molecule signaling pathways to coordinate population wide gene expression through processes called "quorum sensing".[87, 131, 147] Bacterial cells synthesize small organic molecules called autoinducers (AI) and release these diffusible molecules into the surrounding medium. As the number of bacterial cells increase, the concentration of these autoinducers in the surrounding medium also increases. When the concentration of these autoinducers reaches a threshold value, the autoinducers bind to their cognate receptors within the bacterial cells and initiate a signal transduction pathway that leads to population wide changes in gene expression. Quorum sensing enables bacterial cells within a colony to behave cooperatively thus conferring a form of multicellularity to the otherwise unicellular bacterium.[87] Quorum sensing also initiates a number of other processes in bacteria including virulence factor production, antibiotic production, biofilm formation, swarming motility, bioluminescence, root nodulation, sporulation and conjugation.[131]

6.1.3 Developing quorum sensing inhibitors for controlling biofilm formation

Another approach for controlling biofilm formation and related infections is to inhibit the process of quorum sensing. Although quorum sensing is essential for bacterial group behavior, it is not essential for survival[208] and hence inhibiting quorum sensing does not give way to drug-resistant mutations commonly associated with antibacterial

treatments.[209] Quorum sensing circuits in bacteria comprise of small signaling molecules called autoinducers, proteins that synthesize these autoinducers and proteins that function as the cognate receptors for the autoinducers.[87] To inhibit quorum sensing we can disrupt the signaling process by either inhibiting proteins that are involved in the synthesis or sensing of the autoinducers, or we can devise ways of destroying the signaling molecules (autoinducers) itself.[7, 208]

Gram-negative bacteria use small signaling molecules called autoinducer-1 (AI-1) for quorum sensing while gram-positive bacteria use small cyclic peptides called autoinducing peptides (AIP) for signaling.[87] Another class of signaling molecules called autoinducer-2 (AI-2)[210-211] have been identified for both gram-negative and gram-positive bacteria and is a possible means by which different bacterial species can communicate with each other.[212] The AI-1 based quorum sensing circuit involves a class of signaling molecules called the *N*-acylated-L-homoserine lactones (AHLs), while the AI-2 system involves a class of molecules which are based on, or are derivatives of, 4,5-dihydroxy-2,3-pentanedione (DPD).[87] The first AI-1 based quorum sensing circuit was indentified in bioluminescent marine bacterium *Vibrio fischeri*.[129] The quorum sensing circuit in *Vibrio fischeri* is associated with the autoinducer *N*-3-oxohexanoylhomoserine lactone (OHHL) and comprises of the proteins LuxI and LuxR that are involved in the synthesis and detection of OHHL respectively.[7, 87, 130] The AI-1 based quorum-sensing circuits identified in other bacterial species are composed of LuxI-type and LuxR-type proteins and have their own specific autoinducers.[7, 87]

A number of quorum-sensing modulators are reported in the literature, which can target both the AI-1 and AI-2 based quorum-sensing circuits.[8] These small molecule inhibitors

are either structural mimics of AHLs associated with the AI-1 system or structural mimics of DPD and its derivatives associated with the AI-2 system. The X-ray crystal structure of a few LuxR-type proteins bound to their natural AHL ligands have been reported[213-218] and such information has been useful in developing synthetic analogs of the natural AHLs.[8] Blackwell and co-workers have provided a comprehensive review of the structure activity relationship (SAR) for synthetic AHL analogs spanning a number of bacterial species but focusing on the quorum sensing circuits involving the LuxR-type proteins of *Vibrio fischeri* (LuxR), *Pseudomonas aeruginosa* (LasR and RhlR), *Agrobacterium tumefaciens* (TraR) and *Erwinia carotovora* (CarR).[7] Blackwell and co-workers have also reported the synthesis and evaluation of AHL analogs, using small-molecule microarrays and identified quorum-sensing inhibitors for *Vibrio fischeri* and *Chromobacterium violaceum.*[219] Lee, Yoon and co-workers have recently reported the synthesis of AHL analogs against the TraR quorum sensing receptor for *Agrobacterium tumefaciens* and found that some of the analogs were able to inhibit biofilm formation for both *Agrobacterium tumefaciens* and the pathogenic bacteria *Pseudomonas aeruginosa*.[220]

6.1.4 Brominated furanone as quorum sensing inhibitors

Sticher and co-workers have reported the isolation of a number of halogenated furanone compounds from extracts of the marine algae *Delisea pulchra* (Figure 6.1).[221] The isolated furanones have been shown to exhibit antimicrobial properties and were also capable of preventing surface colonization by bacteria.[222] Kjelleberg and co-workers have reported that the biological activity of the isolated haloginated furanones could be due to their interference with AHL based quorum sensing circuits.[223]

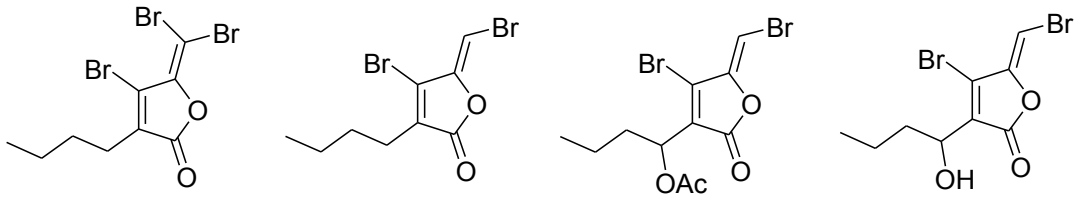

Figure 6.1 Few brominated furanones isolated from extracts of *Delisea pulchra.* Figure adapted from review by Spring and co-workers.[8]

Luk and co-workers have reported a study to identify the key structural elements in brominated furanones, responsible for their inhibitory activity against biofilm formation by *E. coli*.[160] Although *E. coli* itself does not have an AHL-based quorum sensing circuit, it does posess a LuxR-type receptor called SdiA,[224-225] and hence can respond to AHL signals from other bacteria or to synthetic AHL based quorum sensing modulators.[224-225] Luk and co-workers synthesized seven synthetic brominated furanone compounds[160] (Figure 6.2), and identified that the presence of an exocyclic vinyl bromide was crucial but a vinyl bromide within the furanone ring was not crucial for biofilm inhibitory activity. They also identified that a bromine group on the saturated carbon atom decreased biofilm inhibitory activity of the brominated furanones.

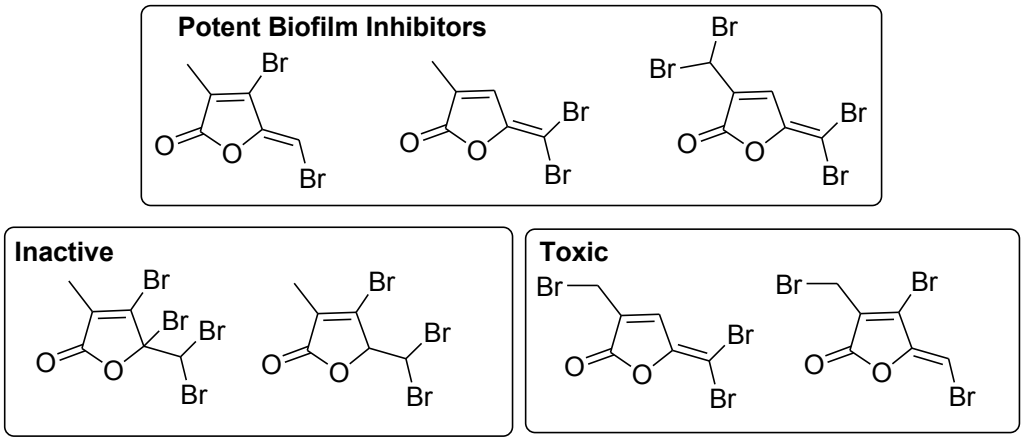

Figure 6.2 Structure of the synthetic brominated furanones synthesized by Luk and co-workers to identify key structural features crucial for inhibitory activity against biofilm formation by *E. coli.* Figure adapted and modified from the report by Luk and co-workers.[160]

6.1.5 Functionalizing surfaces with anti-biofouling agents

There have been a few attempts to functionalize surfaces with brominated furanone.[226-227] These methods involve covalent attachment of the brominated furanones to a surface with an undefined bonding identity. Brominated furanones are believed to be internalized within the bacterial cells, where they bind and inhibit proteins which are part of the quorum sensing circuit.[8] Hence, covalent attachment of brominated furanones to surfaces might prevent their internalization within the bacterial cells. Moreover, the surface immobilization chemistry[227] may also compromise the active structure of the furanones. Surface modifications with anti-biofouling SAMs can also be compromised in time due to formation of a "conditioning" film composed of microbial secretions. This difficulty can be overcome by coating the surface with porous hydrogels, which non-covalently encapsulate quorum-sensing inhibitors. Modulating the release of the inhibitors, together

with the large surface area provided by the hydrogel material, will ensure prevention and control of biofilm formation and provide a multifunctional interface for studying and quorum sensing related processes.

Here, the synthesis of adamantane tethered brominated furanones **1-5** (Scheme 6.1) is reported, for non-covalent encapsulation these furanones in porous hydrogel material[228] which are covalently modified with beta-cyclodextrin (βCD) groups.[229] Its worth noting that the adamantane moiety is also a part of few reported antibacterial drugs.[230]

Scheme 6.1

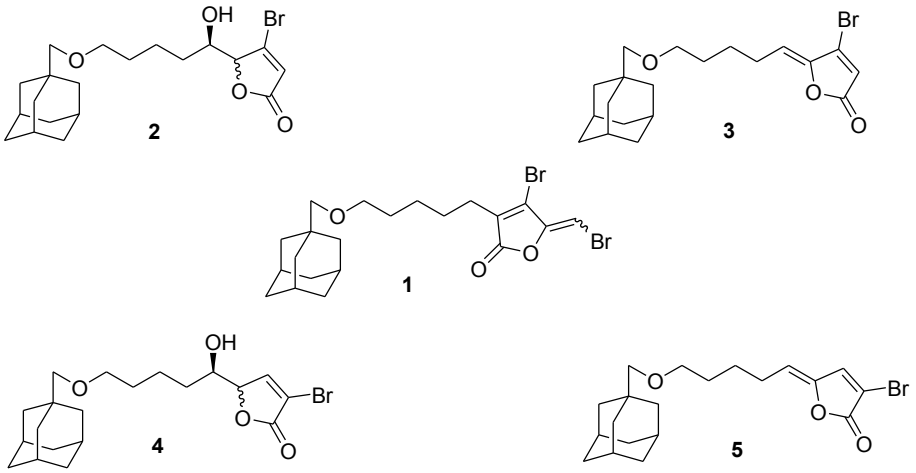

β-cyclodextrin (βCD) molecule has a truncated cone structure ,with a cavity lined with H3, H5 protons and lone pairs of the glycosidic oxygen atoms lying in a plane (Scheme 6.2), making the cavity hydrophobic to encapsulate the hydrophobic adamantane moeity.[231]

Scheme 6.2

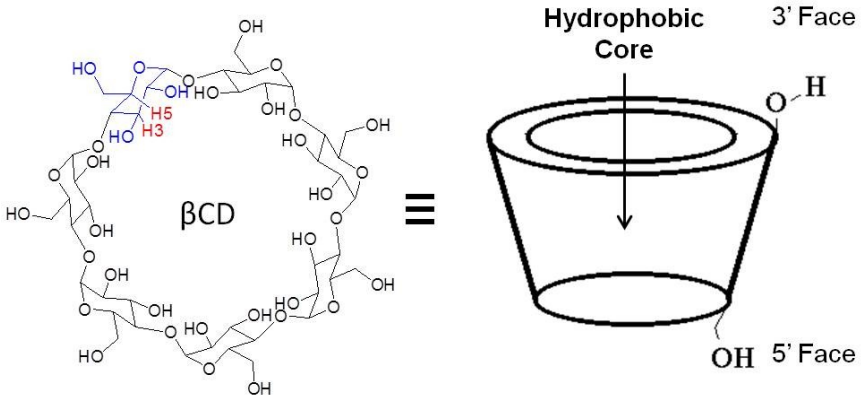

A porous hydrogel material with covalently tethered beta-cyclodextrin (βCD) groups can non-covalently encapsulate the adamantane moiety in compounds **1-5**. This non-covalent encapsulation chemistry (Scheme 6.3) can be used to modulate the release and uptake of these brominated furanones from the hydrogel material.

Scheme 6.3

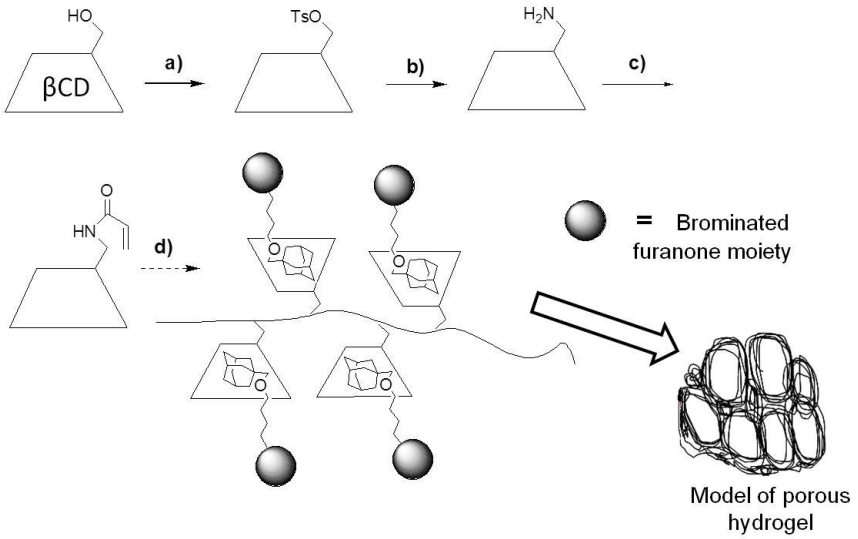

Conditions: Steps **a** through **b**.[232] Steps **c** through **d**[233] (all but encapsulation of adamantane tethered brominated furanones)

6.2 Results and Discussion

6.2.1 Towards the synthesis of adamantane tethered brominated furanone compounds

I first attempted the synthesis of compound **1**, where the brominated furanone moiety is structurally similar to two reported synthetic brominated furanones **6** and **7** (Figure 6.3).[8] Luk and co-workers have reported that compound **6** is active against biofilm formation by *E. coli*.[160] While compound **6** is reported to be non-toxic to *E. coli* at ~ 200 μM,[160] compound **7** was found to be toxic to *E. coli* at 200 μM (see below).

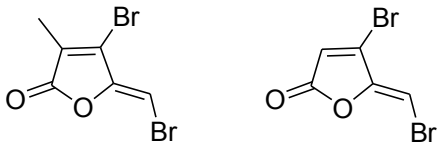

6 **7**

Figure 6.3 Structure of brominated furanones reported in the literature active against biofilm formation by *E. coli.*

The synthesis of compound **1** is depicted in Scheme 6.4. Briefly, nucleophilic substitution of excess of 1,5-dibromopentane with commercially available 1-adamantanemethanol, **1a** provided the bromide **1b** in 18% yield. Deprotonation of diethylmalonate with NaH and nucleophilic substitution of the bromide **1b** provided the diethyl ester **1c** in 64% yield. Base hydrolysis of the diethyl ester **1c** followed by acidic workup provided the diacid **1d** in quantitative yield. Refluxing the diacid **1d** in toluene for 24 h provided the monoacid **1e** in quantitative yield. The ethyl ester **1f** was synthesized from **1e** using Me_3SiCl and EtOH in 75% yield. α-Bromination of **1f** using LDA, Me_3SiCl, followed by NBS provided the α-bromo ethyl ester **1g** in 88% yield.

Treatment of ethylacetoacetate with NaOEt followed by addition of α-bromo ethyl ester provided the diethyl ester **1h**. Base hydrolysis of the diethyl ester **1h** followed by acidic workup provided the monoacid **1i**.

Scheme 6.4

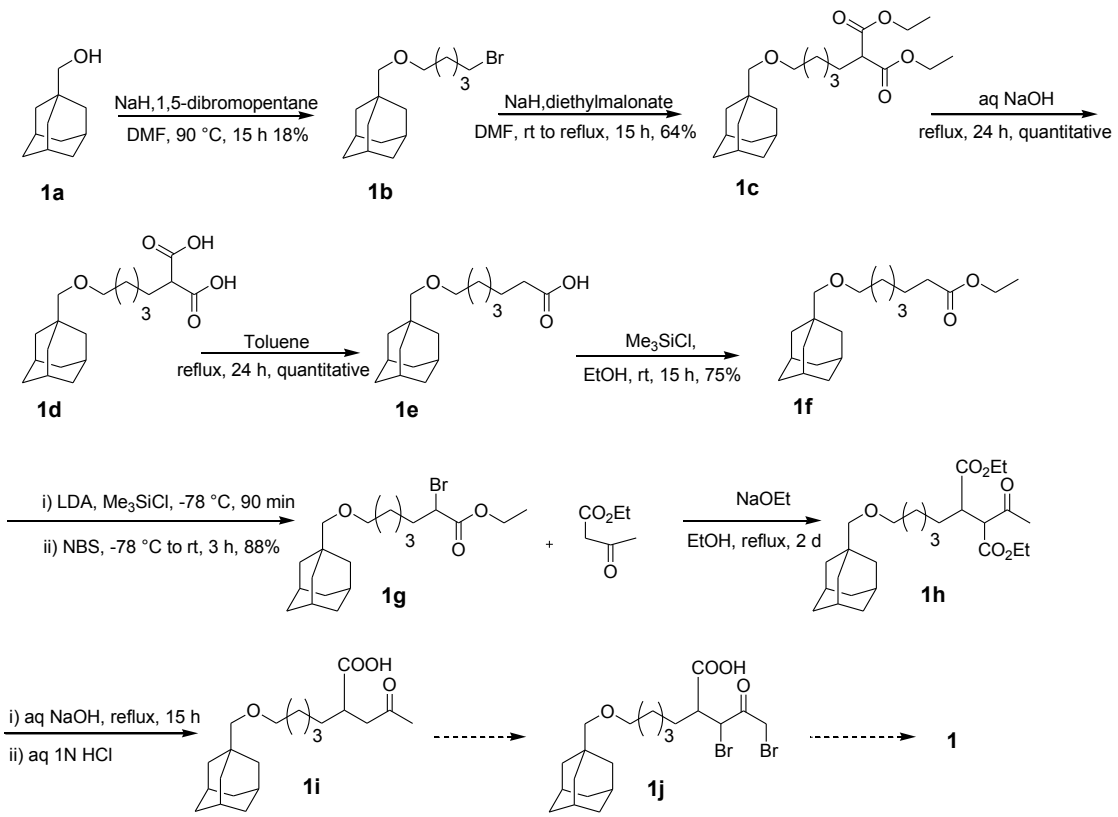

Since the yield for the bromide **1b** in Scheme 7.4 was too low (~18%), a more efficient route to the diethyl ester **1c** was designed. Tosylate **1l** was synthesized from the alcohol **1k**.[234] Compound **1k** was tosylated using TsCl, Et_3N as base and catalytic amount of DMAP to yield the tosylate **1l** in 78% yield. Nucleophilic substitution of the tosylate **1l** with diethylmalonate, NaI and NaH gave the diester **1c** in 84% yield (Scheme 6.5).

Scheme 6.5

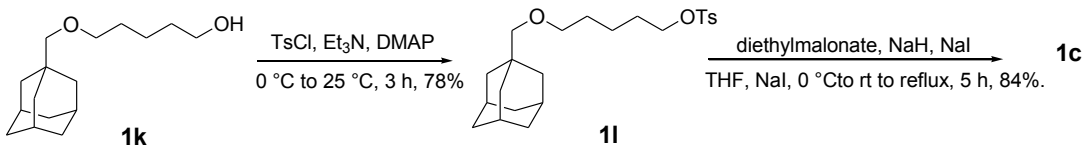

The rest of the sequence for the synthesis of compound **1** is the same as shown in Scheme 6.4. The key step in this synthetic design was the sulfuric acid catalyzed oxidative cyclization[235] of compound **1j**. Although I succeeded in synthesizing compound **1i**, but due to the extremely harsh conditions and low yields for the cyclization step, I failed to synthesize compound **1**.

6.2.2 Synthesis of a new library of adamantane tethered brominated

Since the synthetic scheme for compound **1** was either too long or low yielding, a short and efficient route for the synthesis of the adamantane tethered brominated furanones **2** and **3** was designed. The synthesis outlined in Scheme 6.6 provided the brominated furanone compounds that were structurally different from the desired compound **1** but had features important for activity against bacterial biofouling.[8, 160]

Scheme 6.6

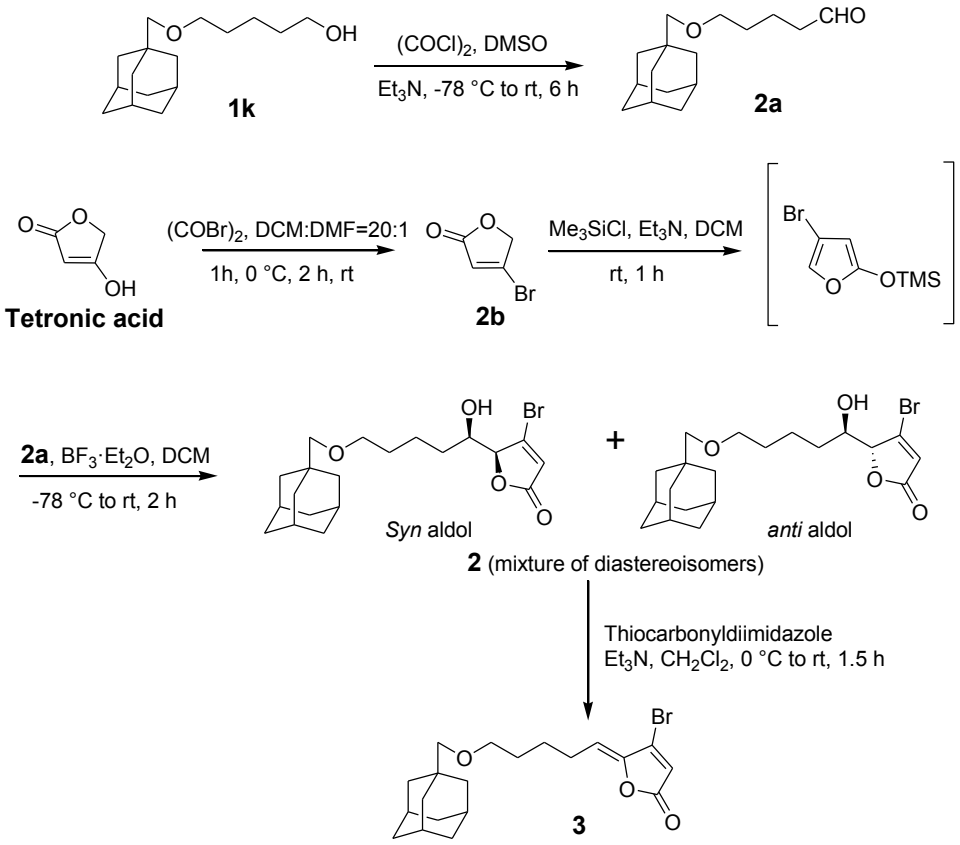

Compound **2a**[234] and **2b**[236] (Scheme 6.6) were synthesized using slight modifications in literature reported procedures. The in-situ generated trimethylsilyl enol ether of **2b** underwent diastereoselective $BF_3 \cdot Et_2O$ catalyzed Mukaiyama aldol reaction with aldehyde **2a** to give a mixture of diastereoisomers **2** (*Syn* aldol : *anti* aldol = 78:22 from ^{1}H NMR).[237] The mixture of diastereoisomers was subjected to dehydration using thiocarbonyldiimidazole and Et_3N and only the *Z* isomer **3** was isolated exclusively after column chromatography.[237-238]

Compounds **4** and **5** can be synthesized using procedures similar to those used for the synthesis of compounds **2** and **3**. The proposed scheme for the synthesis of compounds

4 and **5** is outlined in Scheme 6.7. Compound **4a**[239] was synthesized by bromination of 2-(5H)-furanone in refluxing CCl_4 followed by dehydrobromination (in situ) at rt with Et_3N.

Scheme 6.7

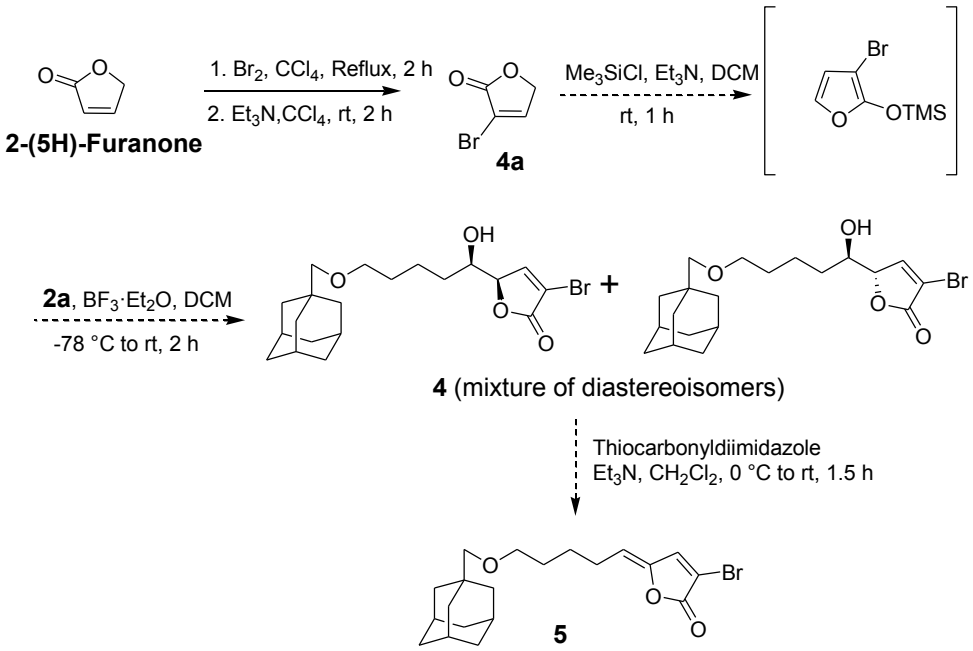

6.2.3 Cytotoxicity study of the adamantane tethered brominated furanone on E.coli.

The adamantane tethered brominated furanone compounds **2** and **3** were first tested for their effect on the growth of bacterial cells. For this study, *E. coli* (RP437) was used as the model bacterium. The cytotoxicity of furanones **2b** and **4a** were also evaluated, which are synthetic precursors for the compounds **3** and **5** respectively. The synthetic brominated furanone compounds **6** and **7** have been reported to be active inhibitors of quorum sensing in *E*. coli and were used as controls in our cytotoxicity assays. The

toxicity of all the brominated furanone compounds (**2**, **2b**, **3** and **4a**) were evaluated at 200 μM since furanone **6** is reported to be non-toxic at concentrations close to 200 μM.[160]

Figure 6.4 shows the growth curves for *E. coli* at 200 μM of the furanone compounds **2b**, **4a**, **2**, **3**, **6** and **7**. The furanones **2**, **2b** and **3** were found to be non-toxic to *E. coli* at 200 μM. Furanone **6** was found to be slightly toxic at 200 μM while furanone **7** was highly toxic to *E. coli* at 200 μM and completely inhibited growth of the bacterium (Figure 7.4). Surprisingly, furanone **4a** which is the structurally similar regioisomer of furanone **2b**, was found to be toxic to *E. coli*.

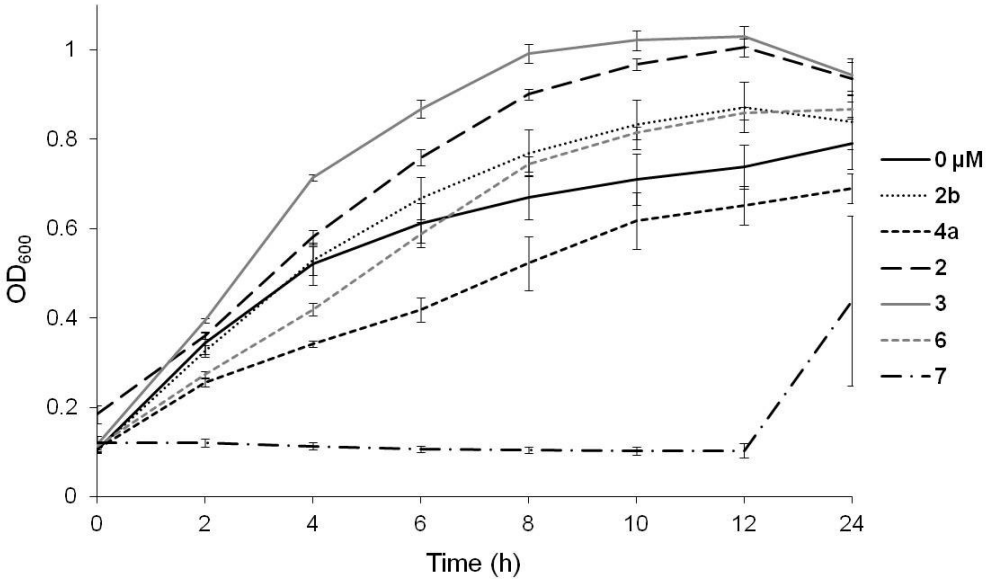

Figure 6.4 Growth curves for *E. coli* in presence of 200 μM of the brominated furanones **2b**, **4a**, **2**, **3**, **6** and **7**.

6.2.4 Inhibition of E. coli biofilm formation using adamantane tethered brominated furanones

The ability of the brominated furanone compounds (**2b**, **4a**, **6** and **7**) and adamantane tethered brominated furanone compounds (**2** and **3**) was further evaluated to inhibit biofilm formation by *E. coli*. A modified crystal violet assay[163, 240-241] was used to estimate the amount of biofilm formed by *E. coli* in the presence of 200 μM of each of the furanones tested. Percent inhibition of biofilm inhibition was calculated using the measured OD_{600} values after crystal violet assay. The equation $[1-(A_{M+B+BF} - A_M)/(A_{M+B} - A_M)] \times 100$ was used for calculating percent inhibition of biofilm formation, where A_{M+B+BF} is the OD_{600} of wells containing media + bacteria + brominated furanones, A_{M+B} is the OD_{600} of wells containing media + bacteria and A_M is the OD_{600} of wells containing only media. Both the adamantane tethered brominated furanones **2** and **3** were found to be very effective in inhibiting biofilm formation by *E. coli* and showed 40.42 ± 8.96% and 40.89 ± 6.10% inhibition respectively. While the non-toxic compound **2b** showed similar inhibition (44.56 ± 5.21%) as shown by **2** and **3**, the cytotoxic brominated furanones **4a**, showed a higher ability to inhibit biofilm formation than compounds **2b**, **2** and **3** with a inhibition of 52.13 ± 5.86%. It was worth noting that both the adamantane tethered brominated furanone **2** and **3**, showed inhibition similar to that shown by compound **6** (45.93 ± 9.46%). Compound **7** was found to be the strongest biofilm inhibitor with an inhibition of 65.31 ± 6.69% (Figure 6.5). It is the toxicity of compound **7** towards *E.coli* which makes it the strongest inhibitor among the library of furanones tested.

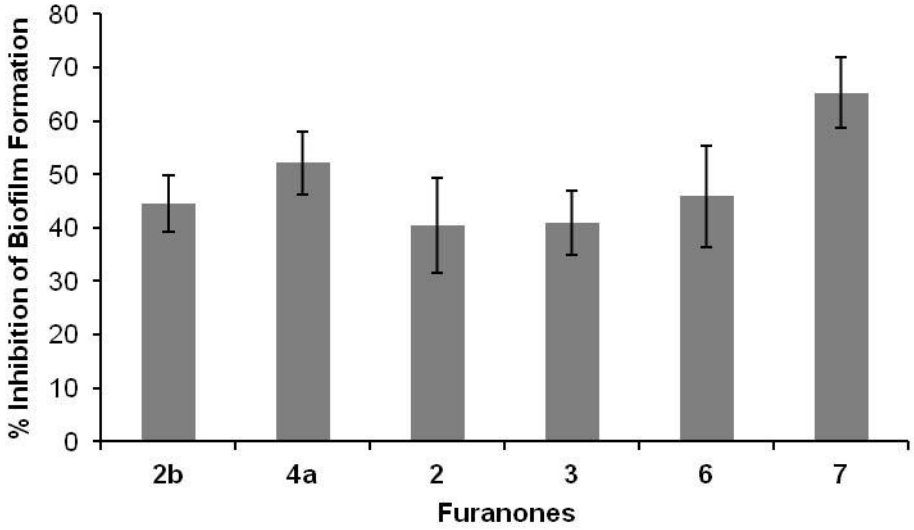

Figure 6.5 Plots for percent inhibition for biofilm formed by *E.coli* at 200 μM of brominated furanones and adamantane tethered brominated furanones.

6.2.5 Possible mode of action of adamantane tethered brominated furanones

It is believed that brominated furanones can interfere with both the AI-1 and AI-2 quorum-sensing circuits.[8] Givskov and co-workers have shown that the inhibitory effects of natural furanones (isolated from *Delsea pulchara*) on the swarming motility of *Serratia liquefaciens* can be reversed by addition of the bacteriums native AHL, demonstrating that furanone compounds are competitive inhibitors of the LuxR-type proteins and that furanones bind to the active site of the protein.[242] Kjelleberg and co-workers have demonstrated that furanones are able to displace radiolabeled native AHL molecule from LuxR,[243] providing further proof that furanones probably bind to the active site of the LuxR-type proteins. Givskov and co-workers have also studied the interaction between halogenated furanones and the LuxR protein, but failed to observe any interaction between them.[214] It is highly probable that both natural and synthetic

brominated furanones probably interact with proteins, which are part of either AI-1 or AI-2 based quorum-sensing circuits, but their mode of action is still uncertain. It is possible that the adamantane tethered brominated furanones **2** and **3**, might be interacting with the AI-2 quorum-sensing circuit or the SdiA LuxR-type receptor in *E. coli.*

6.3 Conclusions and Perspectives

The synthesis of two adamantane tethered brominated furanone compounds **2** and **3**, and the ability of these compounds to inhibit biofilm formation by *E. coli* RP437 is reported. Compound **2** and **3** were found to be non-toxic to *E. coli* at 200 μM and showed 40.42 ± 8.96% and 40.89 ± 6.10% inhibition of biofilm formation respectively. The percent inhibition values were similar to those shown by furanone **6** (45.93 ± 9.46%) at 200 μM. Contrary to what is reported in the literature,[160] the fact that furanone **6** was found to be slightly toxic to *E. coli*, makes compounds **2** and **3** promising candidates for inhibiting quorum sensing in *E. coli*.

Porous hydrogel materials with pendant βCD groups, which can non-covalently encapsulate the synthesized adamantane tethered brominated furanones can be fabricated. This porous hydrogel material can be tested for its ability to inhibit the formation of biofilm by *E. coli* or other bacterial species on surfaces.

It is possible that the adamantane tethered brominated furanones bind to the quorum sensing proteins in *E. coli*. To isolate the protein-furanone complex for structural analysis, βCD functionalized columns can be prepared, which can non-covalently encapsulate the adamantane tethered brominated furanones. These non-covalently encapsulated brominated furanones can potentially capture and isolate the quorum sensing proteins from a medium containing contents of lysed bacterial cells. Hence, the

present study lays the foundation for designing a multifunctional interface for studying and controlling biofilm formation.

6.4 Experimental Section

Synthesis of brominated furanones and adamantane tethered brominated furanones

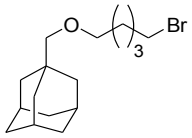

5-(Adamantane-1-yl-methoxy)-1-bromo-pentane (1b)

Dry Solution of **1a** (1.00 g, 6.015 mmol) in DMF (20 mL) was charged with NaH (0.361 g, 60% by wt in mineral oil, 9.023 mmol) at rt and subsequently stirred for 90 min. A solution of 1,5-dibromopentane (5.532 g, 24.06 mmol) in DMF (10 mL) was then added to the reaction mixture and the reaction mixture was heated at 90 °C for 1 d. The reaction was quenched by adding water and the aqueous phase was extracted with EtOAc. The combined organic phase was dried over anhydrous Na_2SO_4 and the crude product was obtained as a yellow oil after evaporation of solvent. The ceude product was purified using flash silica gel column (100% Hexane) to get **1b** (0.342 g, 18%) as yellow oil after evaporation of solvent. R_f = 0.37 (1% EtOAc in Hexane). ^{1}H NMR (300 MHz, $CDCl_3$): 3.45-3.37 (m, 4H), 2.96 (s, 2H, OCH_2- adamantane), 1.94 (br s, 3H, 3 × CH adamantane), 1.90-1.85 (m, 2H, CH_2 pentyl), δ 1.74-1.48 (m, 16H, 6 × CH_2 adamantane, 2 × CH_2 pentyl). ^{13}C NMR (75 MHz, $CDCl_3$): δ 82.2, 71.4, 39.9, 37.5, 34.3, 34.1, 32.9, 28.9, 28.5, 25.2. HRMS: found 337.1135 $[M + Na]^+$, calcd for $[C_{16}H_{27}BrO + Na]^+$ 337.1137.

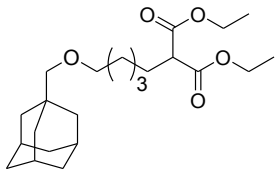

(1c)

Synthesis starting from **1b:**

Dry solution of diethylmalonate (0.118 g, 0.374 mmol) in DMF (3 mL) was charged with NaH (0.0178 g, 60% by wt in mineral oil, 0.449 mmol) at 0 °C and the mixture was to stirred at rt for 30 min. Next a solution of **1b** (0.050 g, 0.375 mmol) in DMF (1.5 mL) was added slowly to the reaction mixture and the mixture was stirred at rt for 20 min and then refluxed overnight at 80 °C. The reaction was quenched with water and aqueous phase was extracted with EtOAc. The organic phase was dried over anhydrous Na_2SO_4 and the crude product obtained as colorless oil after evaporation of solvent. The crude product was purified using flash silica gel column (0%→30% EtOAc in Hexane) to get **3 (**0.095 g, 64%) as a colorless oil after evaporation of solvent.

Synthesis starting from **1k:**

Dry solution of diethylmalonate (1.278, 7.980 mmol) in THF (10 mL) was charged with NaH (0.307 g, 60% by wt in mineral oil, 7.668 mmol) at 0 °C and the mixture was to stirred at rt for 30 min. Next a solution of **1k** (2.534 g, 6.234 mmol) in THF (25 mL) was added slowly to the reaction mixture followed by NaI (0.196 g, 1.309 mmol) and the mixture was to stirred at rt for 20 min and then refluxed for 5 h. The reaction was quenched by adding water and the aqueous phase was extracted with EtOAc. The combined organic phase was dried over anhydrous Na_2SO_4 and the crude product obtained as yellow oil after evaporation of solvent. The crude product was purified using

flash silica gel column (2%→6% EtOAc in Hexane) to get **1c (**2.055 g, 84%) as a colorless oil after evaporation of solvent. R_f 0.59 (10% EtOAc in Hexane), ^{1}H NMR (300 MHz, $CDCl_3$): δ 4.16 (q, J_{H-H} = 7.11 Hz, 4H), 3.35-3.26 (m, 3H), 2.92 (s, 2H, OCH_2- adamantane), 1.93 (br s, 3H, 3 × CH adamantane), 1.89-1.84 (m, 2H, CH_2 pentyl), 1.71-1.49 (m, 16H, 6 × CH_2 adamantane, 2 × CH_2 pentyl), 1.34 (t, J_{H-H} = 3.5 Hz, 2H, CH_2, pentyl), 1.24 (t, J_{H-H} = 6.0 Hz, 6H). ^{13}C NMR (75 MHz, $CDCl_3$): δ 169.7, 82.1, 71.6, 61.4, 52.2, 39.9, 37.4, 29.5, 28.9, 28.5, 27.4, 26.0, 14.3. HRMS: found 417.2598 [M + Na]$^+$, calcd for [$C_{23}H_{38}O_5$ + Na]$^+$ 417.2611.

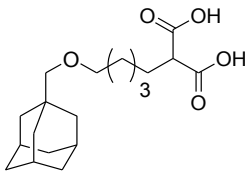

(1d)

Compound **1c** (1.046 g, 2.652 mmol) was suspended in 40 mL solution of 1% NaOH and the mixture was refluxed for 24h. Concentrated HCl was added drop wise to the reaction mixture while stirring vigorously to acidify the reaction mixture to pH 2.0. The aqueous phase was extracted with EtOAc (3 × 100 mL) and the combined organic phase was dried over anhydrous Na_2SO_4 .Compound **1d** (0.899 g, quantitative) was obtained as yellow oil after evaporation of solvent. ^{1}H NMR (300 MHz, $CDCl_3$): δ 10.61 (br s, 2H), 3.41 (m, 3H), 2.99 (s, 2H, OCH_2- adamantane), 1.95 (br s, 5H, 3 × CH adamantane, CH_2 pentyl), 1.72-1.56 (m, 16H, 6 × CH_2, 2 × CH_2 pentyl), 1.39 (br s, 2H). ^{13}C NMR (75 MHz, $CDCl_3$): 174.7, 82.1, 71.9, 51.7, 39.8, 37.4, 34.3, 29.3, 28.9, 28.4, 27.3, 25.9. HRMS: found 361.1985 [M + Na] $^+$, calcd for [$C_{19}H_{30}O_5$ + Na]$^+$ 361.1985.

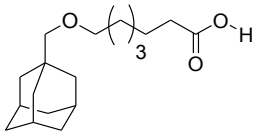

(1e)

A solution of compound **1d** (0.068 g, 0.199 mmol) in toluene (10 mL) was refluxed for 24 h. The solvent was evaporated and the residue dried under vacuum to obtain **1e** (0.717 g, quantitative) as pale yellow solid. ^{1}H NMR (300 MHz, $CDCl_3$): δ 3.37 (t, $J_{H\text{-}H}$ = 6.4 Hz, 2H), 2.99 (s, 2H, OCH_2- adamantane), 2.34 (t, $J_{H\text{-}H}$ = 7.4 Hz, 2H), 1.95 (br s, 5H, 3 × CH adamantane, CH_2 pentyl), 1.73-1.55 (m, 16H, 6 × CH_2, 2 × CH_2 pentyl), 1.38-1.33 (br s, 2H). ^{13}C NMR (75 MHz, $CDCl_3$): 179.91, 82.1, 71.7, 39.9, 37.4, 34.3, 29.5, 29.0, 28.5, 25.9, 24.8. HRMS: found 317.2089 $[M + Na]^+$, calcd for $[C_{18}H_{30}O_3 + Na]^+$ 317.2087.

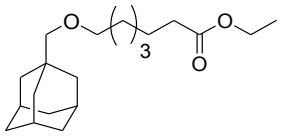

(1f)

To a solution of **1e** (0.816 g, 2.770 mmol) in EtOH (15 mL) was added (0.692 g, 6.371 mmol) of TMS-Cl dropwise and the mixture was stirred at rt overnight. The reaction mixture was concentrated and the residue loaded directly on a silica gel column (0%→10% EtOAc in Hexane) to obtain compound **1f** (0.685 g, 77%) was obtained as colorless oil after evaporation of solvent. R_f = 0.54 (10 % EtOAc: Hexane). ^{1}H NMR (300 MHz, $CDCl_3$): δ 4.12 (q, $J_{H\text{-}H}$ = 7.1 Hz, 2H), 2.95 (s, 2H, OCH_2- adamantane), 2.29 (t, $J_{H\text{-}H}$ = 7.7 Hz, 2H), 1.95 (br s, 5H, 3 × CH adamantane, CH_2 pentyl), 1.74-1.55 (m, 16H, 6 × CH_2 adamantane, 2 × CH_2 pentyl), 1.37-1.28 (m, 2H), 1.23 (t, $J_{H\text{-}H}$ = 6.1 Hz, 3H). ^{13}C NMR (75 MHz, $CDCl_3$): δ 178.04, 82.1, 76.8, 71.8, 39.9, 37.5, 34.6, 34.3, 29.2,

28.5, 26.0, 25.2, 14.5. HRMS: found 345.2393 $[M + Na]^+$, calcd for $[C_{20}H_{34}O_3 + Na]^+$ 345.2400.

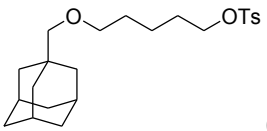

(1l)

A dry solution of **1k** (0.749 g, 2.967 mmol) in DCM (20 mL) was cooled to 0 °C under argon. Triethylamine (0.6 mL, 2.967 mmol) and DMAP (0.025g catalytic) was added to the above solution followed by portion wise addition of toluene-4-sulfonylchloride (0.549 g, 2.878 mmol) over 25 min 0 °C . After stirring for 20 min at 0 °C, the reaction was stirred at 25 °C for 3 h. The reaction was diluted with DCM and the organic layer washed with water (2 × 25 mL) and 1N HCl (2 × 25 mL). The combined organic phase was dried over anhydrous Na_2SO_4 and the crude product obtained as colorless oil after evaporation of solvent. The crude product was purified using flash silica gel column (10% EtOAc in Hexane) to obtain **1l** (0.921 g, 78.75%) as a yellow oil after evaporation of solvent. R_f = 0.50 (25% EtOAc in Hexane). ^{1}H NMR (300 MHz, $CDCl_3$): δ = 7.77 (d, $J_{H\text{-}H}$ = 8.3Hz, 2H), 7.33 (d, $J_{H\text{-}H}$ = 8.53Hz, 2H), 4.02 (t, $J_{H\text{-}H}$ = 6.52Hz, 2H), 3.31 (t, $J_{H\text{-}H}$ = 6.28Hz, 2H), 2.90 (s,2H), 2.43 (s,3H), 1.95 (br s, 3H, 3 × CH adamantane), 1.73-1.70 (m, 8H), 1.68-1.61 (m, 2H), 1.52 (br d, $J_{H\text{-}H}$ = 2.4Hz, 6H), 1.51-1.43 (m, 2H). ^{13}C NMR (75 MHz, $CDCl_3$): δ 144.8, 133.4, 129.9, 128.0, 82.1, 71.3, 70.7, 39.9, 37.4, 34.2, 29.0, 28.8, 28.4, 22.3, 21.8. HRMS: found 429.2060 $[M + Na^+]$, calcd for $[C_{23}H_{34}O_4S + Na]^+$ 429.2070.

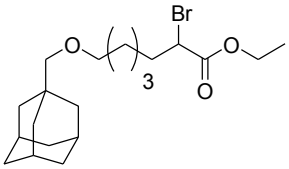

(1g)

n-BuLi (0.21 mL, 1.6 M in Hexane) was added to a solution of N,N-diisopropylamine (0.05 mL, 0.341 mmol) in THF (1.5 mL) at 0 °C. The mixture was stirred at 0 °C for 30 min. The reaction mixture was then cooled to -78 °C and a solution of **1f** (0.100 g, 0.310 mmol) in THF (2 mL) was added drop wise over 5 min to the above reaction mixture. The reaction mixture stirred for the next 30 min and then TMS-Cl (0.07 mL, 0.543 mmol) was added drop wise at -78 °C. The reaction mixture was allowed to stir at -78 °C for the next 90 min followed by addition of N-bromosuccinimide (0.058 g, 0.326 mmol) and stirred at -78 °C for the next 30 min and then warmed to 0 °C over 3 h. The reaction was quenched by adding saturated solution of NH_4Cl and the aqueous phase extracted with EtOAc. The organic layer was dried over anhydrous Na_2SO_4 and the crude product was obtained as brown oil. The crude product was purified using silica gel column (5% EtOAc in Hexane) to obtain **1g** (0.110 g, 88%) as yellow oil after evaporation fo solvent. R_f = 0.55 (10% EtOAc in Hexane). ^{1}H NMR (300 MHz, $CDCl_3$): δ = 4.27-4.19 (m, 3H), 3.37 (t, $J_{H\text{-}H}$ = 9.0 Hz, 2H), 2.95 (s, 2H), 1.96-1.67 (br m, 12H), 1.53 (br s, 10H), 1.31 (t, $J_{H\text{-}H}$ = 6.0 Hz, 2H). ^{13}C NMR (75 MHz, $CDCl_3$): δ 170.0, 82.10, 82.06, 71.44, 62.0, 46.3, 42.5, 39.9, 37.4, 36.3, 35.0, 34.2, 29.4, 28.5, 27.3, 25.6, 14.1. HRMS: found 423.1498 [M + Na^+], calcd for $[C_{20}H_{33}BrO_3 + Na]^+$ 423.1505.

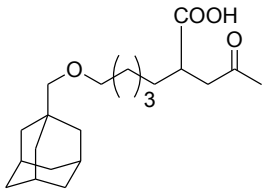

(1i)

NaOEt (0.015 g, 0.221 mmol) was added to a solution of ethyl acetoacetate (0.03 mL, 0.211 mmol) in anhydrous EtOH (0.5 mL). The mixture was heated to reflux and then a solution of compound **1g** (0.085 g, 0.211 mmol) in anhydrous EtOH (2.0 mL) was added to the reaction mixture slowly over 30 min. The reaction mixture was refluxed for 2 d, solvent was evaporated and the residue dissolved in EtOAc. The organic phase was washed with water (10 mL × 2) and the combined organic phase was dried over anhydrous Na_2SO_4. Evaporation of solvent afforded 0.043 g of **1h**, which was directly used in the next step.

Compound **1h** was suspended in 5.0 mL of 1N NaOH (0.405 mmol) and the reaction mixture was refluxed overnight. The reaction mixture was acidified with 1N HCl and the aqueous phase was extracted with EtOAc. The combined organic phase was dried over anhydrous Na_2SO_4 and evaporation of solvents yielded **1i** as a yellow oil (0.029 g, quantitative). R_f = 0.41(80% EtOAc in Hexane). ^{1}H NMR (300 MHz, $CDCl_3$): δ = 3.36 (t, $J_{H\text{-}H}$ = 6.45 Hz, 2H), 2.9-2.87 (m, 2H), 2.57-2.47 (m, 1H), 2.17 (s, 3H), 1.95 (br s, 2H), 1.73-1.62 (br m, 7H), 1.52 (br s, 7H), 1.35 (br m, 4H), 1.26 (s, 2H) ^{13}C NMR (75 MHz, $CDCl_3$): δ 206.9, 82.1, 71.7, 44.7, 40.0, 37.5, 34.3, 31.8, 30.2, 29.9, 29.55, 29.50, 28.5, 27.1, 26.2. HRMS: found 373.2355 [M + Na^+], calcd for $[C_{21}H_{34}O_4 + Na]^+$ 373.2349.

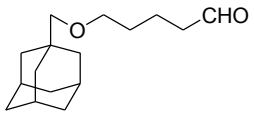

(2a)

A solution of DMSO (0.430 g, 5.506 mmol) in DCM (2.5 mL) was added drop wise over 20 min to a solution of oxalyl chloride, $(COCl)_2$ (0.349 g, 2.753 mmol) in DCM (6 mL) at -78 ºC. The mixture was stirred for 30 min followed by addition of a solution of **1k** (0.632 g, 2.503 mmol) in DCM (6 mL) drop wise over 1 h at -78 ºC. The reaction mixture was stirred at -78 ºC for 2 h followed by addition of Et_3N (1.266 g, 12.514 mmol) drop wise over 15 min at -78 ºC. The reaction mixture was warmed up to rt over 2 h and then diluted by adding 5.0 mL of DCM. The organic phase was washed with dilute HCl followed by saturated solution of $NaHCO_3$. The aqueous phase extracted with DCM and the combined organic phase was dried over anhydrous Na_2SO_4 .The crude product was obtained as yellow oil after evaporation of solvent. The crude product was purified using silica gel column (2% EtOAc in Hexane → 5% EtOAc in Hexane) to give the pure compound **2a**[234] (0.502 g, 80%) as yellow oil after evaporation of solvent. R_f = 0.52 (20% EtOAc in Hexane). ^{1}H NMR (300 MHz, $CDCl_3$): δ = 9.77 (t, $J_{H\text{-}H}$ = 1.77 Hz, 1H), 3.38 (t, $J_{H\text{-}H}$ = 6.14 Hz, 2H), 2.96 (s, 2H), 2.46 (dt, $J_{H\text{-}H}$ = 7.06 Hz, $J_{H\text{-}H}$ = 1.77 Hz, 2H), 1.95 (br s, 3H, 3 × CH adamantane), 1.77-1.55 (br m, 16H). ^{13}C NMR (75 MHz, $CDCl_3$): δ = 202.9, 82.2, 71.1, 43.9, 39.9, 37.4, 34.2, 29.2, 28.5, 19.2. HRMS: found 251.2009 [M + H^+], calcd for $[C_{16}H_{27}O_2]^+$ 251.2006.

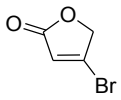

(2b)

To a solution of tetronic acid (0.506 g, 5.053 mmol) in DCM (12 mL) and DMF (0.6 mL) was added oxalyl bromide (1.309 g, 6.064 mmol) drop wise over 1 h at 0 ºC. The color of the solution changed from clear yellow to green during the addition of oxalyl bromide. The reaction mixture was stirred at 0 ºC for 1 h and then at rt for 2 h. 10 mL of water was added to the reaction mixture and the organic layer was separated. The organic phase was washed with saturated solution of $NaHCO_3$ followed by saturated solution of $Na_2S_2O_3$. The aqueous phase extracted with DCM and the combined organic phase was dried over anhydrous Na_2SO_4.The crude product was obtained as a reddish brown solid after evaporation of solvent. The crude product was purified using silica gel column (50% EtOAc in Hexane) to obtain the pure compound **2b**[236] (0.630 g, 76%) as colorless needle shaped crystals after evaporation of solvent. R_f = 0.64 (50% EtOAc in Hexane). ^{1}H NMR (300 MHz, $CDCl_3$): δ = 6.36-6.34 (m, 1H), 4.87-4.85 (m, 2H). ^{13}C NMR (75 MHz, $CDCl_3$): δ = 170.9, 146.3, 121.99, 75.1. HRMS: found 162.9386 [M + H^+], calcd for $[C_4H_4O_2Br]^+$ 162.9389.

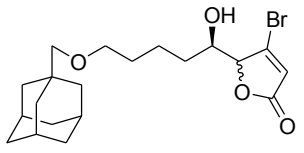

(2)

Step 1: Compound **2b** (0.293 g, 1.801 mmol) was dissolved in DCM (7 mL) and to it was added TMS-Cl (0.332 g, 3.061 mmol) over 5 min at rt, followed by addition of Et_3N (0.619 g, 6.123 mmol) over 10 min at rt. The mixture was stirred at rt for 1 h and then

solvent was removed under vacuum to yield a light pink solid which was protected under argon for later use.

Step 2: $BF_3 \cdot Et_2O$ (0.256g, 1.801 mmol) was added to a solution of compound **2a** (0.451 g, 1.801 mmol) in DCM (15 mL) over 5 min at -78 ºC. The reaction mixture was stirred for the next 5 min at -78 ºC and then a solution of the crude product from step 1 in DCM (8 mL) was added to the reaction mixture drop wise over 30 min at -78 ºC. The reaction mixture was stirred at -78 ºC for 2 h followed by addition of 10 mL of PBS buffer (pH 7.1). The reaction mixture was warmed up to rt and the organic phase was separated. The aqueous phase was extracted with DCM and the combined organic phase was dried over anhydrous Na_2SO_4.The crude product was obtained as colorless oil after evaporation of solvent. The crude product was purified using silica gel column (10% EtOAc in Hexane → 40% EtOAc in Hexane) to obtain **2** (0.353 g, 53%) as pale yellow solid after evaporation of solvent. R_f = 0.28 (30% EtOAc in Hexane). Data for *Syn* aldol: ^{1}H NMR (300 MHz, $CDCl_3$): δ = 6.37-6.36 (m, 1H), 4.88-4.86 (m, 1H), 4.09-4.02 (m, 1H), 3.41 (t, $J_{H\text{-}H}$ = 5.58 HZ, 2H), 2.96 (s, 2H), 1.95 (br s, 3H, 3 × CH adamantane), 1.88-1.51 (br m, 18H). ^{13}C NMR (75 MHz, $CDCl_3$): δ = 170.8, 148.8, 122.9, 87.5, 82.1, 71.5, 69.3, 39.8, 37.3, 33.8, 29.1, 28.3, 22.9. Data for *Anti* aldol: ^{1}H NMR (300 MHz, $CDCl_3$): δ = 6.37-6.36 (m, 1H), 5.11-5.09 (m, 1H), 4.09-4.02 (m, 1H), 3.41 (t, $J_{H\text{-}H}$ = 5.58 Hz, 2H), 2.95 (s, 2H), 1.95 (br s, 3H, 3 × CH adamantane), 1.88-1.51 (br m, 18H). ^{13}C NMR (75 MHz, $CDCl_3$): δ = 170.4, 147.1, 123.3, 88.3, 82.1, 71.5, 69.3, 39.8, 37.3, 34.1, 29.96, 28.3, 22.7. HRMS: found 411.1158 [M - H], calcd for [$C_{20}H_{28}O_4Br$] 411.1165.

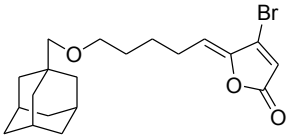

(3)

Thiocarbonyldiimidazole (0.053g, 0.2958 mmol) was added to **2** (0.020g, 0.049 mmol) in DCM (2.0 mL) at 0 ºC. The reaction mixture was stirred for 1 h followed by addition of Et_3N (0.025g, 0.246 mmol) at 0 ºC. The reaction was warmed up to rt and the completion of reaction was confirmed by TLC. The reaction mixture was diluted with DCM and a dry silica gel slurry of the reaction mixture was directly loaded onto the silica gel column (10% EtOAc in Hexane → 15% EtOAc in Hexane). The pure product **3** (0.011g, 57%) was obtained as yellow oil after evaporation of solvent. R_f = 0.56 (20% EtOAc in Hexane). ^{1}H NMR (300 MHz, $CDCl_3$): δ = 6.35 (s, 1H), 5.63 (t, $J_{H\text{-}H}$ = 8.03 Hz, 1H), 3.39 (t, $J_{H\text{-}H}$ = 5.99 Hz, 2H), 2.96 (s, 2H), 2.44 (q, $J_{H\text{-}H}$ = 7.11 Hz, 2H), 1.96 (br s, 3H, 3 × CH adamantane), 1.74-1.52 (br m, 16H). ^{13}C NMR (75 MHz, $CDCl_3$): δ = 167.3, 148.5, 137.2, 119.98, 117.4, 82.2, 71.2, 39.8, 37.3, 34.3, 29.4, 28.5, 26.5, 25.7. HRMS: found 393.1058 [M - H], calcd for [$C_{20}H_{26}O_3Br$] 393.1060.

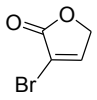

(4a)

A solution of Br_2 (1.748 g, 10.935 mmol) in CCl_4 (5 mL) was added drop wise to a solution of 2-(5H)-furanone (0.599g, 7.124 mmol) in CCl_4 (15 mL) over 20 min at rt. The reaction mixture was and then refluxed for 2 h, followed by addition of Et_3N (1.106 g, 10.935 mmol) at rt. The reaction mixture was stirred at rt for 2 h, which resulted in the formation of a grey precipitate of triethylammonium bromide. The reaction mixture was

filtered to remove the grey precipitate of triethylammonium bromide, the precipitate was washed with CCl_4 and the combined organic phase was washed with water followed by dilute HCl and brine. The aqueous phase was extracted with DCM and the combined organic phase was dried over anhydrous Na_2SO_4. The crude product was obtained as dark brown oil after evaporation of solvent. The crude product was purified using silica gel column (40% EtOAc in Hexane) to obtain the pure product **4a**[239] (0.913g, 77%) as light brown solid after evaporation of solvent. R_f = 0.39 (50% EtOAc in Hexane). ^{1}H NMR (300 MHz, $CDCl_3$): δ = 7.63 (t, J_{H-H} = 1.92 Hz, 1H), 4.86 (d, J_{H-H} = 1.89 Hz, 2H). ^{13}C NMR (75 MHz, $CDCl_3$): δ = 169.1, 149.5, 113.2, 71.7. HRMS: found 162.9385 [M + H^+], calcd for $[C_4H_4O_2Br]^+$ 162.9389.

Preparation of stock solution of the furanone compounds

Stock solutions (10 mM) of all the furanones were prepared in autoclaved DMSO and stored in sterile vials at -20 °C. The stock solutions were thawed at room temperature before use.

Bacterial culture

All chemicals for preparing culture medium for bacterial growth were purchased from Sigma-Aldrich and Fisher Scientific. The *E. coli* strain RP437 was provided by Professor Dacheng Ren (Department of Chemical and Biomedical Engineering, Syracuse University). Overnight cultures of bacteria were grown in Luria-Bertini medium (LB medium) containing 10 g/L tryptone, 10 g/L NaCl and 5 g/L yeast extract at 37 °C in a standard laboratory incubator shaker while shaking at 220 rpm. Water used for preparing the medieum had a resistivity of 18 MΩ cm (Millipore, Billerica, MA). Cyototoxicity and

biofilm inhibition assays were performed in sterile, non-treated, costar polystyrene flat bottom 96-well multititer plates (corning incorporated, corning, NY). Optical density measurements were obtained using Biotek ELx800 (Biotek instruments, Inc, Winooski, VT, USA) plate reader using Gen5 data analysis software.

Cytotoxicity assays

An overnight bacterial culture was diluted and re-grown to an optical density (OD) of 0.05, measured at 600 nm (OD_{600}). 200 μL of bacterial culture was added to the 96-well plates followed by 4 μL of the furanone stock solutions. The outermost wells of the 96-well plates were left unused, but filled with 200 µL of sterile autoclaved water. The 96-well plate was shaken in the incubator shaker at 37 °C and OD_{600} readings were acquired every 0, 2, 4, 6, 8, 10, 12 and 24 h. The plate reader was placed in a sterile laminar flow bio-safety level I hood while acquiring the OD_{600} readings. The OD_{600} values were plotted versus time and the standard deviation in the OD_{600}values was determined over six replicates.

Biofilm inhibition assays

An overnight bacterial culture was diluted and re-grown to an optical density (OD) of 0.05, measured at 600 nm. 200 μL of bacterial culture was added to the 96-well plates followed by 4 μL of the furanone stock solutions. The outermost wells of the 96-well plates were filled with 200 µL of sterile autoclaved water. The 96-well plate was then wrapped in saran wrap and placed in a 37 °C incubator for 24 h. After 24 h, the bacterial broth was withdrawn from each well of the 96-well plate and the wells were allowed to air dry for 30 min. The wells were then rinsed with 200 μL of water once and were dried

again for 30 min. 200 μL of 0.1% crystal violet (CV) solution in water was added to each well to allow biofilm staining for 30 min. The crystal violet solution was removed and the wells were rinsed, three times with 250 μL of water. The plate was air-dried for 30 min, before adding 250 μL of 95% ethanol to each well. The plate was again kept at rt for 30 min and then the contents of each well were mixed gently with a pipette. 100 μL of the solution was then transferred to a fresh 96-well plate and OD was measured at 600 nm (OD_{600}). Percent inhibition of biofilm inhibition was calculated using the measured OD_{600} values after crystal violet assay. We used equation $[1-(A_{M+B+BF} - A_M)/(A_{M+B} - A_M)] \times 100$ for calculating percent inhibition of biofilm formation, where A_{M+B+BF} is the OD_{600} of wells containing media + bacteria + brominated furanones, A_{M+B} is the OD_{600} of wells containing media + bacteria and A_M is the OD_{600} of wells containing only media. The standard deviation in the percent inhibition values was determined over six replicates. The amount of DMSO used to dissolve the adamantane tethered brominated furanones or brominated furanones did not exceed 2% by volume. Narasimhan et al. have reported that DMSO up to 3% by volume has no influence on the growth or formation of biofilm by *E. coli* RP437.[88]

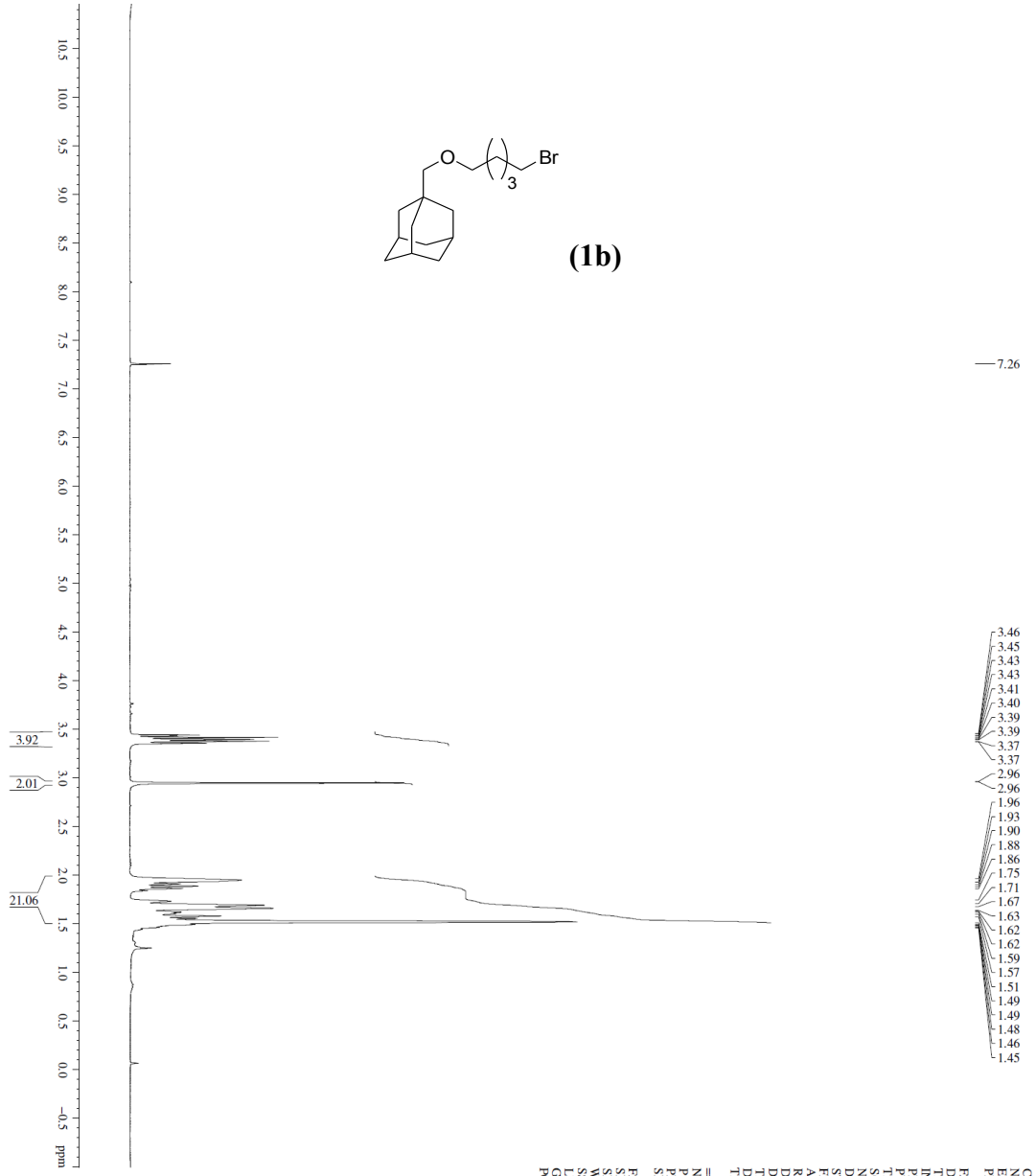
O
Br
3
(1b)
7.26
3.46
3.45
3.43
3.43
3.41
3.40
3.39
3.39
3.37
3.37
2.96
2.96
1.96
1.93
1.90
1.88
1.86
1.75
1.71
1.67
1.63
1.62
1.62
1.59
1.57
1.51
1.49
1.49
1.48
1.46
1.45
3.92
2.01
21.06
10.5 10.0 9.5 9.0 8.5 8.0 7.5 7.0 6.5 6.0 5.5 5.0 4.5 4.0 3.5 3.0 2.5 2.0 1.5 1.0 0.5 0.0 −0.5 ppm
Current Data Parameters
NAME DB1-44-pure
EXPNO 1
PROCNO 1
F2 – Acquisition Parameters
Date_ 20070609
Time 20.09
INSTRUM spect
PROBHD 5 mm QNP 1H/1
PULPROG zg
TD 32768
SOLVENT CDCl3
NS 16
DS 0
SWH 3591.954 Hz
FIDRES 0.109618 Hz
AQ 4.561536 sec
RG 90.5
DW 139.200 usec
DE 54.00 usec
TE 298.2 K
D1 1.00000000 sec
TD0 1
======== CHANNEL f1 ========
NUC1 1H
P1 9.75 usec
PL1 0.00 dB
SFO1 300.1315007 MHz
F2 – Processing parameters
SI 32768
SF 300.1300073 MHz
WDW no
SSB 0
LB 0.00 Hz
GB 0
PC 1.00

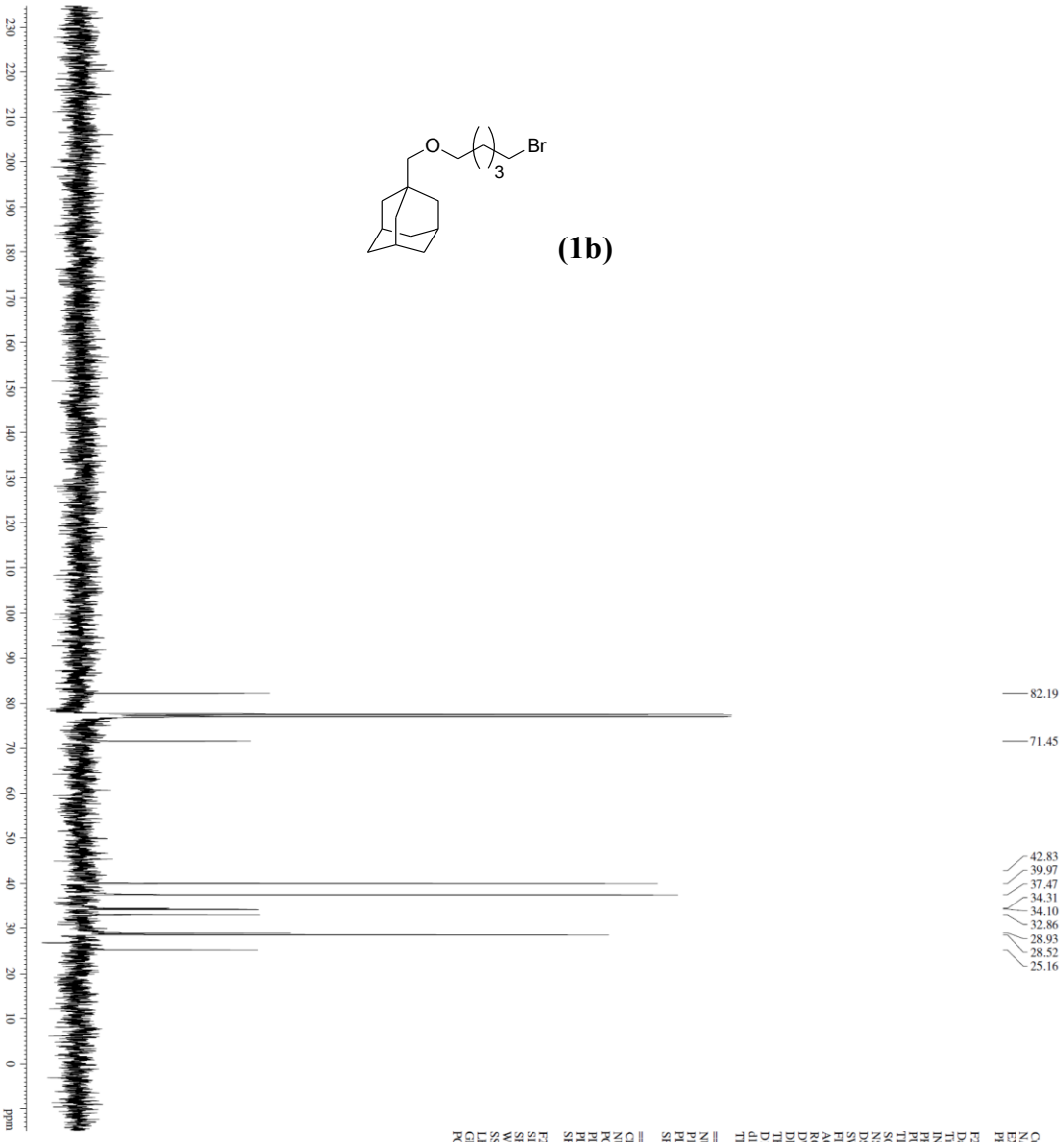

(1b)

Current Data Parameters
NAME DB.144.pure.cumr
EXPNO 2
PROCNO 1

F2 - Acquisition Parameters
Date_ 20070629
Time 19.14 spect
INSTRUM
PROBHD 5 mm QNP 1H/1
PULPROG zgdc30
TD 65536
SOLVENT CDCl3
NS 250
DS 4
SWH 18832.393 Hz
FIDRES 0.287349 Hz
AQ 1.7400308 sec
RG 11585.2
DW 26.550 usec
DE 6.00 usec
TE 298.2 K
D1 0.40000001 sec
d11 0.03000000 sec
TD0 1

======== CHANNEL f1 ========
NUC1 13C
P1 13.70 usec
PL1 0.00 dB
SFO1 75.4760200 MHz

======== CHANNEL f2 ========
CPDPRG2 waltz16
NUC2 1H
PCPD2 95.00 usec
PL2 0.00 dB
PL12 18.00 dB
SFO2 300.1312005 MHz

F2 - Processing parameters
SI 32768
SF 75.4677326 MHz
WDW EM
SSB 0
LB 2.00 Hz
GB 0
PC 1.00

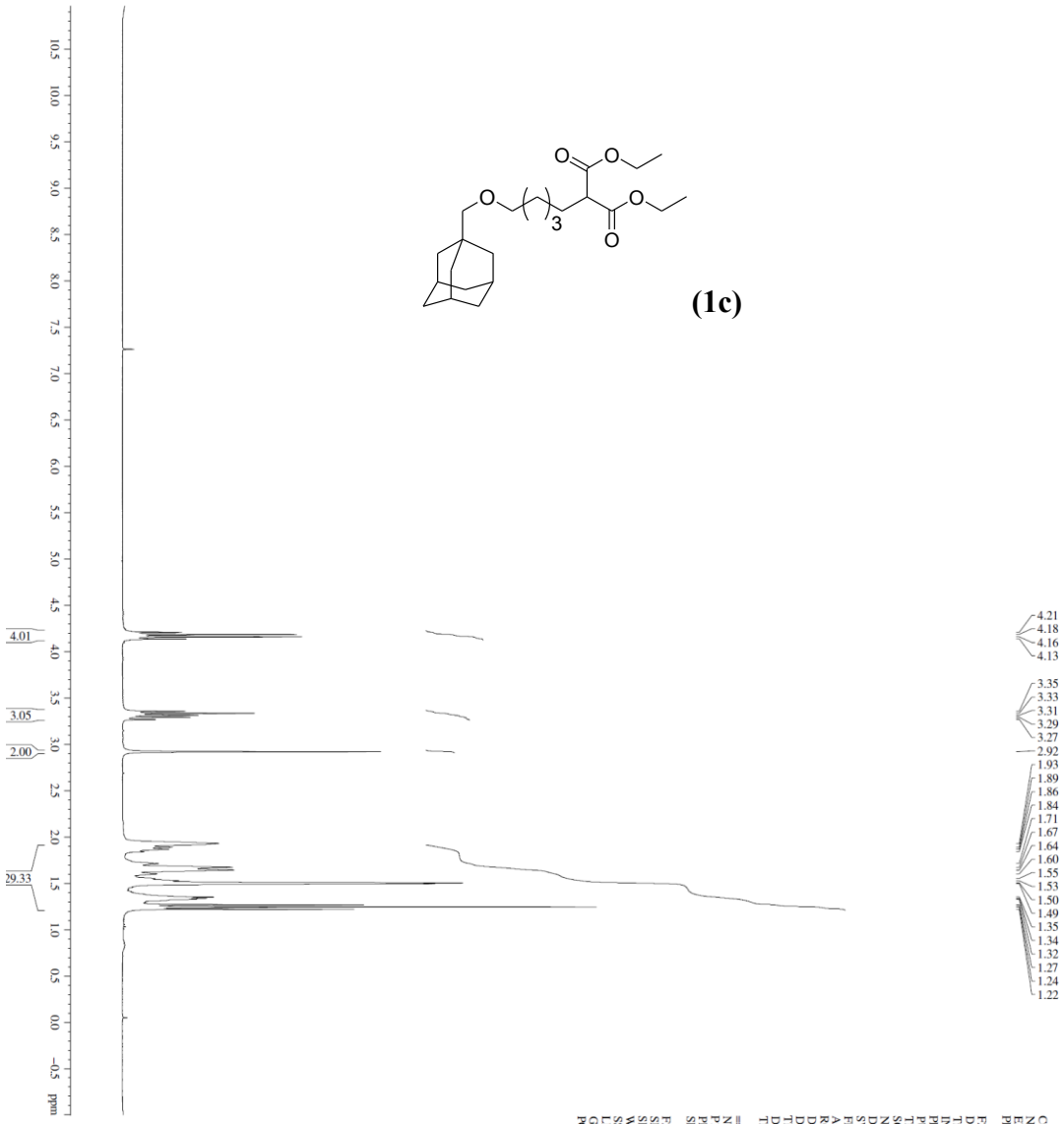
4.01
3.05
2.00
29.33
10.5 10.0 9.5 9.0 8.5 8.0 7.5 7.0 6.5 6.0 5.5 5.0 4.5 4.0 3.5 3.0 2.5 2.0 1.5 1.0 0.5 0.0 −0.5 ppm
4.21
4.18
4.16
4.13
3.35
3.33
3.31
3.29
3.27
2.92
1.93
1.89
1.86
1.84
1.71
1.67
1.64
1.60
1.55
1.53
1.50
1.49
1.35
1.34
1.32
1.27
1.24
1.22
Current Data Parameters
NAME
EXPNO 1
PROCNO 1
F2 - Acquisition Parameters
Date_ 20070629
Time 13.44
INSTRUM spect
PROBHD 5 mm QNP 1H/1
PULPROG zg
TD 32768
SOLVENT CDCl3
NS 16
DS 0
SWH 3591.954 Hz
FIDRES 0.10961 8 Hz
AQ 4.561556 sec
RG 139.200
DW 54.00 usec
DE 297.2 K
TE
D1 1.00000000 sec
TD0 1
CHANNEL f1
NUC1 1H
P1 9.75 usec
PL1 0.00 dB
SFO1 300.1315007 MHz
F2 - Processing parameters
SI 32768
SF 300.1300063 MHz
WDW EM
SSB 0
LB 0.00 Hz
GB 0
PC 1.00

O
O
O
3
O
O
O

(1c)

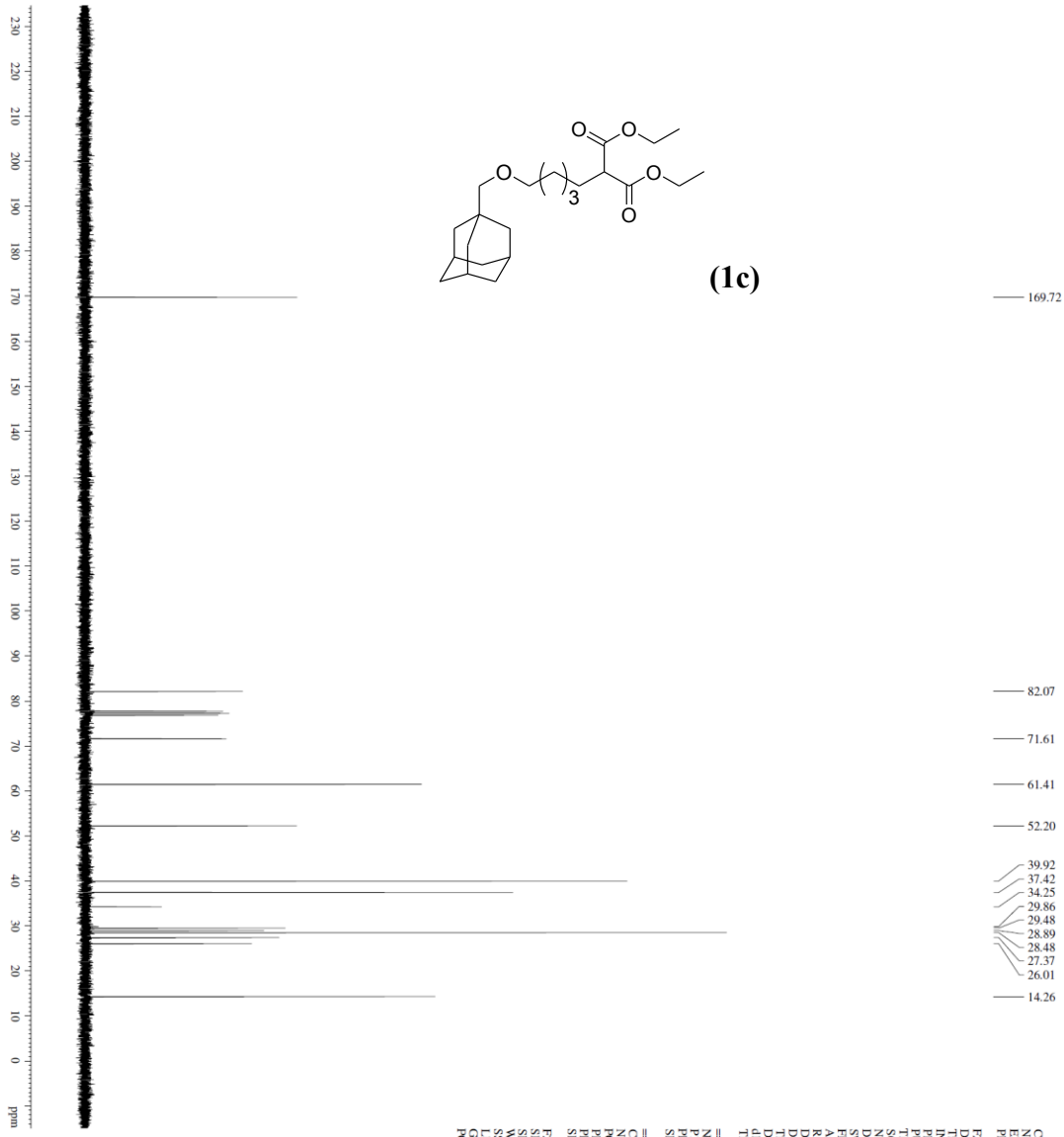
O
O
O
O
O
3
O
(1c)
169.72
82.07
71.61
61.41
52.20
39.92
37.42
34.25
29.86
29.48
28.89
28.48
27.37
26.01
14.26
230 220 210 200 190 180 170 160 150 140 130 120 110 100 90 80 70 60 50 40 30 20 10 0 ppm
Current Data Parameters
NAME DB-1-58_pure cmnr
EXPNO 2
PROCNO 1
F2 – Acquisition Parameters
Date_ 20070629
Time 18.28
INSTRUM spect
PROBHD 5 mm QNP 1H/1
PULPROG zgdc30
TD 65536
SOLVENT CDCl3
NS 250
DS 4
SWH 1883.393 Hz
FIDRES 0.287360 Hz
AQ 1.7400308 sec
RG 5160.6
DW 265.350 usec
DE 6.00 usec
TE 298.2 K
D1 0.40000001 sec
d11 0.03000000 sec
TD0 1
======== CHANNEL f1 ========
NUC1 13C
P1 13.70 usec
PL1 0.00 dB
SFO1 75.4760200 MHz
======== CHANNEL f2 ========
CPDPRG2 waltz16
NUC2 1H
PCPD2 95.00 usec
PL2 0.00 dB
PL12 18.00 dB
SFO2 300.1312005 MHz
F2 – Processing parameters
SI 32768
SF 75.4677350 MHz
WDW no
SSB 0
LB 0.00 Hz
GB 0
PC 1.00

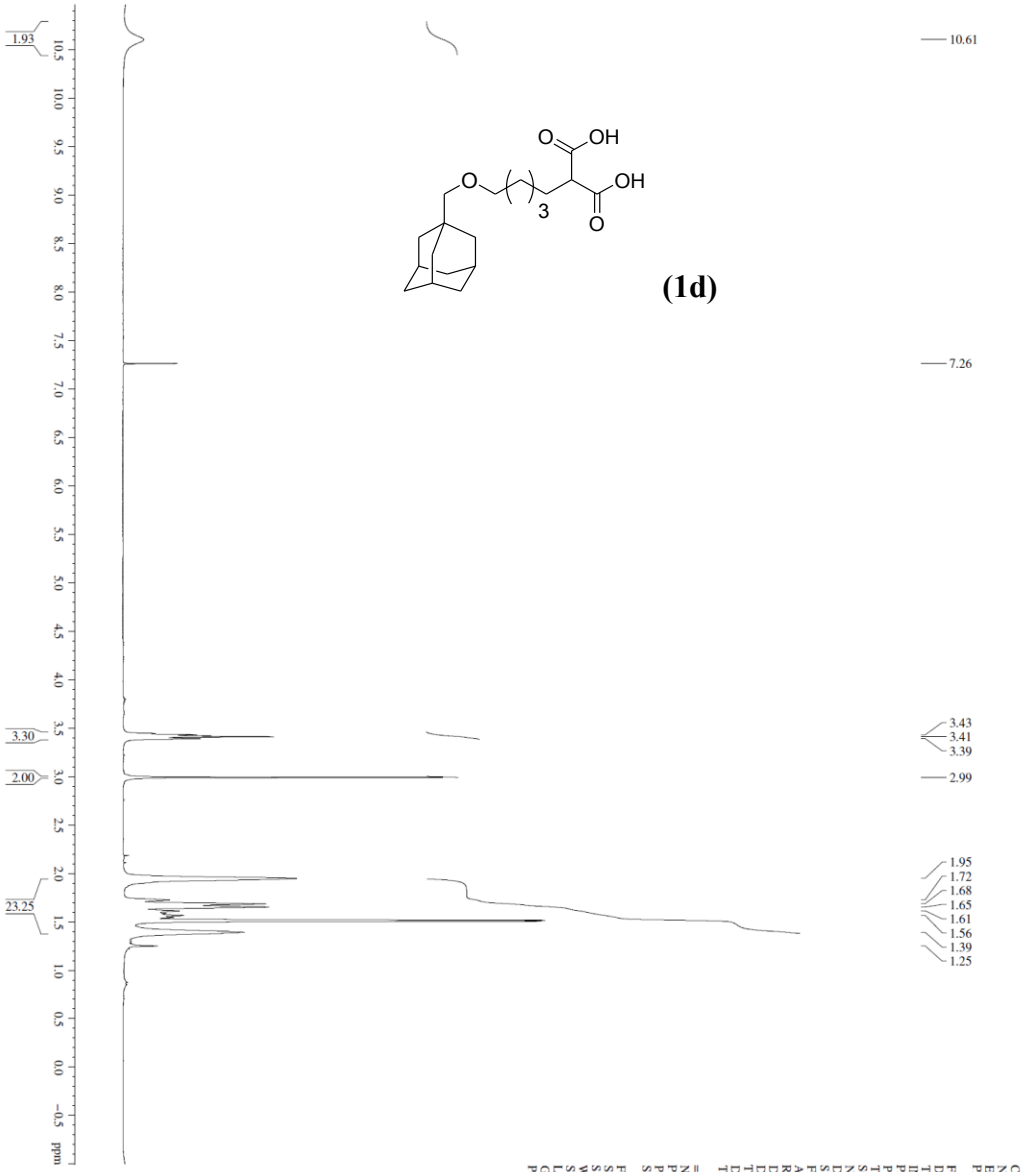

(1d)

Current Data Parameters
NAME DB_1.74.Pure
EXPNO 1
PROCNO 1

F2 - Acquisition Parameters
Date_ 20070706
Time 18.33
INSTRUM spect
PROBHD 5 mm QNP 1H/1
PULPROG zg
TD 32768
SOLVENT CDCl3
NS 30
DS 0
SWH 3591.954 Hz
FIDRES 0.109618 Hz
AQ 4.5613556 sec
RG 71.8
DW 139.200 usec
DE 5.00 usec
TE 298.2 K
D1 1.00000000 sec
TD0 1

======== CHANNEL f1 ========
NUC1 1H
P1 9.75 usec
PL1 0.00 dB
SFO1 300.1315007 MHz

F2 - Processing parameters
SI 32768
SF 300.1300064 MHz
WDW no
SSB 0
LB 0.00 Hz
GB 0
PC 1.00

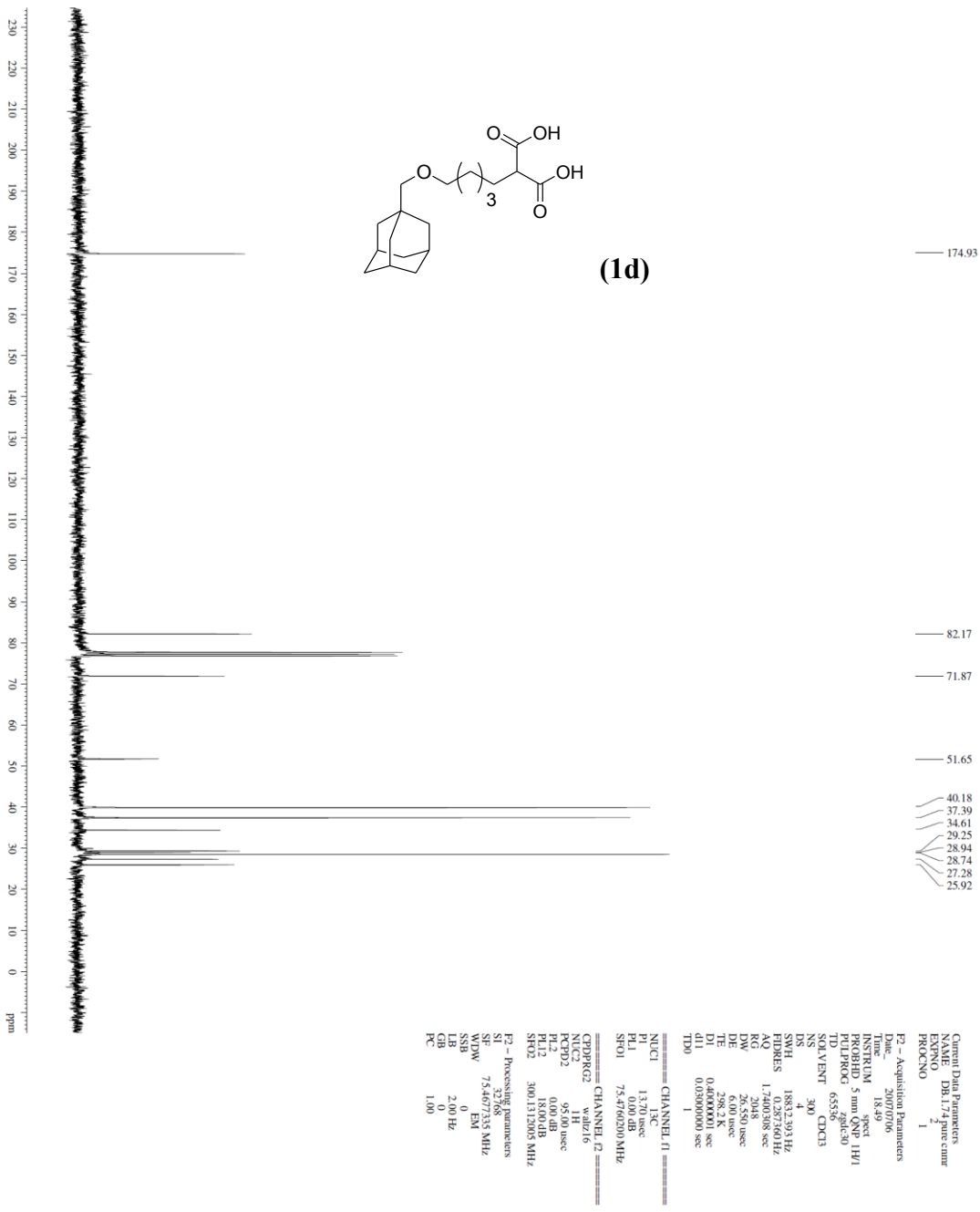

Current Data Parameters
NAME DB-174 pure cmnr
EXPNO 2
PROCNO 1

F2 – Acquisition Parameters
Date_ 20070106
Time 18.49
INSTRUM spect
PROBHD 5 mm QNP 1H/1
PULPROG zgdc30
TD 65536
SOLVENT CDCl3
NS 300
DS 4
SWH 18832.393 Hz
FIDRES 0.287360 Hz
AQ 1.7400308 sec
RG 2048
DW 26.550 usec
DE 6.00 usec
TE 298.2 K
D11 0.03000000 sec
TD0 1

CHANNEL f1
NUC1 13C
P1 13.70 usec
PL1 0.00 dB
SFO1 75.4760200 MHz

CHANNEL f2
CPDPRG2 waltz16
NUC2 1H
PCPD2 95.00 usec
PL2 0.00 dB
PL12 18.00 dB
SFO2 300.1312005 MHz

F2 – Processing parameters
SI 32768
SF 75.4677335 MHz
WDW EM
SSB 0
LB 2.00 Hz
GB 0
PC 1.00

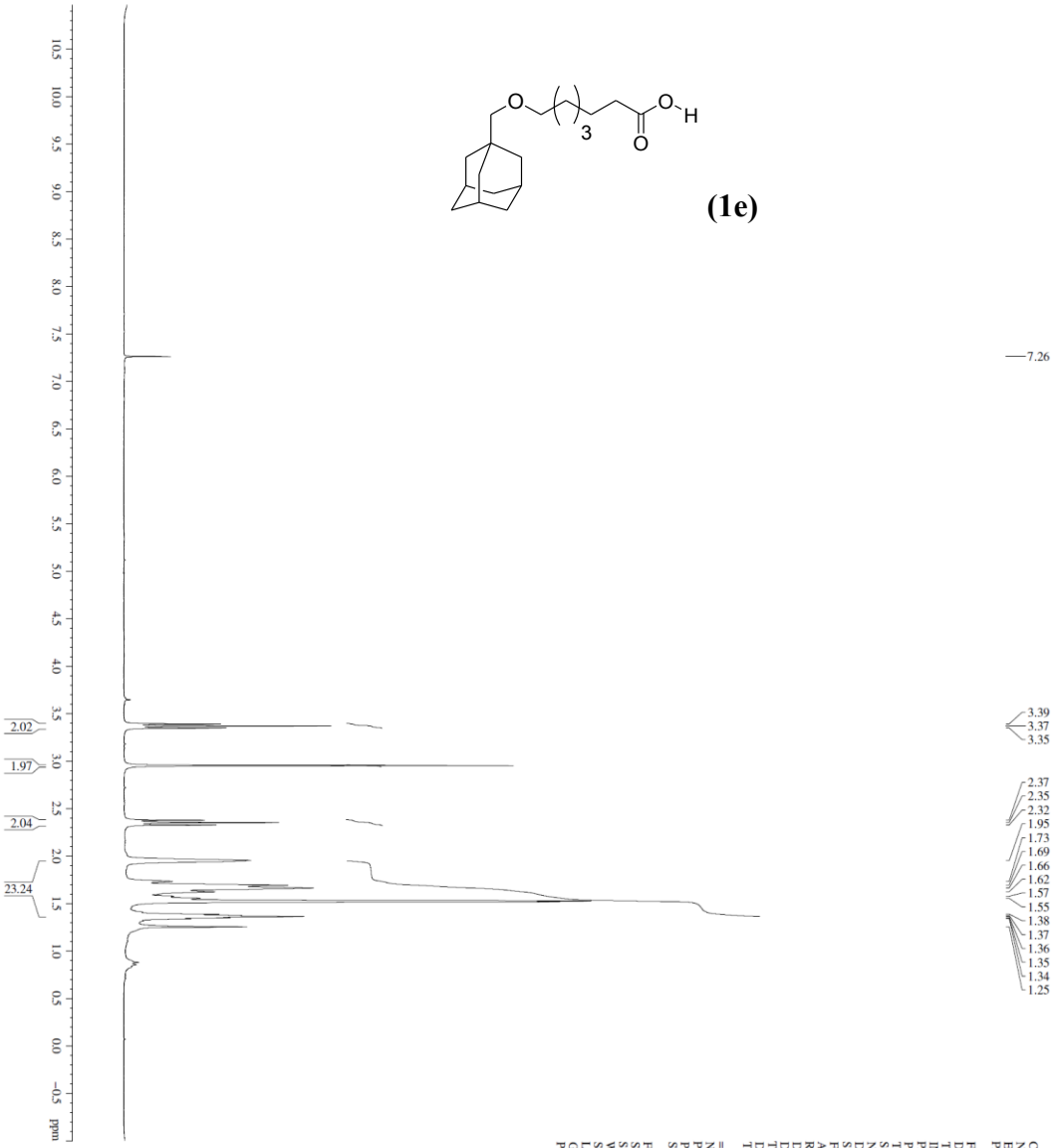
O
3
O
H
O
(1e)
7.26
3.39
3.37
3.35
2.37
2.35
2.32
1.95
1.73
1.69
1.66
1.62
1.57
1.55
1.38
1.37
1.36
1.35
1.34
1.25
2.02
1.97
2.04
23.24
ppm
Current Data Parameters
NAME DB-1.mal decarboxylation
EXPNO 1
PROCNO 1
F2 – Acquisition Parameters
Date_ 20070713
Time 11.26
INSTRUM spect
PROBHD 5 mm QNP 1H/1
PULPROG zg
TD 32768
SOLVENT CDCl3
NS 16
DS 0
SWH 3591.954 Hz
FIDRES 0.109618 Hz
AQ 4.5613556 sec
RG 90.5
DW 139.200 usec
DE 54.00 usec
TE 298.2 K
D1 1.00000000 sec
TD0 1
CHANNEL f1
NUC1 1H
P1 9.75 usec
PL1 0.00 dB
SFO1 300.1315007 MHz
F2 – Processing parameters
SI 32768
SF 300.1300063 MHz
WDW no
SSB 0
LB 0.00 Hz
GB 0
PC 1.00

Current Data Parameters
NAME DB-3-45 decarboxylation CNMR 2
EXPNO 2
PROCNO 1

F2 – Acquisition Parameters
Date_ 20081111
Time 12.02
INSTRUM spect
PROBHD 5 mm QNP 1H/1
PULPROG zgdc30
TD 65536
SOLVENT CDCl3
NS 300
DS 4
SWH 18832.393 Hz
FIDRES 0.287360 Hz
AQ 1.7400308 sec
RG 5160.6
DW 26.550 usec
DE 6.00 usec
TE 300.2 K
D1 0.40000001 sec
d11 0.03000000 sec
TD0 1

======== CHANNEL f1 ========
NUC1 13C
P1 13.70 usec
PL1 0.00 dB
SFO1 75.4760200 MHz

======== CHANNEL f2 ========
CPDPRG2 waltz16
NUC2 1H
PCPD2 95.00 usec
PL2 0.00 dB
PL12 18.00 dB
SFO2 300.1312005 MHz

F2 – Processing parameters
SI 32768
SF 75.4677338 MHz
WDW no
SSB 0
LB 0.00 Hz
GB 0
PC 1.00

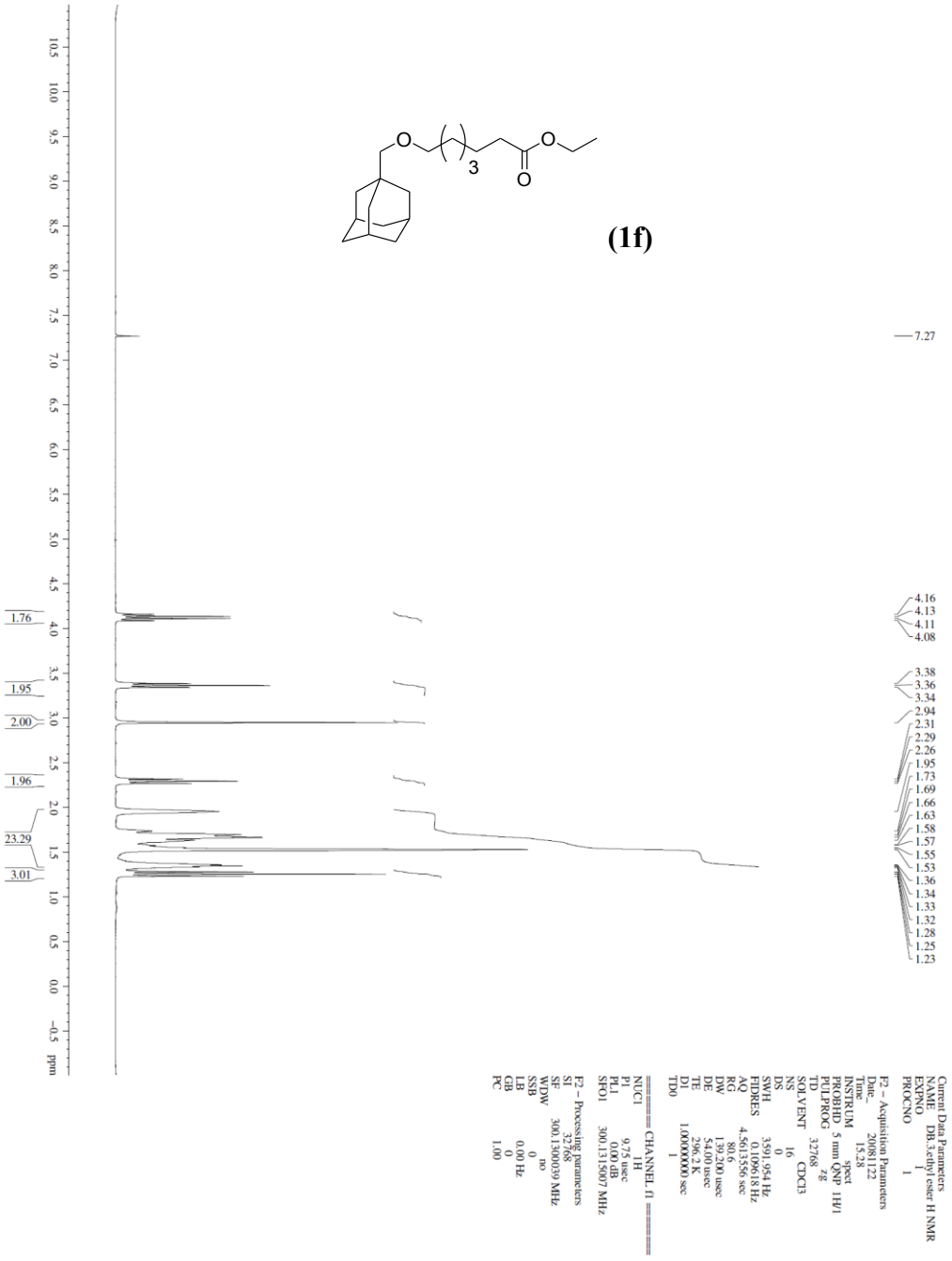
(1f)
7.27
4.16
4.13
4.11
4.08
3.38
3.36
3.34
2.94
2.31
2.29
2.26
1.95
1.73
1.69
1.66
1.63
1.58
1.57
1.55
1.53
1.36
1.34
1.33
1.32
1.28
1.25
1.23
1.76
1.95
2.00
1.96
23.29
3.01
ppm
Current Data Parameters
NAME DR.5ethyl ester H NMR
EXPNO 1
PROCNO 1
F2 – Acquisition Parameters
Date_ 20081122
Time 15.28
INSTRUM spect
PROBHD 5 mm QNP 1H/1
PULPROG zg
TD 32768
SOLVENT CDCl3
NS 16
DS 0
SWH 3591.954 Hz
FIDRES 0.109618 Hz
AQ 4.5613556 sec
RG 80.6
DW 139.200 usec
DE 6.00 usec
TE 294.2 K
D1 1.00000000 sec
TD0 1
CHANNEL f1
NUC1 1H
P1 9.75 usec
PL1 0.00 dB
SFO1 300.1315007 MHz
F2 – Processing parameters
SI 32768
SF 300.1300039 MHz
WDW no
SSB 0
LB 0.00 Hz
GB 0
PC 1.00

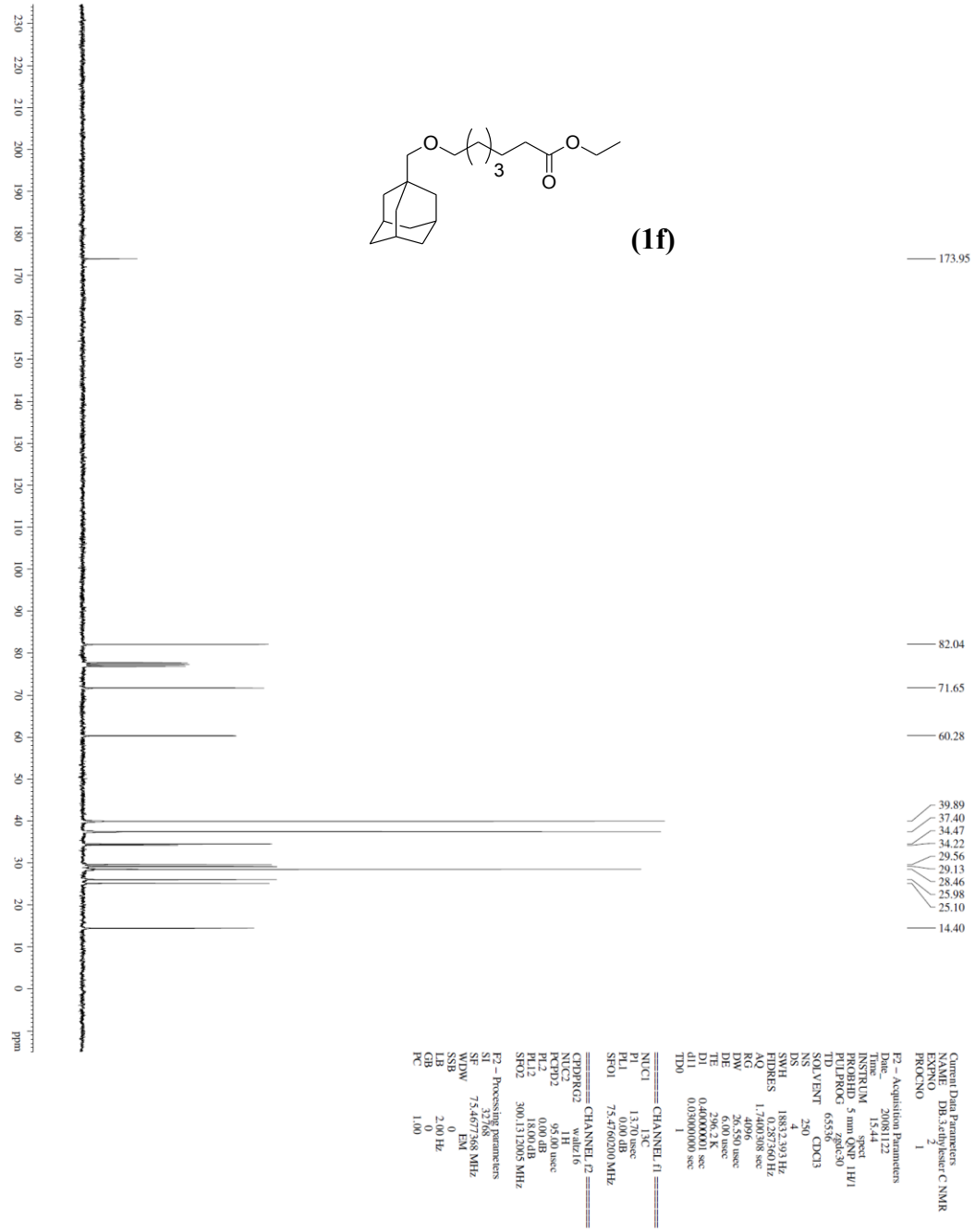
O
3
O
O
(1f)
173.95
82.04
71.65
60.28
39.89
37.40
34.47
34.22
29.56
29.13
28.46
25.98
25.10
14.40
230 220 210 200 190 180 170 160 150 140 130 120 110 100 90 80 70 60 50 40 30 20 10 0 ppm
Current Data Parameters
NAME DB.3.ethylester C NMR
EXPNO 2
PROCNO 1
F2 – Acquisition Parameters
Date_ 20081122
Time 15.44
INSTRUM spect
PROBHD 5 mm QNP 1H/1
PULPROG zgdc30
TD 65536
SOLVENT CDCl3
NS 250
DS 4
SWH 18832.393 Hz
FIDRES 0.287360 Hz
AQ 1.7400308 sec
RG 4096
DW 26.550 usec
DE 6.00 usec
TE 296.2 K
D1 2.00000000 sec
d11 0.03000000 sec
TD0 1
======== CHANNEL f1 ========
NUC1 13C
P1 13.70 usec
PL1 0.00 dB
SFO1 75.4766200 MHz
======== CHANNEL f2 ========
CPDPRG2 waltz16
NUC2 1H
PCPD2 95.00 usec
PL2 0.00 dB
PL12 18.00 dB
SFO2 300.1312005 MHz
F2 – Processing parameters
SI 32768
SF 75.4677368 MHz
WDW EM
SSB 0
LB 2.00 Hz
GB 0
PC 1.00

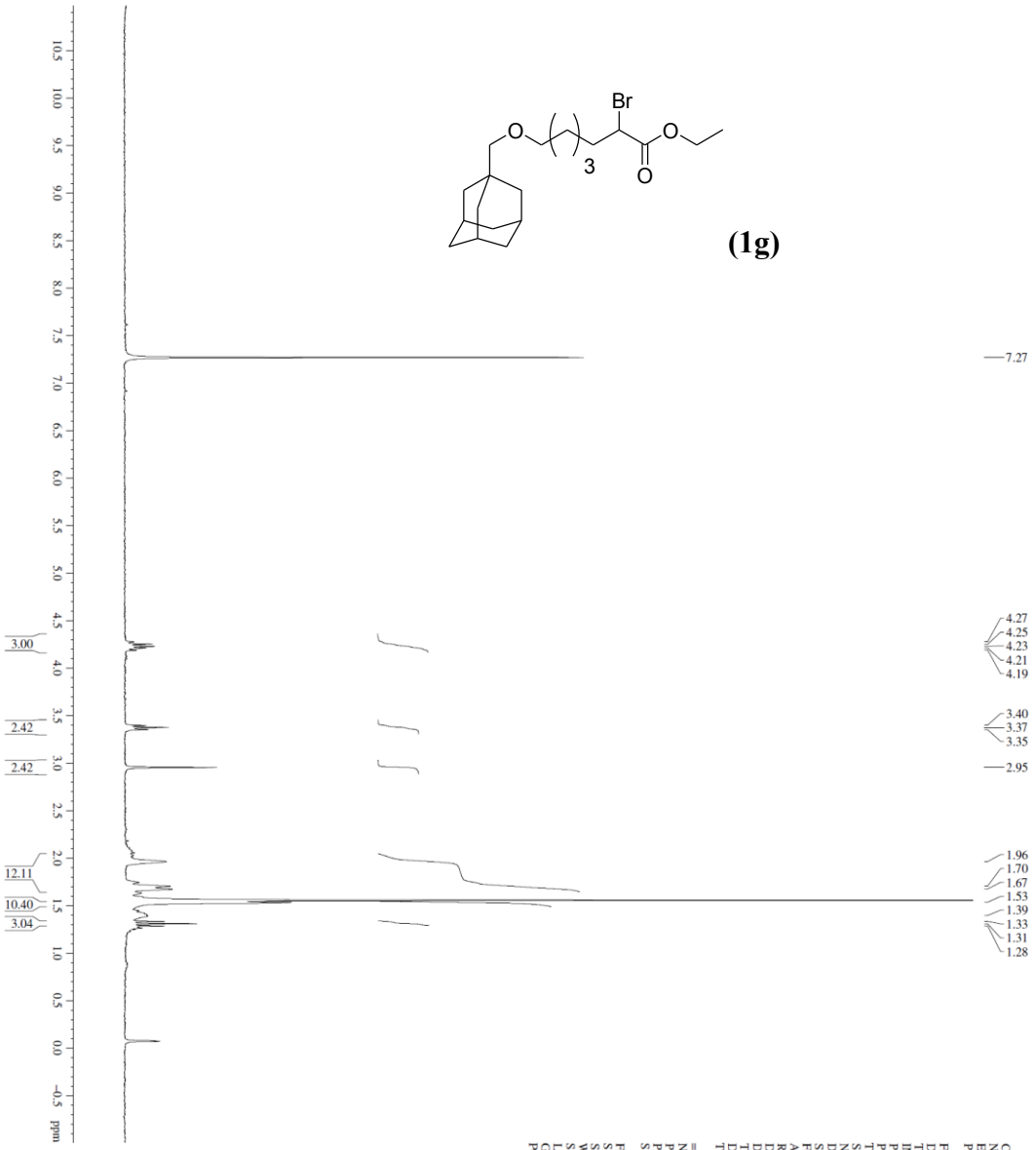
Br
O
O
O
3
(1g)
7.27
4.27
4.25
4.23
4.21
4.19
3.40
3.37
3.35
2.95
1.96
1.70
1.67
1.53
1.39
1.33
1.31
1.28
3.00
2.42
2.42
12.11
10.40
3.04
ppm
Current Data Parameters
NAME DB.3.56.dilute
EXPNO 1
PROCNO 1
F2 – Acquisition Parameters
Date_ 20081013
Time 13.07
INSTRUM spect
PROBHD 5 mm QNP 1H/1
PULPROG zg
TD 32768
SOLVENT CDCl3
NS 10
DS 0
SWH 3591.954 Hz
FIDRES 0.109618 Hz
AQ 4.5613556 sec
RG 1448.2
DW 139.200 usec
DE 5.10 usec
TE 298.2 K
D1 1.00000000 sec
TD0 1
CHANNEL f1
NUC1 1H
P1 9.75 usec
PL1 0.00 dB
SFO1 300.1315007 MHz
F2 – Processing parameters
SI 32768
SF 300.1300039 MHz
WDW EM
SSB 0
LB 1.00 Hz
GB 0
PC 1.00

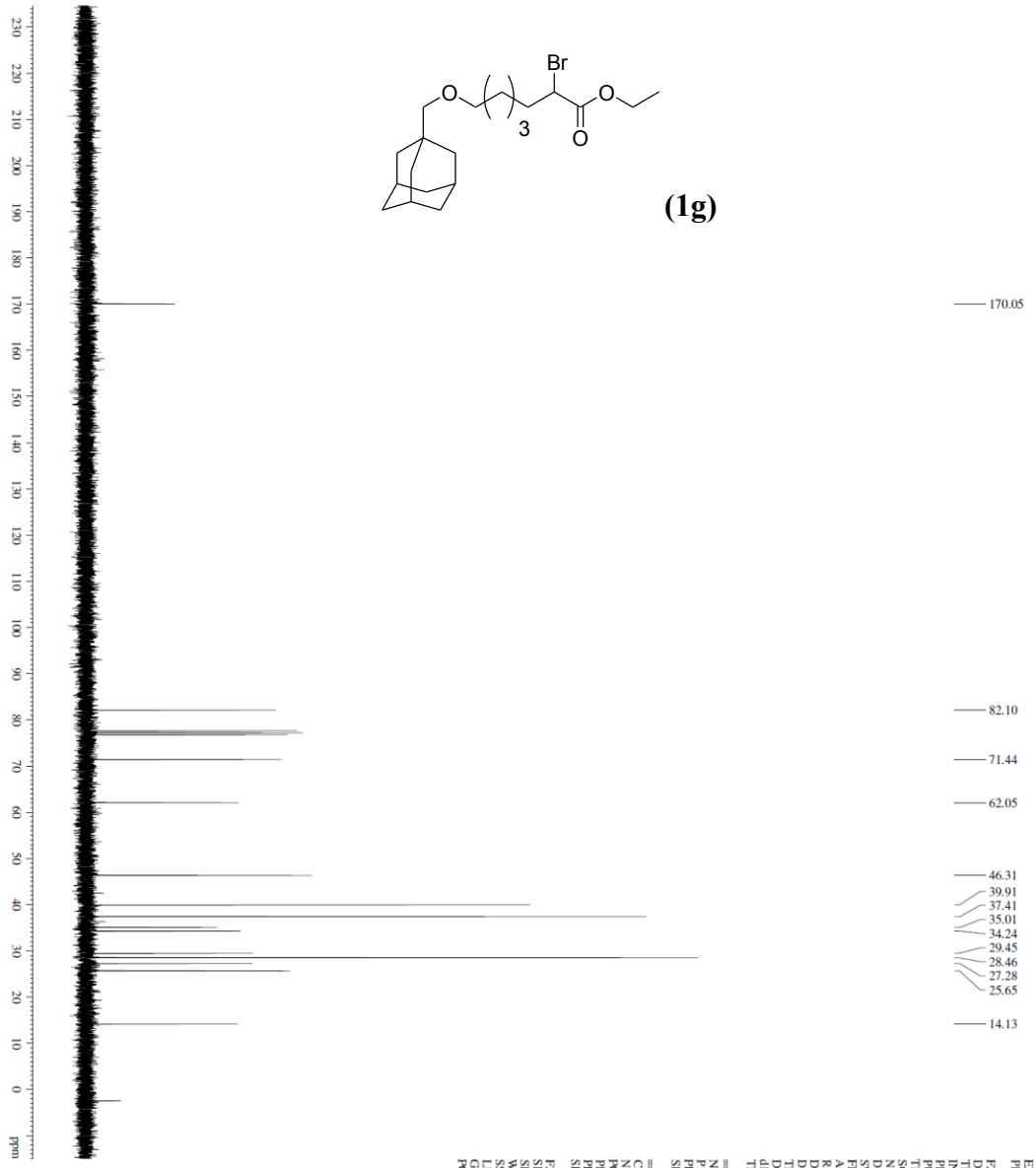
Br
O
O
3
O
O
(1g)
170.05
82.10
71.44
62.05
46.31
39.91
37.41
35.01
34.24
29.45
28.46
27.28
25.65
14.13
230 220 210 200 190 180 170 160 150 140 130 120 110 100 90 80 70 60 50 40 30 20 10 0 ppm
Current Data Parameters
NAME DB-336-FINAL C NMR
EXPNO 2
PROCNO 1
F2 - Acquisition Parameters
Date_ 20081009
Time 17.36
INSTRUM spect
PROBHD 5 mm QNP 1H/1
PULPROG zgdc30
TD 65536
SOLVENT CDCl3
NS 300
DS 4
SWH 18832.393 Hz
FIDRES 0.287360 Hz
AQ 1.7400308 sec
RG 1448.2
DW 26.550 usec
DE 6.00 usec
TE 298.2 K
D1 0.40000001 sec
d11 0.03000000 sec
TD0 1
NUC1 13C
P1 13.70 usec
PL1 0.00 dB
SFO1 75.4760200 MHz
CHANNEL f2
CPDPRG2 waltz16
NUC2 1H
PCPD2 95.00 usec
PL2 0.00 dB
PL12 18.00 dB
SFO2 300.1312005 MHz
F2 - Processing parameters
SI 32768
SF 75.4677368 MHz
WDW no
SSB 0
LB 0.00 Hz
GB 0
PC 1.00

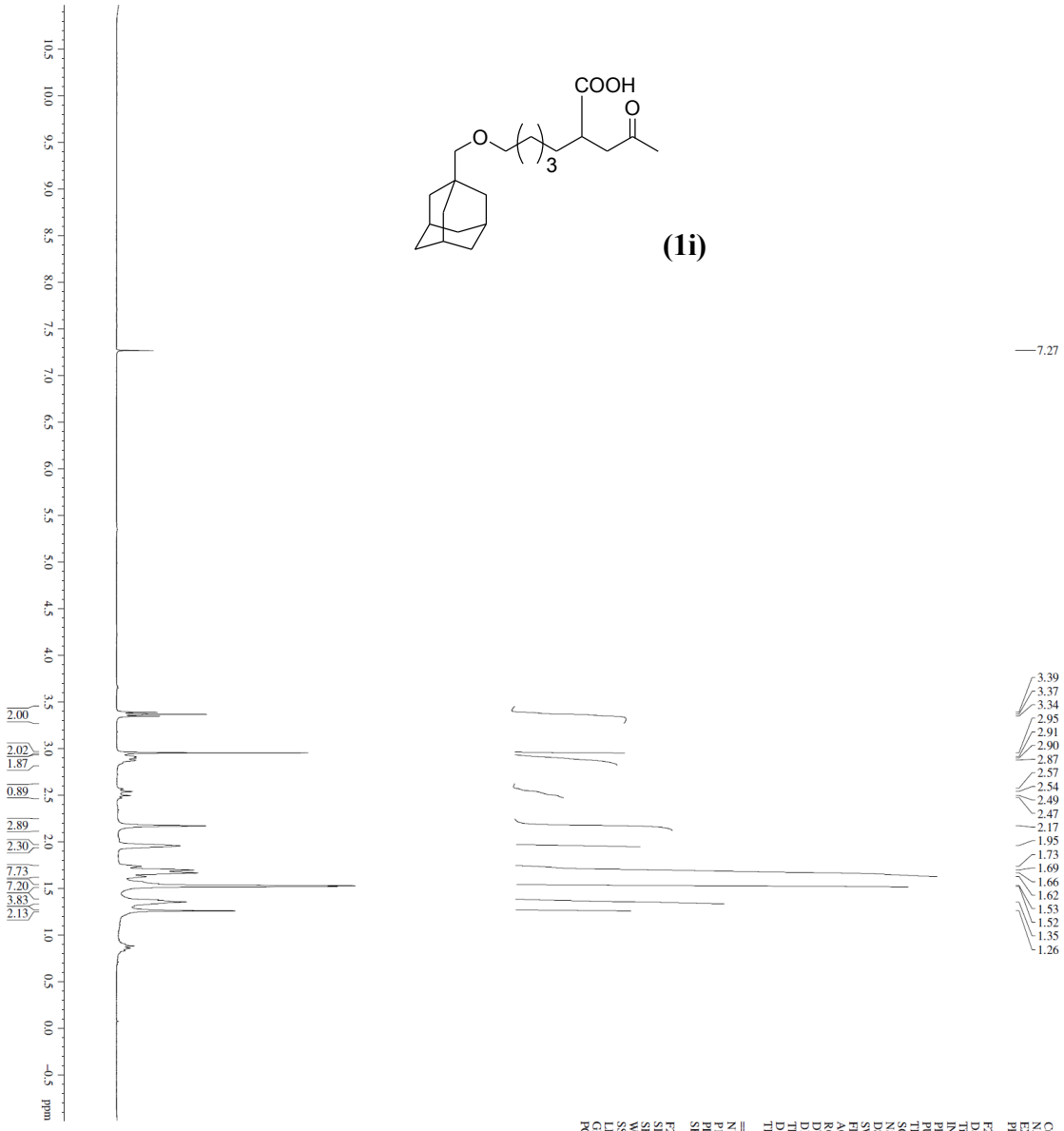
COOH
O
O
3
(1i)
7.27
3.39
3.37
3.34
2.95
2.91
2.90
2.87
2.57
2.54
2.49
2.47
2.17
1.95
1.73
1.69
1.66
1.62
1.53
1.52
1.35
1.26
2.00
2.02
1.87
0.89
2.89
2.30
7.73
7.20
3.83
2.13
ppm
Current Data Parameters
NAME DB-3-58-H NMR
EXPNO 1
PROCNO 1
F2 – Acquisition Parameters
Date_ 20081127
Time 11.18
INSTRUM spect
PROBHD 5 mm QNP 1H/1
PULPROG zg
TD 32768
SOLVENT CDCl3
NS 10
DS 0
SWH 3591.954 Hz
FIDRES 0.109618 Hz
AQ 4.5613556 sec
RG 80.6
DW 139.200 usec
DE 54.00 usec
TE 297.2 K
D1 1.00000000 sec
TD0 1
======== CHANNEL f1 ========
NUC1 1H
P1 9.75 usec
PL1 0.00 dB
SFO1 300.1315007 MHz
F2 – Processing parameters
SI 32768
SF 300.1300039 MHz
WDW no
SSB 0
LB 0.00 Hz
GB 0
PC 1.00

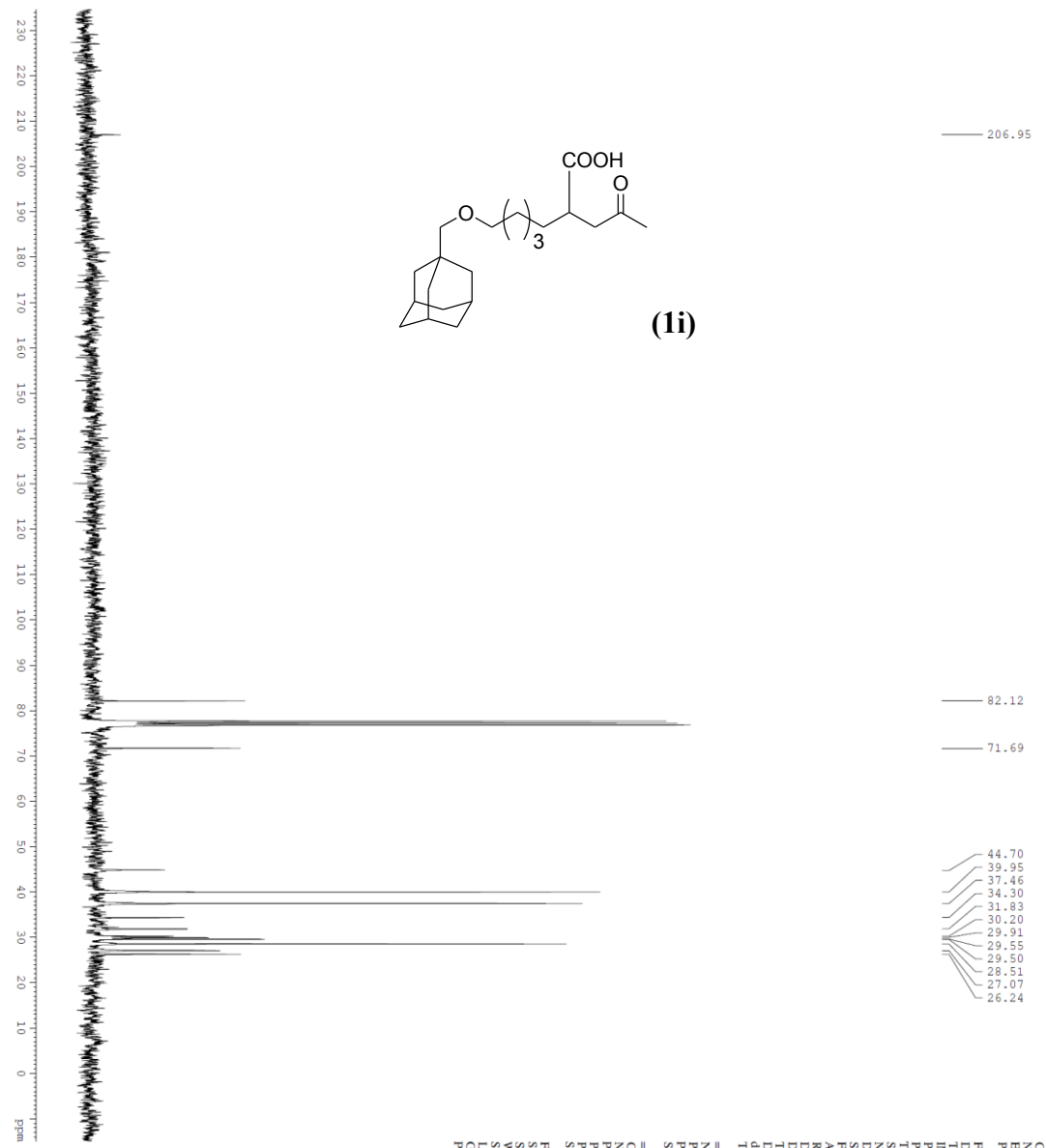

(1i)

Current Data Parameters
NAME DB-3-58-C NMR
EXPNO 2
PROCNO 1

F2 – Acquisition Parameters
Date_ 20081127
Time 11.40
INSTRUM spect
PROBHD 5 mm QNP 1H/1
PULPROG zgdc30
TD 65536
SOLVENT CDCl3
NS 500
DS 4
SWH 18832.393 Hz
FIDRES 0.287360 Hz
AQ 1.7400308 sec
RG 11585.2
DW 26.550 usec
DE 6.00 usec
TE 297.2 K
D1 0.40000001 sec
d11 0.03000000 sec
TD0 1

======== CHANNEL f1 ========
NUC1 13C
P1 13.70 usec
PL1 0.00 dB
SFO1 75.4760200 MHz

======== CHANNEL f2 ========
CPDPRG2 waltz16
NUC2 1H
PCPD2 95.00 usec
PL2 0.00 dB
PL12 18.00 dB
SFO2 300.1312005 MHz

F2 – Processing parameters
SI 32768
SF 75.4677333 MHz
WDW EM
SSB 0
LB 4.00 Hz
GB 0
PC 1.00

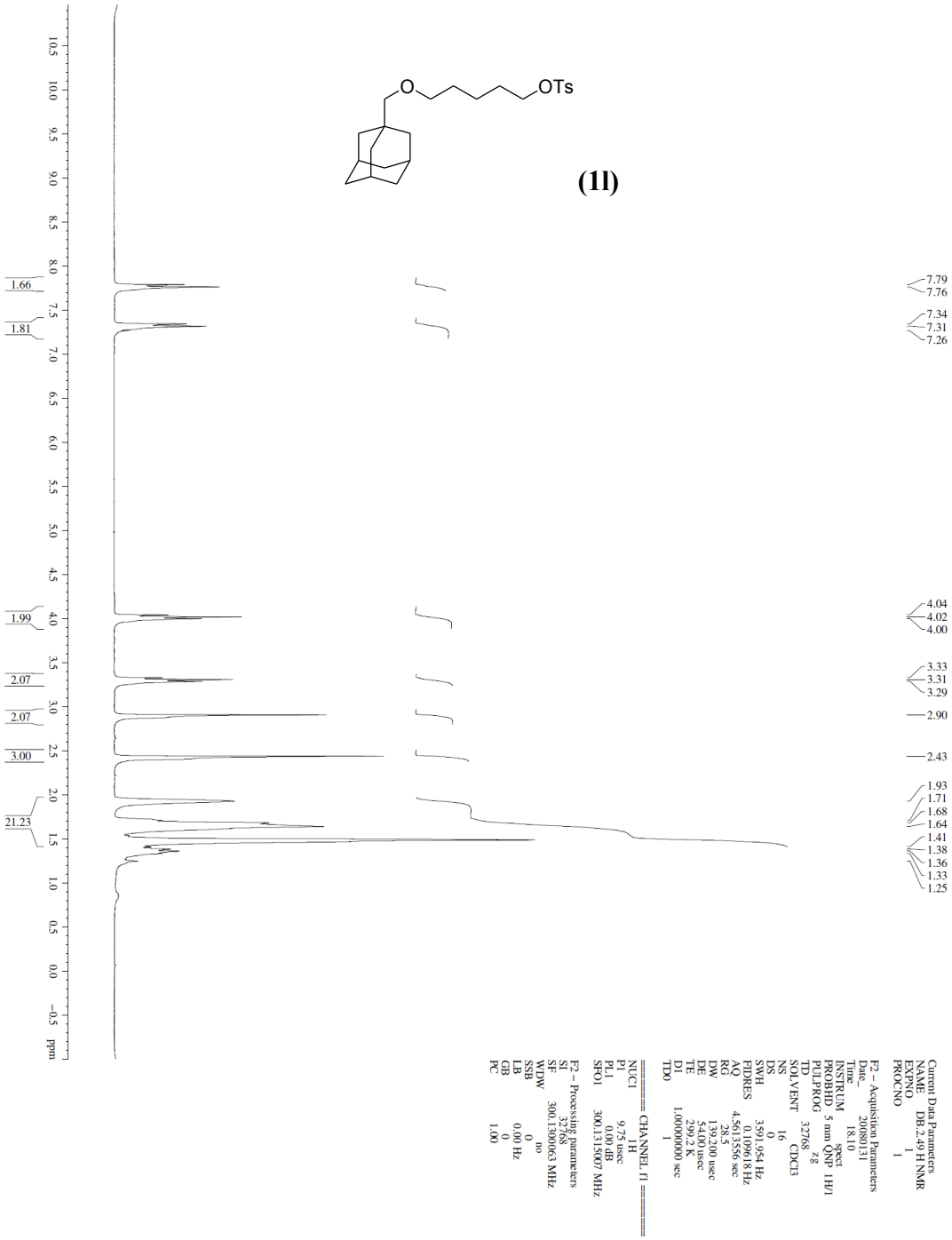
O
OTs
(1l)
7.79
7.76
7.34
7.31
7.26
4.04
4.02
4.00
3.33
3.31
3.29
2.90
2.43
1.93
1.71
1.68
1.64
1.41
1.38
1.36
1.33
1.25
1.66
1.81
1.99
2.07
2.07
3.00
21.23
ppm
Current Data Parameters
NAME DB-2-49 H NMR
EXPNO 1
PROCNO 1
F2 – Acquisition Parameters
Date_ 20080131
Time 18.10
INSTRUM spect
PROBHD 5 mm QNP 1H/1
PULPROG zg
TD 32768
SOLVENT CDCl3
NS 16
DS 0
SWH 3591.954 Hz
FIDRES 0.109618 Hz
AQ 4.5613556 sec
RG 28.5
DW 139.200 usec
DE 5.400 usec
TE 299.2 K
D1 1.00000000 sec
TD0 1
CHANNEL f1
NUC1 1H
P1 9.75 usec
PL1 0.00 dB
SFO1 300.1315007 MHz
F2 – Processing parameters
SI 32768
SF 300.1300063 MHz
WDW no
SSB 0
LB 0.00 Hz
GB 0
PC 1.00

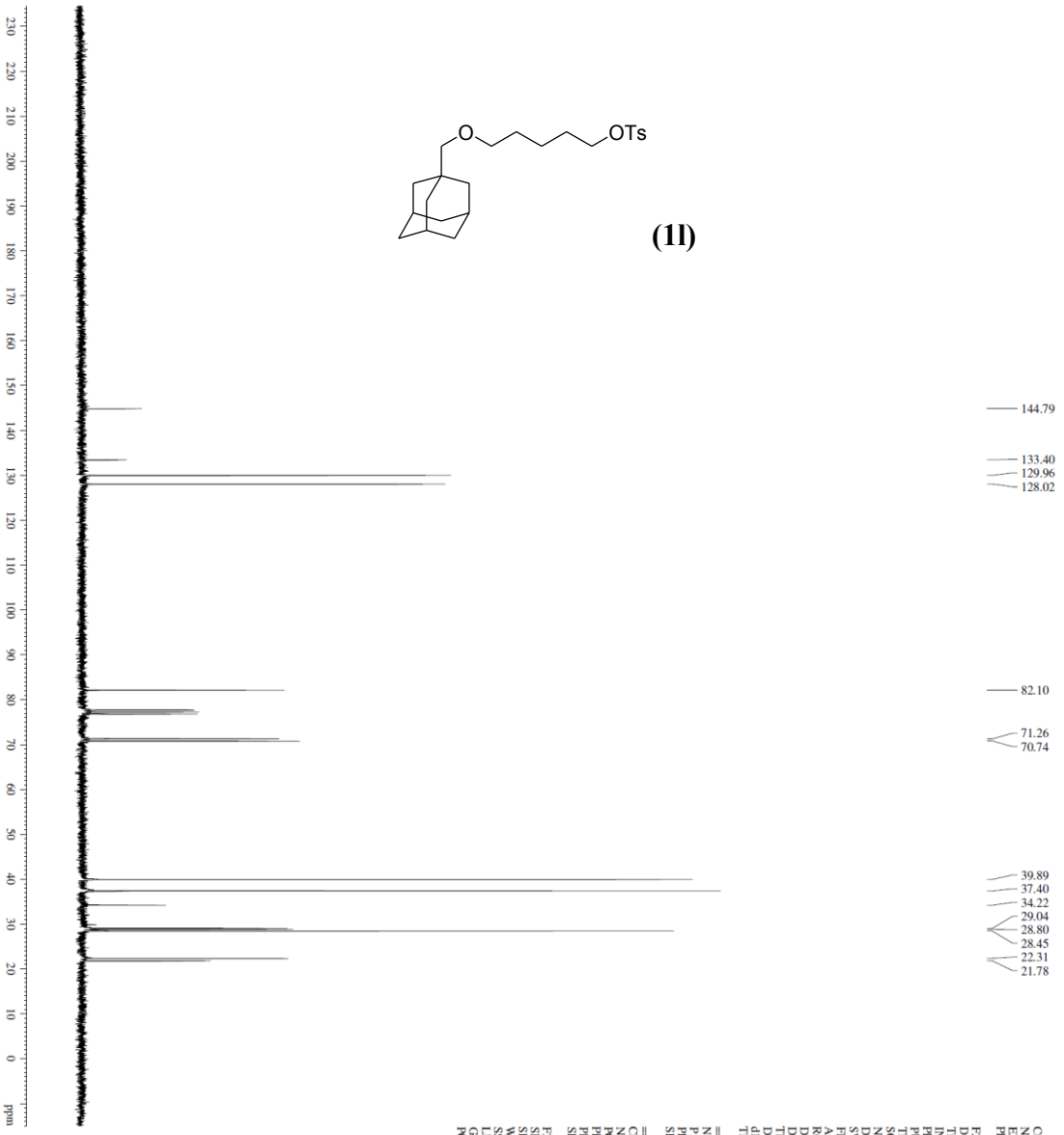

(1l)

Current Data Parameters
NAME DB-2-49-pure cnmr
EXPNO 2
PROCNO 1

F2 – Acquisition Parameters
Date_ 20080131
Time 18.25
INSTRUM spect
PROBHD 5 mm QNP 1H/1
PULPROG zgdc30
TD 65536
SOLVENT CDCl3
NS 4
DS 4
SWH 18832.393 Hz
FIDRES 0.287560 Hz
AQ 1.7400308 sec
RG 4096
DW 26.550 usec
DE 6.00 usec
TE 299.2 K
D1 0.40000001 sec
D11 0.03000000 sec
TD0 1

======== CHANNEL f1 ========
NUC1 13C
P1 13.70 usec
PL1 0.00 dB
SFO1 75.4760200 MHz

======== CHANNEL f2 ========
CPDPRG2 waltz16
NUC2 1H
PCPD2 95.00 usec
PL2 0.00 dB
PL12 18.00 dB
SFO2 300.1312005 MHz

F2 – Processing parameters
SI 32768
SF 75.4677368 MHz
WDW EM
SSB 0
LB 1.00 Hz
GB 0
PC 1.00

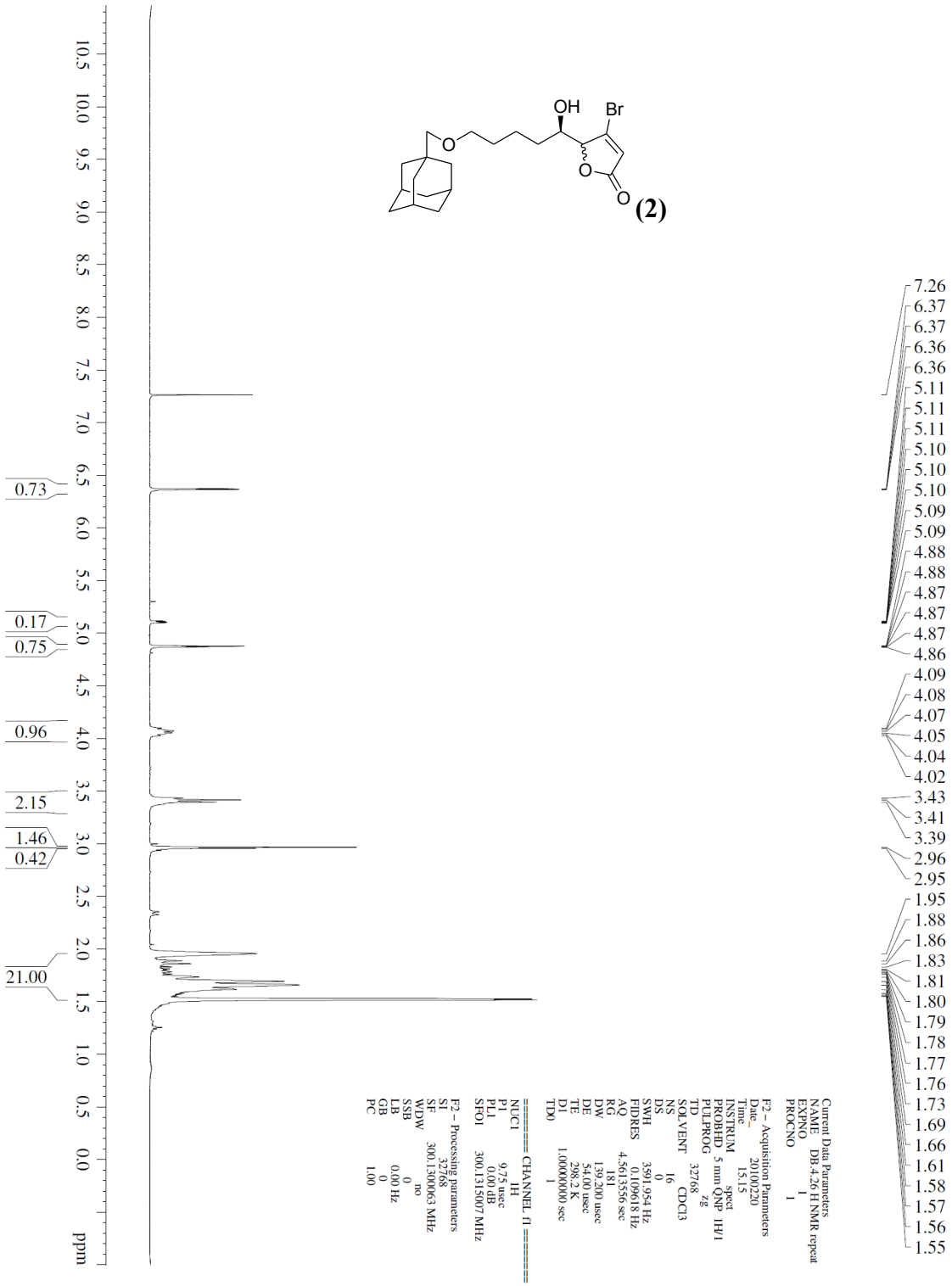
OH
Br
O
O
O
O
(2)
7.26
6.37
6.37
6.36
6.36
5.11
5.11
5.11
5.10
5.10
5.10
5.09
5.09
4.88
4.88
4.87
4.87
4.87
4.86
4.09
4.08
4.07
4.05
4.04
4.02
3.43
3.41
3.39
2.96
2.95
1.95
1.88
1.86
1.83
1.81
1.80
1.79
1.78
1.77
1.76
1.73
1.69
1.66
1.61
1.58
1.57
1.56
1.55
Current Data Parameters
NAME DB.4.26 H NMR repeat
EXPNO 1
PROCNO 1
F2 – Acquisition Parameters
Date_ 20100220
Time 15.15
INSTRUM spect
PROBHD 5 mm QNP 1H/1
PULPROG zg
TD 32768
SOLVENT CDCl3
NS 16
DS 0
SWH 3591.954 Hz
FIDRES 0.109618 Hz
AQ 4.5613556 sec
RG 181
DW 139.200 usec
DE 54.00 usec
TE 298.2 K
D1 1.00000000 sec
TD0 1
========== CHANNEL f1 ==========
NUC1 1H
P1 9.75 usec
PL1 0.00 dB
SFO1 300.1315007 MHz
F2 – Processing parameters
SI 32768
SF 300.1300063 MHz
WDW no
SSB 0
LB 0.00 Hz
GB 0
PC 1.00
0.73
0.17
0.75
0.96
2.15
1.46
0.42
21.00
10.5 10.0 9.5 9.0 8.5 8.0 7.5 7.0 6.5 6.0 5.5 5.0 4.5 4.0 3.5 3.0 2.5 2.0 1.5 1.0 0.5 0.0
ppm

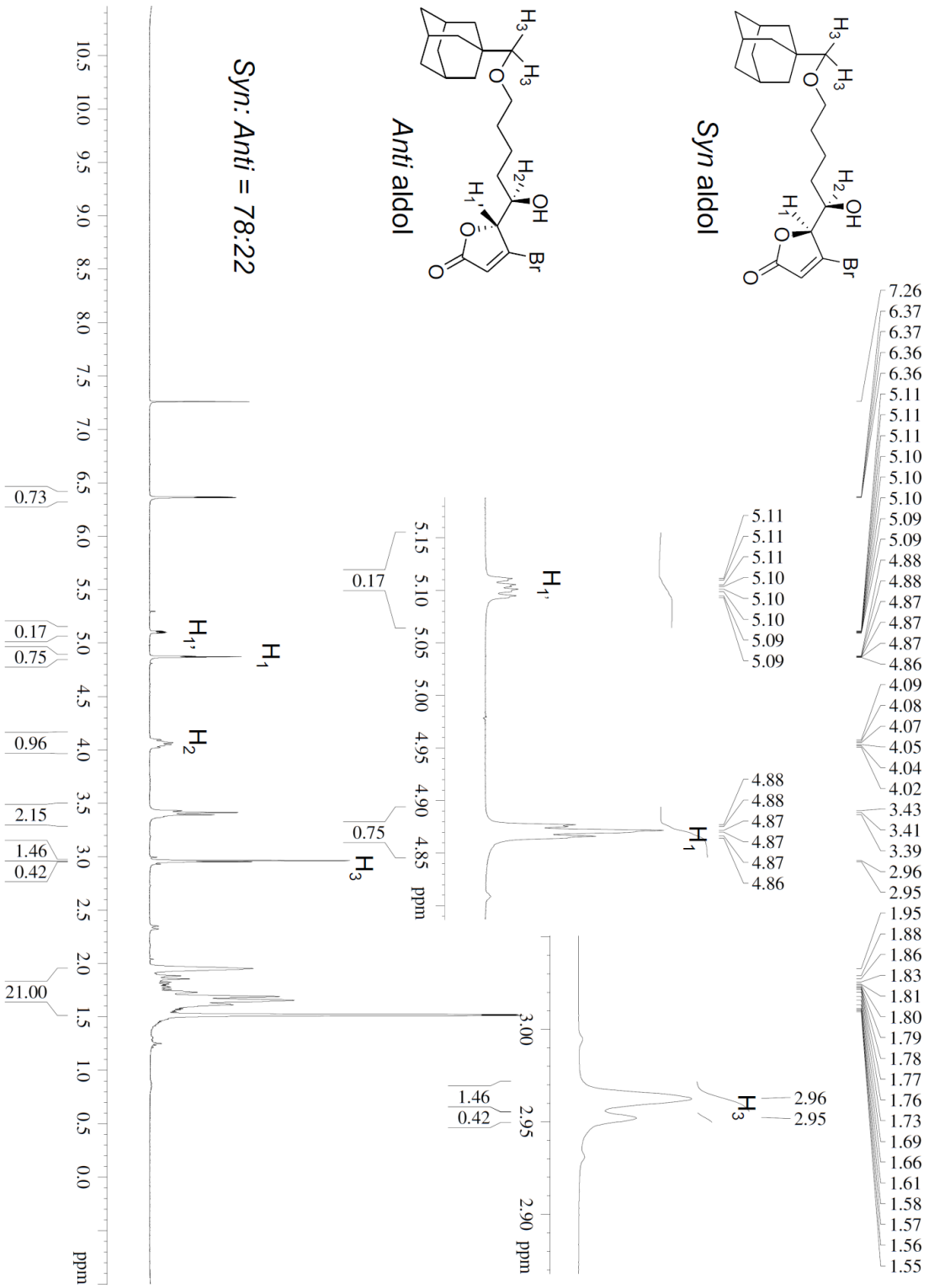
Syn aldol
Anti aldol
Syn: Anti = 78:22
H1
H1'
H2
H3
ppm

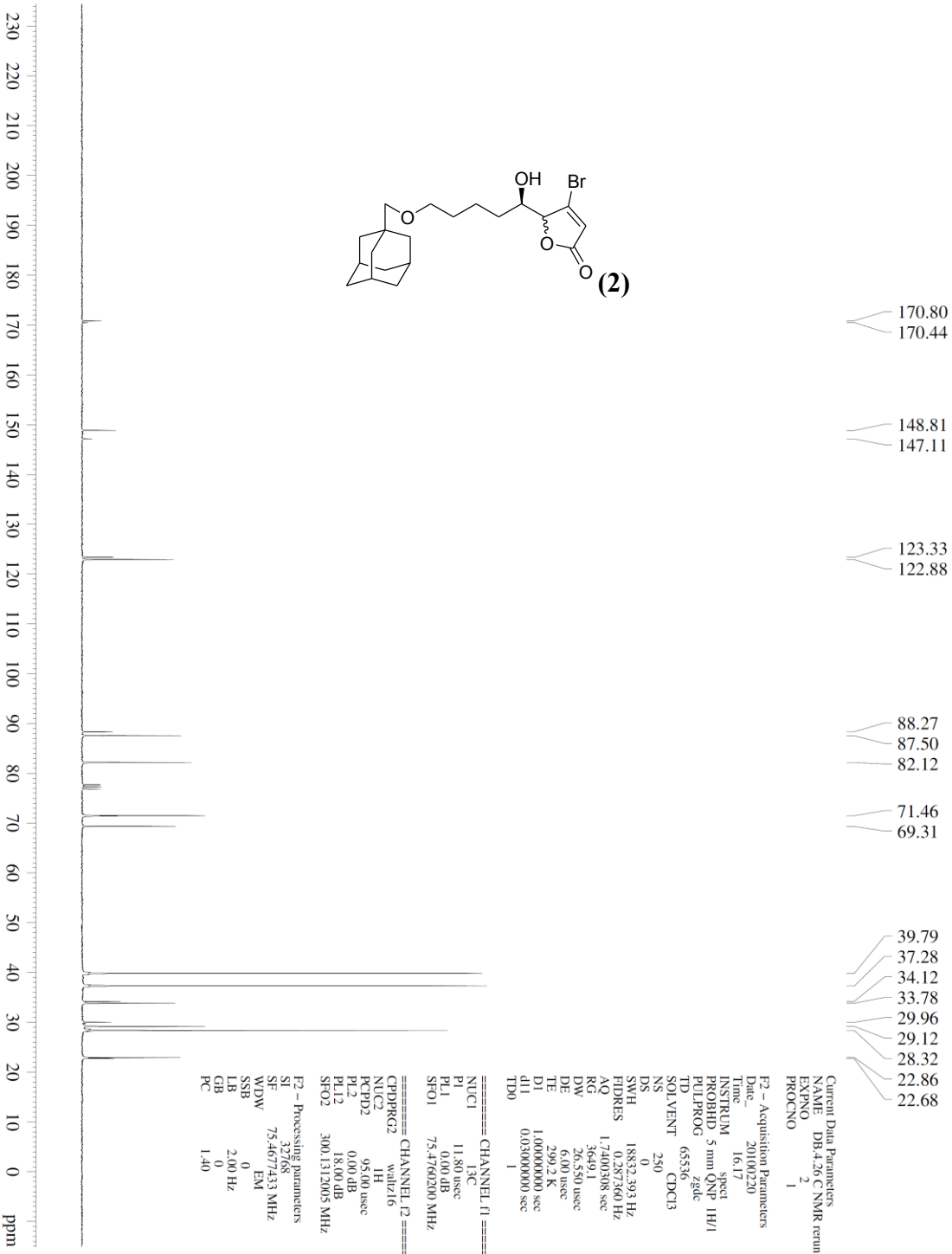
OH
Br
O
O
O
O
(2)
170.80
170.44
148.81
147.11
123.33
122.88
88.27
87.50
82.12
71.46
69.31
39.79
37.28
34.12
33.78
29.96
29.12
28.32
22.86
22.68
Current Data Parameters
NAME DB.4.26 C NMR rerun
EXPNO 2
PROCNO 1
F2 – Acquisition Parameters
Date_ 20100220
Time 16.17
INSTRUM spect
PROBHD 5 mm QNP 1H/1
PULPROG zgdc
TD 65536
SOLVENT CDCl3
NS 250
DS 0
SWH 18832.393 Hz
FIDRES 0.287360 Hz
AQ 1.740308 sec
RG 3649.1
DW 26.550 usec
DE 6.00 usec
TE 299.2 K
D1 1.00000000 sec
d11 0.03000000 sec
TD0 1
========== CHANNEL f1 ==========
NUC1 13C
P1 11.80 usec
PL1 0.00 dB
SFO1 75.4760200 MHz
========== CHANNEL f2 ==========
CPDPRG2 waltz16
NUC2 1H
PCPD2 95.00 usec
PL2 0.00 dB
PL12 18.00 dB
SFO2 300.1312005 MHz
F2 – Processing parameters
SI 32768
SF 75.4677433 MHz
WDW EM
SSB 0
LB 2.00 Hz
GB 0
PC 1.40
230 220 210 200 190 180 170 160 150 140 130 120 110 100 90 80 70 60 50 40 30 20 10 0 ppm

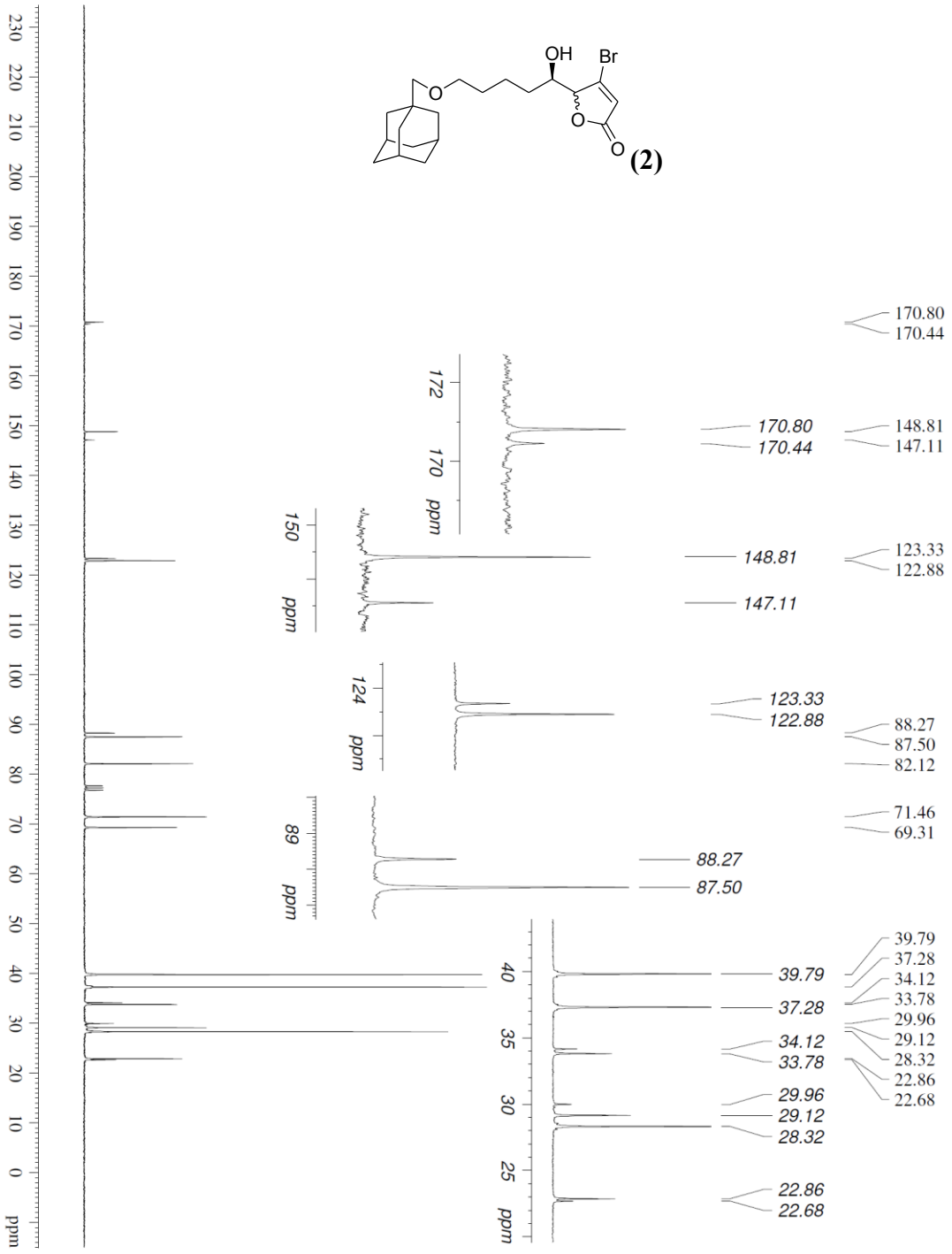
OH
Br
O
O
O
(2)
170.80
170.44
148.81
147.11
123.33
122.88
88.27
87.50
82.12
71.46
69.31
39.79
37.28
34.12
33.78
29.96
29.12
28.32
22.86
22.68
172
170
ppm
150
ppm
124
ppm
89
ppm
40
35
30
25
ppm
230 220 210 200 190 180 170 160 150 140 130 120 110 100 90 80 70 60 50 40 30 20 10 0 ppm

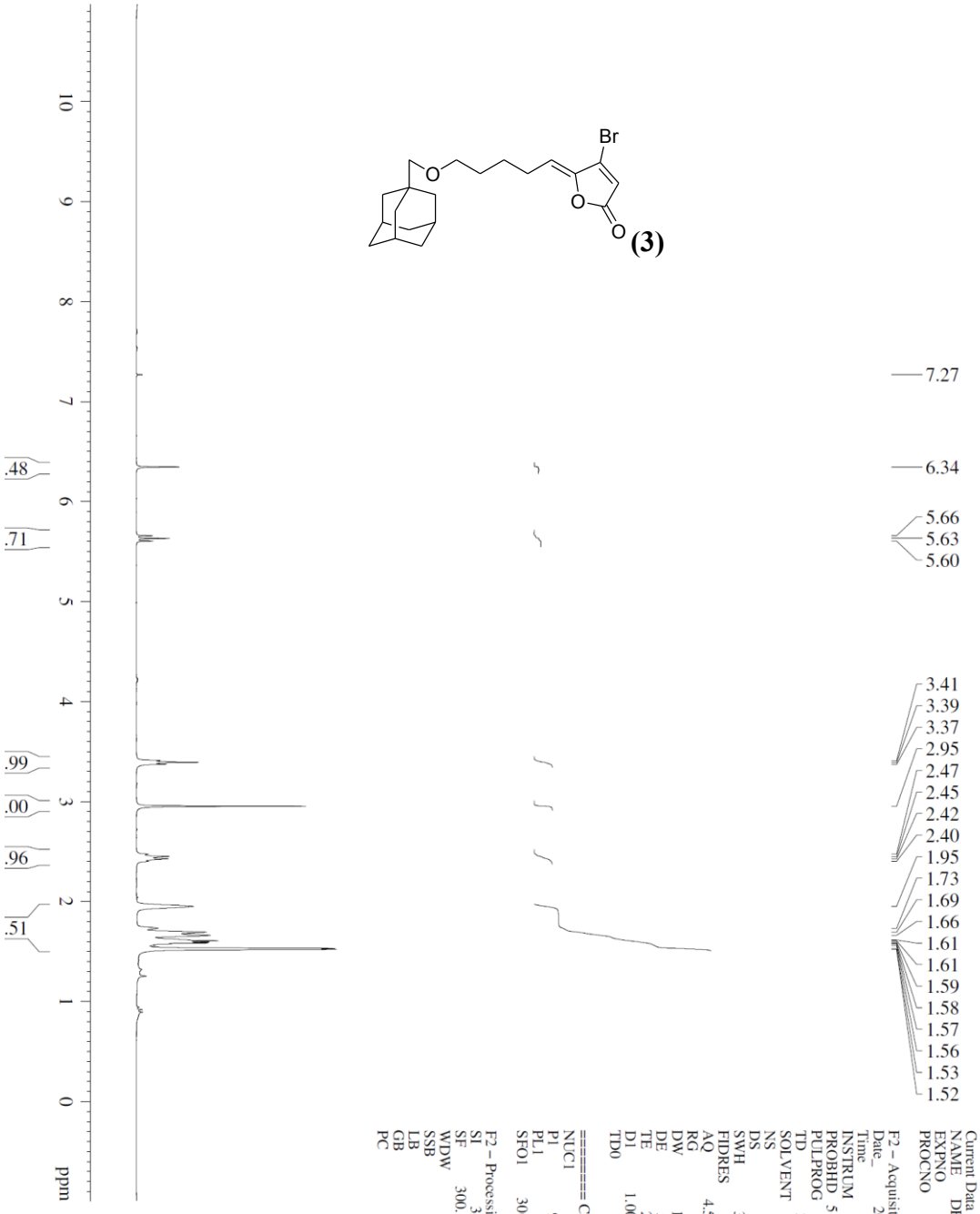
Br
O
O
O
(3)
7.27
6.34
5.66
5.63
5.60
3.41
3.39
3.37
2.95
2.47
2.45
2.42
2.40
1.95
1.73
1.69
1.66
1.61
1.61
1.59
1.58
1.57
1.56
1.53
1.52
.48
.71
.99
.00
.96
.51
ppm
Current Data Parameters
NAME DB.4.34 H NMR
EXPNO 1
PROCNO 1
F2 – Acquisition Parameters
Date_ 20100325
Time 23.24
INSTRUM spect
PROBHD 5 mm QNP 1H/1
PULPROG zg
TD 32768
SOLVENT CDCl3
NS 10
DS 0
SWH 3591.954 Hz
FIDRES 0.109618 Hz
AQ 4.5613556 sec
RG 45.3
DW 139.200 usec
DE 54.00 usec
TE 299.2 K
D1 1.00000000 sec
TD0 1
======== CHANNEL f1 ========
NUC1 1H
P1 9.75 usec
PL1 0.00 dB
SFO1 300.1315007 MHz
F2 – Processing parameters
SI 32768
SF 300.1300039 MHz
WDW no
SSB 0
LB 0.00 Hz
GB 0
PC 1.00

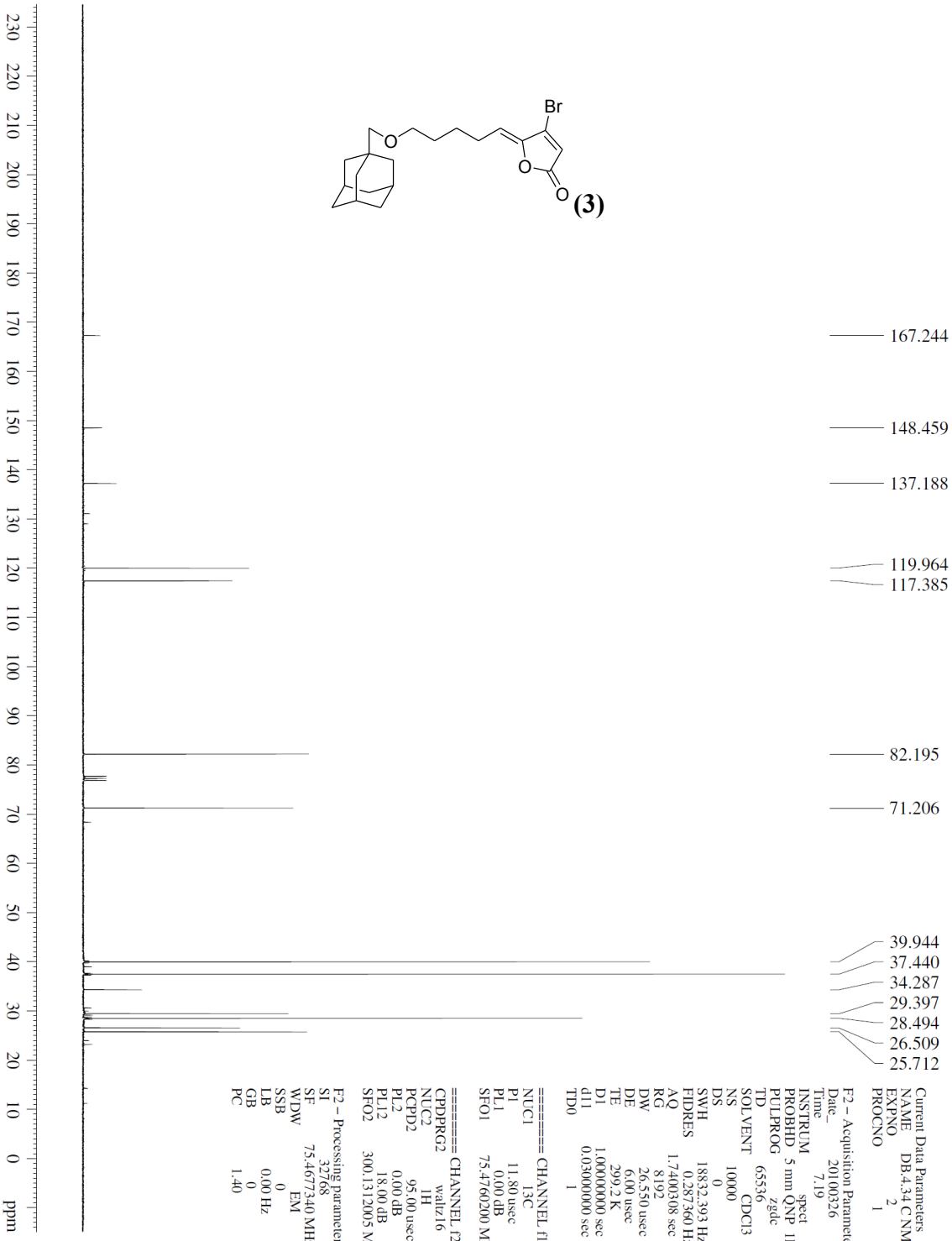
Br
O
O
O
(3)
167.244
148.459
137.188
119.964
117.385
82.195
71.206
39.944
37.440
34.287
29.397
28.494
26.509
25.712
Current Data Parameters
NAME DB4.34 C NMR
EXPNO 2
PROCNO 1
F2 – Acquisition Parameters
Date_ 20100326
Time 7.19
INSTRUM spect
PULPROG zgdc
TD 65536
SOLVENT CDCl3
NS 10000
DS 0
SWH 18832.393 Hz
FIDRES 0.287360 Hz
AQ 1.7400308 sec
RG 8192
DW 26.550 usec
DE 6.00 usec
TE 299.2 K
D1 1.00000000 sec
d11 0.03000000 sec
TD0 1
======== CHANNEL f1 ===
NUC1 13C
P1 11.80 usec
PL1 0.00 dB
SFO1 75.4760200 MHz
======== CHANNEL f2 ===
CPDPRG2 waltz16
NUC2 1H
PCPD2 95.00 usec
PL2 0.00 dB
PL12 18.00 dB
SFO2 300.1312005 MHz
F2 – Processing parameters
SI 32768
SF 75.4677340 MHz
WDW EM
SSB 0
LB 0.00 Hz
GB 0
PC 1.40
230 220 210 200 190 180 170 160 150 140 130 120 110 100 90 80 70 60 50 40 30 20 10 0 ppm

Chapter 7

Squarylated Homoserine Lactones (SHLs) as Structural Mimics of Acylated Homoserine Lactones (AHLs) for Inhibiting Biofilm Formation by *E.coli*

Summary

This work reports the synthesis of a new library of squarylated homoserine lactones (SHLs), which are structural mimics of autionducer-1 (AI-1) based quorum sensing signaling molecules called *N*-acylated homoserine lactones (AHLs). Three alkyl SHLs and three aromatic SHLs were synthesized and their ability to inhibit biofilm formation by the gram-negative bacterium *Escherichia coli* RP437 was evaluated. None of the synthesized SHLs were found to be cytotoxic to *E. coli* but were able to inhibit biofilm formation by the bacterium. The aromatic SHLs in general had a higher ability to inhibit biofilm formation than the alkyl SHLs. Two aromatic SHLs in particular exhibited ≥ 50% inhibition of biofilm formation at 200 μM. These SHLs are believed to inhibit the LuxR-type quorum sensing receptor SdiA in *E.coli* and hence are promising candidates as quorum sensing inhibitors for other gram-negative bacteria.

7.1 Introduction and Goal

7.1.1 N-acylated homoserine lactone (AHL) based quorum-sensing modulators

Gram-negative bacteria commonly use a class of autoinducers (AI) called *N*-acylated-L-homoserine lactones (AHLs) or autoinducer-1 (AI-1) for quorum sensing.[87] The AHLs have the core structure shown in Figure 7.1, which comprises of the L-homoserine lactone ring, unsubstituted at the β- and γ- position and are N-acylated at the α-position.

Although the L-homoserine lactone ring remains the same for all gram-negative bacteria, the AHLs differ in having a unique acyl group (Figure 7.1).

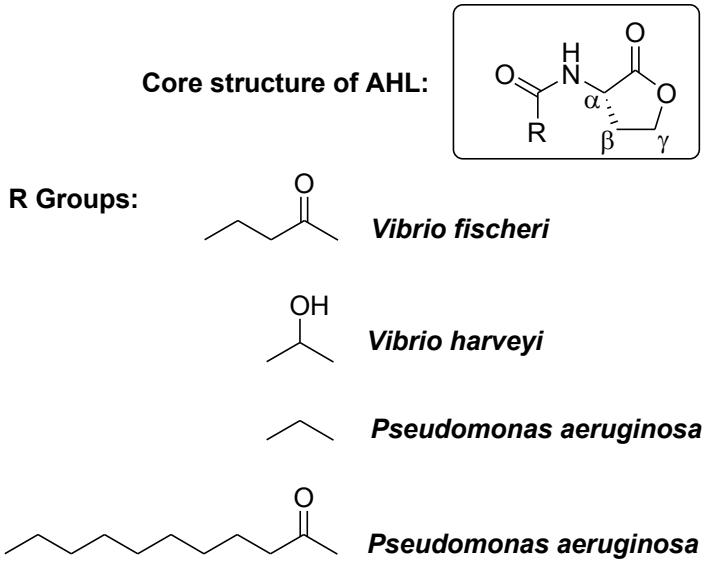

Figure 7.1 Structure of *N*-acylated-L-homoserine lactones (AHLs) for some common gram-negative bacteria. Figure adapted and modified from report by Bassler and co-workers.[131]

The first ever AHL-based quorum-sensing circuit was identified in the marine bioluminescent bacterium *Vibrio fischeri.*[129] The quorum sensing circuit in *V. fischeri* comprises of the protein called LuxI, which is responsible for the synthesis of the native autoinducer signal *N*-oxohexanoylhomoserine lactone (OHHL) and the protein called LuxR, which is the receptor for OHHL.[7, 87, 130] *N*-oxohexanoylhomoserine lactone (OHHL) is synthesized within the bacterium and can diffuse in and out of the cell freely. Although the bacterium synthesizes OHHL throughout its growth, high cell densities are required for the concentration of OHHL within the bacterium to become sufficiently high to initiate binding of OHHL to its cognate receptor LuxR. Once OHHL binds to LuxR, it

initiates a signal transduction pathway, which causes activation of genes responsible for luminescence.[87] Quorum sensing circuits identified in other gram-negative bacteria comprise of LuxI-type synthases and LuxR-type receptors and their own unique AHL signaling molecules. Quorum sensing initiates a number of processes in bacteria including virulence factor production, antibiotic production, biofilm formation, swarming motility, bioluminescence, root nodulation, sporulation and conjugation.[131]

Although quorum sensing is essential for bacterial group behavior, it is not essential for survival[208] and hence inhibiting quorum sensing does not give way to drug-resistant mutations commonly associated with antibacterial treatments.[209] Hence, inhibiting quorum sensing is a promising approach for treating bacterial infection since it overcomes the problem of bacterial antibiotic resistance. Among the many approaches of inhibiting quorum sensing including degradation of the AHLs signal itself[244-245] or inhibition of the LuxI-type protein,[246-247] the most common approach is to develop inhibitors for the LuxR-type receptors.[7, 208]

Blackwell and co-workers have provided a comprehensive review on the structure activity relationship (SAR) for synthetic AHL analogs, spanning a number of bacterial species but focusing primarily on the quorum sensing circuits involving the LuxR-type proteins of *V. fischeri* (LuxR), *Pseudomonas aeruginosa* (LasR and RhlR), *Agrobacterium tumefaciens* (TraR) and *Erwinia carotovora* (CarR).[7] Blackwell and co-workers have also compared the activities of close to 90 AHL analogs across the three gram-negative bacteria *V. fischeri*, *P. aeruginosa* and *A. tumefaciens*, to identify AHL analogs which can modulate the activity of either one or more than one LuxR-type receptor.[159, 248] It is worth noting that the authors identified few LuxR-type protein

agonists than antagonist and that the agonists identified were generally specific for a specific LuxR-type receptor. Hence, the authors were able to identify broad-spectrum inhibitors for the LuxR-type proteins. Blackwell and co-workers have recently reported the synthesis and evaluation of AHL analogs, using small-molecule microarrays and identified quorum-sensing inhibitors for *V. fischeri* and *Chromobacterium violaceum.*[219] Lee, Yoon and co-workers have recently reported the synthesis of AHL analogs against the TraR quorum sensing receptor for *A. tumefaciens* and found that some of the analogs were able to inhibit biofilm formation for both *A. tumefaciens* and the pathogenic bacteria *P. aeruginosa.*[220]

7.1.2 Quorum sensing modulators based on the squarate moiety

One of the disadvantages of using non-native AHLs as quorum sensing modulators is that the LuxR-type receptors exhibit high specificity for their cognate autoinducers,[249] and only slight deviations from the native AHL structure is tolerable without significant loss in binding ability.[249-250] Moreover, the non-native AHLs lack a rigid backbone, providing numerous conformational possibilities for computer based modeling studies.[251-253] The homoserine lactone moiety is also unstable at basic pH and can undergo degradation by mammalian lactonases.[254-256]

The X-ray crystal structure of a few LuxR-type proteins bound to their natural AHL ligands have been reported[213-218] and such information has been useful in developing synthetic analogs of the natural AHLs.[8] Recently, the X-ray crystal structures of binding domains of the LuxR-type receptors with non-native ligands has been reported.[257] A significant portion of the literature pertaining to synthetic quorum sensing modulators

deals with non-native AHLs and hence the non-native AHLs still remain the most studied class of quorum sensing modulators.[8]

Narasimhan et al. have recently reported a new class of biofilm inhibitors, based on the squarate moiety. They tested six squarylated homoserine lactones (SHLs), four squarylated esters and two squarylated amides for their ability to inhibit biofilm formation by *E. coli* RP437.[88] The biofilm inhibition exhibited by the SHLs was also compared to the biofilm inhibition shown by the brominated furanone (**12**)[8, 160] (Figure 7.2).

Squarylated homoserine lactones (SHLs):

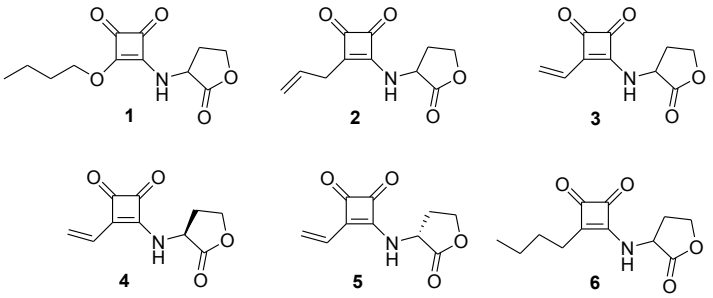

Squarylated esters:

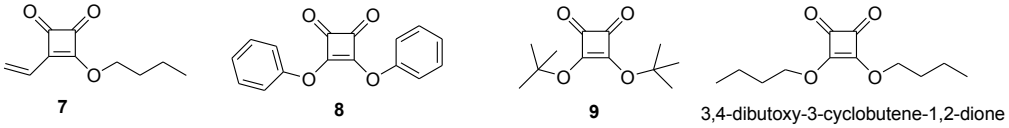

Squarylated amides: *Brominated Furanone:*

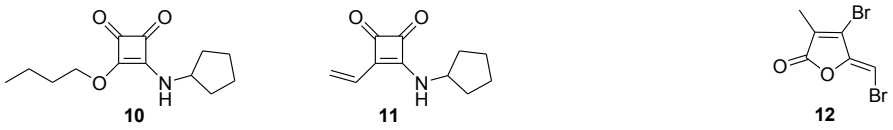

Figure 7.2 Structures of the squarate based mimics of N-acylated homoserinelactones tested by Narasimhan et al. against biofilm formation by *E.coli* RP437. Figure adapted and modified from PhD dissertation by Sri Kamesh Narasimhan.[88]

Although *E. coli* itself does not have an AHL-based quorum sensing circuit, it does have a LuxR-type receptor called SdiA,[224-225] and hence can respond to AHL signals from other bacteria and sense synthetic AHL analogs capable of modulating quorum sensing.[224-225] The squarylated homoserine lactones (SHLs) represent a new class autoinducer-1 (AI-1) mimics,[7] which have the potential to inhibit quorum sensing in *E. coli*. The SHLs are similar in structure to the AHLs since they possess the homoserine lactone moiety, but are chemically different from the AHLs since they possess the rigid and the reactive squarate moiety[258-260] with an alkyl substituent (Figure 7.3).[88] The squarate moiety provides a rigid backbone to the SHLs, allowing one to vary the alkyl group without much loss in conformational rigidity. The two carbonyl groups of the squarate moiety are potential hydrogen bond acceptors and can help the SHLs bind to the quorum sensing receptor efficiently. The SHLs also lack native amide bonds and have a lower tendency to undergo degradation by enzymes.[258-259] Additionally, the reactive squarate moiety enhances the electrophilicity of the SHLs and can help in covalently modifying reactive amino acid residues in the active site of the quorum sensing receptors.[249, 261]

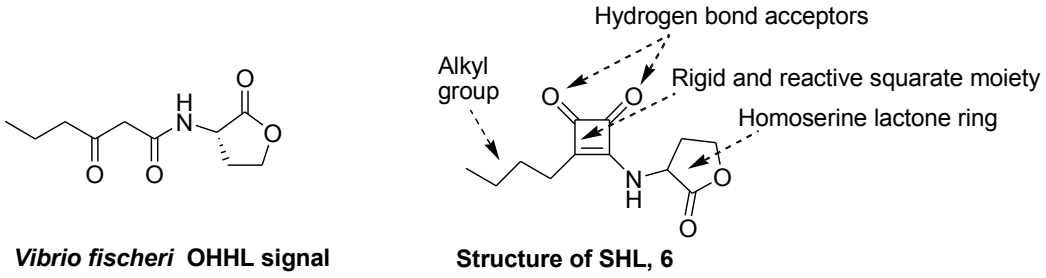

Figure 7.3 Structural comparison of the *Vibrio fischeri N*-oxohexanoylhomoserine lactone (OHHL) signal and SHL **6**.[88]

Among all the squarate based AHL mimics tested by Narasimhan et al., compound **3** exhibited the highest percent inhibition of biofilm formation by *E. coli* RP437 at 200 μM. Compound **3** exhibited ~57% inhibition of biofilm formation followed by ~56% inhibition shown by the brominated furanone **12** and ~48% shown by compound **6**. It is worth noting that squarate based AHL mimics tested were generally non-toxic to *E.coli* RP437.[88]

Here, the synthesis and ability of six new SHLs namely the alkyl SHLs **13**, **14**, **15** and the aromatic SHLs **16**, **17** and **18** (Figure 7.4),[**] to inhibit the biofilm formation by *E.coli* RP437 is reported. An improved and optimized synthesis of the SHLs is also reported.

7.2 Results and Discussion

7.2.1 Synthesis of a new library of squarylated homoserine lactones (SHLs)

Blackwell and co-workers have recently reviewed the structure activity relationship (SAR) for a range of non-natural AHL analogs, primarily focusing on the quorum sensing circuits involving the LuxR-type proteins of *V. fischeri* (LuxR), *P. aeruginosa* (LasR and RhlR), *A. tumefaciens* (TraR) and *E. carotovora* (CarR).[7] They concluded that the length of the acyl chain was very critical for the activity of non-native AHL analogs and the analogs having chain length similar to the native AHLs generally exhibited high activity. Additionally, incorporation of aromatic substituent's in the acyl chain generally yielded analogs with inhibitory activity.

Motivated by the above finding by Blackwell and co-workers[7] and the recent work done by Narasimhan et al.,[88] a set of new SHLs with alkyl (**13**, **14** and **15**) or aromatic

[**] Sijie Yang synthesized SHLs **15** and **16**. Nisha Varghese synthesized SHL **17** and precursor for SHL **18** (**18 b**). Department of Chemistry, Syracuse University, Syracuse, NY.

(**16**, **17** and **18**) substituent's (Figure 7.4) were synthesized. The ability of the newly synthesized SHLs to inhibit biofilm formation by *E. coli* RP437 was evaluated and was compared to biofilm inhibitory activity of SHL **6**[88] and the brominated furanone **12**[160] at 200 μM.

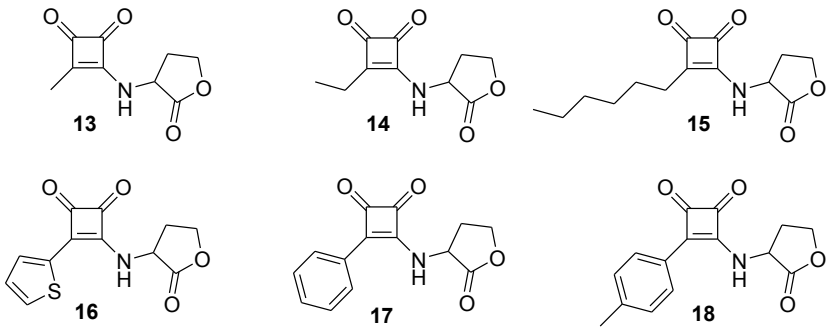

Figure 7.4 A library of new squarylated homoserine lactones (SHLs) containing alkyl or aromatic substituent's.

7.2.2 Improved synthesis for the squrylated homoserine lactones

The general synthetic scheme used by Narasimhan et al. is outlined in Scheme 7.1. Briefly, the squarate ester 3,4-dibutoxy-3-cyclobutene-1,2-dione was treated with alkyl lithium (RLi) or alkyl magnesium bromide (RMgBr) as the alkylating agent, followed by addition of trifluoroacetic anhydride (TFAA). Addition of an aqueous solution of NH_4Cl followed by work up and purification yielded the intermediate (I).[88, 262] Reaction of the intermediate (I) with (±) α-amino-γ-butyrolactone hydrobromide in tetrahydrofuran (THF) or dichloromethane (DCM) as solvent and N,N-diisopropylethylamine (DIPEA) as base resulted in the formation of the SHL (II).[88]

Scheme 7.1

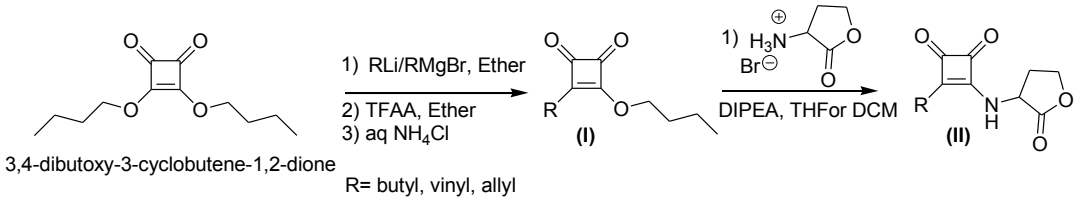

The synthesis of SHL **13** following Scheme 7.1 and using methyl lithium (MeLi) as the alkylating agent was first attempted. Although the corresponding intermediate (I) for SHL **13** was successfully isolated, the final product could not be isolated even after multiple attempts. Hence, a synthetic scheme essentially similar to Scheme 7.1 but now employing EtOH as solvent[263] and triethylamine (TEA) as base was worked out for the final step (Scheme 7.2). The crude product was purified by column chromatography and then re-precipitated using diethyl ether (Et_2O) from a solution of **13** in ethyl acetate (EtOAc) or dichloromethane (DCM).

Scheme 7.2

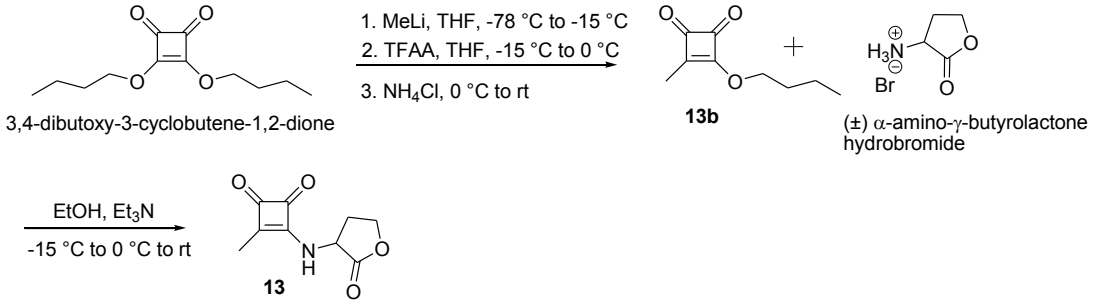

The SHL **14** was synthesized employing slight modification in the synthetic design outlined in Scheme 7.2. While the intermediate **13b** for SHL **13** was synthesized in one-pot,[262] the intermediate **14b** for SHL **14** was synthesized in two steps.[264] The synthesis of SHL **14** is outlined in Scheme 7.3. Compound **6** was synthesized similarly.

Scheme 7.3

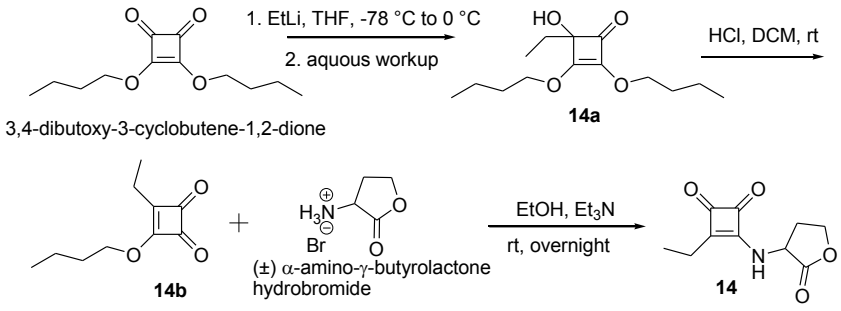

7.2.3 Cytotoxicity studies using squarylated homoserine lactones on E. coli

The effect of the synthesized alkyl SHLs **6**, **13**, **14**, **15** and aromatic SHLs **16**, **17**, **18** on the growth of *E. coli* RP437 was evaluated. Since the SHLs synthesized by Narasimhan et al.[88] were shown to be non-toxic to *E.coli* RP437 at 200 μM, the newly synthesized SHL were also tested for cytotoxic effects at 200 μM. All the SHLs tested were found to be non-toxic to *E. coli* RP437 at 200 μM. Since the brominated furanone **12** was shown to be toxic to *E.coli* at 200 μM (chapter 6), **12** was used as a control in this study. Interestingly, all the SHL were found to promote the growth of bacteria. Beyond 2 h, the optical density (OD_{600}) values at 600 nm for all the SHL in Figure 7.5 were consistently higher than the OD_{600} values in the absence of SHLs.

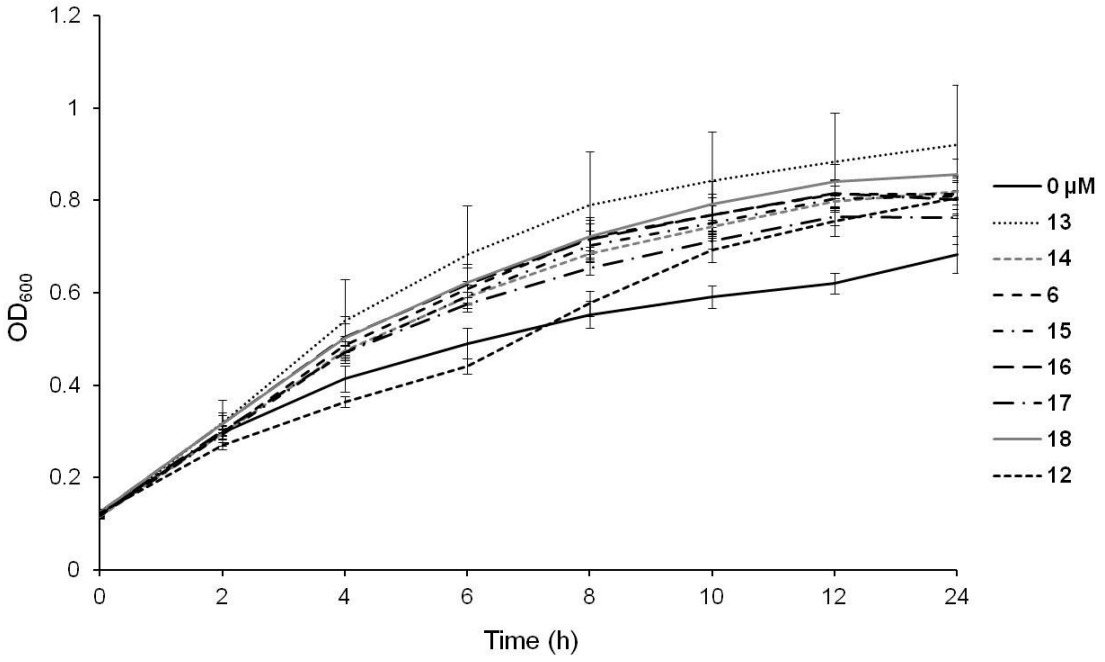

Figure 7.5 Growth for *E. coli* RP437 in presence of 200 μM of squarylated homoserine lactone (SHLs) or brominated furanone.

7.2.4 Inhibition of E. coli biofilm formation by squarylated homoserine lactones

The ability of the SHLs to inhibit biofilm formation by *E. coli* was studied next. A modified crystal violet assay[163, 240-241] was used to estimate the amount of biofilm formed by *E. coli* in the presence of 200 μM of each of the SHLs. Percent inhibition of biofilm inhibition was calculated using the OD_{600} values after crystal violet assay. The equation $[1-(A_{M+B+C} - A_M)/(A_{M+B} - A_M)] \times 100$ was used for calculating percent inhibition of biofilm formation, where A_{M+B+C} is the OD_{600} of wells containing media + bacteria + compounds, A_{M+B} is the OD_{600} of wells containing media + bacteria and A_M is the OD_{600} of wells containing only media. All the SHLs tested were found to inhibit biofilm formation by *E. coli*. The SHL **18** exhibited the highest inhibition with a percent

inhibition of 55.26 ± 5.66% (Figure 7.6), followed by SHL **17** (52.62 ± 6.05%), SHL **16** (43.76 ± 7.68%) and SHL **15** (41.51 ± 7.66%). The SHLs **13** and **14** exhibited the lowest inhibition of biofilm formation with a percent inhibition of 35.60 ± 10.29% and 33.89 ± 8.91% respectively. It was noted that the percent inhibition of biofilm exhibited by SHL **6** (44.56 ± 4.58%), was similar to that reported by Narasimhan et al.[88] It is interesting to note that although SHL **17** and **18** were non-toxic to *E.coli*, they still exhibited a higher percent inhibition of biofilm formation than that exhibited by the mildly toxic brominated furanone **12** (50.30 ± 5.13%). The aromatic SHLs were also found to have a higher ability to inhibit biofilm formation when compared to the alkyl SHLs (Figure 7.6).

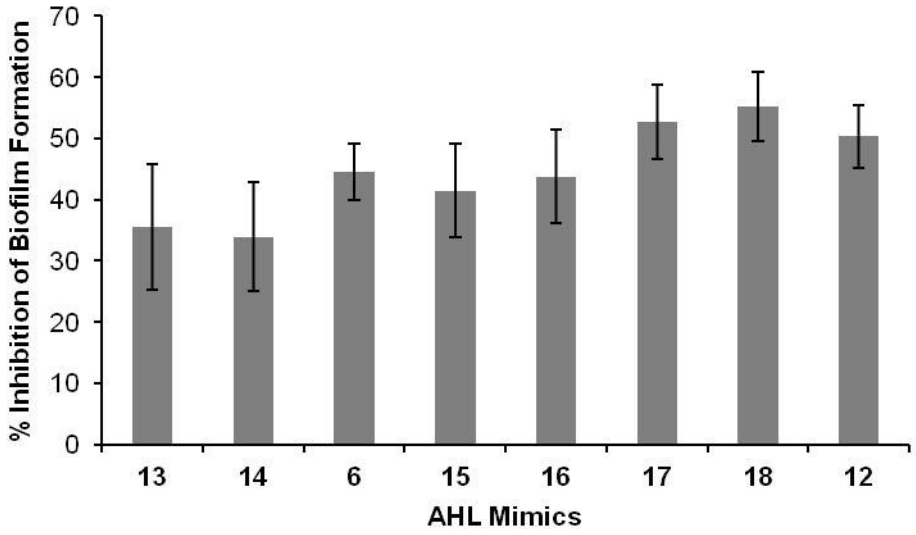

Figure 7.6 Percent inhibition of biofilm exhibited by the synthesized squarylated homoserine lactones (SHLs) and brominated furanone **12** at 200 μM.

This study shows that the SHLs are promising candidates as novel inhibitors of quorum sensing in bacteria. Although the mode of action of these SHLs is not known, the SHLs probably bind and inhibit the LuxR-type receptor (SdiA)[224-225] in *E. coli.*

7.3 Conclusion and Perspectives

The synthesis of a new library of squarylated homoserine lactones (SHLs), which are structural mimics of autionducer-1 (AI-1) based quorum sensing signaling molecules called *N*-acylated homoserine lactones (AHLs) is reported. The synthesized SHLs were found to be non-toxic to *E.coli* RP437 at 200 μM. Although all the SHLs showed inhibition of biofilm formation by *E.coli* at 200 μM, two SHLs in particular **17** and **18**, exhibited higher percent of inhibition than the mildly toxic brominated furanone **12**. Among all the SHLs tested, the aromatic SHLs had a higher ability to inhibit biofilm formation than the alkyl SHLs. Preliminary investigation (results not included) has indicated that the synthesized library of SHLs exhibit no cytotoxicity towards mammalian cells (Swiss 3T3 albino fibroblasts) at 200 μM, hence these SHLs are promising drug candidates for biofilm related infections.

The ability of the SHLs to inhibit biofilm formation by other pathogenic bacteria such as *P. aeruginosa* can be further studied. Computer simulated binding of the SHLs to the active site of LuxR-type receptors can also help to decipher the mechanism of action of these SHLs.

7.4 Experimental Section

General information for synthesis of squarylated homoserine lactones (SHLs)

The processes involving reactants sensitive to moisture or air were carried out under an atmosphere of argon using oven-dried glassware. Reagents and solvents were reagent grade and used as supplied unless otherwise mentioned. THF was distilled from sodium benzophenone. Solvents were removed under reduced pressure using rotary evaporator

below 40 ºC. Silica Gel 60 F_{254} precoated plates (0.25-mm thickness, EMD) were used for TLC and a solution of phosphomolybdic acid/ceric sulfate/sulfuric acid (10g : 1.25 g : 8% 250 mL), followed by charring at ~ 150 ºC, was used for visualization. Flash column chromatography was performed using SILICYCLE, Silica-P Flash Silica Gel with 40-63µ mesh size. NMR spectra (^{1}H, ^{13}C) were recorded on 300 MHz or 500 MHz Bruker instrument 300. ^{1}H chemical shifts are reported in ppm relative to $CDCl_3$ δ 7.26. ^{13}C chemical shifts are reported relative to $CDCl_3$ δ 77.23, DMSO-d_6 δ 39.5 and CD_3CN δ 1.94. High Resolution Mass Spectra (HRMS) or Ligh Resolution Mass Spectra (LRMS) samples were analyzed by positive ion electrospray or electron impact.

Details for the synthesis of squarylated homoserine lactones (SHLs)

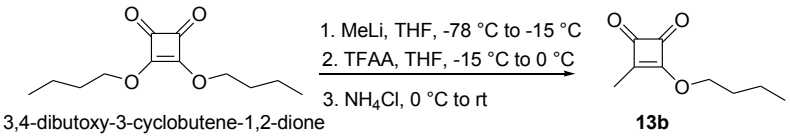

1.6 M MeLi (0.55 mL, 0.884 mmol) in Et_2O was added drop wise to a solution of 3,4-dibutoxy-3-cyclobutene-1,2-dione (0.200 g, 0.884 mmol) in THF (10.0 mL) at to -78 °C. The reaction mixture was allowed to stir at -78 °C for 30 min and then warmed up to -15 °C slowly. The reaction mixture was stirred at -15 °C for 2 h followed by addition of TFAA (0.15 mL, 1.061 mmol). The progress of the reaction was monitored on TLC till no more consumption of starting material was observed. A solution of 10% NH_4Cl in water was added to the reaction mixture and the aqueous phase was extracted with EtOAc. The combined organic potions were dried over anhydrous Na_2SO_4 and evaporation of organic solvents afforded the crude product as yellow oil. The crude product was purified using silica gel column (10% EtOAc in Hexanes) to obtain **13b**

(0.044 g, 35.84%) as a light yellow oil after evaporation of solvent. R_f = 0.52, (30% EtOAc in Hexanes). ^{1}H NMR (300 MHz, $CDCl_3$): δ 4.72 (t, J_{H-H} = 6.6 Hz, 2H), 2.21 (s, 3H), 1.85-1.76 (m, 2H), 1.52-1.36 (m, 2H), 0.97 (t, J_{H-H} = 7.35 Hz, 3H). ^{13}C NMR (75 MHz, $CDCl_3$): δ 199.2, 196.2, 193.8, 180.2, 74.5, 31.8, 18.5, 13.6, 9.7.

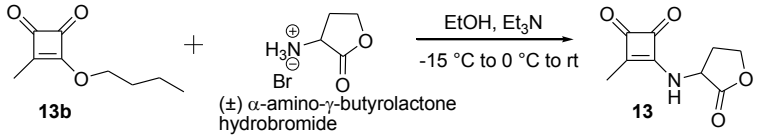

A solution of **13b** (0.033 g, 0.196 mmol) in EtOH (2.0 mL) was added to a solution of **(±)** α-amino-γ-butyrolactone hydrobromide (0.039 g, 0.216 mmol) in EtOH (2.0 mL) at -15 °C. The reaction mixture was allowed to stir at -15 °C for 15 min followed by addition of Et_3N (0.08 mL, 0.059 mmol) drop wise at the same temperature. The reaction was monitored on TLC (25% EtOAc in Hexanes and 100 % EtOAc separately). Once complete consumption of starting material was observed on TLC, a dry silica gel slurry of the crude reaction mixture was prepared and the slurry was loaded on to silica gel column and purified (100% EtOAc) to obtain the pure **13** (0.020 g, 52.22%) as viscous colorless oil after evaporation of solvent. The viscous oil was dissolved in EtOAc or DCM and the product was re-precipitated by addition in Et_2O. The mixture was placed in -20 °C overnight. The solvent was carefully removed using a glass pipette and the remaining precipitate was dried under vacuum to provide **13** as a sticky white solid. R_f = 0.20, (100% EtOAc). ^{1}H NMR (300 MHz, $CDCl_3$): δ 7.08 (br, s, 1H), 5.08-5.05 (m, 1H), 4.55-4.36 (m, 2H), 2.51-2.40 (m, 2H), 2.19 (s, 3H).

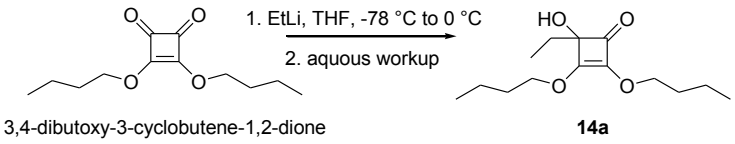

3,4-dibutoxy-3-cyclobutene-1,2-dione **14a**

To a solution of 3,4-dibutoxy-3-cyclobutene-1,2-dione (0.200 g, 0.884 mmol) in THF (6.0 mL) was added 1.7 M EtLi (0.57 mL, 0.972 mmol) at -78 °C and the reaction mixture for allowed to stir at -78 °C for 30 min. The progress of the reaction was monitored on TLC (20% EtOAc in Hexanes) and another batch of 1.7 M EtLi (0.57 mL, 0.972 mmol) was added since there was no progress. The reaction was monitored on TLC until there no more starting material left. Water was added to the reaction mixture drop wise at -78 °C and the reaction mixture was slowly warmed up to rt. The aqueous phase was extracted with EtOAc. The combined organic portions were dried over anhydrous Na_2SO_4 and evaporation of organic solvents afforded the crude product as yellow oil. The crude product was purified using silica gel column (10% EtOAc in Hexanes → 20% EtOAc in Hexanes) to obtain the pure **14a** (0.057 g, 25.42%) as yellow oil after evaporation of solvent. R_f = 0.20, (25% EtOAc in Hexanes). ^{1}H NMR (300 MHz, $CDCl_3$): δ 4.44-4.28 (m, 2H), 4.23-4.18 (m, 2H), 3.22 (br s, 1H), 1.91-1.69 (m, 4H), 1.63-1.58 (m, 2H), 1.46-1.35 (m, 4H), 0.96-0.88 (m, 9H).

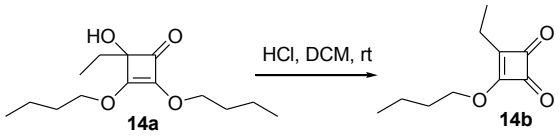

14a **14b**

To a solution of compound **14a** (0.057 g, 0.223 mmol) in DCM (3.0 mL) was added 2 drops of 12 N HCl at rt.[264] The reaction mixture was stirred at rt and monitored on TLC (25% EtOAc in Hexanes) for complete consumption of starting material. The reaction

mixture was diluted with DCM (5.0 mL) and the organic phase was washed with water (10.0 mL × 3). The organic phase was dried over anhydrous Na_2SO_4 and evaporation of solvent afforded the crude product as yellow oil. The crude product was purified using silica gel column (10% EtOAc in Hexanes → 20% EtOAc in Hexanes) to obtain pure **14b** (0.038 g, 95%) as canary yellow oil after evaporation of solvent. R_f = similar to the R_f of 3,4-dibutoxy-3-cyclobutene-1,2-dione (25% EtOAc in Hexanes). ^{1}H NMR (300 MHz, $CDCl_3$): δ 4.71(t, $J_{H\text{-}H}$ = 6.57 Hz, 2H), 2.62 (q, $J_{H\text{-}H}$ = 7.62 Hz, 2H), 1.83-1.74 (m, 2H), 1.50-1.38 (m, 2H), 1.25 (t, $J_{H\text{-}H}$ = 7.56 Hz, 3H), 0.96 (t, $J_{H\text{-}H}$ = 7.32 Hz, 3H). LRMS: found 182 [M^+], calcd for $[C_{10}H_{14}O_3]^+$ 182.

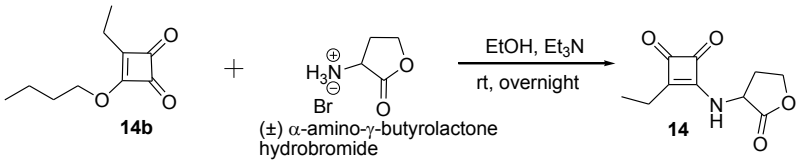

To a solution of (±) α-amino-γ-butyrolactone hydrobromide (0.041 g, 0.223 mmol) in EtOH (1.0 mL) was added Et_3N (0.08 mL, 0.609 mmol). The mixture was stirred for 5 min followed by addition of a solution of compound **14b** (0.037 g, 0.203 mmol) in EtOH (2.0 mL). The progress of the reaction was monitored on TLC (25% EtOAc in Hexanes and 80% EtOAc in Hexanes separately). Once TLC indicated complete consumption of starting material, a dry silica gel slurry was prepared of the reaction mixture and was loaded on to a silica gel column and purified (100% EtOAc) to obtain pure **14** (0.037 g, 87.86%) as a colorless viscous oil after evaporation of solvent. EtOAc or DCM and the product was re-precipitated by addition in Et_2O. The mixture was placed in -20 °C overnight. The solvent was carefully removed using a glass pipette and the remaining

precipitate was dried under vaccum to provide **14** as a sticky white solid. R_f = 0.31, (100% EtOAc). ^{1}H NMR (300 MHz, $CDCl_3$): δ 7.54 (d, J_{H-H} = 7.89 Hz, 1H), 5.13-5.03 (m, 1H), 4.49 (t, J_{H-H} = 9.12 Hz, 1H), 4.37-4.10 (m, 1H), 2.84-2.75 (m, 1H), 2.61 (q, J_{H-H} = 7.62 Hz, 2H), 2.50-2.43 (m, 1H), 1.25 (t, J_{H-H} = 7.53 Hz, 3H).

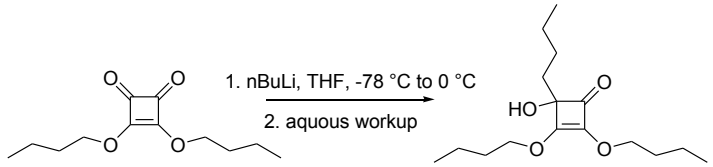

To a solution of 3,4-dibutoxy-3-cyclobutene-1,2-dione (0.400 g, 1.768 mmol) in THF (10.0 mL) was added 2.5 M n-BuLi (0.707 mL, 1.768 mmol) at -78 °C drop wise. The reaction mixture gradually turned from colorless to pale yellow during the addition of n-BuLi. The reaction mixture was stirred at -78 °C for the next 20 min and monitored by TLC (20% EtOAc in Hexanes), which confirmed formation of product. TLC after 1 h showed little progress hence another batch of 2.5 M n-BuLi (0.884 mmol) was added to the reaction mixture at -78 °C. The progress of the reaction was monitored on TLC until complete consumption of starting material. Water was added to the reaction mixture drop wise at -78 °C and the reaction mixture was slowly warmed up to rt. The aqueous phase was extracted with EtOAc. The combined organic portions were dried over anhydrous Na_2SO_4 and evaporation of organic solvents afforded the crude product as yellow oil. The crude product was purified using silica gel column (20% EtOac in Hexanes) to afford pure **6a** (0.324 g, 64.53%) as colorless oil after evaporation of solvent. R_f = 0.23, (20% EtOAc). ^{1}H NMR (300 MHz, $CDCl_3$): δ 4.45-4.30 (m, 2H), 4.23 (t, J_{H-H} = 6.54 Hz, 2H), 2.74 (s, 1H), 1.88-1.58 (m, 6H), 1.50-1.25 (m, 8H), 0.99-0.87 (m, 9H). ^{13}C NMR (75

MHz, $CDCl_3$): δ 187.9, 168.2, 132.8, 86.5, 73.03, 70.7, 32.6, 31.9, 31.6, 27.3, 22.9, 18.86, 18.76, 14.0, 13.8, 13.7.

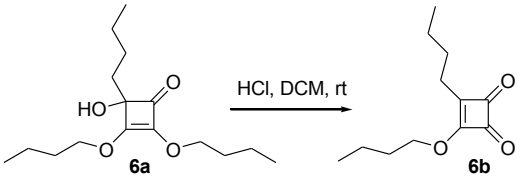

To a solution of compound **6a** (0.304 g, 1.069 mmol) in DCM (7.0 mL) was added 3 drops of 12 N HCl at rt. The reaction mixture was stirred at rt for 20 min rt. After 20 min TLC (20% EtOAc in Hexanes) showed complete consumption of starting material. The reaction mixture was diluted by adding DCM (10 mL) and the organic phase was washed with water (10.0 mL × 3). The organic phase was dried over anhydrous Na_2SO_4 and evaporation of solvent afforded the crude product as light brown oil. The crude product was purified using silica gel column (15% EtOAc in Hexanes) to afford pure **6b** (0.201 g, 89.23%) as yellow oil after evaporation of solvent. R_f = 0.51, (20% EtOAc). ^{1}H NMR (300 MHz, $CDCl_3$): δ 4.72 (t, $J_{H\text{-}H}$ = 6.60 Hz, 2H), 2.61-2.56 (m, 2H), 1.83-1.70 (m, 2H), 1.68-1.60 (m, 2H), 1.50-1.38 (m, 4H), 0.98-0.90 (m, 6H). ^{13}C NMR (75 MHz, $CDCl_3$): δ 198.7, 195.6, 194.4, 184.5, 74.4, 31.9, 27.9, 24.8, 22.8, 18.6, 13.6.

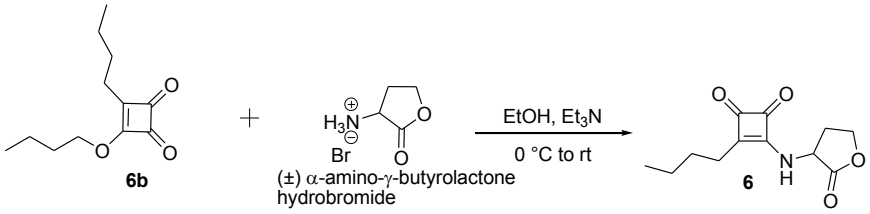

To a solution of compound **6b** (0.105 g, 0.498 mmol) in EtOH (5.0 mL) was added (±) α-amino-γ-butyrolactone hydrobromide (0.099 g, 0.548 mmol) at 0 °C and to the solution

was added Et_3N (0.22 mL, 1.495 mmol) drop wise at 0 °C. The progress of the reaction was monitored on TLC (20% EtOAc in Hexanes and 70% EtOAc in Hexanes seperately) until complete consumption of starting material. A dry silica gel slurry was prepared of the reaction mixture and was loaded on to a silica gel column and purified (70% EtOAc in Hexanes to 100% EtOAc) to obtain pure **6** (0.084 g, 71.32%) as a colorless viscous oil after evaporation of solvent. EtOAc or DCM and the product was re-precipitated by addition in Et_2O. The mixture was placed in -20 °C overnight. The solvent was carefully removed using a glass pipette and the remaining precipitate was dried under vaccum to provide **6** as white solid. R_f = 0.20, (70% EtOAc in Hexanes). ^{1}H NMR (300 MHz, CD_3CN): δ 7.01 (br s, 1H), 5.06-4.97 (m, 1H), 4.46-4.25 (m, 2H), 2.74-2.53 (m, 3H), 2.41-2.30 (m, 1H), 1.68-1.58 (m, 2H), 1.45-1.33 (m, 2H), 0.94 (t, J_{H-H} = 7.20 Hz, 3H). ^{13}C NMR (75 MHz, $CDCl_3$): δ 192.5, 184.7, 175.8, 174.7, 65.9, 53.1, 31.0, 28.2, 25.2, 23.1, 13.9. HRMS: found 237.0998 [M^+], calcd for $[C_{12}H_{15}NO_4]^+$ 237.0996.

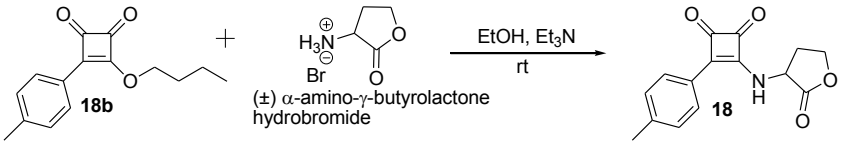

To a solution of (±) α-amino-γ-butyrolactone hydrobromide (0.041 g, 0.225 mmol) in EtOH (3.0 mL) was added Et_3N (0.09 mL, 0.614 mmol) at rt. The reaction mixture was stirred at rt for 10 min followed by addition of **18b** (0.050 g, 0.205 mmol). The progress of the reaction was monitored on TLC (20% EtOAc in Hexanes and 80% EtOAc in Hexanes). The reaction mixture was then stirred overnight at rt. TLC after overnight reaction showed complete consumption of starting material. A dry silica gel slurry was

prepared of the reaction mixture and was loaded on to a silica gel column and purified (80% EtOAc in Hexanes) to obtain pure **18** (0.053 g, 94.77%) as a pale yellow solid after evaporation of solvent. The solid was dried, crushed and washed with hexanes (1 mL × 3) and then dried under vacuum. R_f = 0.55, (80% EtOAc in Hexanes). ^{1}H NMR (300 MHz, DMSO-d_6): δ 9.28 (br s, 1H), 7.89 (d, J_{H-H} = 7.95 Hz, 2H), 7.39 (d, J_{H-H} = 7.86 Hz, 2H), 5.33-5.26 (m, 1H), 4.49-4.30 (m, 2H), 2.71-2.63 (m, 1H), 2.43 (br s, 1H), 2.38 (s, 3H). ^{13}C NMR (75 MHz, DMSO-d_6): δ 192.3, 188.9, 178.9, 174.7, 162.98, 141.4, 129.8, 126.3, 126.2, 65.5, 52.8, 29.2, 21.3. HRMS: found 271.0836 [M^+], calcd for $[C_{15}H_{13}NO_4]^+$ 271.0839.

Bacterial culture, cytotoxcity assays and biofilm inhibition assays **(same as described in chapter 6)**

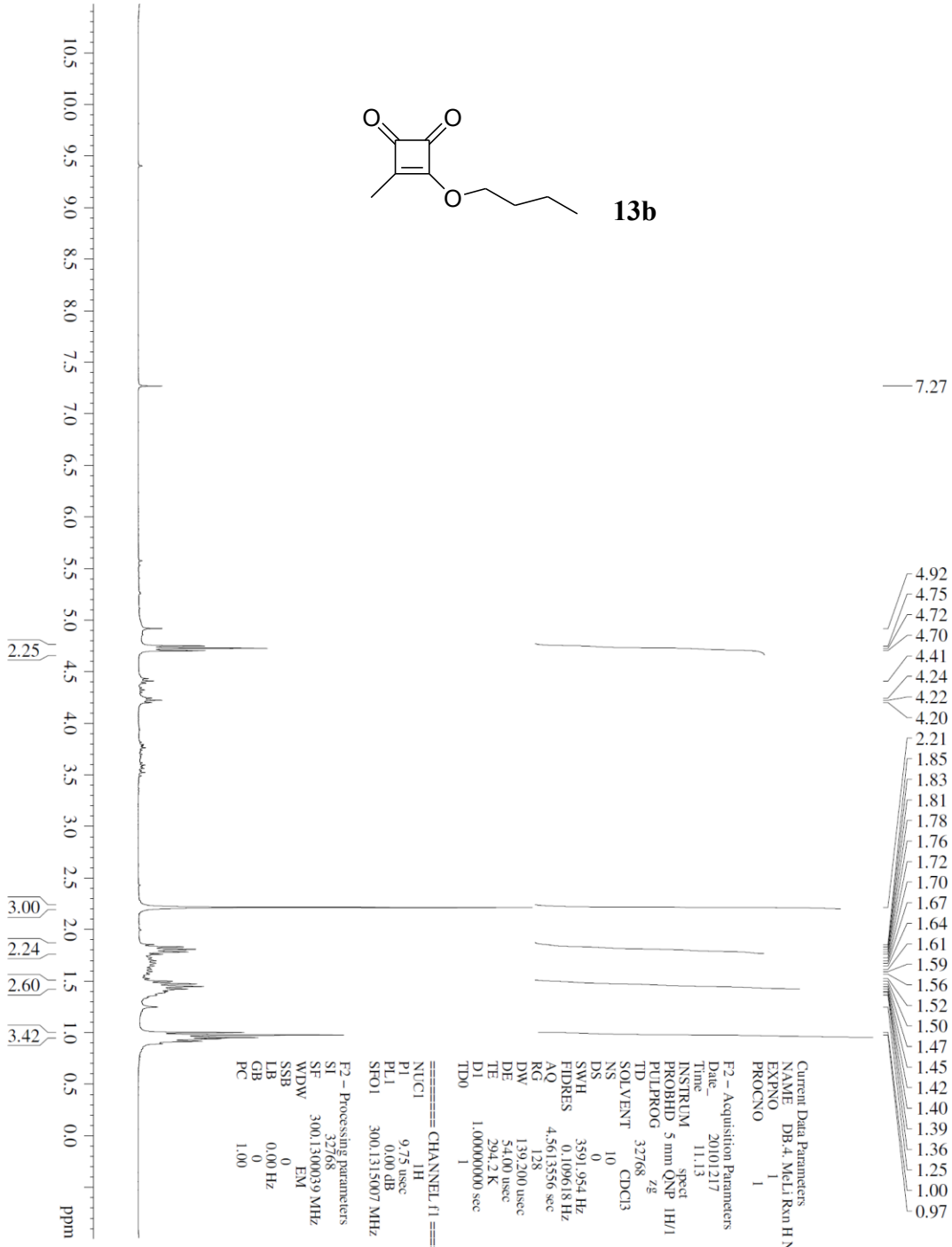
13b
7.27
4.92
4.75
4.72
4.70
4.41
4.24
4.22
4.20
2.21
1.85
1.83
1.81
1.78
1.76
1.72
1.70
1.67
1.64
1.61
1.59
1.56
1.52
1.50
1.47
1.45
1.42
1.40
1.39
1.36
1.25
1.00
0.97
2.25
3.00
2.24
2.60
3.42
ppm
Current Data Parameters
NAME DB.4. MeLi Rxn H NMR
EXPNO 1
PROCNO 1
F2 – Acquisition Parameters
Date_ 20101217
Time 11.13
INSTRUM spect
PROBHD 5 mm QNP 1H/1
PULPROG zg
TD 32768
SOLVENT CDCl3
NS 10
DS 0
SWH 3591.954 Hz
FIDRES 0.109618 Hz
AQ 4.5613556 sec
RG 128
DW 139.200 usec
DE 54.00 usec
TE 294.2 K
D1 1.00000000 sec
TD0 1
======== CHANNEL f1 ========
NUC1 1H
P1 9.75 usec
PL1 0.00 dB
SFO1 300.1315007 MHz
F2 – Processing parameters
SI 32768
SF 300.1300039 MHz
WDW EM
SSB 0
LB 0.00 Hz
GB 0
PC 1.00

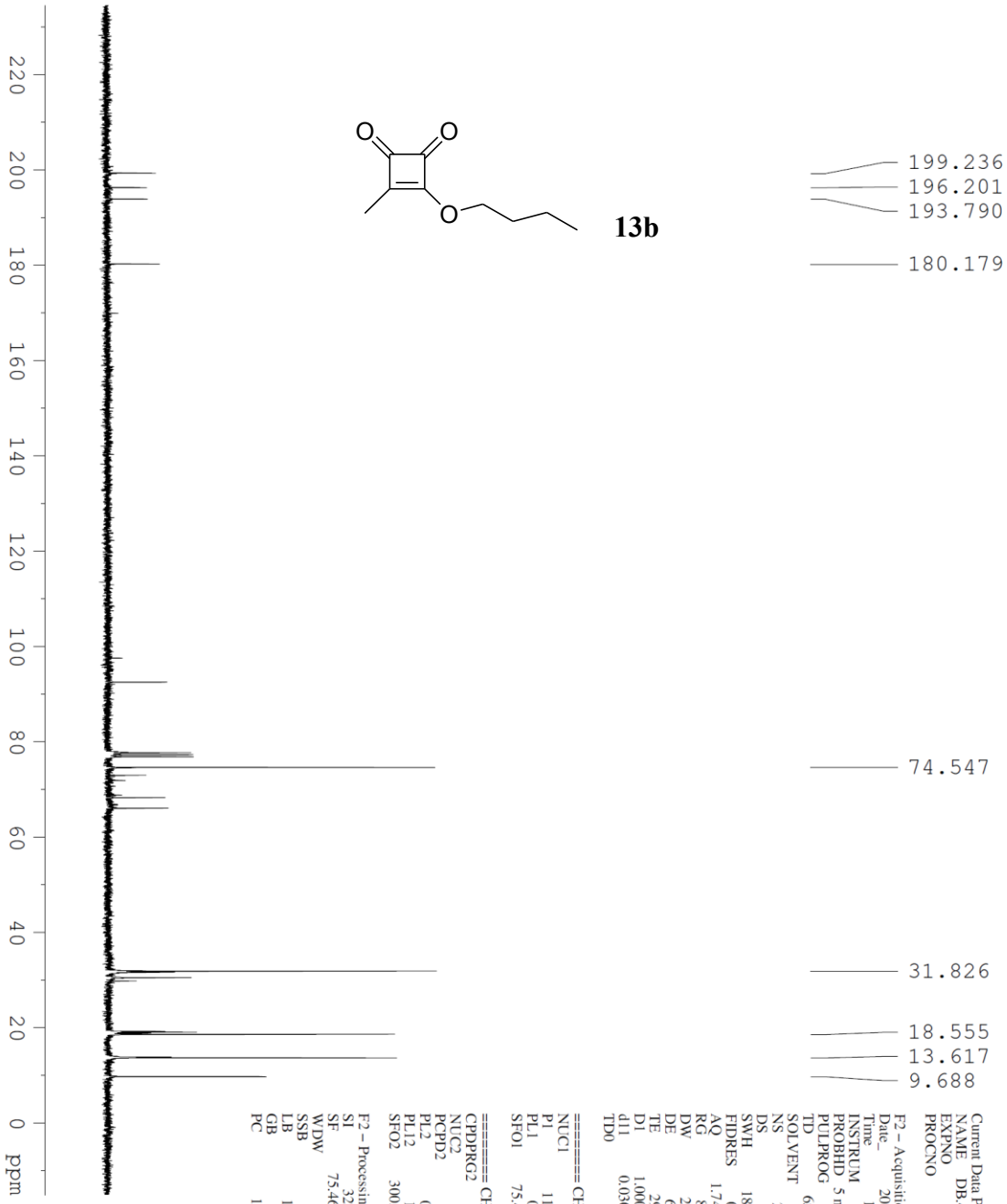
O
O
O
13b
199.236
196.201
193.790
180.179
74.547
31.826
18.555
13.617
9.688
220
200
180
160
140
120
100
80
60
40
20
0
ppm
Current Data Parameters
NAME DB.4.MeLi Rxn C N
EXPNO 2
PROCNO 1
F2 – Acquisition Parameters
Date_ 20101217
Time 11.30
INSTRUM spect
PROBHD 5 mm QNP 1H/1
PULPROG zgdc
TD 65536
SOLVENT CDCl3
NS 200
DS 0
SWH 18832.393 Hz
FIDRES 0.287360 Hz
AQ 1.740308 sec
RG 8192
DW 26.550 usec
DE 6.00 usec
TE 294.2 K
D1 1.00000000 sec
d11 0.03000000 sec
TD0 1
======== CHANNEL f1 ========
NUC1 13C
P1 11.80 usec
PL1 0.00 dB
SFO1 75.4760200 MHz
======== CHANNEL f2 ========
CPDPRG2 waltz16
NUC2 1H
PCPD2 95.00 usec
PL2 0.00 dB
PL12 18.00 dB
SFO2 300.1312005 MHz
F2 – Processing parameters
SI 32768
SF 75.4677412 MHz
WDW EM
SSB 0
LB 1.00 Hz
GB 0
PC 1.40

13
7.27
7.09
7.07
5.31
5.08
5.05
4.55
4.52
4.49
4.36
2.51
2.47
2.44
2.40
2.32
2.19
0.96
0.92
1.34
1.23
2.07
3.00
Current Data Parameters
NAME DB-4.132 ETHER PPT 2
EXPNO 1
PROCNO 1
F2 – Acquisition Parameters
Date_ 20110415
Time 17.32
INSTRUM spect
PROBHD 5 mm QNP 1H/1
PULPROG zg
TD 32768
SOLVENT CDCl3
NS 16
DS 0
SWH 3591.954 Hz
FIDRES 0.109618 Hz
AQ 4.5613556 sec
RG 456.1
DW 139.200 usec
DE 54.00 usec
TE 295.2 K
D1 1.00000000 sec
TD0 1
======== CHANNEL f1 ========
NUC1 1H
P1 9.75 usec
PL1 0.00 dB
SFO1 300.1315007 MHz
F2 – Processing parameters
SI 32768
SF 300.1300039 MHz
WDW EM
SSB 0
LB 2.00 Hz
GB 0
PC 1.00
10.5 10.0 9.5 9.0 8.5 8.0 7.5 7.0 6.5 6.0 5.5 5.0 4.5 4.0 3.5 3.0 2.5 2.0 1.5 1.0 0.5 0.0
PPM

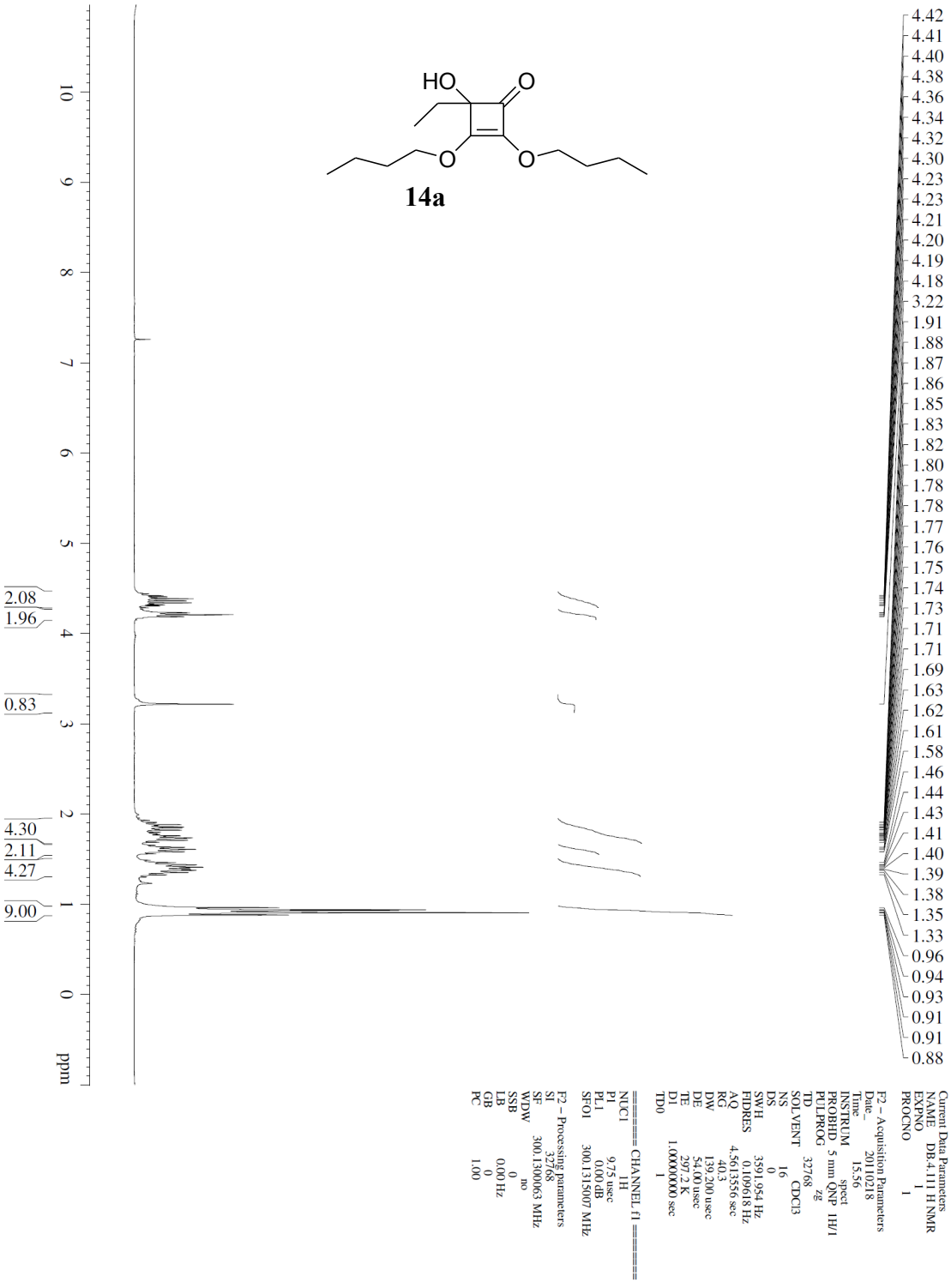
HO
O
O
O
14a
ppm
2.08
1.96
0.83
4.30
2.11
4.27
9.00
4.42
4.41
4.40
4.38
4.36
4.34
4.32
4.30
4.23
4.23
4.21
4.20
4.19
4.18
3.22
1.91
1.88
1.87
1.86
1.85
1.83
1.82
1.80
1.78
1.78
1.77
1.76
1.75
1.74
1.73
1.71
1.71
1.69
1.63
1.62
1.61
1.58
1.46
1.44
1.43
1.41
1.40
1.39
1.38
1.35
1.33
0.96
0.94
0.93
0.91
0.91
0.88
Current Data Parameters
NAME DB-4-111 H NMR
EXPNO 1
PROCNO 1
F2 – Acquisition Parameters
Date_ 20110218
Time 15.56
INSTRUM spect
PROBHD 5 mm QNP 1H/1
PULPROG zg
TD 32768
SOLVENT CDCl3
NS 16
DS 0
SWH 3591.954 Hz
FIDRES 0.109618 Hz
AQ 4.5613556 sec
RG 40.3
DW 139.200 usec
DE 54.00 usec
TE 297.2 K
D1 1.00000000 sec
TD0 1
======== CHANNEL f1 ========
NUC1 1H
P1 9.75 usec
PL1 0.00 dB
SFO1 300.1315007 MHz
F2 – Processing parameters
SI 32768
SF 300.1300063 MHz
WDW no
SSB 0
LB 0.00 Hz
GB 0
PC 1.00

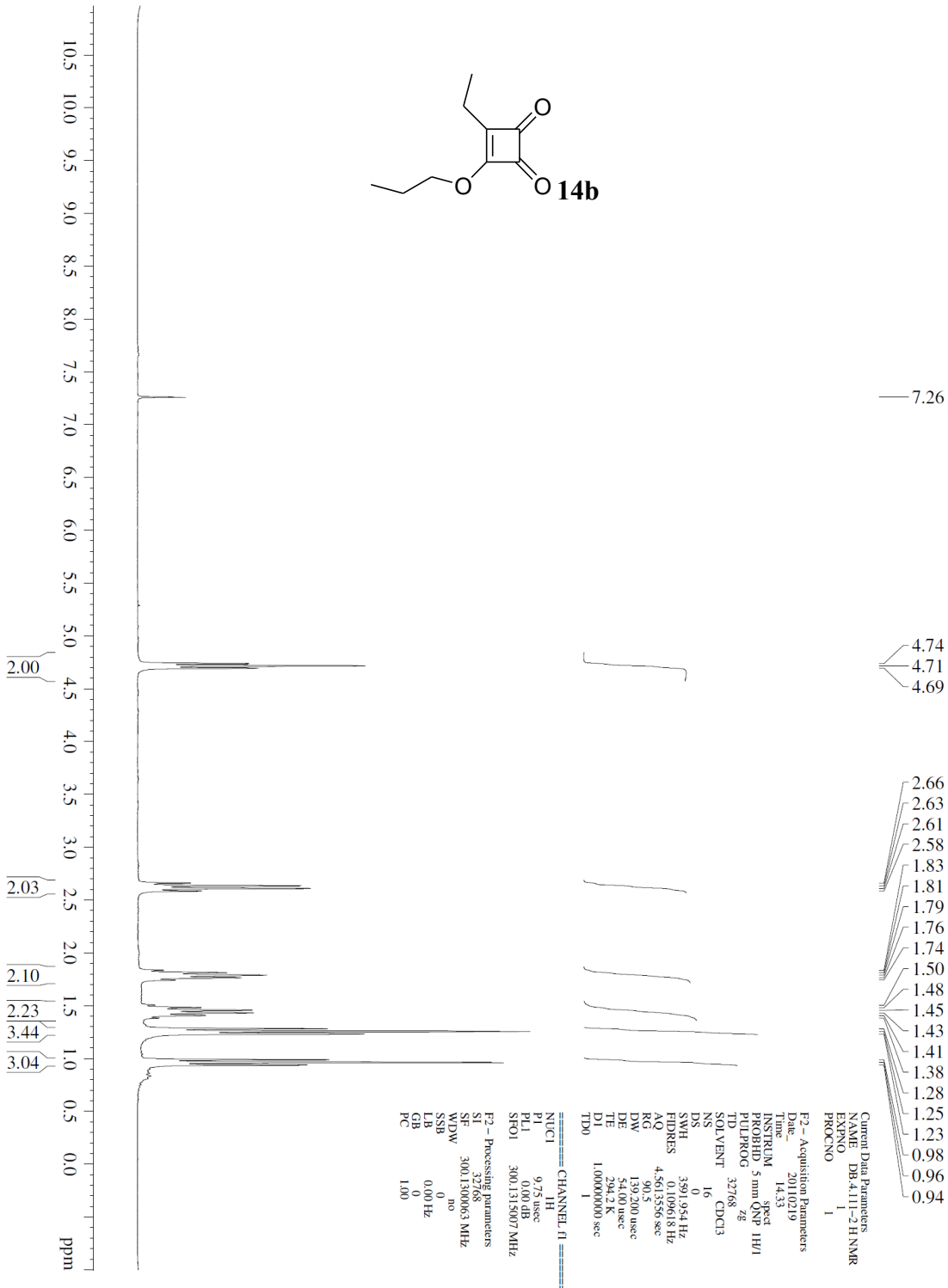
14b
7.26
4.74
4.71
4.69
2.66
2.63
2.61
2.58
1.83
1.81
1.79
1.76
1.74
1.50
1.48
1.45
1.43
1.41
1.38
1.28
1.25
1.23
0.98
0.96
0.94
2.00
2.03
2.10
2.23
3.44
3.04
ppm

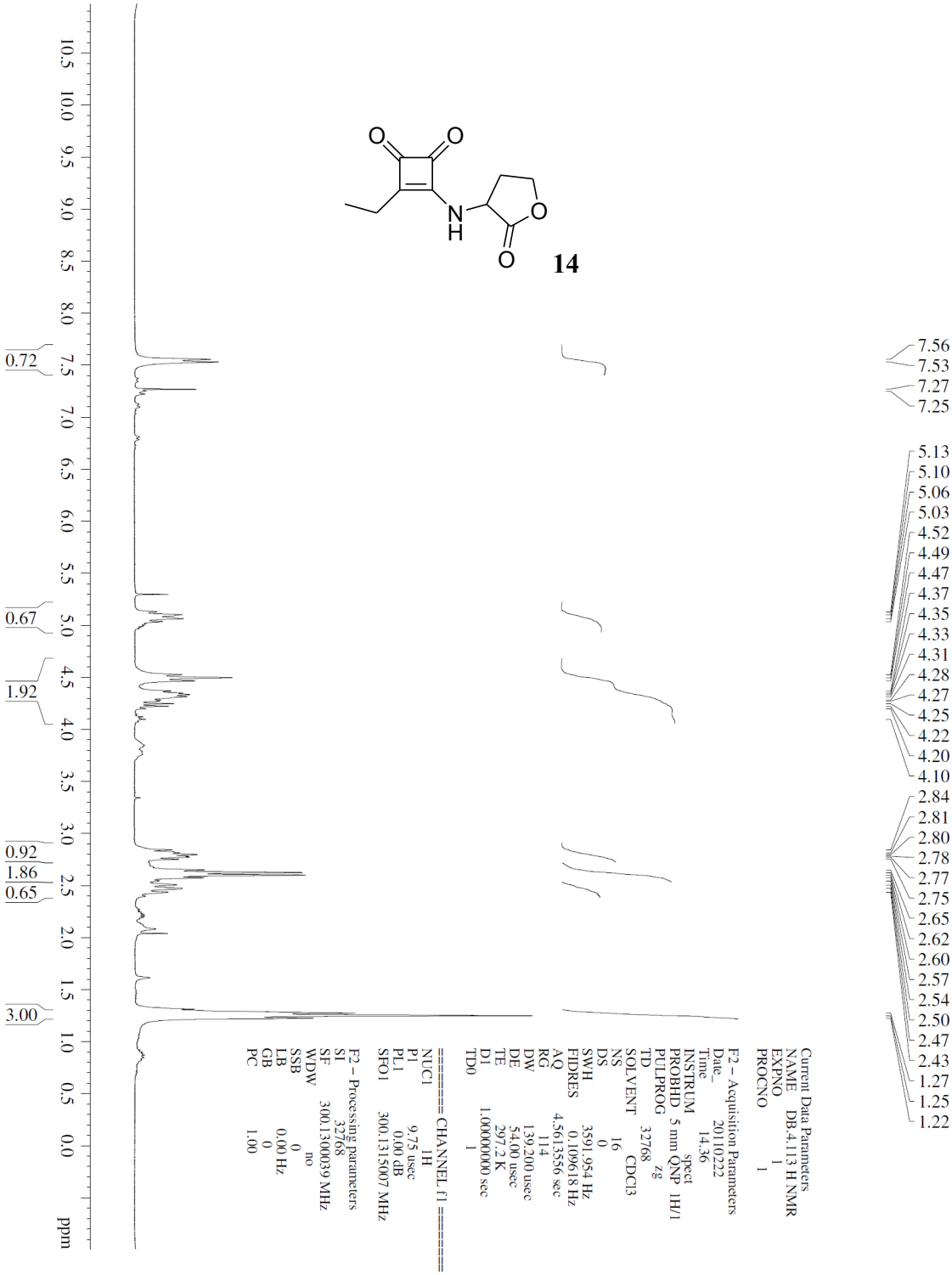
14
7.56
7.53
7.27
7.25
5.13
5.10
5.06
5.03
4.52
4.49
4.47
4.37
4.35
4.33
4.31
4.28
4.27
4.25
4.22
4.20
4.10
2.84
2.81
2.80
2.78
2.77
2.75
2.65
2.62
2.60
2.57
2.54
2.50
2.47
2.43
1.27
1.25
1.22
Current Data Parameters
NAME DB-4.113 H NMR
EXPNO 1
PROCNO 1
F2 – Acquisition Parameters
Date_ 20110222
Time 14.36
INSTRUM spect
PROBHD 5 mm QNP 1H/1
PULPROG zg
TD 32768
SOLVENT CDCl3
NS 16
DS 0
SWH 3591.954 Hz
FIDRES 0.109618 Hz
AQ 4.56133556 sec
RG 114
DW 139.200 usec
DE 54.00 usec
TE 297.2 K
D1 1.00000000 sec
TD0 1
======== CHANNEL f1 ========
NUC1 1H
P1 9.75 usec
PL1 0.00 dB
SFO1 300.1315007 MHz
F2 – Processing parameters
SI 32768
SF 300.1300039 MHz
WDW no
SSB 0
LB 0.00 Hz
GB 0
PC 1.00
0.72
0.67
1.92
0.92
1.86
0.65
3.00
10.5 10.0 9.5 9.0 8.5 8.0 7.5 7.0 6.5 6.0 5.5 5.0 4.5 4.0 3.5 3.0 2.5 2.0 1.5 1.0 0.5 0.0
ppm

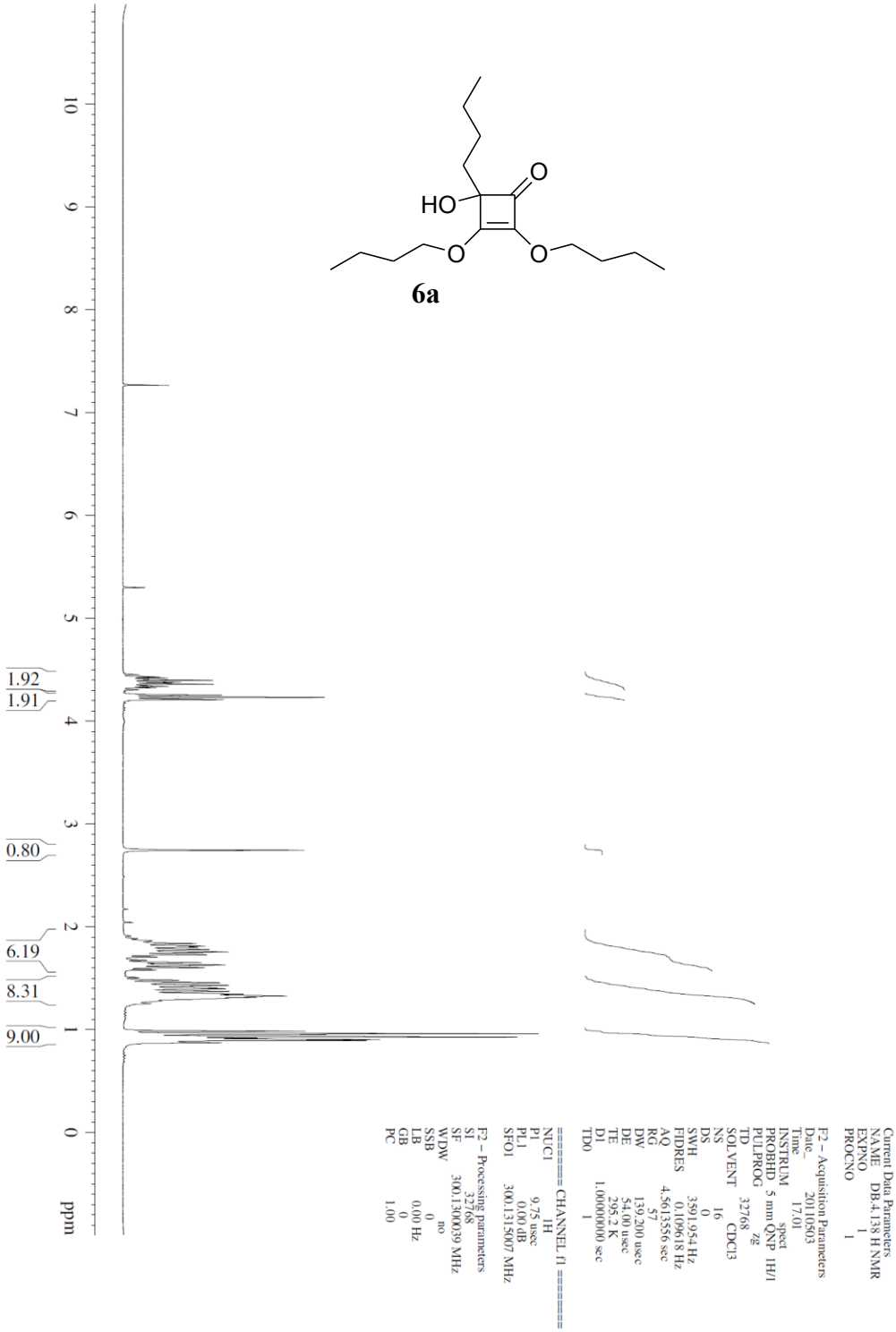
HO
O
O
O
6a
1.92
1.91
0.80
6.19
8.31
9.00
10
9
8
7
6
5
4
3
2
1
0
ppm
7.27
7.26
4.43
4.42
4.41
4.39
4.38
4.37
4.36
4.35
4.34
4.32
4.25
4.23
4.21
2.74
1.86
1.83
1.81
1.80
1.78
1.77
1.75
1.73
1.70
1.67
1.65
1.64
1.63
1.60
1.58
1.48
1.45
1.43
1.42
1.40
1.40
1.37
1.34
1.34
1.32
1.31
1.30
1.28
1.25
0.99
0.98
0.96
0.96
0.95
0.93
0.93
0.92
0.90
0.90
0.89
0.87
Current Data Parameters
NAME DB-4-138 H NMR
EXPNO 1
PROCNO 1
F2 - Acquisition Parameters
Date_ 20110503
Time 17.01
INSTRUM spect
PROBHD 5 mm QNP 1H/1
PULPROG zg
TD 32768
SOLVENT CDCl3
NS 16
DS 0
SWH 3591.954 Hz
FIDRES 0.109618 Hz
AQ 4.561356 sec
RG 57
DW 139.200 usec
DE 54.00 usec
TE 295.2 K
D1 1.00000000 sec
TD0 1
======== CHANNEL f1 ========
NUC1 1H
P1 9.75 usec
PL1 0.00 dB
SFO1 300.1315007 MHz
F2 - Processing parameters
SI 32768
SF 300.1300039 MHz
WDW no
SSB 0
LB 0.00 Hz
GB 0
PC 1.00

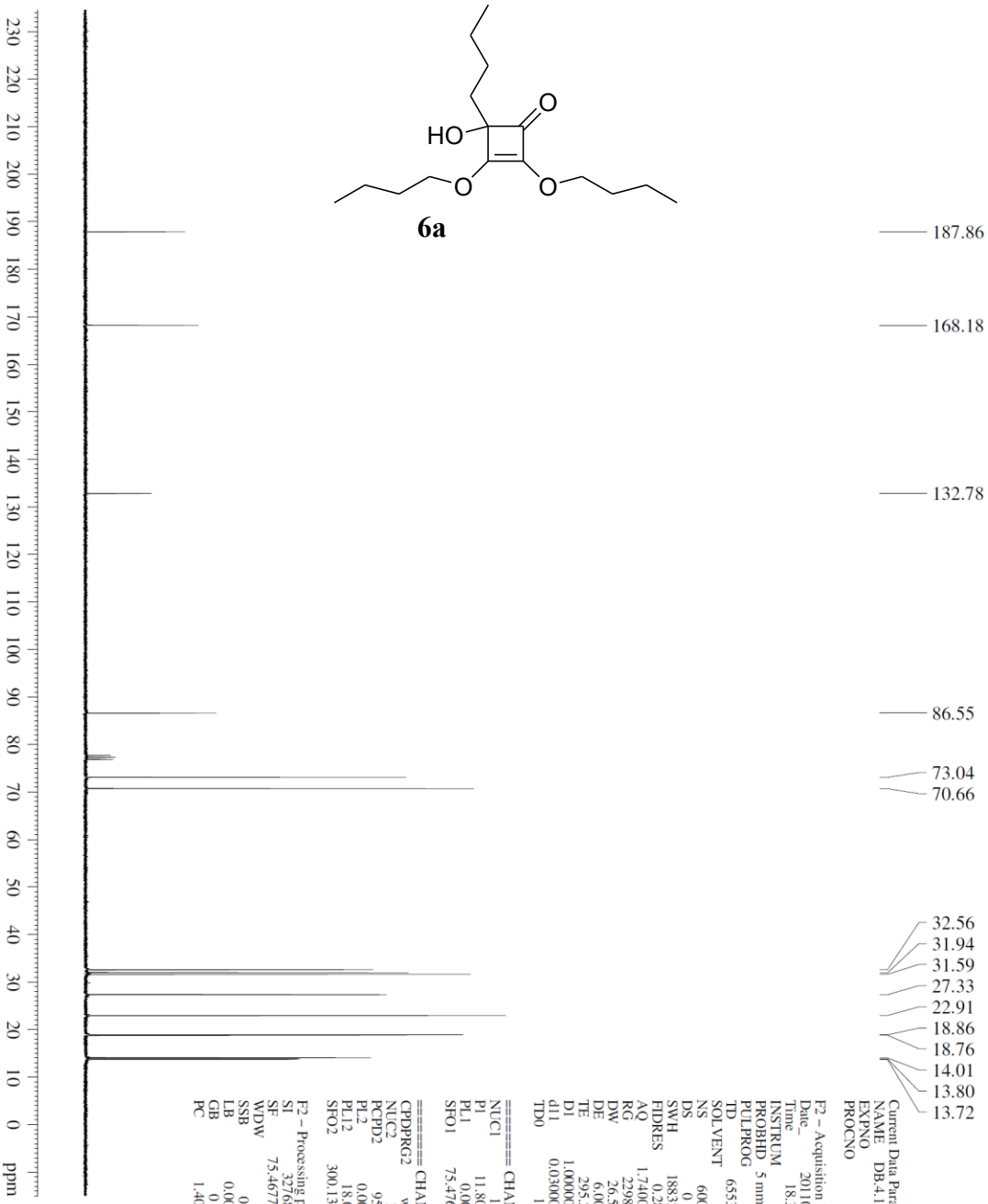
HO
O
O
O
6a
187.86
168.18
132.78
86.55
73.04
70.66
32.56
31.94
31.59
27.33
22.91
18.86
18.76
14.01
13.80
13.72
Current Data Parameters
NAME DB.4.138 C NMR
EXPNO 2
PROCNO 1
F2 – Acquisition Parameters
Date_ 20110503
Time 18.39
INSTRUM spect
PROBHD 5 mm QNP 1H/1
PULPROG zgdc
TD 65536
SOLVENT CDCl3
NS 600
DS 0
SWH 18832.393 Hz
FIDRES 0.287360 Hz
AQ 1.7400308 sec
RG 2298.8
DW 26.550 usec
DE 6.00 usec
TE 295.2 K
D1 1.00000000 sec
d11 0.03000000 sec
TD0 1
======== CHANNEL f1 ========
NUC1 13C
P1 11.80 usec
PL1 0.00 dB
SFO1 75.4760200 MHz
======== CHANNEL f2 ========
CPDPRG2 waltz16
NUC2 1H
PCPD2 95.00 usec
PL2 0.00 dB
PL12 18.00 dB
SFO2 300.1312005 MHz
F2 – Processing parameters
SI 32768
SF 75.4677387 MHz
WDW no
SSB 0
LB 0.00 Hz
GB 0
PC 1.40
230 220 210 200 190 180 170 160 150 140 130 120 110 100 90 80 70 60 50 40 30 20 10 0 ppm

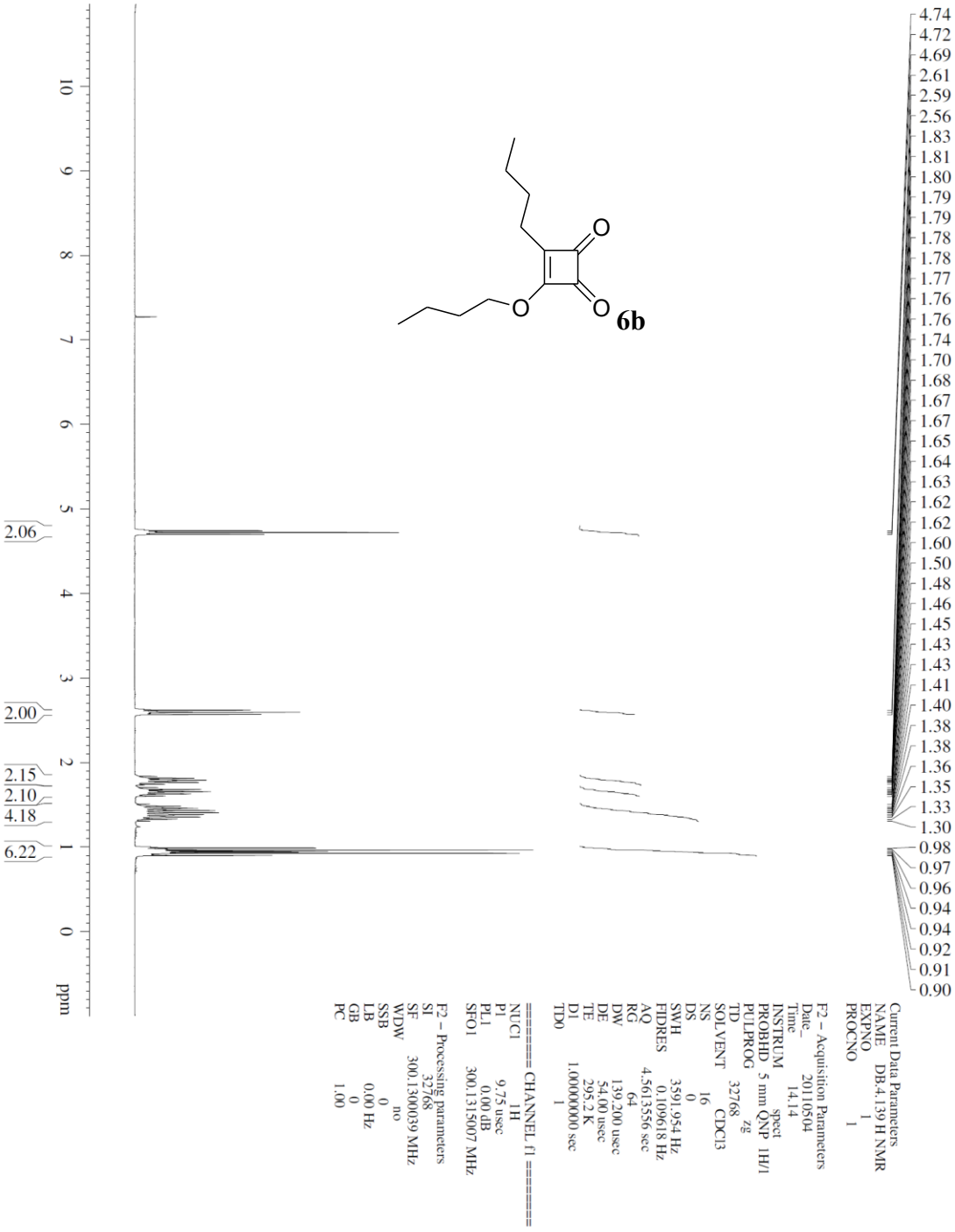
6b
2.06
2.00
2.15
2.10
4.18
6.22
ppm
Current Data Parameters
NAME DB.4.139.H NMR
EXPNO 1
PROCNO 1
F2 – Acquisition Parameters
Date_ 20110504
Time 14.14
INSTRUM spect
PROBHD 5 mm QNP 1H/1
PULPROG zg
TD 32768
SOLVENT CDCl3
NS 16
DS 0
SWH 3591.954 Hz
FIDRES 0.109618 Hz
AQ 4.5613556 sec
RG 64
DW 139.200 usec
DE 54.00 usec
TE 295.2 K
D1 1.00000000 sec
TD0 1
======== CHANNEL f1 ========
NUC1 1H
P1 9.75 usec
PL1 0.00 dB
SFO1 300.1315007 MHz
F2 – Processing parameters
SI 32768
SF 300.1300039 MHz
WDW no
SSB 0
LB 0.00 Hz
GB 0
PC 1.00

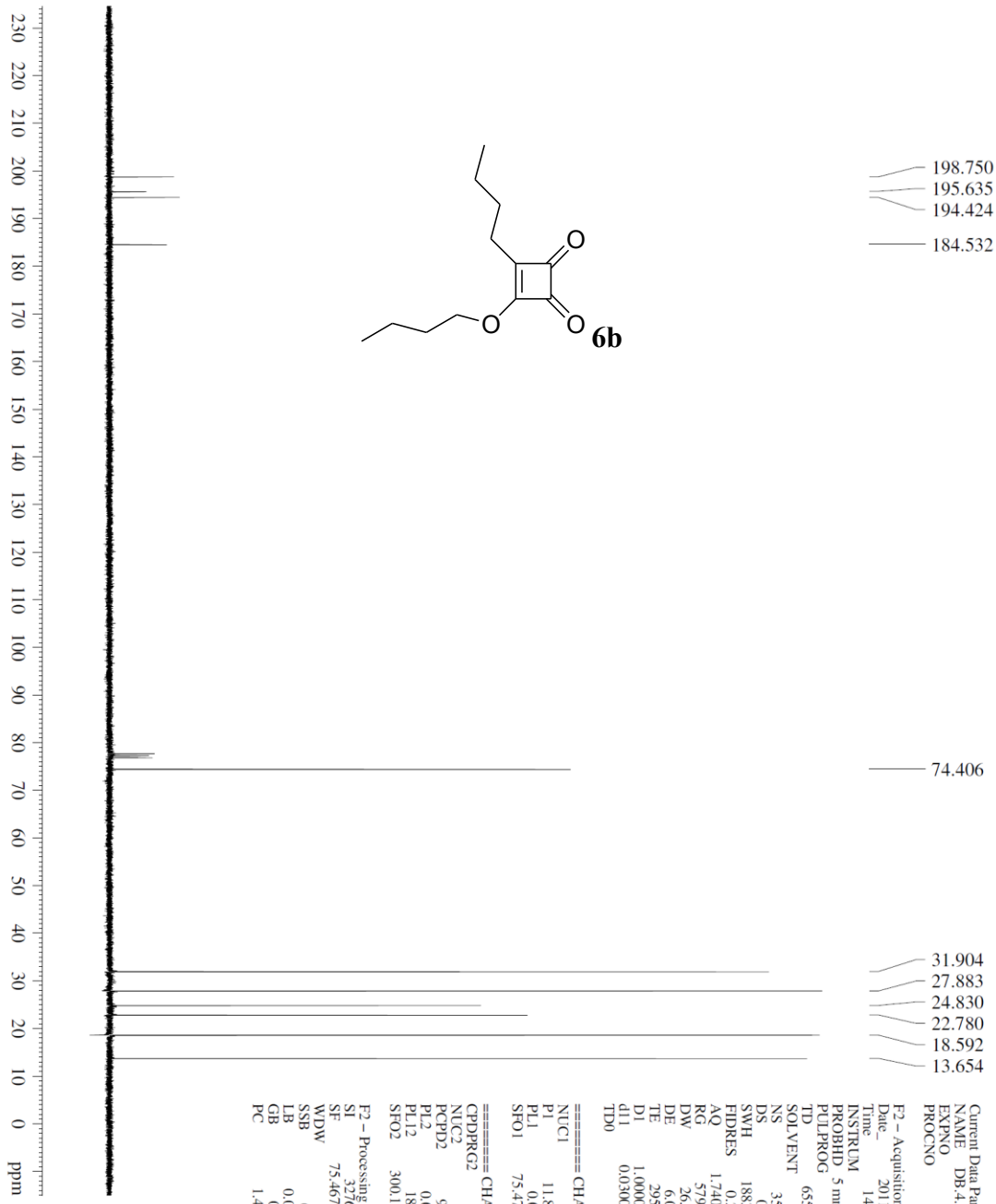
198.750
195.635
194.424
184.532
74.406
31.904
27.883
24.830
22.780
18.592
13.654
6b
Current Data Parameters
NAME DB.4.139 C NMR
EXPNO 2
PROCNO 1
F2 – Acquisition Parameters
Date_ 20110504
Time 14.37
INSTRUM spect
PROBHD 5 mm QNP 1H/1
PULPROG zgdc
TD 65536
SOLVENT CDCl3
NS 350
DS 0
SWH 18832.393 Hz
FIDRES 0.287360 Hz
AQ 1.7400308 sec
RG 5792.6
DW 26.550 usec
DE 6.00 usec
TE 295.2 K
D1 1.00000000 sec
d11 0.03000000 sec
TD0 1
======== CHANNEL f1 ========
NUC1 13C
P1 11.80 usec
PL1 0.00 dB
SFO1 75.4760200 MHz
======== CHANNEL f2 ========
CPDPRG2 waltz16
NUC2 1H
PCPD2 95.00 usec
PL2 0.00 dB
PL12 18.00 dB
SFO2 300.1312005 MHz
F2 – Processing parameters
SI 32768
SF 75.4677404 MHz
WDW no
SSB 0
LB 0.00 Hz
GB 0
PC 1.40
230 220 210 200 190 180 170 160 150 140 130 120 110 100 90 80 70 60 50 40 30 20 10 0 ppm

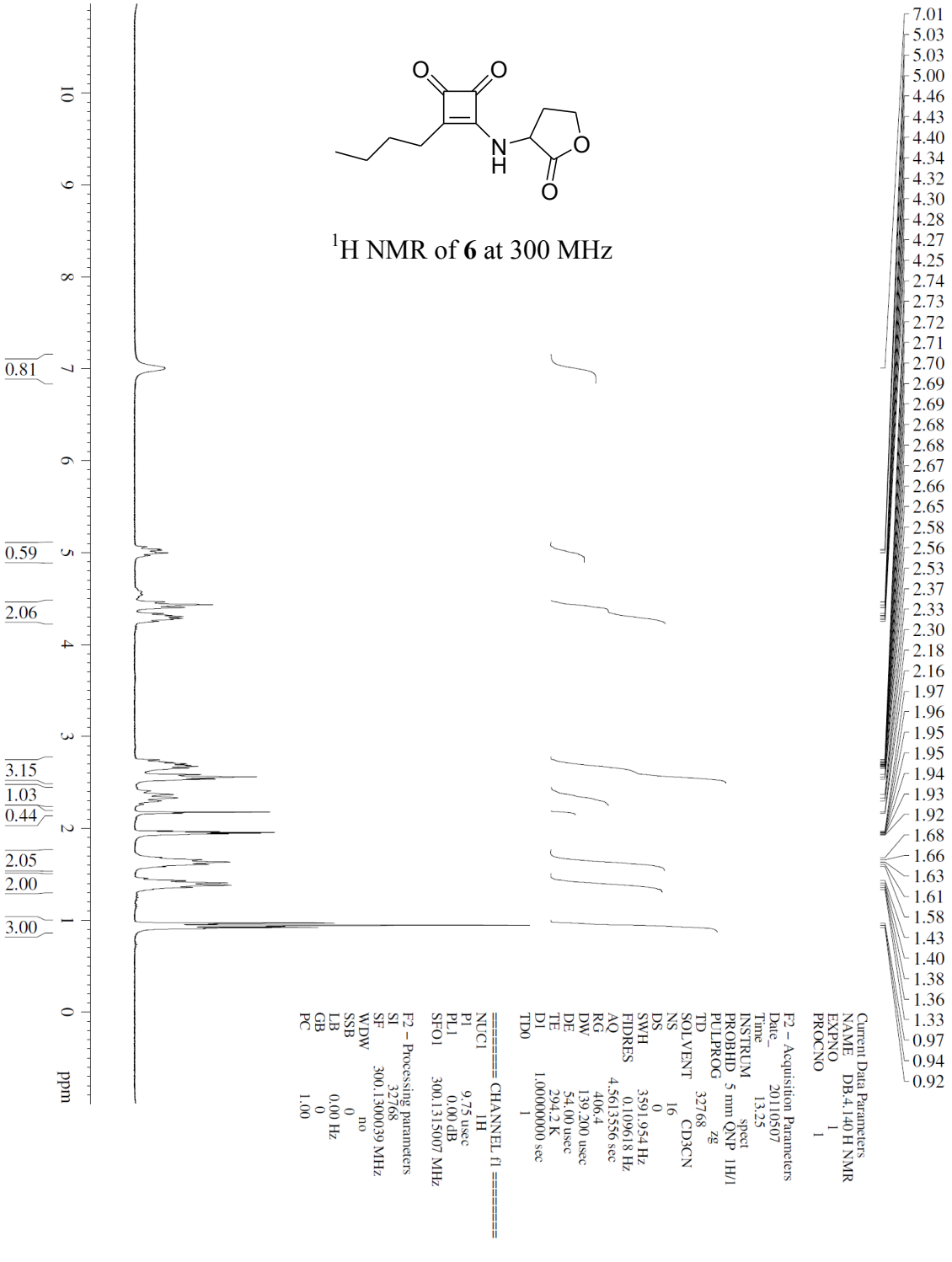

^{1}H NMR of **6** at 300 MHz

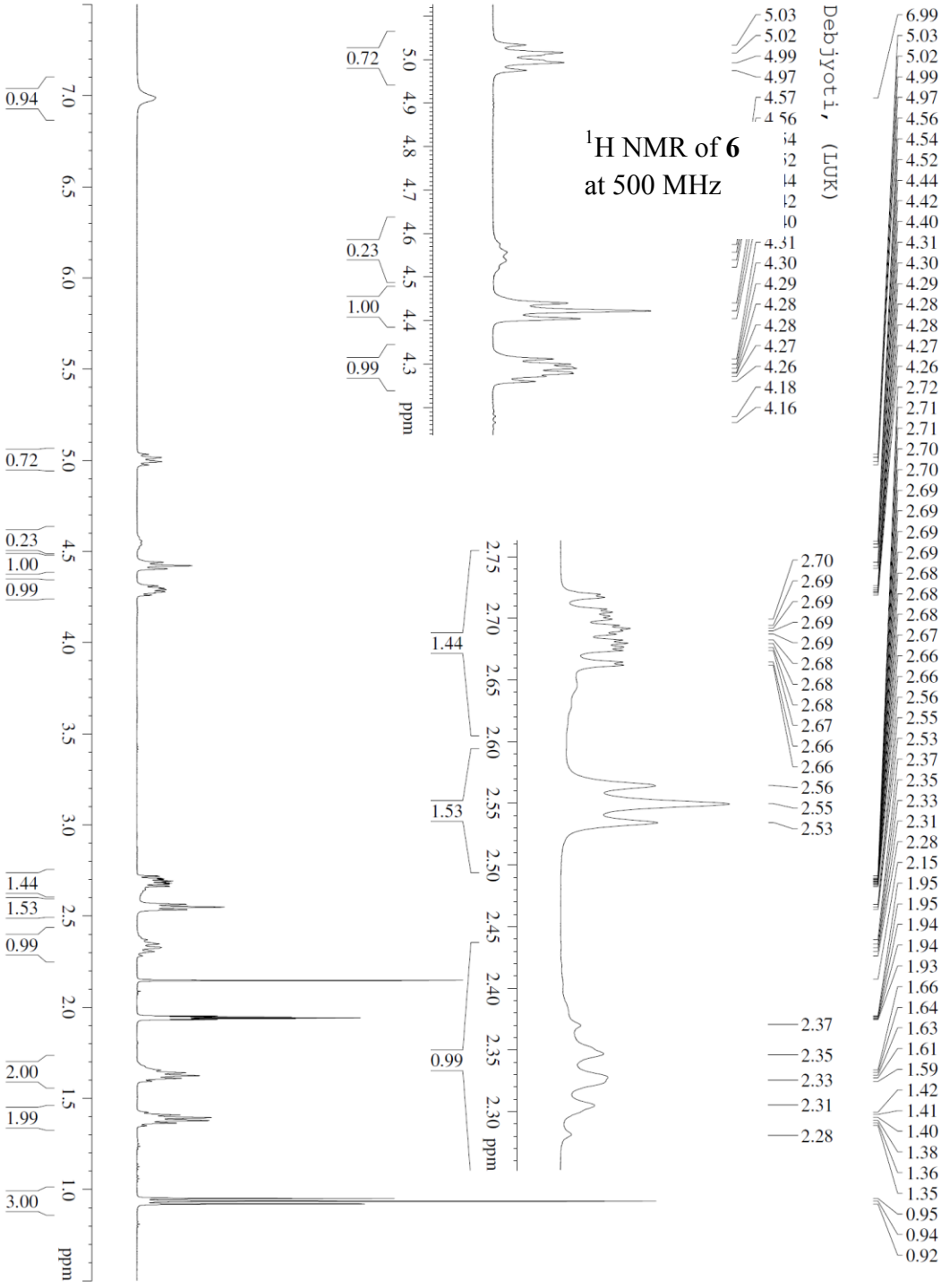
Debjyoti, (LUK)
^{1}H NMR of **6**
at 500 MHz
ppm

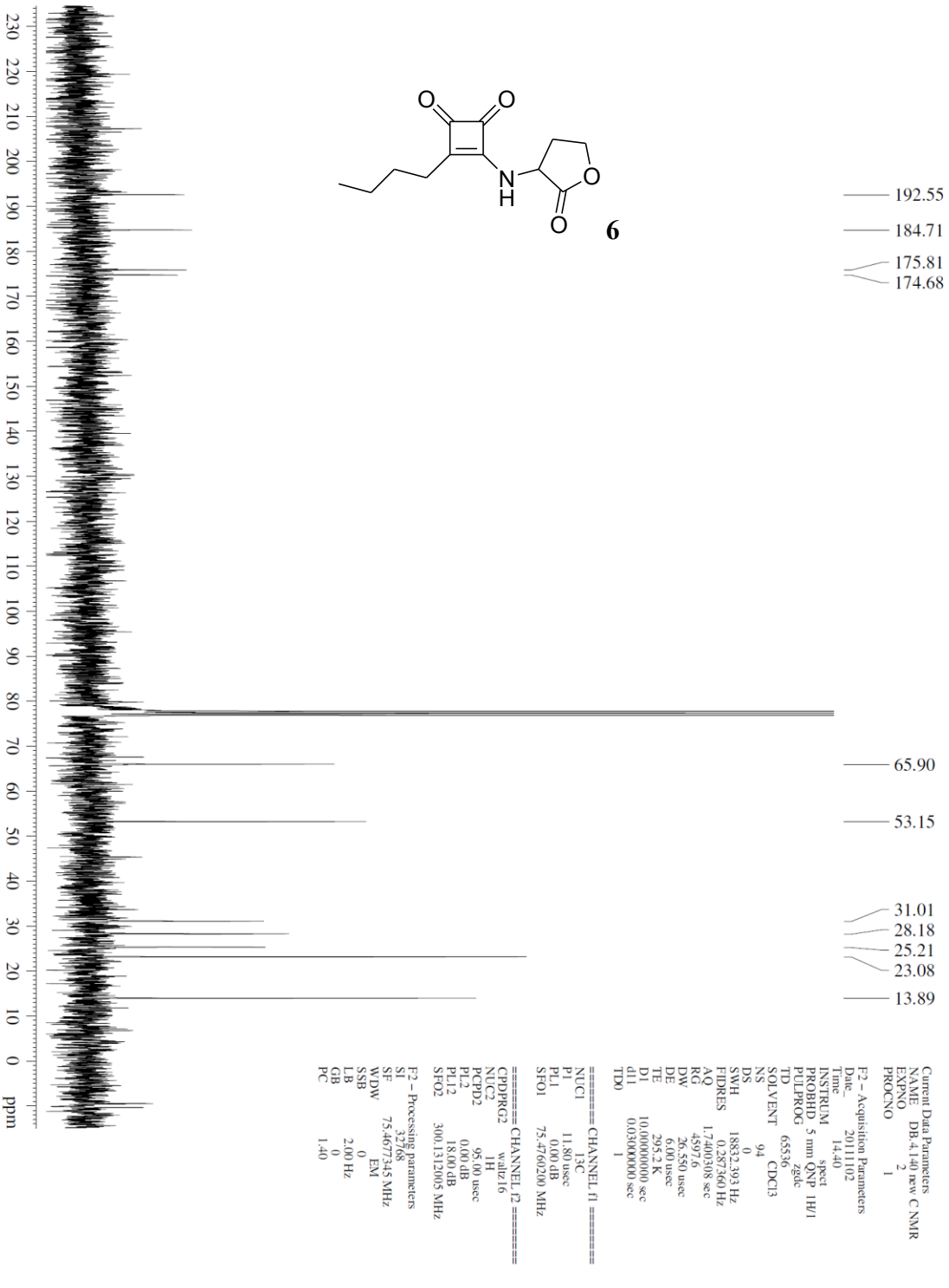
O
O
N
H
O
O
6
192.55
184.71
175.81
174.68
65.90
53.15
31.01
28.18
25.21
23.08
13.89
230 220 210 200 190 180 170 160 150 140 130 120 110 100 90 80 70 60 50 40 30 20 10 0 ppm
Current Data Parameters
NAME DB-4-140 new C NMR
EXPNO 2
PROCNO 1
F2 - Acquisition Parameters
Date_ 20111102
Time 14.40
INSTRUM spect
PROBHD 5 mm QNP 1H/1
PULPROG zgdc
TD 65536
SOLVENT CDCl3
NS 94
DS 0
SWH 18832.393 Hz
FIDRES 0.287360 Hz
AQ 1.7400308 sec
RG 4597.6
DW 26.550 usec
DE 6.00 usec
TE 295.2 K
D1 10.00000000 sec
d11 0.03000000 sec
TD0 1
======== CHANNEL f1 ========
NUC1 13C
P1 11.80 usec
PL1 0.00 dB
SFO1 75.4760200 MHz
======== CHANNEL f2 ========
CPDPRG2 waltz16
NUC2 1H
PCPD2 95.00 usec
PL2 0.00 dB
PL12 18.00 dB
SFO2 300.1312005 MHz
F2 - Processing parameters
SI 32768
SF 75.4677345 MHz
WDW EM
SSB 0
LB 2.00 Hz
GB 0
PC 1.40

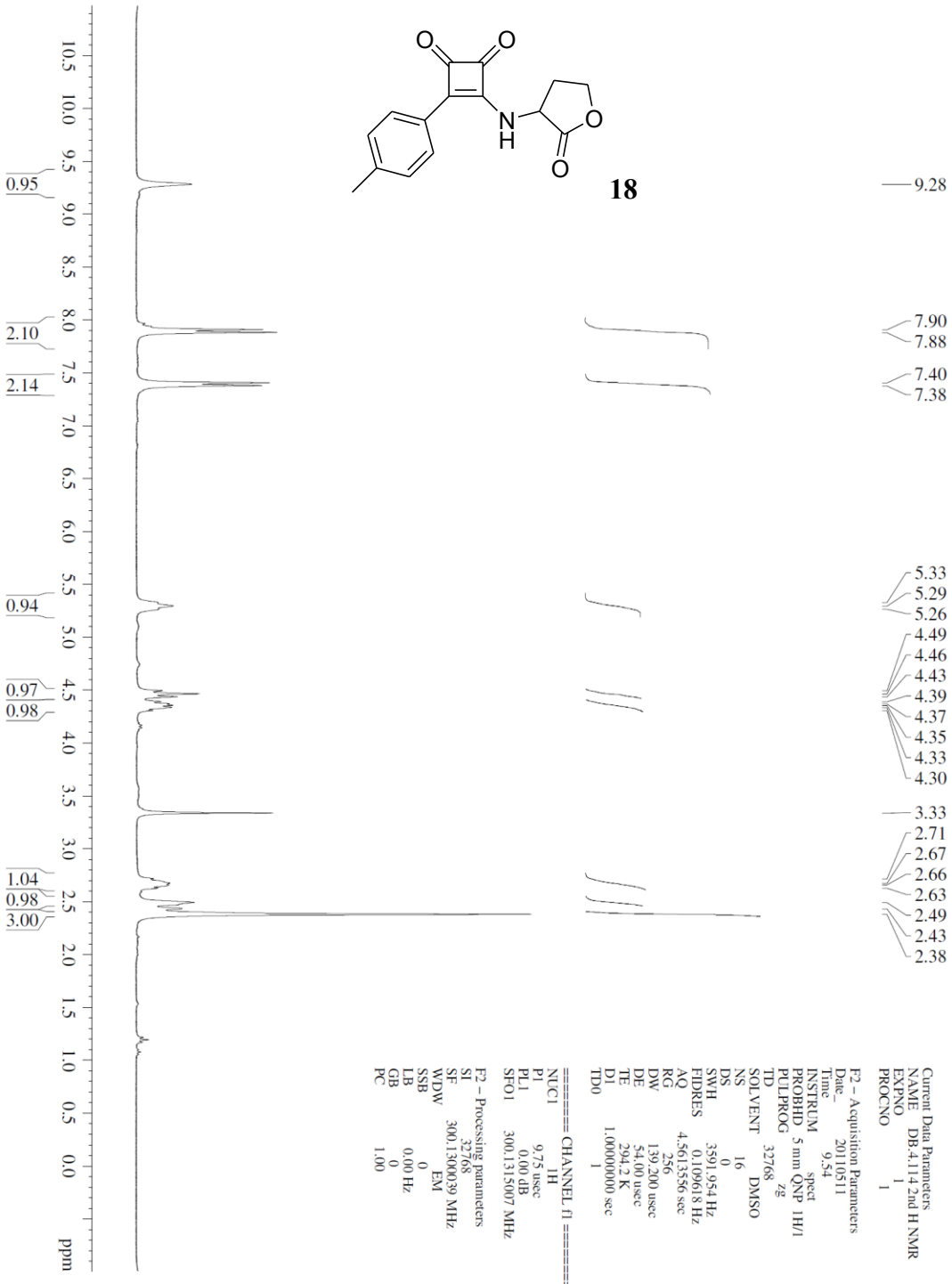
18
9.28
7.90
7.88
7.40
7.38
5.33
5.29
5.26
4.49
4.46
4.43
4.39
4.37
4.35
4.33
4.30
3.33
2.71
2.67
2.66
2.63
2.49
2.43
2.38
0.95
2.10
2.14
0.94
0.97
0.98
1.04
0.98
3.00
ppm
Current Data Parameters
NAME DB-4.114 2nd H NMR
EXPNO 1
PROCNO 1
F2 - Acquisition Parameters
Date_ 20110511
Time 9.54
INSTRUM spect
PROBHD 5 mm QNP 1H/1
PULPROG zg
TD 32768
SOLVENT DMSO
NS 16
DS 0
SWH 3591.954 Hz
FIDRES 0.109618 Hz
AQ 4.5613556 sec
RG 256
DW 139.200 usec
DE 54.00 usec
TE 294.2 K
D1 1.00000000 sec
TD0 1
======== CHANNEL f1 ========
NUC1 1H
P1 9.75 usec
PL1 0.00 dB
SFO1 300.1315007 MHz
F2 - Processing parameters
SI 32768
SF 300.1300039 MHz
WDW EM
SSB 0
LB 0.00 Hz
GB 0
PC 1.00

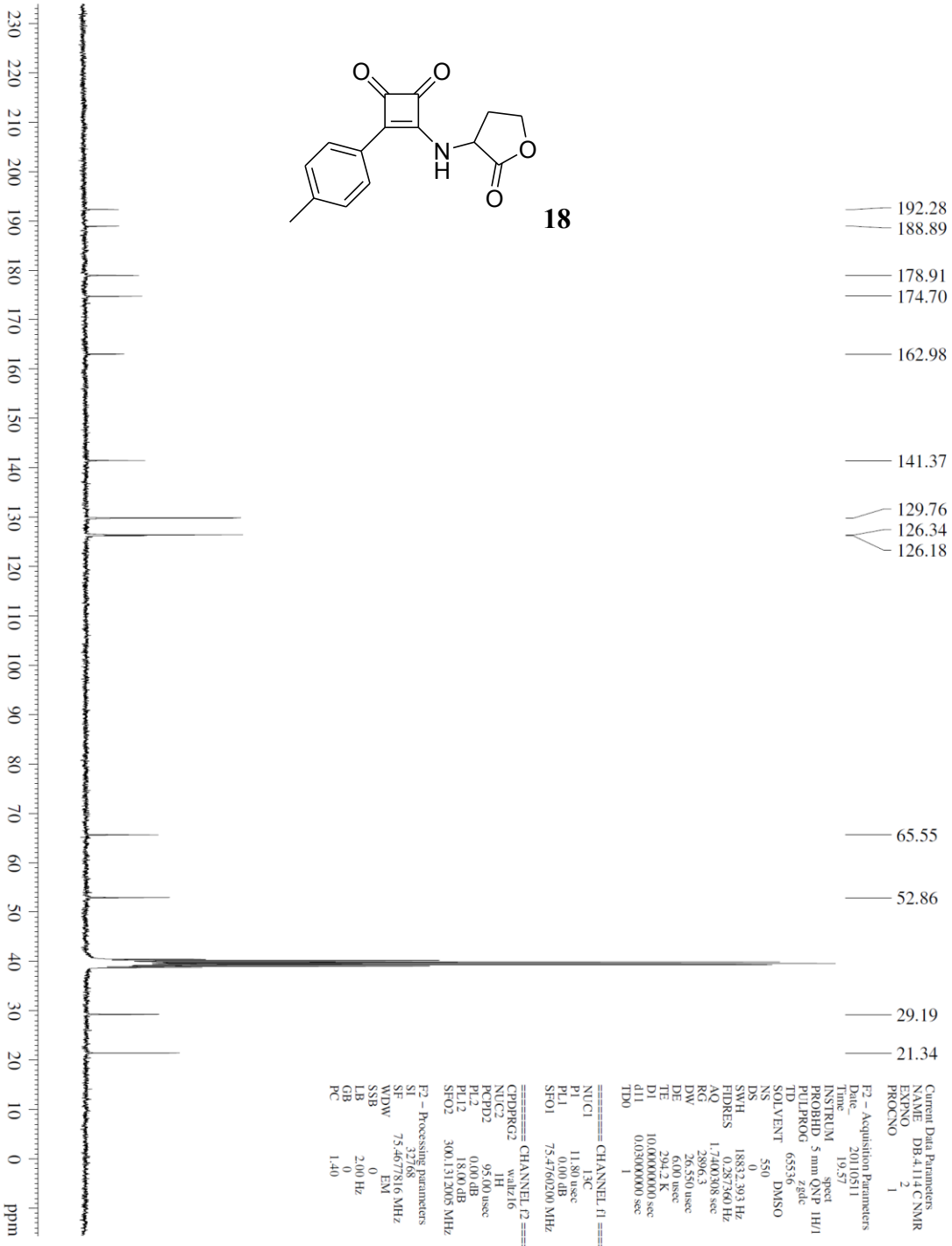
18
192.28
188.89
178.91
174.70
162.98
141.37
129.76
126.34
126.18
65.55
52.86
29.19
21.34
230 220 210 200 190 180 170 160 150 140 130 120 110 100 90 80 70 60 50 40 30 20 10 0 ppm
Current Data Parameters
NAME DB 4 114 C NMR
EXPNO 2
PROCNO 1
F2 - Acquisition Parameters
Date_ 20110511
Time 19.57
INSTRUM spect
PROBHD 5 mm QNP 1H/1
PULPROG zgdc
TD 65536
SOLVENT DMSO
NS 550
DS 0
SWH 18832.393 Hz
FIDRES 0.287360 Hz
AQ 1.7400308 sec
RG 2896.3
DW 26.550 usec
DE 6.00 usec
TE 294.2 K
D1 10.0000000 sec
d11 0.0300000 sec
TD0 1
======== CHANNEL f1 ========
NUC1 13C
P1 11.80 usec
PL1 0.00 dB
SFO1 75.4760200 MHz
======== CHANNEL f2 ========
CPDPRG2 waltz16
NUC2 1H
PCPD2 95.00 usec
PL2 0.00 dB
PL12 18.00 dB
SFO2 300.1312005 MHz
F2 - Processing parameters
SI 32768
SF 75.4677816 MHz
WDW EM
SSB 0
LB 2.00 Hz
GB 0
PC 1.40

Chapter 8

A Summary on Controlling Biofouling by Surface Engineering and Molecular Inhibition

Introduction

This dissertation presents two approaches for controlling biofouling caused by protein adsorption,[1-2] mammalian cell adhesion[3-4] and biofilm formation.[5-6] First is a surface chemist approach involving *surface engineering* and second is a chemical biologist approach involving *molecular inhibition* of biofilm formation. Biofouling is a complex phenomenon and is not well understoodat the molecular level. For example, biofilm formation is associated with five stages, which begins with attachment of the planktonic bacterial cells on the surface, microcolony formation, secretion of polysaccharides, maturation of the biofilm and eventual dispersal of the bacterial cells from the biofilm.[18] Bacterial cells within the biofilm are protected from environmental stress and are resistant to antibiotics. Hence, one viable approach for treating biofilm-related infections is to prevent the formation biofilm in the first place. Biofilm formation can be controlled by either fabricating surfaces that can resist the formation of biofilm or by inhibiting the process of quorum sensing[87] that initiates biofilm formation.

For surface engineering, I have used self-assembled monolayers (SAMs) of ω-functionalized alkanethiols on gold (Au).[39] These SAMs have a well-defined structure and present chemical functionalities which are resistant towards different biofouling events such as protein adsorption, mammalian cell adhesion and biofilm formation. For molecular inhibition, I have synthesized organic molecules, which are structural mimics

of signaling molecules called autoinducers (AI) that initiate quorum sensing in bacteria. Quorum sensing initiates a number of processes in bacteria including biofilm formation,[87] hence inhibiting quorum sensing is a viable approach of treating biofilm related bacterial infections. Antibiotics generally target vital cellular processes that are important for the survival of bacterial cells, as a result, bacteria tend to develop resistance against antibiotics over time. It is believed that bacteria are unlikely to develop resistance against quorum sensing inhibitors and hence developing quorum-sensing inhibitors can help us overcome the problem of bacterial antibiotic resistance.[8]

Controlling Biofouling by Surface Engineering

Theories for bioinert surfaces

A number of theories have been proposed to rationalize why SAMs presening oligo(ethylene glycol) (OEG) on gold resists the adsorption of proteins. Whitesides and co-workers proposed that SAMs presenting OEG on gold resist the adsorption of proteins because protein adsorption on such a surface will be associated with thermodynamically unfavorable desolvation and loss of conformational freedom of the OEG chains (steric repulsion effect).[28, 70, 118] But steric repulsion effect is more relevant in case of long polymeric chains of ethylene glycol such as poly(ethylene glycol) (PEG) and less relevant in case of small polymeric chains of ethylene glycol such as OEG.[265-267] Hence steric repulsion theory alone was insufficient to explain the bioinert properties of SAMs presenting OEG. Grunze and co-workers used surface force measurements to discover that proteins approaching SAMs presenting OEG on gold (Au) experience a long-range repulsive interaction and that this repulsive interaction was completely independent of the

steric repulsion effect.[90] Grunze and co-workers also proposed that this long-range repulsive interaction might be a direct consequence of the structured interfacial water associated with SAMs presenting OEG on gold (Au).[89, 108] But there was no experimental evidence to suggest if such long-range repulsive interactions were responsible for making SAMs other than those presenting OEG bioinert. Hence, a rational explanation for resistance of protein adsorption by bioinert SAMs was still lacking at this point.

Whitesides and co-workers hypothesized that if SAMs present zwitterionic groups, such a surface can mimic the surface (or skin) of proteins and can prevent protein adsorption since proteins do not come together in solution.[94] But proteins do aggregate in solution and protein aggregation is a major problem faced by the biopharmaceutical industry. Hence, the "protein skin" theory had its own share of problems. Whitesides and co-workers then proposed a set of properties which bioinert SAMs on gold (Au) should possess. They proposed that chemical functionalities presented by bioinert SAMs should be polar but neutral in charge, should only possess hydrogen bond acceptors and lack hydrogen bond donors.[95]

The kosmotrope theory

Franz Hofmeister made an empirical observation, which led to the discovery that certain ions referred to as kosmotropes had the ability to salt proteins out of solution whereas certain ions referred to as chaotropes had the ability to salt proteins into solution.[99] Kosmotropic ions were also found to preserve the native structure of proteins whereas chaotropic ions were found to denature proteins.[98-99] A similar ability to stabilize the native structure biomolecules was also observed in case of small organic compounds

called osmolytes. Osmolytes are small organic compounds which are secreted within cells of aquatic organisms to combat osmotic stress.[268] Osmolytes such as trimethylamine N-oxide (TMAO), betaine, sarcosine, taurine, octopine and glycerol may be referred to as "organic kosmotropes", whereas protein denaturants such as urea and guanidinium salts may be referred to as "organic chaotropes". It was discovered that that such organic kosmostropes have a tendency to remain preferentially excluded from the vicinity of proteins in solution.[98] Luk[74, 92] and Kane[96] independently hypothesized that if organic kosmotropes are covalently immobilized on sufaces, such surfaces can in principle resist the adsorption of protein since proteins will have a tendency to remain preferentially excluded from such a surface.

Templating a structured interfacial water layer- A key step in making surfaces bioinert

Self-assembled monolayers (SAMs) presenting OEG on gold (Au) are able to resist the adsorption of proteins. Interestingly, SAMs presenting OEG on silver (Ag) are unable to resist the adsorption of proteins.[27] This difference in behavior is due to difference in structures of these SAMs on the surface of gold (Au) and silver (Ag). While the SAMs on silver (Ag) are upright and are associated with an extended all-trans conformation for both the alkanethiolate and OEG chains, the alkanethiolate chains on gold (Au) are tilted at an angle of ~30° to the surface normal with an all-trans extended conformation but the OEG chains have a helical conformation.[89] Theoretical calculations conducted by Kreuzer and co-workers suggests that due to the helical conformation of the OEG chains on gold (Au), the OEG moieties are able to bind water molecules and should be associated with structured interfacial water layer.[108] Grunze and co-workers

hypothesized that this structured interfacial water layer may be responsible for the ability of SAMs presenting OEG on gold (Au) to resist the adsorption of proteins.[89]

Polyol-terminated alkanethiolate SAMs on gold (Au) can template a structured interfacial water layer

Mrksich and co-workers synthesized a polyol-terminated alkanethiol, terminated in the polyol with the stereochemistry of D-mannitol.[74] They hypothesized that such polyol-terminated alkanethiolate SAMs on gold (Au) can help template a structured interfacial water layer by hydrogen bonding water molecules via the terminal hydroxyl groups.[74, 92] It is possible that such as structured interfacial water can act as a barrier and make the surface invisible to attachment of biological entities such as proteins, bacterial cells, mammalian cells and biofilm.

Self-assembled monolayers (SAMs) presenting D-mannitol are more resistant to mammalian cell adhesion than SAMs presenting tri(ethylene glycol) (EG_3OH)

Mammalian cell adhesion on surface is one consequence of protein adsorption on surface.[269] Once proteins adsorb onto a surface, they can present ligands such as the tripeptide Arg-Gly-Asp (RGD), which has specific affinity for the cell surface receptor integrin. This binding event then initiates a number of processes such as proliferation, migration and signaling.[78]

Studying the resistance towards mammalian cell adhesion is a more stringent test for bioinertness of SAMs than studying the resistance towards protein adsorption.[3] While a surface tends to get coated with complete monolayer of protein within minutes, mammalian cell adhesion on a surface generally lasts longer (over weeks).

Mrksich and co-workers demonstrated that although SAMs presenting D-mannitol on gold (Au) had similar ability to resist the adsorption of proteins as compared to SAMs presenting tri(ethylene glycol) (EG_3OH), but SAMs presenting D-mannitol were more resistant towards adhesion of mammalian cells (Swiss 3T3 albino fibroblasts) than SAMs presenting EG_3OH.[74] Mrksich and co-workers used microcontact printing[39] to create circular patterns of methyl-terminated SAMs, surrounded by either SAMs presenting D-mannitol or EG_3OH, where the methyl-terminated SAMs were conducive to protein adsorption and mammalian cell adhesion. They found that the D-mannitol SAMs were able to keep the mammalian cells adhered within the boundaries of the circular patterns up to four times longer than EG_3OH SAMs.[74] This method of creating micropatterned substrates and conducting mammalian culture provides a quantitative measure of the relative bioinertness of SAMs. Hence, the longer a bioinert SAMs can keep the adhered mammalian cells confined within the micropatterns, the more bioinert it is.

Self-assembled monolayers (SAMs) presenting D-mannitol are more resistant to biofilm formation than SAMs presenting tri(ethylene glycol) (EG_3OH)

Recently, Ren and co-workers have demonstrated that patterned substrates where D-mannitol SAMs or EG_3OH SAMs surrounded square patterns of methyl-terminated SAMs, were able to keep biofilm formed by a red fluorescent strain of *E. coli* RP437 confined within the square patterns for long periods. Interestingly, the D-mannitol SAMs were again able to keep the attached biofilm confined within the square patterns much longer than the EG_3OH SAMs.[76]

Influence of the stereochemistry of polyol-terminated alkanethiolate SAMs on gold (Au) on their ability to resist biofouling

Although the D-mannitol SAMs on gold were able to resist adhesion of mammalian cells and biofilm formation much longer than EG_3OH SAMs, there is no study to correlate the stereochemistry of polyol-terminated SAMs to their ability to resist various forms of biofouling such as protein adsorption, mammalian cell adhesion and biofilm formation.

Mammalian cell adhesion on a surface is known to be influenced by the stereochemistry of the surface. Addadi and co-workers have demonstrated that epithelial cells adhere differently on the enantiomeric crystal faces of calcium tartrate tetrahydrate. While epithelial cells could adhere on the (R,R) face of the crystal, they were unable to adhere on the (S,S) face of the crystal.[84] Sun and Chi and co-workers have demonstrated that immune cells adhere differently on monolayers presenting derivatives of either D-cysteine or L-cysteine on gold (Au). While the cells had a rounded morphology and were fewer in number on the surface presenting the D isomer, the cells were well spread and more in number on the surface presenting the L isomer.[85]

Stereochemical effects during protein adsorption on SAMs presenting chiral polyols

Motivated by the above findings, I synthesized a set of enantiomeric chiral polyol-terminated alkanethiols. I synthesized a pair of enantiomeric alditol-terminated alkanethiols, terminated in the sugar alcohols D-gulitol and L-gulitol and a pair of enantiomeric aldonamide-terminated alkanethiols, terminated in the sugar alcohols D-mannonamide and L-mannonamide (Chapter 2). I studied the effect of chirality of these

polyol SAMs on their ability of resist the adsorption of three proteins namely bovine serum albumin (BSA), lysozyme and fibrinogen, which is one of the stickiest proteins known. I used the synthesized alkanethiols to form enantiomeric and racemic SAMs on the surface of gold (Au). Both the enantiomeric and racemic SAMs were found to resist the adsorption of proteins when compared to methyl SAMs. Interestingly, the racemic SAMs were able to resist the adsorption of proteins much more efficiently than the enantiomeric SAMs.

Stereochemical effects during mammalian cell adhesion on SAMs presenting chiral polyols

Since I observed a racemic enhancement in the bioinertness of these chiral polyol-terminated SAMs towards protein adsorption, I next examined the ability of these chiral polyol-terminated SAMs to resist the adhesion of mammalian cells (Swiss 3T3 albino fibroblasts) (Chapter 3). I created patterned substrates where either enantiomeric or racemic SAMs of mannonamide- or gulitol-terminated alkanethiols surrounded circular patterns of methyl-terminated SAMs. I found that only racemic mannonamide SAMs were able to resist the adhesion of mammalian cells and were able to keep the adhered mammalian cells confined within the circular patterns for up to 10 days. In case of the gulitol SAMs, the SAMs presenting D-gulitol were more bioinert as compared to the SAMs presenting the enantiomer L-gulitol. While SAMs presenting D-gulitol were able to keep the mammalian cells confined within the circular patterns for up to 19 days, L-gulitol SAMs failed at 13 days. Interestingly, the SAMs presenting the racemic mixture of the gulitol-terminated alkanethiols were more resistant to mammalian cell adhesion

than SAMs presenting the enantiomers alone. The racemic gulitol SAMs were able to keep the adhered mammalian cells confined within the circular patterns for up to 23 days.

I also observed that SAMs formed by diastereoisomeric aldonamide-terminated alkanethiols namely D-gulonamide and D-gluconamide had different ability to resist the adhesion of mammalian cells. While SAMs presenting D-gulonamide confined the adhered mammalian cells within the circular patterns for up to 2 days, SAMs presenting D-gluconamide were able to keep the mammalian cells confined for up to 5 days.

Although polyol SAMs are hydrophilic in nature, I concluded that hydrophilic surfaces in general may not be bioinert. I created patterned substrates where amine-terminated SAMs surrounded square patterns of methyl-terminated SAMs. When these patterned substrates were presented to mammalian cell culture, the amine SAMs were unable to resist the adhesion of mammalian cell. Interestingly, within one day of mammalian cell culture, the regions presenting the amine SAMs were completely covered with a monolayer of cells while there were very few cells on the region presenting the methyl SAMs. Eventually on day 3, the regions presenting both amine and methyl SAMs were completely covered by a monolayer of cells. I concluded that although amine SAMs are charged and hydrophilic under physiological conditions, amine on surfaces are most likely chaotropic in nature and cause extensive protein adsorption and denaturation followed by mammalian cell adhesion. The regions presenting the methyl SAMs most likely supported a layer of hydrated proteins, which could prevent mammalian cell adhesion temporarily. Eventually, the adsorbed proteins on the regions presenting the

methyl SAMs might denature completely, expose the RGD groups, and hence allow mammalian cell adhesion.

Stereochemical effects during biofilm formation on SAMs presenting chiral polyols

Chapter 4 presents the results on confining biofilm formed by the bacterium *Escherichia coli* within micrometer sized cell adhesive patterns of methyl-terminated SAMs, surrounded by bioinert chiral polyol-terminated SAMs. The biofilm experiments were conducted in a flow cell and I used a red fluorescent *E. coli* strain to monitor the formation of biofilm *in situ*. Interestingly, racemic SAMs of both mannonamide- and gulitol-terminated alkanethiols were found to confine the biofilms within the micropatterns longer than the SAMs presenting either enantiomer. The racemic polyol SAMs were able to keep the biofilms confined within the micropatterns for up to 20 days. Hence, a racemic enhancement in the bioinertness of these polyol SAMs was observed towards resisting protein adsorption, mammalian cell adhesion and biofilm formation. I also discovered that these patterned substrates were able to indentify two phases of biofilm formation. During the first phase of biofilm formation (which lasted for about 2 days) the fluorescent signal was weak on the regions presenting the methyl SAMs but was strong on the regions presenting the polyol SAMs. After about 2 days in the first phase, the fluorescent signal started to disappear from the regions presenting the polyol SAMs but strong fluorescent signal appeared on the regions presenting the methyl SAMs and remain confined on these regions for long periods (~ 20 days). I hypothesize that during the first phase of biofilm formation, there is a hydrated layer of adsorbed biomolecules or proteins on the regions presenting the methyl SAMs, which makes these

regions temporarily bioinert towards attachment of bacterial cells. The polyol SAMs on the other hand resist the adsorption of proteins or other biomolecules but allow temporary attachment of bacteria, probably via non-specific hydrogen bonding. After about 2 days in the first phase, the bacterial cells migrated from the regions presenting the polyol SAMs to the circular micropatterns presenting the methyl SAMs and start forming biofilm on these micropatterns. The formed biofilm then remained confined within the micropatterns that marked the second phase of biofilm formation on these patterned substrates.

Since we observed a racemic enhancement of bioinertness for both the aldonamide- and alditol-terminated alkanethiolate SAMs on gold (Au), I believe that this racemic enhancement might be a common feature among SAMs presenting chiral polyol. The enantiomeric, racemic and diastereisomeric polyol-terminated SAMs might be associated with a different and unique interfacial water structure, which translates into their bioinertness and contributes to the chiral discrimination observed during protein adsorption, mammalian cell adhesion and biofilm formation.

Transferring the bioinert properties of polyol SAMs from gold (Au) to native oxides of titanium (TiO_2)and iron oxide (Fe_3O_4)

Chapter 5 presents the synthesis of chiral polyol-terminated alkanephosphonic acids to form SAMs on surface of native metal oxides, particularly TiO_2 and Fe_3O_4. Preliminary results on the ability of these polyol SAMs on TiO_2 to resist the adhesion of mammalian cells (Swiss 3T3 albino fibroblasts) were withheld prior to more careful evaluation of the TiO_2 surface, whereas data were presented on the ability of these polyol SAMs on Fe_3O_4

to solubilize Fe_3O_4 (magnetite) nanoparticles in aqueous media. I synthesized three chiral polyol-terminated alkanephosphonic acids that terminated in the sugar alcohols D-mannitol, L-mannitol and D-gulitol with the aim of forming alkanephosphonate SAMs on TiO_2 and Fe_3O_4. Alkanephosphonic acids are common coatings for surface of native metal oxide or alloys such as iron,[44] steel,[45] aluminum,[45-46] copper[45] and even mica.[48] While mammalian cell adhesion is undesirable for certain titanium based medical implants such a cardiovascular implants,[190] it is highly desirable for titanium based bone implants for better osseointegration.[191] The polyol-terminated alkanephosphonic acids can be used to form SAMs on the surface of TiO_2 to evaluate the ability of the polyol SAMs to resist the adhesion of mammalian cells. Titanium is desirable as a material for studying tissue biomaterial interaction since titanium is comparatively cheaper than gold and combines the light weight of aluminum and strength of steel. The ability to resist mammalian cell adhesion on titanium can be extremely beneficial in preventing infection and rejection associated with certain titanium based medical implants. Further work to characterize the SAM modified TiO_2 surface will be necessary prior to interpreting the results with polyol SAMs on this important surface.

I also used the D-gulitol-terminated alkanephosphonic acid to synthesize D-gulitol modified magnetite nanoparticles (D-GPA MNPs), to study the solubility and stability of these modified nanoparticles in water. The D-gulitol alkanephosphonic acid modified magnetite nanoparticles (D-GPA MNPs) were found to be soluble and stable towards agglomeration in water as compared to the unmodified magnetite nanoparticles (MNPs).

Future work for polyol-terminated alkanethiolate SAMs:

Although I observed a racemic enhancement of bioinertness for the chiral polyol-terminated SAMs, it would be interesting to note if combinations other than 1:1 mixtures of the enantiomeric polyol-terminated alkanethiols in such SAMs can exhibit an enhancement in bioinertness. Here, I would like to acknowledge Professor James Kallmerten (PhD defense committee member) for suggesting the use of scalemic mixtures of the synthesized polyol-terminated alkanethiols to fabricate SAMs on gold (Au) and investigate their resistance to protein adsorption, mammalian cell adhesion and biofilm formation relative to both enentiomeric and racemic SAMs.

Future work for polyol-terminated alkanephosphonate SAM modified magnetite nanoparticles:

Water-soluble magnetite nanoparticles have applications in magnetic resonance imaging (MRI), drug delivery and hyperthermia. These water-soluble D-GPA MNPs can be functionalized with targeting ligands or antibodies and can have potential application in targeted drug delivery and magnetic resonance imaging. Further characterization of the D-GPA MNPs using thermo gravimetric analysis (TGA), infrared (IR) analysis can be conducted to confirm the presence of the alkenphosphonate SAMs on the surface of these nanoparticles.

Controlling Biofilm Formation by Molecular Inhibition

Another approach of controlling biofilm formation is to develop inhibitors for a class of organic molecules called autoinducers, which are responsible for regulating bacterial group behavior such as biofilm formation.[8] Chapter 6 reports the synthesis of derivatives

of a class of molecules called brominated furanones, which are known to inhibit biofilm formation in *E. coli.* These brominated furanone compounds are considered structural mimics of two classes of signaling molecules, which are associated with quorum sensing in gram-negative bacteria such as *E. coli*. Among the two kinds of signaling molecules, one class of signaling molecules are referred to as autoinducer-1 (AI-1) or acylated homoserine lactones (AHLs) and the other class of signaling molecules are referred to as autoinducer-2 (AI-2) or borate complexes or derivatives of 4,5-dihydroxy-2,3-pentanedione.[8, 87]

Immobilizing brominated furanones covalently on surfaces is one viable approach for controlling biofilm formation on surfaces[226-227] But the reported covalent immobilization chemistry involves radicals and might cause loss of the active structure of the furanones.[160] Moreover, the brominated furanones need to be internalized within the bacterial cells so they can bind and inhibit the quorum sensing proteins. Hence, I hypothesize to synthesize adamanatane derivatives of brominated furanones, which can be non-covalently encapsulated within porous hydrogel materials containing pendent beta-cyclodextrin (βCD) groups.[233] This hydrogel material has the potential of being used as a general antifouling coat for a wide variety of surfaces. With this aim, I synthesized two adamantane tethered brominated furanones and found that the compounds alone could inhibit biofilm formation by the bacterium *E. coli* by up to ~40% at 200 μM. The synthesized adamantane tethered brominated furanones were found to be non-toxic to *E. coli* at 200 μM and their biofilm inhibitory activity compared well to the inhibitory activity exhibited by brominated furanones reported in the literature.[160]

Chapter 7 reports the synthesis of a new library of novel squarate based molecules named squarylated homoserine lactones (SHLs),[88] which are structural mimics of the bacterial autoinducer molecules called AHLs. The synthesized SHLs were found to be non-toxic to *E. coli* at 200 μM and were able to exhibit inhibition of biofilm formation by the bacterium ranging from 30-40%.

Future work for controlling biofouling by molecular inhibition:

Hydrogel materials can be fabricated to non-covalently encapsulate the adamantane tethered brominated furanones, which can then be tested for their ability to inhibit biofilm formation on a model surface such as glass or steel.

Preliminary investigation (results not included) has indicated that the synthesized library of SHLs exhibit no cytotoxicity towards mammalian cells (Swiss 3T3 albino fibroblasts) at 200 μM, hence these SHLs are promising drug candidates for biofilm related infections.

References

1. Banerjee, I.; Pangule, R. C.; Kane, R. S., Antifouling Coatings: Recent Developments in the Design of Surfaces That Prevent Fouling by Proteins, Bacteria, and Marine Organisms. *Adv. Mater.* **2011,** 23, 690-718.

2. Magnani, A.; Peluso, G.; Margarucci, S.; Chittur, K. K., Protein adsorption and cellular/tissue interactions. *Integr. Biomater. Sci.* **2002**, 669-689.

3. Mrksich, M.; Whitesides, G. M., Using self-assembled monolayers to understand the interactions of man-made surfaces with proteins and cells. *Annu. Rev. Biophys. Biomol. Struct.* **1996,** 25, 55-78.

4. Anderson, J. M., Biological responses to materials. *Annu. Rev. Mater. Res.* **2001,** 31, 81-110.

5. Costerton, J. W.; Lewandowski, Z.; Caldwell, D. E.; Korber, D. R.; Lappin-Scott, H. M., Microbial biofilms. *Annu. Rev. Microbiol.* **1995,** 49, 711-45.

6. Costerton, J. W.; Stewart, P. S.; Greenberg, E. P., Bacterial biofilms: a common cause of persistent infections. *Science* **1999,** 284, 1318-1322.

7. Geske, G. D.; O'Neill, J. C.; Blackwell, H. E., Expanding dialogues: From natural autoinducers to non-natural analogs that modulate quorum sensing in Gram-negative bacteria. *Chem. Soc. Rev.* **2008,** 37, 1432-1447.

8. Galloway, W. R. J. D.; Hodgkinson, J. T.; Bowden, S. D.; Welch, M.; Spring, D. R., Quorum sensing in Gram-negative bacteria: Small molecule modulation of AHL and AI-2 quorum sensing pathways. *Chem. Rev.* **2011,** 111, 28-67.

9. Adamson, A. W.; Gast, A. P.; Editors, *Physical Chemistry of Surfaces, Sixth Edition*. Wiley-Interscience: New York, 1997; p 784 pp.

10. Israelachvili, J.; Wennerstrom, H., Role of hydration and water structure in biological and colloidal interactions. *Nature* **1996,** 379, 219-25.

11. Nandi, N.; Bhattacharyya, K.; Bagchi, B., Dielectric Relaxation and Solvation Dynamics of Water in Complex Chemical and Biological Systems. *Chem. Rev.* **2000,** 100, 2013-2045.

12. Ramsden, J. J., Puzzles and paradoxes in protein adsorption. *Chem. Soc. Rev.* **1995,** 24, 73-8.

13. Haynes, C. A.; Sliwinsky, E.; Norde, W., Structural and electrostatic properties of globular proteins at a polystyrene-water interface. *J. Colloid Interface Sci.* **1994,** 164, 394-9.

14. Lee, Y.-S.; Mrksich, M., Protein chips, from concept to practice. *Trends Biotechnol.* **2002,** 20, S14-S18.

15. Zhu, H.; Snyder, M., Protein chip technology. *Curr. Opin. Chem. Biol.* **2003,** 7, 55-63.

16. Houseman, B. T.; Huh, J. H.; Kron, S. J.; Mrksich, M., Peptide chips for the quantitative evaluation of protein kinase activity. *Nat. Biotechnol.* **2002,** 20, 270-274.

17. Kononen, J.; Bubendorf, L.; Kallioneimi, A.; Barlund, M.; Schraml, P.; Leighton, S.; Torhorst, J.; Mihatsch, M.; Suater, G.; Kallioneimi, O.-P., Tissue microarrays for high-throughput molecular profiling of tumor specimens. *Nat. Med.* **1998,** 4, 844-847.

18. Stoodley, P.; Sauer, K.; Davies, D. G.; Costerton, J. W., Biofilms as complex differentiated communities. *Annu. Rev. Microbiol.* **2002,** 56, 187-209.

19. Sauer, K.; Camper, A. K.; Ehrlich, G. D.; Costerton, J. W.; Davies, D. G., Pseudomonas aeruginosa displays multiple phenotypes during development as a biofilm. *J. Bacteriol.* **2002,** 184, 1140-1154.

20. Deziel, E.; Comeau, Y.; Villemur, R., Initiation of biofilm formation by Pseudomonas aeruginosa 57RP correlates with emergence of hyperpiliated and highly adherent phenotypic variants deficient in swimming, swarming, and twitching motilities. *J. Bacteriol.* **2001,** 183, 1195-1204.

21. Lawrence, J. R.; Korber, D. R.; Hoyle, B. D.; Costerton, J. W.; Caldwell, D. E., Optical sectioning of microbial biofilms. *J. Bacteriol.* **1991,** 173, 6558-67.

22. de Beer, D.; Stoodley, P.; Lewandowski, Z., Liquid flow in heterogeneous biofilms. *Biotechnol. Bioeng.* **1994,** 44, 636-41.

23. Hall-Stoodley, L.; Costerton, J. W.; Stoodley, P., Bacterial biofilms: From the natural environment to infectious diseases. *Nat. Rev. Microbiol.* **2004,** 2, 95-108.

24. Parsek, M. R.; Singh, P. K., Bacterial biofilms: An emerging link to disease pathogenesis. *Annu. Rev. Microbiol.* **2003,** 57, 677-701.

25. Coetser, S. E.; Cloete, T. E., Biofouling and biocorrosion in industrial water systems. *Crit. Rev. Microbiol.* **2005,** 31, 213-232.

26. Ward, K. H.; Olson, M. E.; Lam, K.; Costerton, J. W., Mechanism of persistent infection associated with peritoneal implants. *J. Med. Microbiol.* **1992,** 36, 406-13.

27. Mrksich, M.; Whitesides, G. M., Using self-assembled monolayers that present oligo(ethylene glycol) groups to control the interactions of proteins with surfaces. *ACS Symposium Series* **1997,** 680, 361-373.

28. Prime, K. L.; Whitesides, G. M., Self-assembled organic monolayers: model systems for studying adsorption of proteins at surfaces. *Science* **1991,** 252, 1164-7.

29. Chen, C. S.; Mrksich, M.; Huang, S.; Whitesides, G. M.; Ingber, D. E., Geometric control of cell life and death. *Science* **1997,** 276, 1425-1428.

30. Gupta, V. K.; Skaife, J. J.; Dubrovsky, T. B.; Abbott, N. L., Optical amplification of ligand-receptor binding using liquid crystals. *Science* **1998,** 279, 2077-2080.

31. Simon, K. A.; Burton, E. A.; Han, Y.; Li, J.; Huang, A.; Luk, Y.-Y., Enhancing Cell Adhesion and Confinement by Gradient Nanotopography. *J. Am. Chem. Soc.* **2007,** 129, 4892-4893.

32. Gupta, V. K.; Abbott, N. L., Self-Assembled Monolayers Formed from Alkanethiols on Obliquely Deposited Films of Gold as Uniform Anchors of Nematic Liquid Crystalline Phases. *Langmuir* **1996,** 12, 2587-93.

33. Skaife, J. J.; Abbott, N. L., Quantitative Characterization of Obliquely Deposited Substrates of Gold by Atomic Force Microscopy: Influence of Substrate Topography on Anchoring of Liquid Crystals. *Chem. Mater.* **1999,** 11, 612-623.

34. Laibinis, P. E.; Whitesides, G. M.; Allara, D. L.; Tao, Y. T.; Parikh, A. N.; Nuzzo, R. G., Comparison of the structures and wetting properties of self-assembled monolayers of n-alkanethiols on the coinage metal surfaces, copper, silver, and gold. *J. Am. Chem. Soc.* **1991,** 113, 7152-67.

35. Walczak, M. M.; Chung, C.; Stole, S. M.; Widrig, C. A.; Porter, M. D., Structure and interfacial properties of spontaneously adsorbed n-alkanethiolate monolayers on evaporated silver surfaces. *J. Am. Chem. Soc.* **1991,** 113, 2370-8.

36. Nuzzo, R. G.; Allara, D. L., Adsorption of bifunctional organic disulfides on gold surfaces. *J. Am. Chem. Soc.* **1983,** 105, 4481-3.

37. Porter, M. D.; Bright, T. B.; Allara, D. L.; Chidsey, C. E. D., Spontaneously organized molecular assemblies. 4. Structural characterization of n-alkyl thiol monolayers on gold by optical ellipsometry, infrared spectroscopy, and electrochemistry. *J. Am. Chem. Soc.* **1987,** 109, 3559-68.

38. Bain, C. D.; Whitesides, G. M., Molecular-level control over surface order in self-assembled monolayer films of thiols on gold. *Science* **1988,** 240, 62-3.

39. Love, J. C.; Estroff, L. A.; Kriebel, J. K.; Nuzzo, R. G.; Whitesides, G. M., Self-Assembled Monolayers of Thiolates on Metals as a Form of Nanotechnology. *Chem. Rev.* **2005,** 105, 1103-1169.

40. Muskal, N.; Turyan, I.; Mandler, D., Self-assembled monolayers on mercury surfaces. *J. Electroanal. Chem.* **1996,** 409, 131-136.

41. Li, Z.; Chang, S.-C.; Williams, R. S., Self-Assembly of Alkanethiol Molecules onto Platinum and Platinum Oxide Surfaces. *Langmuir* **2003,** 19, 6744-6749.

42. Carvalho, A.; Geissler, M.; Schmid, H.; Michel, B.; Delamarche, E., Self-assembled monolayers of eicosanethiol on palladium and their use in microcontact printing. *Langmuir* **2002,** 18, 2406-2412.

43. Love, J. C.; Wolfe, D. B.; Haasch, R.; Chabinyc, M. L.; Paul, K. E.; Whitesides, G. M.; Nuzzo, R. G., Formation and Structure of Self-Assembled Monolayers of Alkanethiolates on Palladium. *J. Am. Chem. Soc.* **2003,** 125, 2597-2609.

44. Felhosi, I.; Keresztes, Z.; Kalman, E., Surface modification of iron by self-assembly of phosphonates. *Proc. - Electrochem. Soc.* **2001,** 2001-22, 386-392.

45. Van Alsten, J. G., Self-Assembled Monolayers on Engineering Metals: Structure, Derivatization, and Utility. *Langmuir* **1999,** 15, 7605-7614.

46. Gao, W.; Dickinson, L.; Grozinger, C.; Morin, F. G.; Reven, L., Self-Assembled Monolayers of Alkylphosphonic Acids on Metal Oxides. *Langmuir* **1996,** 12, 6429-6435.

47. Gawalt, E. S.; Avaltroni, M. J.; Koch, N.; Schwartz, J., Self-Assembly and Bonding of Alkanephosphonic Acids on the Native Oxide Surface of Titanium. *Langmuir* **2001,** 17, 5736-5738.

48. Woodward, J. T.; Schwartz, D. K., In Situ Observation of Self-Assembled Monolayer Growth. *J. Am. Chem. Soc.* **1996,** 118, 7861-7862.

49. Kane, R. S.; Takayama, S.; Ostuni, E.; Ingber, D. E.; Whitesides, G. M., Patterning proteins and cells using soft lithography. *Biomaterials* **1999,** 20, 2363-2376.

50. Dubois, L. H.; Nuzzo, R. G., Synthesis, structure, and properties of model organic surfaces. *Annu. Rev. Phys. Chem.* **1992,** 43, 437-63.

51. Semaltianos, N. G.; Wilson, E. G., Investigation of the surface morphology of thermally evaporated thin gold films on mica, glass, silicon and calcium fluoride substrates by scanning tunneling microscopy. *Thin Solid Films* **2000,** 366, 111-116.

52. Skaife, J. J.; Brake, J. M.; Abbott, N. L., Influence of Nanometer-Scale Topography of Surfaces on the Orientational Response of Liquid Crystals to Proteins Specifically Bound to Surface-Immobilized Receptors. *Langmuir* **2001,** 17, 5448-5457.

53. Nuzzo, R. G.; Zegarski, B. R.; Dubois, L. H., Fundamental studies of the chemisorption of organosulfur compounds on gold(111). Implications for molecular self-assembly on gold surfaces. *J. Am. Chem. Soc.* **1987,** 109, 733-40.

54. Fischer, D.; Curioni, A.; Andreoni, W., Decanethiols on Gold: The Structure of Self-Assembled Monolayers Unraveled with Computer Simulations. *Langmuir* **2003,** 19, 3567-3571.

55. Bain, C. D.; Troughton, E. B.; Tao, Y. T.; Evall, J.; Whitesides, G. M.; Nuzzo, R. G., Formation of monolayer films by the spontaneous assembly of organic thiols from solution onto gold. *J. Am. Chem. Soc.* **1989,** 111, 321-35.

56. Yang, G.; Amro, N. A.; Starkewolfe, Z. B.; Liu, G.-y., Molecular-Level Approach To Inhibit Degradations of Alkanethiol Self-Assembled Monolayers in Aqueous Media. *Langmuir* **2004,** 20, 3995-4003.

57. Schlenoff, J. B.; Li, M.; Ly, H., Stability and Self-Exchange in Alkanethiol Monolayers. *J. Am. Chem. Soc.* **1995,** 117, 12528-36.

58. Zhong, C.-J.; Woods, N. T.; Dawson, G. B.; Porter, M. D., Formation of thiol-based monolayers on gold: implications from open circuit potential measurements. *Electrochem. Commun.* **1999,** 1, 17-21.

59. Hasan, M.; Bethell, D.; Brust, M., The Fate of Sulfur-Bound Hydrogen on Formation of Self-Assembled Thiol Monolayers on Gold: 1H NMR Spectroscopic Evidence from Solutions of Gold Clusters. *J. Am. Chem. Soc.* **2002,** 124, 1132-1133.

60. Andreoni, W.; Curioni, A.; Gronbeck, H., Density functional theory approach to thiols and disulfides on gold. Au(111) surface and clusters. *Int. J. Quantum Chem.* **2000,** 80, 598-608.

61. Drawhorn, R. A.; Abbott, N. L., Anchoring of Nematic Liquid Crystals on Self-Assembled Monolayers Formed from Alkanethiols on Semitransparent Films of Gold. *J. Phys. Chem.* **1995,** 99, 16511-15.

62. Gupta, V. K.; Miller, W. J.; Pike, C. L.; Abbott, N. L., Using Isotropic, Nematic, and Smectic Fluids for the Study of Self-Assembled Monolayers Formed from Alkanethiols on Gold. *Chem. Mater.* **1996,** 8, 1366-1369.

63. Wilderbeek, H. T. A.; Van der Meer, F. J. A.; Feldman, K.; Broer, D. J.; Bastiaansen, C. W. M., Alignment of liquid crystals on self-assembled monolayers using ultra-thin gold films. *Adv. Mater.* **2002,** 14, 655-658.

64. Gupta, V. K.; Abbott, N. L., Azimuthal anchoring transition of nematic liquid crystals on self-assembled monolayers formed from odd and even alkanethiols. *Phys. Rev. E Stat. Phys., Plasmas, Fluids, Relat. Interdiscip. Top.* **1996,** 54, R4540-R4543.

65. Gupta, V. K.; Abbott, N. L., Design of surfaces for patterned alignment of liquid crystals on planar and curved substrates. *Science* **1997,** 276, 1533-1536.

66. Follonier, S.; Miller, W. J. W.; Abbott, N. L.; Knoesen, A., Characterization of the molecular orientation of self-assembled monolayers of alkanethiols on obliquely

deposited gold films by using infrared-visible sum-frequency spectroscopy. *Langmuir* **2003,** 19, 10501-10509.

67. Mrksich, M.; Sigal, G. B.; Whitesides, G. M., Surface Plasmon Resonance Permits in Situ Measurement of Protein Adsorption on Self-Assembled Monolayers of Alkanethiolates on Gold. *Langmuir* **1995,** 11, 4383-5.

68. Bandyopadhyay, D.; Prashar, D.; Luk, Y.-Y., Anti-Fouling Chemistry of Chiral Monolayers: Enhancing Biofilm Resistance on Racemic Surface. *Langmuir* **2011,** 27, 6124-6131.

69. Bandyopadhyay, D.; Prashar, D.; Luk, Y.-Y., Stereochemical effects of chiral monolayers on enhancing the resistance to mammalian cell adhesion. *Chem. Commun.* **2011,** 47, 6165-6167.

70. Prime, K. L.; Whitesides, G. M., Adsorption of proteins onto surfaces containing end-attached oligo(ethylene oxide): a model system using self-assembled monolayers. *J. Am. Chem. Soc.* **1993,** 115, 10714-21.

71. Xia, Y.; Whitesides, G. M., Soft lithography. *Angew. Chem., Int. Ed.* **1998,** 37, 550-575.

72. Choi, K. M.; Rogers, J. A., A Photocurable Poly(dimethylsiloxane) Chemistry Designed for Soft Lithographic Molding and Printing in the Nanometer Regime. *J. Am. Chem. Soc.* **2003,** 125, 4060-4061.

73. Clarson, S. J.; Semlyen, J. A., *Siloxane Polymers*. Prentice Hall: Englewood Cliffs, NJ, 1993; p 673 pp.

74. Luk, Y.-Y.; Kato, M.; Mrksich, M., Self-Assembled Monolayers of Alkanethiolates Presenting Mannitol Groups Are Inert to Protein Adsorption and Cell Attachment. *Langmuir* **2000,** 16, 9604-9608.

75. Hou, S.; Burton, E. A.; Simon, K. A.; Blodgett, D.; Luk, Y.-Y.; Ren, D., Inhibition of Escherichia coli biofilm formation by self-assembled monolayers of functional alkanethiols on gold. *Appl. Environ. Microbiol.* **2007,** 73, 4300-4307.

76. Hou, S.; Burton, E. A.; Wu, R. L.; Luk, Y.-Y.; Ren, D., Prolonged control of patterned biofilm formation by bio-inert surface chemistry. *Chem. Commun.* **2009**, 1207-1209.

77. Hynes, R. O., Integrins: versatility, modulation, and signaling in cell adhesion. *Cell* **1992,** 69, 11-25.

78. Ruoslahti, E.; Pierschbacher, M. D., New perspectives in cell adhesion: RGD and integrins. *Science* **1987,** 238, 491-7.

79. Banerjee, I.; Pangule, R. C.; Kane, R. S., Antifouling Coatings: Recent Developments in the Design of Surfaces That Prevent Fouling by Proteins, Bacteria, and Marine Organisms. *Adv. Mater.* **2011,** 23, 690-718.

80. Ostuni, E.; Chapman, R. G.; Liang, M. N.; Meluleni, G.; Pier, G.; Ingber, D. E.; Whitesides, G. M., Self-assembled monolayers that resist the adsorption of proteins and the adhesion of bacterial and mammalian cells. *Langmuir* **2001,** 17, 6336-6343.

81. Wei, J.; Ravn, D. B.; Gram, L.; Kingshott, P., Stainless steel modified with poly(ethylene glycol) can prevent protein adsorption but not bacterial adhesion. *Colloids Surf., B* **2003,** 32, 275-291.

82. Roosjen, A.; van der Mei, H. C.; Busscher, H. J.; Norde, W., Microbial Adhesion to Poly(ethylene oxide) Brushes: Influence of Polymer Chain Length and Temperature. *Langmuir* **2004,** 20, 10949-10955.

83. Zhao, Y.-H.; Zhu, X.-Y.; Wee, K.-H.; Bai, R., Achieving Highly Effective Non-biofouling Performance for Polypropylene Membranes Modified by UV-Induced Surface Graft Polymerization of Two Oppositely Charged Monomers. *J. Phys. Chem. B* **2010,** 114, 2422-2429.

84. Hanein, D.; Geiger, B.; Addadi, L., Differential adhesion of cells to enantiomorphous crystal surfaces. *Science* **1994,** 263, 1413-16.

85. Sun, T.; Han, D.; Rhemann, K.; Chi, L.; Fuchs, H., Stereospecific Interaction between Immune Cells and Chiral Surfaces. *J. Am. Chem. Soc.* **2007,** 129, 1496-1497.

86. Mrksich, M.; Whitesides, G. M., Using self-assembled monolayers to understand the interactions of man-made surfaces with proteins and cells. *Annu. Rev. Biophys. Biomol. Struct.* **1996,** 25, 55-78.

87. Waters, C. M.; Bassler, B. L., Quorum sensing: Cell-to-cell communication in bacteria. *Annu. Rev. Cell Dev. Biol.* **2005,** 21, 319-346.

88. Narasimhan, S. K. Structured unnatural molecules: Inducing molecular folding, enabling matured mammalian cell adhesion and inhibiting bacterial biofilm formation. Syracuse University, Syracuse, 2010.

89. Harder, P.; Grunze, M.; Dahint, R.; Whitesides, G. M.; Laibinis, P. E., Molecular Conformation in Oligo(ethylene glycol)-Terminated Self-Assembled Monolayers on

Gold and Silver Surfaces Determines Their Ability To Resist Protein Adsorption. *J. Phys. Chem. B* **1998,** 102, 426-436.

90. Feldman, K.; Haehner, G.; Spencer, N. D.; Harder, P.; Grunze, M., Probing Resistance to Protein Adsorption of Oligo(ethylene glycol)-Terminated Self-Assembled Monolayers by Scanning Force Microscopy. *J. Am. Chem. Soc.* **1999,** 121, 10134-10141.

91. Chapman, R. G.; Ostuni, E.; Takayama, S.; Holmlin, R. E.; Yan, L.; Whitesides, G. M., Surveying for Surfaces that Resist the Adsorption of Proteins. *J. Am. Chem. Soc.* **2000,** 122, 8303-8304.

92. Luk, Y.-Y. I. Bio-inertness and stereochemical control of cell adhesion on chiral surfaces and II. Surface chemistry of self-assembled monolayers and nano-colloids. Ph.D. Thesis, University of Chicago, Chicago, 2001.

93. Chapman, R. G.; Ostuni, E.; Liang, M. N.; Meluleni, G.; Kim, E.; Yan, L.; Pier, G.; Warren, H. S.; Whitesides, G. M., Polymeric Thin Films That Resist the Adsorption of Proteins and the Adhesion of Bacteria. *Langmuir* **2001,** 17, 1225-1233.

94. Holmlin, R. E.; Chen, X.; Chapman, R. G.; Takayama, S.; Whitesides, G. M., Zwitterionic SAMs that Resist Nonspecific Adsorption of Protein from Aqueous Buffer. *Langmuir* **2001,** 17, 2841-2850.

95. Ostuni, E.; Chapman, R. G.; Holmlin, R. E.; Takayama, S.; Whitesides, G. M., A Survey of Structure-Property Relationships of Surfaces that Resist the Adsorption of Protein. *Langmuir* **2001,** 17, 5605-5620.

96. Kane, R. S.; Deschatelets, P.; Whitesides, G. M., Kosmotropes Form the Basis of Protein-Resistant Surfaces. *Langmuir* **2003,** 19, 2388-2391.

97. Jiang, S.; Cao, Z., Ultralow-Fouling, Functionalizable, and Hydrolyzable Zwitterionic Materials and Their Derivatives for Biological Applications. *Adv. Mater.* **2010,** 22, 920-932.

98. Zhang, Y.; Cremer, P. S., Chemistry of hofmeister anions and osmolytes. *Annu. Rev. Phys. Chem.* **2010,** 61, 63-83.

99. Kunz, W.; Henle, J.; Ninham, B. W., 'Zur Lehre von der Wirkung der Salze' (About the science of the effect of salts): Franz Hofmeister's historical papers. *Curr. Opin. Colloid Interface Sci.* **2004,** 9, 19-37.

100. Collins, K. D., Ions from the Hofmeister series and osmolytes: effects on proteins in solution and in the crystallization process. *Methods* **2004,** 34, 300-311.

101. Vrbka, L.; Vondrasek, J.; Jagoda-Cwiklik, J.; Vacha, R.; Jungwirth, P., Quantification and rationalization of the higher affinity of sodium over potassium to protein surfaces. *Proc. Natl. Acad. Sci. U. S. A.* **2006,** 103, 15440-15444.

102. Uejio, J. S.; Schwartz, C. P.; Duffin, A. M.; Drisdell, W. S.; Cohen, R. C.; Saykally, R. J., Characterization of selective binding of alkali cations with carboxylate by x-ray absorption spectroscopy of liquid microjets. *Proc. Natl. Acad. Sci. U. S. A.* **2008,** 105, 6809-6812.

103. Zhang, Y.; Cremer, P. S., The inverse and direct Hofmeister series for lysozyme. *Proc. Natl. Acad. Sci. U. S. A.* **2009,** 106, 15249-15253.

104. Gekko, K.; Timasheff, S. N., Mechanism of protein stabilization by glycerol: preferential hydration in glycerol-water mixtures. *Biochemistry* **1981,** 20, 4667-76.

105. Lee, J. C.; Timasheff, S. N., The stabilization of proteins by sucrose. *J. Biol. Chem.* **1981,** 256, 7193-201.

106. Herberhold, H.; Royer, C. A.; Winter, R., Effects of Chaotropic and Kosmotropic Cosolvents on the Pressure-Induced Unfolding and Denaturation of Proteins: An FT-IR Study on Staphylococcal Nuclease. *Biochemistry* **2004,** 43, 3336-3345.

107. Seraydarian, K.; Mommaerts, W. F., Density gradient separation of sarcotubular vesicles and other particulate constituents of rabbit muscle. *J. Cell Biol.* **1965,** 26, 641-56.

108. Wang, R. L. C.; Kreuzer, H. J.; Grunze, M., Molecular Conformation and Solvation of Oligo(ethylene glycol)-Terminated Self-Assembled Monolayers. *J. Phys. Chem. B* **1997,** 101, 9767-9773.

109. Hower, J. C.; He, Y.; Bernards, M. T.; Jiang, S., Understanding the nonfouling mechanism of surfaces through molecular simulations of sugar-based self-assembled monolayers. *J. Chem. Phys.* **2006,** 125, 214704/1-214704/7.

110. Hower, J. C.; He, Y.; Jiang, S., A molecular simulation study of methylated and hydroxyl sugar-based self-assembled monolayers: Surface hydration and resistance to protein adsorption. *J. Chem. Phys.* **2008,** 129, 215101/1-215101/7.

111. Chen, S.; Li, L.; Zhao, C.; Zheng, J., Surface hydration: Principles and applications toward low-fouling/nonfouling biomaterials. *Polymer* **2010,** 51, 5283-5293.

112. Pinto, B. M.; Liu, H., Design and synthesis of selenonium and sulfonium ions related to the naturally occurring glucosidase inhibitor salacinol. *Can. J. Chem.* **2006,** 84, 1351-1362.

113. Bjerknes, R., Neutrophil phagocytosis: influence of opsonins, neutrophil activation, and microbial characteristics. *Phagocyte Funct.* **1998**, 187-216.

114. Coleman, D. L., Regulation of macrophage phagocytosis. *Eur. J. Clin. Microbiol.* **1986,** 5, 1-5.

115. Saba, T. M.; Di Luzio, N. R., Comparative evaluation of the influence of opsonins on hepatic, spenic, and pulmonary phagocytosis. *Proc. Soc. Exp. Biol. Med.* **1967,** 125, 630-3.

116. Vanzi, F.; Madan, B.; Sharp, K., Effect of the Protein Denaturants Urea and Guanidinium on Water Structure: A Structural and Thermodynamic Study. *J. Am. Chem. Soc.* **1998,** 120, 10748-10753.

117. Xu, C.; Ng, S. C.; Chan, H. S. O., Self-assembly of perfunctionalized beta -cyclodextrins on a quartz crystal microbalance for real-time chiral recognition. *Langmuir* **2008,** 24, 9118-9124.

118. Pale-Grosdemange, C.; Simon, E. S.; Prime, K. L.; Whitesides, G. M., Formation of self-assembled monolayers by chemisorption of derivatives of oligo(ethylene glycol) of structure HS(CH2)11(OCH2CH2)mOH on gold. *J. Am. Chem. Soc.* **1991,** 113, 12-20.

119. Noelken, M. E.; Timasheff, S. N., Preferential solvation of bovine serum albumin in aqueous guanidine hydrochloride. *J. Biol. Chem.* **1967,** 242, 5080-5.

120. Reisler, E.; Haik, Y.; Eisenberg, H., Bovine serum albumin in aqueous guanidine hydrochloride solutions. Preferential and absolute interactions and comparison with other systems. *Biochemistry* **1977,** 16, 197-203.

121. Simpson, R. B.; Kauzmann, W., Kinetics of protein denaturation. I. Behavior of the optical rotation of ovalbumin in urea solutions. *J. Am. Chem. Soc.* **1953,** 75, 5139-52.

122. Tanford, C., Isothermal unfolding of globular proteins in aqueous urea solutions. *J. Am. Chem. Soc.* **1964,** 86, 2050-9.

123. Chen, X.; Sagle, L. B.; Cremer, P. S., Urea orientation at protein surfaces. *J. Am. Chem. Soc.* **2007,** 129, 15104-15105.

124. Vanderah, D. J.; Vierling, R. J.; Walker, M. L., Oligo(ethylene oxide) Self-Assembled Monolayers with Self-Limiting Packing Densities for the Inhibition of Nonspecific Protein Adsorption. *Langmuir* **2009,** 25, 5026-5030.

125. Hanein, D.; Sabanay, H.; Addadi, L.; Geiger, B., Selective interactions of cells with crystal structures; implications for the mechanism of cell adhesion. *J. Cell Sci.* **1993,** 104, 275-88.

126. Fuhrhop, J. H.; Schnieder, P.; Boekema, E.; Helfrich, W., Lipid bilayer fibers from diastereomeric and enantiomeric N-octylaldonamides. *J. Am. Chem. Soc.* **1988,** 110, 2861-7.

127. Harrison, M. A.; Rae, I. F., *General Techniques of Cell culture*. 1st ed.; Cambridge University Press: Cambridge, 1997.

128. Porter, J. R., Antony van Leeuwenhoek: tercentenary of his discovery of bacteria. *Bacteriol Rev* **1976,** 40, 260-9.

129. Nealson, K. H.; Platt, T.; Hastings, J. W., Cellular control of the synthesis and activity of the bacterial luminescent system. *J. Bacteriol.* **1970,** 104, 313-22.

130. Eberhard, A.; Burlingame, A. L.; Eberhard, C.; Kenyon, G. L.; Nealson, K. H.; Oppenheimer, N. J., Structural identification of autoinducer of Photobacterium fischeri luciferase. *Biochemistry* **1981,** 20, 2444-9.

131. Camilli, A.; Bassler, B. L., Bacterial Small-Molecule Signaling Pathways. *Science* **2006,** 311, 1113-1116.

132. Liang, M. N.; Smith, S. P.; Metallo, S. J.; Choi, I. S.; Prentiss, M.; Whitesides, G. M., Measuring the forces involved in polyvalent adhesion of uropathogenic Escherichia coli to mannose-presenting surfaces. *Proc. Natl. Acad. Sci. U. S. A.* **2000,** 97, 13092-13096.

133. Habash, M.; Reid, G., Microbial biofilms: their development and significance for medical device-related infections. *J. Clin. Pharmacol.* **1999,** 39, 887-898.

134. McKenney, D.; Huebner, J.; Muller, E.; Wang, Y.; Goldmann, D. A.; Pier, G. B., The ica locus of Staphylococcus epidermidis encodes production of the capsular polysaccharide/adhesin. *Infect. Immun.* **1998,** 66, 4711-4720.

135. McKenney, D.; Pouliot, K. L.; Wang, Y.; Murthy, V.; Ulrich, M.; Doring, G.; Lee, J. C.; Goldmann, D. A.; Pier, G. B., Broadly protective vaccine for Staphylococcus aureus based on an in vivo-expressed antigen. *Science* **1999,** 284, 1523-1527.

136. Hudson, M. C.; Ramp, W. K.; Frankenburg, K. P., Staphylococcus aureus adhesion to bone matrix and bone-associated biomaterials. *FEMS Microbiol. Lett.* **1999,** 173, 279-284.

137. Joh, D.; Wann, E. R.; Kreikemeyer, B.; Speziale, P.; Hook, M., Role of fibronectin-binding MSCRAMMs in bacterial adherence and entry into mammalian cells. *Matrix Biol.* **1999,** 18, 211-223.

138. Burton, E. A.; Simon, K. A.; Hou, S.; Ren, D.; Luk, Y.-Y., Molecular Gradients of Bioinertness Reveal a Mechanistic Difference between Mammalian Cell Adhesion and Bacterial Biofilm Formation. *Langmuir* **2009,** 25, 1547-1553.

139. Govan, J. R.; Deretic, V., Microbial pathogenesis in cystic fibrosis: mucoid Pseudomonas aeruginosa and Burkholderia cepacia. *Microbiol Rev* **1996,** 60, 539-74.

140. Branda, S. S.; Vik, A.; Friedman, L.; Kolter, R., Biofilms: the matrix revisited. *Trends Microbiol.* **2005,** 13, 20-26.

141. Ryder, C.; Byrd, M.; Wozniak, D. J., Role of polysaccharides in Pseudomonas aeruginosa biofilm development. *Curr. Opin. Microbiol.* **2007,** 10, 644-648.

142. Matsukawa, M.; Greenberg, E. P., Putative exopolysaccharide synthesis genes influence Pseudomonas aeruginosa biofilm development. *J. Bacteriol.* **2004,** 186, 4449-4456.

143. Friedman, L.; Kolter, R., Two genetic loci produce distinct carbohydrate-rich structural components of the Pseudomonas aeruginosa biofilm matrix. *J. Bacteriol.* **2004,** 186, 4457-4465.

144. Jackson, K. D.; Starkey, M.; Kremer, S.; Parsek, M. R.; Wozniak, D. J., Identification of psl, a locus encoding a potential exopolysaccharide that is essential for Pseudomonas aeruginosa PAO1 biofilm formation. *J. Bacteriol.* **2004,** 186, 4466-4475.

145. Ma, L.; Jackson, K. D.; Landry, R. M.; Parsek, M. R.; Wozniak, D. J., Analysis of Pseudomonas aeruginosa conditional Psl variants reveals roles for the Psl polysaccharide in adhesion and maintaining biofilm structure postattachment. *J. Bacteriol.* **2006,** 188, 8213-8221.

146. Ma, L.; Conover, M.; Lu, H.; Parsek Matthew, R.; Bayles, K.; Wozniak Daniel, J., Assembly and development of the Pseudomonas aeruginosa biofilm matrix. *PLoS Pathog* **2009,** 5, e1000354.

147. Davies, D. G.; Parsek, M. R.; Pearson, J. P.; Iglewski, B. H.; Costerton, J. W.; Greenberg, E. P., The involvement of cell-to-cell signals in the development of a bacterial biofilm. *Science* **1998,** 280, 295-298.

148. Latifi, A.; Winson, M. K.; Foglino, M.; Bycroft, B. W.; Stewart, G. S. A. B.; Lazdunski, A.; Williams, P., Multiple homologs of LuxR and LuxI control expression of virulence determinants and secondary metabolites through quorum sensing in Pseudomonas aeruginosa PAO1. *Mol. Microbiol.* **1995,** 17, 333-43.

149. Passador, L.; Cook, J. M.; Gambello, M. J.; Rust, L.; Iglewski, B. H., Expression of Pseudomonas aeruginosa virulence genes requires cell-to-cell communication. *Science* **1993,** 260, 1127-30.

150. Ochsner, U. A.; Koch, A. K.; Fiechter, A.; Reiser, J., Isolation and characterization of a regulatory gene affecting rhamnolipid biosurfactant synthesis in Pseudomonas aeruginosa. *J. Bacteriol.* **1994,** 176, 2044-54.

151. Ochsner, U. A.; Reiser, J., Autoinducer-mediated regulation of rhamnolipid biosurfactant synthesis in Pseudomonas aeruginosa. *Proc. Natl. Acad. Sci. U. S. A.* **1995,** 92, 6424-8.

152. Gambello, M. J.; Iglewski, B. H., Cloning and characterization of the Pseudomonas aeruginosa lasR gene, a transcriptional activator of elastase expression. *J. Bacteriol.* **1991,** 173, 3000-9.

153. Pearson, J. P.; Gray, K. M.; Passador, L.; Tucker, K. D.; Eberhard, A.; Iglewski, B. H.; Greenberg, E. P., Structure of the autoinducer required for expression of Pseudomonas aeruginosa virulence genes. *Proc. Natl. Acad. Sci. U. S. A.* **1994,** 91, 197-201.

154. Pesci, E.; Pearson, J. P.; Seed, P. C.; Iglewski, B. H., Regulation of las and rhl quorum sensing in Pseudomonas aeruginosa. *J. Bacteriol.* **1997,** 179, 3127-3132.

155. Pesci, E. C.; Iglewski, B. H., The chain of command in Pseudomonas quorum sensing. *Trends Microbiol.* **1997,** 5, 132-4; discussion 134-5.

156. Latifi, A.; Foglino, M.; Tanaka, K.; Williams, P.; Lazdunski, A., A hierarchical quorum-sensing cascade in Pseudomonas aeruginosa links the transcriptional activators LasR and RhlR (VsmR) to expression of the stationary-phase sigma factor RpoS. *Mol. Microbiol.* **1996,** 21, 1137-1146.

157. Nickel, J. C.; Ruseska, I.; Wright, J. B.; Costerton, J. W., Tobramycin resistance of Pseudomonas aeruginosa cells growing as a biofilm on urinary catheter material. *Antimicrob. Agents Chemother.* **1985,** 27, 619-24.

158. Cochrane, D. M. G.; Brown, M. R. W.; Anwar, H.; Weller, P. H.; Lam, K.; Costerton, J. W., Antibody response to Pseudomonas aeruginosa surface protein antigens in a rat model of chronic lung infection. *J. Med. Microbiol.* **1988,** 27, 255-61.

159. Geske, G. D.; O'Neill, J. C.; Miller, D. M.; Mattmann, M. E.; Blackwell, H. E., Modulation of bacterial quorum sensing with synthetic ligands: Systematic evaluation of N-acylated homoserine lactones in multiple species and new insights into their mechanisms of action. *J. Am. Chem. Soc.* **2007,** 129, 13613-13625.

160. Han, Y.; Hou, S.; Simon, K. A.; Ren, D.; Luk, Y.-Y., Identifying the important structural elements of brominated furanones for inhibiting biofilm formation by Escherichia coli. *Bioorg. Med. Chem. Lett.* **2008,** 18, 1006-1010.

161. Lowery, C. A.; Abe, T.; Park, J.; Eubanks, L. M.; Sawada, D.; Kaufmann, G. F.; Janda, K. D., Revisiting AI-2 Quorum Sensing Inhibitors: Direct Comparison of Alkyl-DPD Analogues and a Natural Product Fimbrolide. *J. Am. Chem. Soc.* **2009,** 131, 15584-15585.

162. Richards, J. J.; Melander, C., Controlling bacterial biofilms. *ChemBioChem* **2009,** 10, 2287-2294.

163. Rogers, S. A.; Huigens, R. W., III; Melander, C., A 2-Aminobenzimidazole That Inhibits and Disperses Gram-Positive Biofilms through a Zinc-Dependent Mechanism. *J. Am. Chem. Soc.* **2009,** 131, 9868-9869.

164. Davies, D. G.; Marques, C. N. H., A fatty acid messenger is responsible for inducing dispersion in microbial biofilms. *J. Bacteriol.* **2009,** 191, 1393-1403.

165. Pringle, J. H.; Fletcher, M., Influence of substratum hydration and adsorbed macromolecules on bacterial attachment to surfaces. *Appl. Environ. Microbiol.* **1986,** 51, 1321-5.

166. Khan, M. M. T.; Ista, L. K.; Lopez, G. P.; Schuler, A. J., Experimental and Theoretical Examination of Surface Energy and Adhesion of Nitrifying and Heterotrophic Bacteria Using Self-Assembled Monolayers. *Environ. Sci. Technol.* **2011,** 45, 1055-1060.

167. Bevis, B. J.; Glick, B. S., Rapidly maturing variants of the Discosoma red fluorescent protein (DsRed). *Nat. Biotechnol.* **2002,** 20, 1159.

168. Allison, D. G.; Sutherland, I. W., The role of exopolysaccharides in adhesion of freshwater bacteria. *J. Gen. Microbiol.* **1987,** 133, 1319-27.

169. Busscher, H. J.; Sjollema, J.; Van der Mei, H. C., Relative Importance of Surface Free Energy as a Measure of Hydrophobicity in Bacterial Adhesion to Solid Surfaces. In *Microbial Cell Surface Hydrophobicity*

Doyle, R. J.; Rosenberg, M., Eds. American Society for Microbiology: Washington, DC, 1990; pp 335-359.

170. Lawrence, J. R.; Delaquis, P. J.; Korber, D. R.; Caldwell, D. E., Behavior of *Pseudomonas fluorescens* Within the Hydrodynamic Boundary Layers of Surface Microenvironments. *Microb. Ecol* **1987,** 14, 1-14.

171. Marshall, K. C.; Stout, R.; Mitchell, R., Mechanism of the initial events in the sorption of marine bacteria to surfaces. *J. Gen. Microbiol.* **1971,** 68, 337-48.

172. Wiencek, K. M.; Fletcher, M., Bacterial adhesion to hydroxyl- and methyl-terminated alkanethiol self-assembled monolayers. *J. Bacteriol.* **1995,** 177, 1959-66.

173. Towbin, H.; Staehelin, T.; Gordon, J., Electrophoretic transfer of proteins from polyacrylamide gels to nitrocellulose sheets: Procedure and some applications. *Proc. Natl. Acad. Sci. U. S. A.* **1979,** 76, 4350-4.

174. Hower, J. C.; Bernards, M. T.; Chen, S.; Tsao, H.-K.; Sheng, Y.-J.; Jiang, S., Hydration of "Nonfouling" Functional Groups. *J. Phys. Chem. B* **2009,** 113, 197-201.

175. Jacques, J.; Collet, A.; Wilen, S. H., *Enantiomers, Racemates, and Resolutions*. John Wiley and Sons: New York, 1981; p 447 pp.

176. Hibbing, M. E.; Fuqua, C.; Parsek, M. R.; Peterson, S. B., Bacterial competition: surviving and thriving in the microbial jungle. *Nat. Rev. Microbiol.* **2010,** 8, 15-25.

177. O'Toole, G. A.; Kolter, R., Flagellar and twitching motility are necessary for Pseudomonas aeruginosa biofilm development. *Mol. Microbiol.* **1998,** 30, 295-304.

178. Laurent, S.; Forge, D.; Port, M.; Roch, A.; Robic, C.; Vander Elst, L.; Muller, R. N., Magnetic Iron Oxide Nanoparticles: Synthesis, Stabilization, Vectorization, Physicochemical Characterizations, and Biological Applications. *Chem. Rev.* **2008,** 108, 2064-2110.

179. Murray, C. B.; Kagan, C. R.; Bawendi, M. G., Synthesis and characterization of monodisperse nanocrystals and close-packed nanocrystal assemblies. *Annu. Rev. Mater. Sci.* **2000,** 30, 545-610.

180. Portet, D.; Denizot, B.; Rump, E.; Lejeune, J.-J.; Jallet, P., Nonpolymeric Coatings of Iron Oxide Colloids for Biological Use as Magnetic Resonance Imaging Contrast Agents. *J. Colloid Interface Sci.* **2001,** 238, 37-42.

181. Ulman, A., Self-assembled monolayers of alkyltrichlorosilanes: building blocks for future organic materials. *Adv. Mater.* **1990,** 2, 573-82.

182. Xiao, S.-J.; Textor, M.; Spencer, N. D.; Sigrist, H., Covalent Attachment of Cell-Adhesive, (Arg-Gly-Asp)-Containing Peptides to Titanium Surfaces. *Langmuir* **1998,** 14, 5507-5516.

183. Kiely, J. D.; Houston, J. E., Contact Hysteresis and Friction of Alkanethiol Self-Assembled Monolayers on Gold. *Langmuir* **1999,** 15, 4513-4519.

184. Geissler, U.; Hempel, U.; Wolf, C.; Scharnweber, D.; Worch, H.; Wenzel, K. W., Collagen type I-coating of Ti6Al4V promotes adhesion of osteoblasts. *J. Biomed. Mater. Res.* **2000,** 51, 752-760.

185. Anselme, K.; Linez, P.; Bigerelle, M.; Le Maguer, D.; Le Maguer, A.; Hardouin, P.; Hildebrand, H. F.; Iost, A.; Leroy, J. M., The relative influence of the topography and chemistry of Ti6Al4V surfaces on osteoblastic cell behavior. *Biomaterials* **2000,** 21, 1567-1577.

186. Carley, A. F.; Roberts, J. C.; Roberts, M. W., Dissociative chemisorption and localized oxidation states at titanium surfaces. *Surf. Sci.* **1990,** 225, L39-L41.

187. Roberts, M. W.; Tomellini, M., Mixed oxidation states of titanium at the metal-oxide interface. *Catal. Today* **1992,** 12, 443-52.

188. Lu, G.; Bernasek, S. L.; Schwartz, J., Oxidation of a polycrystalline titanium surface by oxygen and water. *Surf. Sci.* **2000,** 458, 80-90.

189. Brunette, D. M.; Tengvall, P.; Textor, M.; Thomsen, P.; Editors, *Titanium in Medicine: Material Science, Surface Science, Engineering, Biological Responses and Medical Applications*. 2001; p 1019 pp.

190. Olin, C., Titanium in cardiac and cardiovascular applications. *Titanium Med.* **2001**, 889-907.

191. Sul, Y.-T.; Kang, B.-S.; Johansson, C.; Um, H.-S.; Park, C.-J.; Albrektsson, T., The roles of surface chemistry and topography in the strength and rate of osseointegration of titanium implants in bone. *J. Biomed. Mater. Res., Part A* **2009,** 89A, 942-950.

192. Gawalt, E. S.; Avaltroni, M. J.; Danahy, M. P.; Silverman, B. M.; Hanson, E. L.; Midwood, K. S.; Schwarzbauer, J. E.; Schwartz, J., Bonding Organics to Ti Alloys: Facilitating Human Osteoblast Attachment and Spreading on Surgical Implant Materials. *Langmuir* **2003,** 19, 200-204.

193. Yee, C.; Kataby, G.; Ulman, A.; Prozorov, T.; White, H.; King, A.; Rafailovich, M.; Sokolov, J.; Gedanken, A., Self-Assembled Monolayers of Alkanesulfonic and -phosphonic Acids on Amorphous Iron Oxide Nanoparticles. *Langmuir* **1999,** 15, 7111-7115.

194. Sahoo, Y.; Pizem, H.; Fried, T.; Golodnitsky, D.; Burstein, L.; Sukenik, C. N.; Markovich, G., Alkyl Phosphonate/Phosphate Coating on Magnetite Nanoparticles: A Comparison with Fatty Acids. *Langmuir* **2001,** 17, 7907-7911.

195. Veiseh, O.; Gunn, J. W.; Kievit, F. M.; Sun, C.; Fang, C.; Lee, J. S. H.; Zhang, M., Inhibition of tumor-cell invasion with chlorotoxin-bound superparamagnetic nanoparticles. *Small* **2009,** 5, 256-264.

196. Veiseh, O.; Sun, C.; Gunn, J.; Kohler, N.; Gabikian, P.; Lee, D.; Bhattarai, N.; Ellenbogen, R.; Sze, R.; Hallahan, A.; Olson, J.; Zhang, M., Optical and MRI Multifunctional Nanoprobe for Targeting Gliomas. *Nano Lett.* **2005,** 5, 1003-1008.

197. Sun, C.; Veiseh, O.; Gunn, J.; Fang, C.; Hansen, S.; Lee, D.; Sze, R.; Ellenbogen, R. G.; Olson, J.; Zhang, M., In vivo MRI detection of gliomas by chlorotoxin-conjugated superparamagnetic nanoprobes. *Small* **2008,** 4, 372-379.

198. Lartigue, L.; Oumzil, K.; Guari, Y.; Larionova, J.; Guerin, C.; Montero, J.-L.; Barragan-Montero, V.; Sangregorio, C.; Caneschi, A.; Innocenti, C.; Kalaivani, T.; Arosio, P.; Lascialfari, A., Water-Soluble Rhamnose-Coated Fe3O4 Nanoparticles. *Org. Lett.* **2009,** 11, 2992-2995.

199. El-Boubbou, K.; Zhu, D. C.; Vasileiou, C.; Borhan, B.; Prosperi, D.; Li, W.; Huang, X., Magnetic Glyco-Nanoparticles: A Tool To Detect, Differentiate, and Unlock the Glyco-Codes of Cancer via Magnetic Resonance Imaging. *J. Am. Chem. Soc.* **2010,** 132, 4490-4499.

200. Lartigue, L.; Innocenti, C.; Kalaivani, T.; Awwad, A.; Sanchez Duque, M. d. M.; Guari, Y.; Larionova, J.; Guerin, C.; Montero, J.-L. G.; Barragan-Montero, V.; Arosio, P.; Lascialfari, A.; Gatteschi, D.; Sangregorio, C., Water-Dispersible Sugar-Coated Iron Oxide Nanoparticles. An Evaluation of their Relaxometric and Magnetic Hyperthermia Properties. *J. Am. Chem. Soc.* **2011,** 133, 10459-10472.

201. Shen, X.; Wu, Y.-L.; Wu, Y., Enantioselective synthesis of ethyl 4,5,7,8,9-penta-O-acetyl-2,6-anhydro-3-deoxy-D-erythro-L-gluca-nononate: a 2-monodeoxygenated derivative of "2-keto-3-deoxy-D-glycero-D-galacto-nononic acid". *Helv. Chim. Acta* **2000,** 83, 943-953.

202. Vonlanthen, D.; Leumann, C. J., Hydroxycyclopentanone derivatives from D-mannose via ring closing metathesis: An improved synthesis of a key intermediate of tricyclo-DNA. *Synthesis* **2003**, 1087-1090.

203. Bhattacharya, A. K.; Thyagarajan, G., Michaelis-Arbuzov rearrangement. *Chem. Rev.* **1981,** 81, 415-30.

204. Qiao, L.; Vederas, J. C., Synthesis of a C-phosphonate disaccharide as a potential inhibitor of peptidoglycan polymerization by transglycosylase. *J. Org. Chem.* **1993,** 58, 3480-2.

205. Grison, C.; Petek, S.; Finance, C.; Coutrot, P., Synthesis and antibacterial activity of mechanism-based inhibitors of KDO8P synthase and DAH7P synthase. *Carbohydr. Res.* **2005,** 340, 529-537.

206. Cegelski, L.; Marshall, G. R.; Eldridge, G. R.; Hultgren, S. J., The biology and future prospects of antivirulence therapies. *Nat. Rev. Microbiol.* **2008,** 6, 17-27.

207. Marra, A., Can virulence factors be viable antibacterial targets? *Expert Rev. Anti-Infect. Ther.* **2004,** 2, 61-72.

208. Rasmussen, T. B.; Givskov, M., Quorum sensing inhibitors: A bargain of effects. *Microbiology* **2006,** 152, 895-904.

209. Hentzer, M.; Wu, H.; Andersen, J. B.; Riedel, K.; Rasmussen, T. B.; Bagge, N.; Kumar, N.; Schembri, M. A.; Song, Z.; Kristoffersen, P.; Manefield, M.; Costerton, J. W.; Molin, S.; Eberl, L.; Steinberg, P.; Kjelleberg, S.; Hoiby, N.; Givskov, M., Attenuation of Pseudomonas aeruginosa virulence by quorum sensing inhibitors. *Embo J.* **2003,** 22, 3803-3815.

210. Chen, X.; Schauder, S.; Potier, N.; Van Dorsselaer, A.; Pelczer, I.; Bassler, B. L.; Hughson, F. M., Structural identification of a bacterial quorum-sensing signal containing boron. *Nature* **2002,** 415, 545-549.

211. Thiel, V.; Vilchez, R.; Sztajer, H.; Wagner-Doebler, I.; Schulz, S., Identification, quantification, and determination of the absolute configuration of the bacterial quorum-sensing signal auto-inducer-2 by gas chromatography-mass spectrometry. *ChemBioChem* **2009,** 10, 479-485.

212. Xavier, K. B.; Bassler, B. L., LuxS quorum sensing: More than just a numbers game. *Curr. Opin. Microbiol.* **2003,** 6, 191-197.

213. Hilgers, M. T.; Ludwig, M. L., Crystal structure of the quorum-sensing protein LuxS reveals a catalytic metal site. *Proc. Natl. Acad. Sci. U. S. A.* **2001,** 98, 11169-11174.

214. Koch, B.; Liljefors, T.; Persson, T.; Nielsen, J.; Kjelleberg, S.; Givskov, M., The LuxR receptor: The sites of interaction with quorum-sensing signals and inhibitors. *Microbiology* **2005,** 151, 3589-3602.

215. Vannini, A.; Volpari, C.; Di Marco, S., Crystal structure of the quorum-sensing protein TraM and its interaction with the transcriptional regulator TraR. *J. Biol. Chem.* **2004,** 279, 24291-24296.

216. Vannini, A.; Volpari, C.; Gargioli, C.; Muraglia, E.; Cortese, R.; De Francesco, R.; Neddermann, P.; Di Marco, S., The crystal structure of the quorum sensing protein TraR bound to its autoinducer and target DNA. *Embo J.* **2002,** 21, 4393-4401.

217. Zhang, R.-g.; Pappas, K. M.; Brace, J. L.; Miller, P. C.; Oulmassov, T.; Molyneaux, J. M.; Anderson, J. C.; Bashkin, J. K.; Winans, S. C.; Joachimiak, A., Structure of a bacterial quorum-sensing transcription factor complexed with pheromone and DNA. *Nature* **2002,** 417, 971-974.

218. Bottomley, M. J.; Muraglia, E.; Bazzo, R.; Carfi, A., Molecular insights into quorum sensing in the human pathogen Pseudomonas aeruginosa from the structure of the virulence regulator LasR bound to its autoinducer. *J. Biol. Chem.* **2007,** 282, 13592-13600.

219. Praneenararat, T.; Geske, G. D.; Blackwell, H. E., Efficient Synthesis and Evaluation of Quorum-Sensing Modulators Using Small Molecule Macroarrays. *Org. Lett.* **2009,** 11, 4600-4603.

220. Kim, C.; Kim, J.; Park, H.-Y.; Park, H.-J.; Kim, C. K.; Yoon, J.; Lee, J.-H., Development of inhibitors against TraR quorum-sensing system in Agrobacterium tumefaciens by molecular modeling of the ligand-receptor interaction. *Mol. Cells* **2009,** 28, 447-453.

221. de Nys, R.; Wright, A. D.; Konig, G. M.; Sticher, O., New halogenated furanones from the marine alga Delisea pulchra (cf. fimbriata). *Tetrahedron* **1993,** 49, 11213-20.

222. De Nys, R.; Steinberg, P. D.; Willemsen, P.; Dworjanyn, S. A.; Gabelish, C. L.; King, R. J., Broad spectrum effects of secondary metabolites from the red alga Delisea pulchra in antifouling assays. *Biofouling* **1995,** 8, 259-71.

223. Givskov, M.; de Nys, R.; Manefield, M.; Gram, L.; Maximilien, R.; Eberl, L.; Molin, S.; Steinberg, P. D.; Kjelleberg, S., Eukaryotic interference with homoserine lactone-mediated prokaryotic signaling. *J. Bacteriol.* **1996,** 178, 6618-6622.

224. Smith Jenee, N.; Dyszel Jessica, L.; Soares Jitesh, A.; Ellermeier Craig, D.; Altier, C.; Lawhon Sara, D.; Adams, L. G.; Konjufca, V.; Curtiss, R., 3rd; Slauch James, M.; Ahmer Brian, M. M., SdiA, an N-acylhomoserine lactone receptor, becomes active during the transit of Salmonella enterica through the gastrointestinal tract of turtles. *PLoS One* **2008,** 3, e2826.

225. Van Houdt, R.; Aertsen, A.; Moons, P.; Vanoirbeek, K.; Michiels, C. W., N-acyl-L-homoserine lactone signal interception by Escherichia coli. *FEMS Microbiol. Lett.* **2006,** 256, 83-89.

226. Baveja, J. K.; Willcox, M. D. P.; Hume, E. B. H.; Kumar, N.; Odell, R.; Poole-Warren, L. A., Furanones as potential anti-bacterial coatings on biomaterials. *Biomaterials* **2004,** 25, 5003-5012.

227. Hume, E. B. H.; Baveja, J.; Muir, B.; Schubert, T. L.; Kumar, N.; Kjelleberg, S.; Griesser, H. J.; Thissen, H.; Read, R.; Poole-Warren, L. A.; Schindhelm, K.; Willcox, M.

D. P., The control of Staphylococcus epidermidis biofilm formation and in vivo infection rates by covalently bound furanones. *Biomaterials* **2004,** 25, 5023-5030.

228. Simon, K. A. Water-in-water emulsions and templated synthesis of heterogeneous biocatalysts with enhanced activity, and, Enhancing anti-fouling chemistry for confining mammalian cell adhesion by gradient nanotopography. Syracuse University, Syracuse, 2010.

229. Ogoshi, T.; Takashima, Y.; Yamaguchi, H.; Harada, A., Chemically-Responsive Sol-Gel Transition of Supramolecular Single-Walled Carbon Nanotubes (SWNTs) Hydrogel Made by Hybrids of SWNTs and Cyclodextrins. *J. Am. Chem. Soc.* **2007,** 129, 4878-4879.

230. Kelly, J. M.; Quack, G.; Miles, M. M., In vitro and in vivo activities of aminoadamantane and aminoalkylcyclohexane derivatives against Trypanosoma brucei. *Antimicrob. Agents Chemother.* **2001,** 45, 1360-1366.

231. Dodziuk, H., Molecules with holes - cyclodextrins. *Cyclodextrins Their Complexes* **2008**, 1-30.

232. Muderawan, I. W.; Ong, T. T.; Lee, T. C.; Young, D. J.; Ching, C. B.; Ng, S. C., A reliable synthesis of 2- and 6-amino-β-cyclodextrin and permethylated-β-cyclodextrin. *Tetrahedron Lett.* **2005,** 46, 7905-7907.

233. Harada, A.; Kobayashi, R.; Takashima, Y.; Hashidzume, A.; Yamaguchi, H., Macroscopic self-assembly through molecular recognition. *Nat Chem* **2011,** 3, 34-7.

234. Wennekes, T.; Van den Berg, R. J. B. H. N.; Donker, W.; van der Marel, G. A.; Strijland, A.; Aerts, J. M. F. G.; Overkleeft, H. S., Development of Adamantan-1-yl-

methoxy-Functionalized 1-Deoxynojirimycin Derivatives as Selective Inhibitors of Glucosylceramide Metabolism in Man. *J. Org. Chem.* **2007,** 72, 1088-1097.

235. Manny, A. J.; Kjelleberg, S.; Kumar, N.; de Nys, R.; Read, R. W.; Steinberg, P., Reinvestigation of the sulfuric acid-catalyzed cyclization of brominated 2-alkyllevulinic acids to 3-alkyl-5-methylene-2(5H)-furanones. *Tetrahedron* **1997,** 53, 15813-15826.

236. Le Vezouet, R.; White, A. J. P.; Burrows, J. N.; Barrett, A. G. M., Synthetic studies on the CDEF ring system of lactonamycin. *Tetrahedron* **2006,** 62, 12252-12263.

237. Boukouvalas, J.; Beltran, P. P.; Lachance, N.; Cote, S.; Maltais, F.; Pouliot, M., A new, highly stereoselective synthesis of β-unsubstituted (Z)-γ-alkylidenebutenolides using bromine as a removable stereocontrol element. *Synlett* **2007**, 219-222.

238. Burghart, J.; Bruckner, R., Total synthesis of Naturally configured pyrrhoxanthin, a carotenoid butenolide from plankton. *Angew. Chem., Int. Ed.* **2008,** 47, 7664-7668.

239. Ochoa de Echaguen, C.; Ortuno, R. M., The bromination of β-angelica lactone revisited: synthesis of new 3-bromo-5-methylene- and 3-bromo-5-methyl-2(5H)-furanones. *Tetrahedron* **1994,** 50, 12457-62.

240. Huigens, R. W., III; Ma, L.; Gambino, C.; Moeller, P. D. R.; Basso, A.; Cavanagh, J.; Wozniak, D. J.; Melander, C., Control of bacterial biofilms with marine alkaloid derivatives. *Mol. BioSyst.* **2008,** 4, 614-621.

241. Bunders, C. A.; Richards, J. J.; Melander, C., Identification of aryl 2-aminoimidazoles as biofilm inhibitors in Gram-negative bacteria. *Bioorg. Med. Chem. Lett.* **2010,** 20, 3797-3800.

242. Rasmussen, T. B.; Manefield, M.; Andersen, J. B.; Eberl, L.; Anthoni, U.; Christophersen, C.; Steinberg, P.; Kjelleberg, S.; Givskov, M., How Delisea pulchra furanones affect quorum sensing and swarming motility in Serratia liquefaciens MG1. *Microbiology* **2000,** 146, 3237-3244.

243. Manefield, M.; De Nys, R.; Kumar, N.; Read, R.; Givskov, M.; Steinberg, P.; Kjelleberg, S., Evidence that halogenated furanones from Delisea pulchra inhibit acylated homoserine lactone (AHL)-mediated gene expression by displacing the AHL signal from its receptor protein. *Microbiology* **1999,** 145, 283-291.

244. Kapadnis, P. B.; Hall, E.; Ramstedt, M.; Galloway, W. R. J. D.; Welch, M.; Spring, D. R., Towards quorum-quenching catalytic antibodies. *Chem. Commun.* **2009**, 538-540.

245. De Lamo Marin, S.; Xu, Y.; Meijler, M. M.; Janda, K. D., Antibody catalyzed hydrolysis of a quorum sensing signal found in Gram-negative bacteria. *Bioorg. Med. Chem. Lett.* **2007,** 17, 1549-1552.

246. Rasmussen, T. B.; Givskov, M., Quorum-sensing inhibitors as anti-pathogenic drugs. *Int. J. Med. Microbiol.* **2006,** 296, 149-161.

247. Hentzer, M.; Givskov, M., Pharmacological inhibition of quorum sensing for the treatment of chronic bacterial infections. *J. Clin. Invest.* **2003,** 112, 1300-1307.

248. Hodgkinson, J. T.; Welch, M.; Spring, D. R., Learning the Language of Bacteria. *ACS Chem. Biol.* **2007,** 2, 715-717.

249. Amara, N.; Mashiach, R.; Amar, D.; Krief, P.; Spieser, S. A. H.; Bottomley, M. J.; Aharoni, A.; Meijler, M. M., Covalent Inhibition of Bacterial Quorum Sensing. *J. Am. Chem. Soc.* **2009,** 131, 10610-10619.

250. Galloway, W. R. J. D.; Hodgkinson, J. T.; Welch, M.; Spring, D. R., Mastering the chemical language of bacteria. *Chem. Biol.* **2009,** 16, 913-914.

251. Kim, C.; Kim, J.; Park, H.-Y.; Lee, J.-H.; Park, H.-J.; Kim, C. K.; Yoon, J., Structural understanding of quorum-sensing inhibitors by molecular modeling study in Pseudomonas aeruginosa. *Appl. Microbiol. Biotechnol.* **2009,** 83, 1095-1103.

252. Geske, G. D.; O'Neill, J. C.; Miller, D. M.; Wezeman, R. J.; Mattmann, M. E.; Lin, Q.; Blackwell, H. E., Comparative analyses of N-acylated homoserine lactones reveal unique structural features that dictate their ability to activate or inhibit quorum sensing. *ChemBioChem* **2008,** 9, 389-400.

253. Ahumedo, M.; Diaz, A.; Vivas-Reyes, R., Theoretical and structural analysis of the active site of the transcriptional regulators LasR and TraR, using molecular docking methodology for identifying potential analogues of acyl homoserine lactones (AHLs) with anti-quorum sensing activity. *Eur. J. Med. Chem.* **2010,** 45, 608-615.

254. Glansdorp, F. G.; Thomas, G. L.; Lee, J. K.; Dutton, J. M.; Salmond, G. P. C.; Welch, M.; Spring, D. R., Synthesis and stability of small molecule probes for Pseudomonas aeruginosa quorum sensing modulation. *Org. Biomol. Chem.* **2004,** 2, 3329-3336.

255. Ozer, E. A.; Pezzulo, A.; Shih, D. M.; Chun, C.; Furlong, C.; Lusis, A. J.; Greenberg, E. P.; Zabner, J., Human and murine paraoxonase 1 are host modulators of Pseudomonas aeruginosa quorum-sensing. *FEMS Microbiol. Lett.* **2005,** 253, 29-37.

256. Yang, F.; Wang, L.-H.; Wang, J.; Dong, Y.-H.; Hu, J. Y.; Zhang, L.-H., Quorum quenching enzyme activity is widely conserved in the sera of mammalian species. *FEBS Lett.* **2005,** 579, 3713-3717.

257. Zou, Y.; Nair, S. K., Molecular basis for the recognition of structurally distinct autoinducer mimics by the Pseudomonas aeruginosa LasR quorum sensing signaling receptor. *Chem. Biol.* **2009,** 16, 961-970.

258. Sejwal, P.; Han, Y.; Shah, A.; Luk, Y.-Y., Water-driven chemoselective reaction of squarate derivatives with amino acids and peptides. *Org. Lett.* **2007,** 9, 4897-4900.

259. Sejwal, P. I. Water-driven chemoselective reactions of squarate derivatives with amino acids and peptides: Mechanism and applications. II. Biocompatible hydrogels: Transferring bioinert chemistry from surfaces to 3-dimensional materials. 2008.

260. Sejwal, P.; Narasimhan, S. K.; Prashar, D.; Bandyopadhyay, D.; Luk, Y.-Y., Selective Immobilization of Peptides Exclusively via N-Terminus Cysteines by Water-Driven Reactions on Surfaces. *J. Org. Chem.* **2009,** 74, 6843-6846.

261. Zang, T.; Lee, B. W. K.; Cannon, L. M.; Ritter, K. A.; Dai, S.; Ren, D.; Wood, T. K.; Zhou, Z. S., A naturally occurring brominated furanone covalently modifies and inactivates LuxS. *Bioorg. Med. Chem. Lett.* **2009,** 19, 6200-6204.

262. Reed, M. W.; Pollart, D. J.; Perri, S. T.; Foland, L. D.; Moore, H. W., Synthesis of 4-substituted-3-alkoxy-3-cyclobutene-1,2-diones. *J. Org. Chem.* **1988,** 53, 2477-82.

263. Ferrer, S.; Pasto, M.; Rodriguez, B.; Riera, A.; Pericas, M. A., Chiral derivatives of semisquaric acid as new modular ligands for asymmetric catalysis. *Tetrahedron Asymmetry* **2003,** 14, 1747-1752.

264. Liebeskind, L. S.; Fengl, R. W.; Wirtz, K. R.; Shawe, T. T., An improved method for the synthesis of substituted cyclobutenediones. *J. Org. Chem.* **1988,** 53, 2482-8.

265. Andrade, J. D.; Hlady, V., Protein adsorption and materials biocompatibility: a tutorial review and suggested hypotheses. *Adv. Polym. Sci.* **1986,** 79, 1-63.

266. Jeon, S. I.; Lee, J. H.; Andrade, J. D.; De Gennes, P. G., Protein-surface interactions in the presence of polyethylene oxide. I. Simplified theory. *J. Colloid Interface Sci.* **1991,** 142, 149-58.

267. Jeon, S. I.; Andrade, J. D., Protein-surface interactions in the presence of polyethylene oxide. II. Effect of protein size. *J. Colloid Interface Sci.* **1991,** 142, 159-66.

268. Yancey, P. H.; Clark, M. E.; Hand, S. C.; Bowlus, R. D.; Somero, G. N., Living with water stress: evolution of osmolyte systems. *Science* **1982,** 217, 1214-22.

269. Mrksich, M., A surface chemistry approach to studying cell adhesion. *Chem. Soc. Rev.* **2000,** 29, 267-273.

VITA

NAME OF AUTHOR: Debjyoti Bandyopadhyay

PLACE OF BIRTH: New Delhi, India

DATE OF BIRTH: December 12, 1982

GRADUATE AND UNDERGRADUATE SCHOOLS ATTENDED:
Syracuse University, Syracuse, New York
University of Delhi, New Delhi, India

DEGREES AWARDED:
Master of Philosophy in Chemistry, 2008, Syracuse University, Syracuse, New York
Master of Science in Chemistry, 2005, University of Delhi, New Delhi, India
Bachelor of Science in Chemistry, 2003, University of Delhi, New Delhi, India

AWARDS AND HONORS:
Outstanding Teaching Assistant: William D. Johnson Award, Syracuse University, 2010

Lectureship in Chemical Sciences in joint Council for Scientific & Industrial Research (CSIR)-University Grants Commission (UGC) - National Eligibility Test (NET), for lectureship at a university/college in India, 2005

PROFESSIONAL EXPERIENCE:
Teaching Assistant, Department of Chemistry, Syracuse University, 2006-2011
Research Assistant, Department of Chemistry, Syracuse University, 2006-2011